The physical properties of magnetic inks

James Martin McCoy

The Physical Properties
of
Magnetic Inks

James Martin McCoy B.Sc.
(Graduate Society)

Thesis submitted to the University of Durham in
Candidature for the Degree of Doctor of Philosophy,
September, 1988

Statement of Copyright

To my Mother and in Memory of my Father.

Declaration

The work contained in this thesis was carried out by the author between 1984 and 1988 while a postgraduate student in the Physics Department at the University of Durham. Work carried out in collaboration with other parties is clearly acknowledged at the appropriate point. None of the work contained in this thesis has been submitted in candidature for any other degree.

So every journey that I make
Leads me ...
To some new ambush, to some fresh mistake.

(Philip Larkin, Nursery Tale)

Abstract

The magnetic particle inspection (MPI) method is a widely used non destructive testing (NDT) technique for ferrous structures. Magnetic inks used in MPI are suspensions of fine ferro/ferrimagnetic particles which, when applied to a magnetized test specimen, delineate surface flaws. This work is an investigation of some of the properties of magnetic ink systems and some aspects of their interaction with defect leakage flux. Reviews of magnetism, the MPI method and leakage flux at defects are given. The construction, characterization and automation of a 1.2 T electromagnet vibrating sample magnetometer, used for magnetic measurements on the inks, is described. The instrument has a resolution of better than $10^{-9}\,\mathrm{JT}^{-1}$. A 2D model of indication formation in MPI, based upon the simulation of many particles in the neighbourhood of a defect, is presented. Results of the rôle of several of the model parameters are given. Results indicate that carrier coefficients of viscosity at the lower end of the range investigated ($\eta = 0.3\,\mathrm{mPas}$) are optimum. The size and contrast of an indication increases with defect size. The contrast and rate of formation of contrast increase with defect aspect ratio. The effect of the contrast paint layer thickness indicates that the recommendation of the British Standard, BS 5044 (1973), is qualitatively correct. Experimental observations of particles in field gradients reveals a discrepancy between theoretical and observed behaviour which is attributed, in particular, to unobservable voids in the particles. Detailed characterization of the particles shows them to be aggregates of $20 - 200\,\mathrm{nm}$ crystallites which are probably single domain particles. The morphology of larger aggregates is related to measurements of the low field susceptibility. Evidence from intensive magnetic measurements supports the relationship between magnetic properties and aggregate characteristics. A '$\ln t$' magnetic viscosity effect is reported. At 77 K, the coefficient of magnetic viscosity has a maximum near the coercivity field.

Acknowledgements

It is my privilege to acknowledge the assistance and support given to me by many people during the course of this work.

I thank Professors B.H. Bransden and A.W. Wolfendale for making available to me the facilities of the Department of Physics at the University of Durham.

I am very grateful to my supervisor, Dr. B.K. Tanner for his continued support, enthusiasm, encouragement and good ideas throughout the duration of this work. The support of Dr. W.D. Corner is also much appreciated. I have been fortunate in sharing some of my time in Durham with Dr. S.N.M. Willcock and Dr. S.R. Hoon. Their assistance and knowledge, particularly with regard to the second Durham VSM, is greatly appreciated. The insight and expertise of Dr. D.B. Lambrick has also been important and is much appreciated. Others I thank from the Solid State Physics Research Group at the University of Durham include Dr. M.J. Hawton, Mr. N. Loxley, Miss A. Birkett and Dr. C.D.H. Williams. I am grateful for the advice and help given to me by Dr. A. Wooding and Dr. N. Mason from the Chemistry Department.

My two industrial supervisors, Mr. G.A. Raine and Dr. A.W. Wagg, have both contributed greatly and their support and expertise has been very much appreciated. I would also like to thank Dr. D. Paige, Dr. L.L. Morgan and Mr. S.T. Brown from British Gas.

I am indebted to the late Dr. G.J. Russell from the School of Engineering and Applied Science for his cooperation in the electron microscopy studies. I also thank Dr. M.G. Hetherington and Dr. J.P. Jakubovics for the use of the High Voltage Electron Microscope at Oxford.

The expert technical advice, assistance and support of Mr. P. Foley, Mr. D. Oliver and Mr. J. Scott is much appreciated. In addition, I express my thanks to the staff of the Teaching Workshop, Mr. D. Jobling, Mr. P. Armstrong and Mr. G. Teasdale, for their technical expertise, their good advice and the skill with which they fabricated the VSM parts. I am grateful to all of the members of the Physics Electronics Workshop, under the direction of Mr. T. Jackson, particularly for their maintenance of the VSM power supply unit.

Thanks are due also to all of the staff of the University of Durham Computer Centre, particularly Mr. B.R. Lander. I thank Miss K.L. Gittens for the care and precision with which she drew most of the diagrams in this thesis and also Mr. M. Lee for his preparation of the photographs.

Finally, I wish to express my sincere gratitude to the Science and Engineering Research Council, British Gas Plc. and the Central Electricity Generating Board, all of whose financial support has made this research possible.

List of Publications

Tanner, B.K., McCoy, J.M., Willcock, S.N.M., Hetherington, M.G. and Jakubovics, J.P. *The structure and behaviour of inks for magnetic particle inspection* J. Mater. Sci. Letts. **5**, 296 (1986)

McCoy, J.M. and Tanner, B.K. *Simulation of Particle Trajectories in Magnetic Particle Inspection* IEEE Trans. Magn. **MAG-24**, 1665 (1988)

Contents

Chapter 1

Introduction

This work describes a study of some of the properties of magnetic ink systems and of their interaction with defect leakage fields in the non-destructive testing (NDT) technique of magnetic particle inspection (MPI). The MPI technique is used to reveal the presence of cracks and defects in steel structures and welds such as are commonly used in the gas and oil industries. Magnetic inks are suspensions of fine ferro- or ferrimagnetic particles in a suitable carrier liquid. The test specimen is first magnetized and then the magnetic ink is applied to the surface. Any surface-breaking or near surface-breaking defects running in a direction perpendicular to the magnetizing direction produce magnetic flux leakage fields localized at the defects. The magnetic field gradients localized at the defects cause forces to act on the suspended magnetic ink particles and attract them to the defect line. The local increase in particle number density at the defect renders the defect visible to an observer. This description constitutes a brief account of the use and the underlying physics of the technique of MPI.

This thesis is a report of an attempt to elucidate in greater depth some aspects of the underlying physics. Specifically, the work focusses on the properties of the MPI particles themselves and their behaviour in leakage field gradients.

To this end, the first two chapters are intended to constitute something of a review or a background of some of the topics which are required later on and which permeate the whole thesis. The first of the two includes a brief review of the important concepts and ideas underlying magnetism. In addition to this, the specific subject of fine particle magnetism, which is of such importance in the understanding of the properties of magnetic inks, is introduced and surveyed. The chapter after that deals in great depth exclusively with the subjects of MPI and magnetic flux leakage at defects.

Once these topics have been dealt with, the thesis goes on in the following chapter, Chapter 4, to describe the construction, characterization and automation of a 1.2T electromagnet vibrating sample magnetometer (VSM). This intrument was used for investigating the magnetic properties of the magnetic ink systems. Most of the VSM data presented in this thesis was obtained from this instrument.

The next chapter, Chapter 5, describes the formulation of a 2D model of the indication formation process. This model is a classical dynamics model based on the simulation of the trajectories of a large number of particles in the neighbourhood of a defect leakage field. The numerical solution of the equations of motion of the particles is described in detail.

Chapter 6 presents some results obtained from the indication formation model described in Chapter 5. The chapter attempts to obtain information about the rôle played by several of the model parameters in the indication formation process.

The following chapter, Chapter 7, reports a series of experiments which involved the direct observation of the motions of individual MPI particles moving in a magnetic field gradient. This study was originally intended to constitute a test of the

model developed in Chapter 5. In addition to this, however, it succeeds in revealing some important properties of some of the particles themselves.

Details of the characterization of the particulate component of magnetic ink systems are given in Chapter 8. A variety of techniques are described which were used to determine the nature of the MPI particles. Important results are presented concerning the microstructure of the particles and aggregates. Optical microscopy observations of particles in an applied field could be successfully correlated with some of the magnetic properties of the systems measured using a VSM.

Chapter 9 reports a more intensive study of the magnetic properties of magnetic ink systems. The relationship between aggregate characteristics and magnetic properties which was found in Chapter 8 is investigated in more depth. Finally, details of a magnetic viscosity effect found in these systems are reported.

The final chapter brings together the most important conclusions of the whole work. In addition to this, the author makes some suggestions for some possible refinements and for some possible ways of achieving further elucidation of some of the material presented in this thesis.

Chapter 2

Introductory Magnetism and Fine Particle Magnetism

2.1 Introduction

The first purpose of this chapter is to give a brief introduction to the main ideas and concepts of magnetism. Because the treatment is brief, extensive coverage of the quantum mechanical description of magnetism is omitted. Elements of such a description are only given when and where it is relevant. The second purpose is to give an introduction to the subject of fine particle magnetism, or, the magnetism of small particles. Sommerfeld SI units will be employed exclusively for all magnetic quantities throughout this and all other chapters.

2.2 Basic Field Concepts

Confusion often arises over the quantities the magnetic field, $\mathbf{H}$, the induction in free space, $\mathbf{B}_0$ (also sometimes called the magnetic field), and the induction in a magnetized medium, $\mathbf{B}$. Here, the magnetic field, $\mathbf{H}$, has units of ampères per metre (Am^{-1}) and the inductions in free space and in a medium, $\mathbf{B}_0$ and $\mathbf{B}$ respectively, have units of tesla (T) or webers per square metre (Wb m^{-2}). $\mathbf{B}$ and $\mathbf{B}_0$ are also called the magnetic flux density. There are differences between these which will be clarified here.

In free space (or a vacuum), things are relatively straightforward and there is a simple proportionality between the magnetic field, $\mathbf{H}$, and the induction, $\mathbf{B}$,

$$\mathbf{B} = \mu_0 \mathbf{H} \tag{2.1}$$

μ_0 is the permeability of free space ($4\pi \times 10^{-7}$ henrys per metre (Hm^{-1})). However, since this is in free space, the induction, $\mathbf{B}$, is exactly the same as $\mathbf{B}_0$, the free space induction, and so

$$\mathbf{B}_0 = \mu_0 \mathbf{H} \qquad \text{in free space.} \tag{2.2}$$

In a magnetized medium the situation is more complicated. The induction, $\mathbf{B}$, is given by

$$\mathbf{B} = \mu_0(\mathbf{H} + \mathbf{M}) \qquad \text{in a medium.} \tag{2.3}$$

But from equation (2.2) this can be written as

$$\mathbf{B} = \mathbf{B}_0 + \mu_0 \mathbf{M} \tag{2.4}$$

Here $\mathbf{M}$ is the magnetization per unit volume and has units of ampères per metre (Am^{-1}) or joules per tesla per cubic metre ($\mathrm{JT}^{-1}\mathrm{m}^{-3}$). Equation (2.4) clarifies the difference between the two types of induction. The free space induction, $\mathbf{B}_0$, is the induction which would be present in free space were the medium to be removed and the induction in a medium, $\mathbf{B}$, is that induction which is actually present in the medium.

The magnetization per unit volume, $\mathbf{M}$, is related to the magnetic dipole moment, $\mathbf{m}$, a quantity which will be discussed in more detail in the next section. $\mathbf{m}$

has units of ampère square metres (Am^2) or joules per tesla (JT^{-1}). A volume element, dV, of material has a magnetic dipole moment, $d\mathbf{m}$, given by

$$d\mathbf{m} = \mathbf{M}\, dV \qquad 2.5$$

Hence the magnetization per unit volume is the magnetic dipole moment per unit volume.

Sometimes it is more convenient to consider the magnetization per unit mass rather than the magnetization per unit volume. The magnetization per unit mass, σ, is simply related to the magnetization per unit volume via the density of the material, ρ, by the equation

$$\sigma = \frac{\mathbf{M}}{\rho} \qquad 2.6$$

σ has units of ampère square metres per kilogramme (Am^2kg^{-1}) or joules per tesla per kilogramme ($JT^{-1}kg^{-1}$).

Equation (2.3) can also be written as

$$\mathbf{B} = \mu_0 \mu_r \mathbf{H} \qquad 2.7$$

where $\mu_r (= 1 + M/H)$ is called the relative permeability of the magnetized material and is dimensionless. Another quantity which is closely related to the relative permeability is the volume susceptibility, χ_v, which is also dimensionless and which is defined by

$$\chi_v = \mu_r - 1 \qquad 2.8a$$

or

$$\chi_v = \frac{M}{H} \qquad 2.8b$$

Loosely speaking, these two quantities, μ_r and χ_v, are measures of magnetic response or how the magnetization of a substance changes under the application of a magnetic field at a particular magnetic field. In linear, isotropic, homogeneous media χ_v and μ_r are scalar quantities, but most generally, in media where this is not the case they are both tensors.

In the same way that the magnetization per unit mass, σ, is related to the magnetization per unit volume, $\mathbf{M}$, by the density, ρ, so the mass susceptibility, χ_m, is related to the volume susceptibility in a similar manner. The two quantities are related in an obvious way by

$$\chi_m = \frac{\sigma}{H} = \frac{\chi_v}{\rho} \qquad 2.9$$

These definitions of susceptibility are not universal and other authors may define them in different ways (for example, Crangle (1977)).

Equation (2.7) is also sometimes written as

$$\mathbf{B} = \mu \mathbf{H} \qquad 2.10$$

that is, with the use of the definition

$$\mu = \mu_0 \mu_r \qquad 2.11$$

The quantity μ is called the absolute permeability (as distinct from the relative permeability) and has dimensions of henrys per metre (Hm^{-1}). The reciprocal of the absolute permeability is called the reluctivity, ν. That is

$$\nu = \frac{1}{\mu} = \frac{1}{\mu_0 \mu_r} \qquad 2.12$$

The reluctivity has units of metres per henry (mH^{-1}).

2.3 The Magnetic Dipole Moment

We will now to go into greater detail about the magnetic dipole moment, $\mathbf{m}$, because this is of such basic importance in magnetism. The concept of the magnetic dipole moment is an example of a case in which the classical object can help to elucidate the quantum mechanical object.

Classically, a current, I, flowing around the perimeter of a loop of area a produces a magnetic dipole moment, $\mathbf{m}$, which is given by

$$\mathbf{m} = Ia\hat{\mathbf{n}} \qquad 2.13$$

Here $\hat{\mathbf{n}}$ is a unit vector perpendicular to the plane of the current loop. At the atomic level atoms also have magnetic dipole moments. Obviously, their precise origin is not exactly the same as for their classical counterparts. However, the analogy with macroscopic current loops of charged electrons orbiting in atoms and so constituting some sort of microscopic current loop is useful to describe magnetic dipole moments on the quantum mechanical level.

Before dealing with the origins of atomic or molecular magnetic dipole moments, two more important points will be presented here which are of particular relevance to Chapter 5. The first point is concerned with the magnetostatic energy possessed by a magnetic dipole moment, $\mathbf{m}$, in an applied magnetic field, $\mathbf{B}_0$. It can be simply shown (see, for example, Duffin (1980), p198 or Chikazumi (1964), p4) that the magnetostatic energy, $E_{\mathbf{B}_0}$, is given by

$$E_{\mathbf{B}_0} = -\mathbf{m}\cdot\mathbf{B}_0 \qquad 2.14$$

Obviously the minimum energy orientation of $\mathbf{m}$ occurs when $\mathbf{m}$ is parallel to $\mathbf{B}_0$.

The second point is concerned with the magnetic dipole-dipole interaction energy or the magnetostatic interaction energy between two magnetic dipole moments, $\mathbf{m}_1$ and $\mathbf{m}_2$. This interaction arises from each magnetic dipole moment 'feeling' the magnetic field, $\mathbf{B}_0$, produced by the other magnetic dipole moment and, consequently, suffering an interaction energy in accordance with equation (2.14). This interaction energy, E_m^{12}, is given by (see, for example, Chikazumi (1964), p5, and also, for the magnetic field produced by a single magnetic dipole moment, Kittel (1976), p507 (although these authors do not use SI units))

$$E_m^{12} = -\frac{\mu_0}{4\pi}\left[\frac{\mathbf{m}_1\cdot\mathbf{m}_2}{R_{12}^3} - \frac{3(\mathbf{m}_1\cdot\mathbf{R}_{12})(\mathbf{m}_2\cdot\mathbf{R}_{12})}{R_{12}^5}\right] \qquad 2.15$$

Here $\mathbf{R}_{12}$ is the position vector between the magnetic dipole moments $\mathbf{m}_1$ and $\mathbf{m}_2$.

Atomic magnetic dipole moments arise from properties of the electrons associated with the atoms and from the interaction of the electrons with a magnetic

field. A charged electron orbiting in an atom constitutes an ampèrian current loop and so a magnetic dipole moment is associated with the electronic motion. In the absence of any external torques acting, the angular momentum of the orbiting electron remains constant. A direct proportionality exists between the magnetic dipole moment, **m**, and the angular momentum, **G**, (see, for example, Bleaney and Bleaney (1976), p164) which is given by

$$\mathbf{m} = \gamma \mathbf{G} \qquad 2.16$$

γ is called the gyromagnetic ratio or the magnetogyric ratio and for pure orbital electron motion is given by

$$\gamma = -\frac{e}{2m_e} \qquad 2.17$$

In this equation e is the magnitude of the electronic charge and m_e is the electron rest mass. As well as there being a magnetic dipole moment associated with the electron's orbital angular momentum, a magnetic dipole moment is associated with the electron's intrinsic angular momentum (spin) in a manner which is also given by equation (2.16), although for this pure spin angular momentum, γ is twice the value given by equation (2.17), that is, $\gamma = -e/m_e$. Thus, the total angular momentum of the atom (neglecting nuclear properties) is the vector sum of both the orbital and spin angular momenta elements of all of the electrons associated with the atom. In the same way, the total magnetic dipole moment of the whole atom is given by a similar vector sum. The linear relationship between the atom's total angular momentum and its total magnetic dipole moment is preserved, but the proportionality constant is not necessarily the same. The relationship between these two quantities is an important one. Because most free atoms possess non-zero electronic angular momentum vectors it follows that most free atoms would be expected to possess permanent magnetic dipole moments.

2.4 Classes of Magnetic Behaviour

Rarely do atoms exist in the free state. Usually atoms are incorporated into molecules or ionic systems. In such systems the electronic behaviour is not as is described above for individual atoms but is modified in the following way. As a result of the interactions between the electrons in bound neighbouring atoms or ions, the total magnetic dipole moment of an individual molecule or ionic system is usually zero in the absence of an applied magnetic field. The reason for this is that the stable state of the bound system corresponds to that state in which no net magnetic dipole moment exists. Hence, the conclusion here is that usually molecules or systems which have ionic constituents do not possess permanent magnetic dipole moments in the absence of an applied magnetic field. However, when placed in an applied magnetic field these substances can acquire net magnetic dipole moments. This effect can be explained by the magnetic field's causing a precessional motion of the electronic orbits in accordance with Larmor's theorem. This means that the electrons acquire additional angular momentum and, hence, produce magnetic dipole moments. If this is the sole source of the magnetic dipole moments then the substance is said to be *diamagnetic*. In diamagnetic substances the magnetic dipole moments are aligned antiparallel to the applied magnetic field (essentially as a consequence of Lenz's law). This means that the susceptibility is always negative. The susceptibility is also temperature-independent because the effect is internal to each atom. Finally the susceptibility is also independent of the applied field (that is, it is linear). The magnitude of the diamagnetic volume susceptibility is typically

$\chi_v \sim -10^{-5}$ or less. Diamagnetism is by far the most common class of magnetic behaviour and, whatever other classes may additionally occur, it is always present.

In the previous paragraph it was stated that most substances possess no magnetic dipole moments in the absence of an applied magnetic field. *Paramagnetism* is the name given to the magnetism of those substances which do possess magnetic dipole moments even in the absence of an applied magnetic field. For these substances, the stable bound states permit non-zero atomic, molecular or ionic magnetic dipole moments. However, in the absence of an applied magnetic field, these magnetic dipole moments are free to orientate themselves at random subject to thermal agitation and so the substance as a whole has no net magnetization. Only under the application of an applied magnetic field do the individual magnetic dipole moments tend to align themselves, and they do so parallel to the applied magnetic field. This corresponds to the lowest energy state (equation (2.14)). The susceptibility is, thus, positive and the paramagnetic volume susceptibility is typically $\chi_v \sim 10^{-3}$. The susceptibility is independent of the applied field but is dependent on the temperature. This latter point is hardly surprising since the degree of magnetic dipole moment alignment (and, hence, net magnetization) is subject to thermal agitation. The temperature-dependence of the susceptibility of many paramagnetic substances follows Curie's law which is given by

$$\chi_v = \frac{C}{T} \qquad 2.18$$

where C is the Curie constant and T is the absolute temperature. Interactions between the objects carrying the magnetic dipole moments can modify Curie's law to become

$$\chi_v = \frac{C}{T - \theta_w} \qquad 2.19$$

This is the Curie-Weiss law and θ_w is known as the Weiss constant and may be positive or negative but depends on the particular substance. Even though paramagnetic substances have a simultaneous occurrence of diamagnetism, the magnitude of the paramagnetic effect is so large in comparison that it completely masks the diamagnetic effect.

The most complex class of magnetic behaviour is known as *ferromagnetism*. (We also include in this class, because of their close relationship, *antiferromagnetism* and *ferrimagnetism*.) Below a certain temperature, substances in this class have their magnetic dipole moments spontaneously ordered even in the absence of an applied magnetic field. Hence, these substances can exhibit a non-zero magnetization in the absence of an applied magnetic field. This class of magnetic behaviour, because it is most relevant to this work, will now be discussed in more detail.

2.5 Microscopic Ferromagnetism

Magnetic ordering is a purely quantum mechanical effect and it cannot arise in classical physics. (The proof of this is known as van Leeuwen's theorem and is excellently discussed by Van Vleck (Van Vleck (1932), p94).) Fortunately, simple classical analogues can be used to describe most of the main concepts.

The characteristic feature of ferromagnetic substances is the spontaneous ordering of magnetic dipole moments even in the absence of an applied magnetic field. At zero kelvin (0 K) the alignment of all the moments in one direction is perfect.

As the temperature is increased above this, however, the ordering becomes increasingly destroyed by thermal agitation until a temperature is reached which is known as the Curie temperature, T_c, at which the ordering mechanism becomes inactive. Above the Curie temperature the substance behaves as a normal paramagnet and its volume susceptibility is given by the Curie-Weiss law (equation (2.17)) with the Weiss constant, θ_w, having a value very close to the Curie temperature, T_c. The best known examples of ferromagnets are the transition metals iron, cobalt and nickel. The Curie temperatures of these ferromagnetic elements (Fe 1043 K; Co 1388 K; Ni 627 K) are below their melting points and this explains why single phase liquid ferromagnets do not exist.

The origin of this spontaneous ordering will be explained. Historically, the first explanation was given by Weiss in 1907 (Weiss (1907)) and it invoked the presence of a strong internal magnetic field or 'molecular field' to account for the ordering. This field was assumed to be caused by interactions between the molecules. This theory was successful at explaining the temperature-dependence of the saturation magnetization (a quantity to be defined shortly) of the ferromagnetic transition elements but was incapable of describing magnetic behaviour close to the critical region (the Curie temperature) or of incorporating spin waves (elementary excitations of the atomic spins which occur at low temperatures). Still the detailed origin of the 'Weiss molecular field' was not clear. The problem essentially was that the magnitude of the magnetic field needed to be as large as $\sim 10^3$T to account for its effect and there was no obvious cause of so large a field.

The problem was solved by Heisenberg in 1928 (Heisenberg (1928)). Heisenberg, originally considering the case of hydrogen, showed that there is a coupling between unpaired spins of the electrons of two neighbouring atoms. This coupling, an 'exchange interaction', arises for purely quantum mechanical reasons. No classical analogy exists. The result is that, as a consequence of arguments based on Pauli's exclusion principle, if the two electrons have parallel spins they are mutually repelled and if they have antiparallel spins they are mutually attracted. Moreover, the energy associated with this interaction, the exchange energy, is electrostatic in origin. The energy of interaction of atoms i and j, $\mathrm{H}_{\mathrm{ex}}^{ij}$, where each atom has a spin quantum number $\mathbf{S}_i$ and $\mathbf{S}_j$ respectively, is proportional to the inner product, $\mathbf{S}_i \cdot \mathbf{S}_j$, and is given by

$$\mathrm{H}_{\mathrm{ex}}^{ij} = -2J_{ij}\,\mathbf{S}_i \cdot \mathbf{S}_j \qquad 2.20$$

J_{ij} is known as the exchange constant or the exchange integral and derives from the spatial wavefunctions of the i and j electrons. In the rigourous quantum mechanical treatment treatment $\mathrm{H}_{\mathrm{ex}}^{ij}$ is actually an operator and $\mathrm{H}_{\mathrm{ex}}^{ij}$ is just one part of the total Hamiltonian operator. The total exchange Hamiltonian for a solid comprised of many (N) atoms consists of the sum over all i and j $(i \neq j)$, or

$$\mathrm{H}_{\mathrm{ex}} = -2 \sum_{\substack{i=1 \\ i \neq j}}^{N} \sum_{\substack{j=1 \\ j \neq i}}^{N} J_{ij}\,\mathbf{S}_i \cdot \mathbf{S}_j \qquad 2.21$$

This quantity, H_{ex}, is known as the Heisenberg Hamiltonian. (This operator, frequently simplified to include only nearby atoms in the summations, is often used as the starting point for more advanced treatments of ferromagnetism.) The most important quantity from equations (2.20) and (2.21) for our discussion is the exchange constant, J_{ij}. The exchange constant in principle can be either positive or

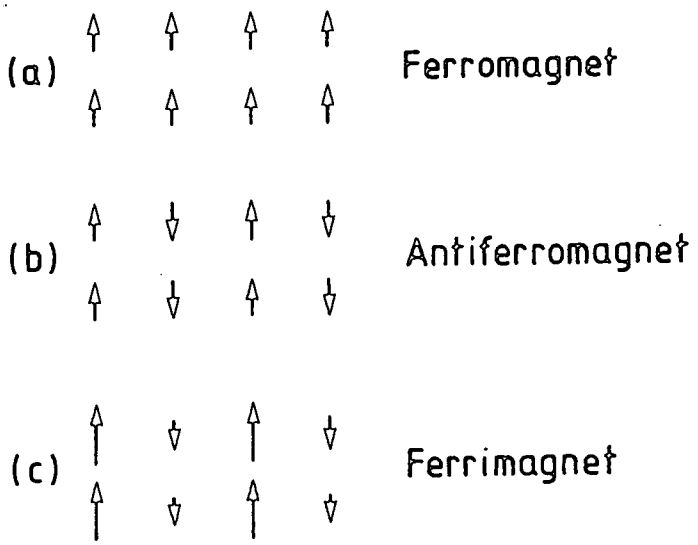

Figure 2.1 Schematic representation of the ordering of magnetic dipole moments for (*a*) ferromagnet, (*b*) antiferromagnet, (*c*) ferrimagnet.

negative. If J_{ij} is positive then the minimum in exchange energy occurs when $\mathbf{S}_i$ and $\mathbf{S}_j$ are parallel. If J_{ij} is negative the minimum occurs when $\mathbf{S}_i$ and $\mathbf{S}_j$ are antiparallel. A positive value of $-J_{ij}$ produces ferromagnetism and a negative value of J_{ij} produces antiferromagnetism or ferrimagnetism.

Thus, we have a basic explanation of ferromagnetic ordering. The occurrence of all the spins being mutually parallel corresponds to the spontaneous ordering of all the magnetic dipole moments. Antiferromagnetic and ferrimagnetic ordering involves the magnetic dipole moments on neighbouring sites being antiparallel. In antiferromagnetism there is an exact compensation between the magnitudes of oppositely-directed vectors and so the substance as a whole has no net magnetization. In ferrimagnetism the magnitudes of the neighbouring magnetic dipole moment vectors do not compensate exactly and so a net magnetization in one direction exists. The ordering of the moments for these three classes of magnetism is shown schematically in figure 2.1.

Whilst the exchange interaction provides the basis of an explanation of magnetic ordering, the treatment given above constitutes something of an over-simplification. The exchange interaction described above is only one type of exchange interaction, namely *direct exchange*. Other more complicated mechanisms also exist. *Superexchange* occurs when neighbouring magnetic atoms/ions are separated by a non-magnetic atom/ion. The electrons of the non-magnetic atom/ion mediate an exchange interaction between the two magnetic atoms/ions which is of larger magnitude than their direct exchange interaction. Superexchange is responsible for the magnetic ordering in ferrites. *Indirect exchange* is present in rare earth metals and involves the coupling of neighbouring electrons in the partially filled $f-$shells via their interactions with the conduction electrons. *Itinerant exchange* is the main exchange mechanism for metals and this mechanism refers to an exchange interaction between the conduction electrons. It is an itinerant exchange interaction which is responsible for the ferromagnetism of the three ferromagnetic transition metals. For most metals in general and the three ferromagnetic transition metals in particular an exchange interaction based on localized magnetic dipole moments,

for example direct exchange, is inappropriate. In the case of the transition metals this is because the $3d$ electrons which, loosely speaking, provide the magnetic dipole moments are non-localized and move quite freely in bands throughout the metal. Further details of the theory of itinerant electron magnetism will not be discussed here. The main purpose of our discussion has been to give a brief idea of the phenomena without giving unnecessary detail.

2.6 Macroscopic Ferromagnetism

This section is concerned with the characteristic manifestations of microscopic ferromagnetic ordering which are present on the macroscopic scale. Here 'macroscopic' is to be understood to refer to length scales at which it is possible to treat atomic properties such as atomic spins and atomic dipole moments at discrete lattice sites as producing quantities which are continuous functions of position. These length scales, however, may still be rather small (maybe ~ 100Å).

Above the Curie temperature ferromagnets behave as paramagnets in their magnetic properties. Below the Curie temperature, however, they are drastically different. Magnetizations having values many orders of magnitude greater than those of paramagnets at the same applied magnetic field are produced. In addition to this the magnetization varies non-linearly with the applied magnetic field in a complicated fashion. The characteristic plot of this behaviour is shown in figure 2.2.

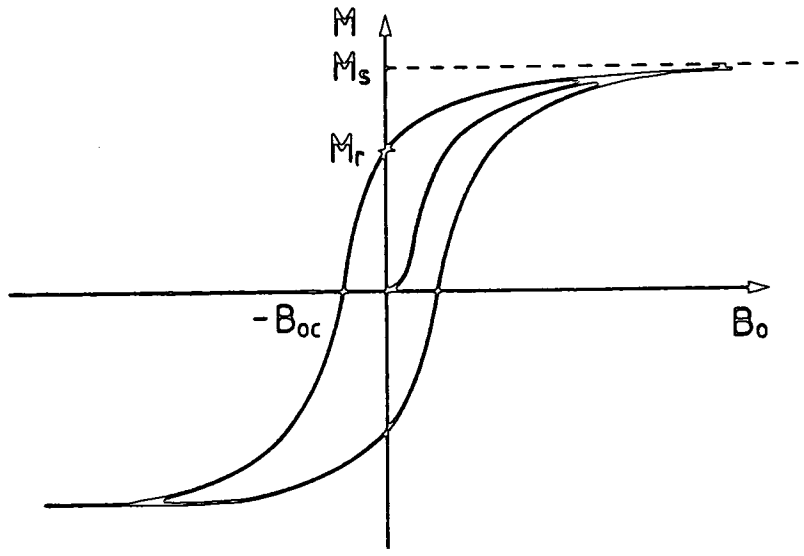

Figure 2.2 The magnetization curve showing the saturation magnetization, M_s, the remanence, M_r, and the coercivity, $-B_{0c}$.

From figure 2.2 it can be seen that if the substance starts from an initially unmagnetized state in zero applied field (that is, at the origin) and then the magnetic field is gradually increased then the magnetization, M, also increases. This first part of the magnetization curve is the virgin curve or the initial magnetization curve. For very small applied magnetic fields the magnetization in this part of the curve is reversible and a gradual reduction of the field back to zero moves the magnetization back exactly along the curve to the origin. If the applied magnetic field continues to increase then the magnetization also increases until it reaches a stage where the rate of increase with field is drastically reduced. This region of the magnetization curve is known as the saturation region. In this region, as the field

continues to increase, the magnetization asymptotically approaches a fixed value of the magnetization, M_s, which is defined as the saturation magnetization and which is the magnetization value which would be measured in an infinite applied magnetic field. (Incidentally, practical estimates of M_s are obtained by plotting the values of M in the saturation region against $1/B_0$ and extrapolating the resulting curve back to the line $(1/B_0) = 0$.) If the applied magnetic field is now reduced the magnetization does not retrace its original path once it has left the saturation region. Instead it passes through the M-axis at a finite positive value of the magnetization which is defined as the remanence, M_r. The remanence corresponds to the previously mentioned common characteristic of a ferromagnet of being capable of exhibiting a non-zero magnetization even in the absence of an applied magnetic field. Upon the application of a reverse magnetic field the magnetization falls and becomes zero at a value of the applied field which is defined as the coercivity or the coercive force, $-B_{0c}$. The coercivity is the reverse applied field which is required to reduce the magnetization to zero from positive saturation. Further increase in the reverse applied field results in negative saturation of the magnetization, approaching the value $-M_s$. Reduction of the reverse field back to zero moves the magnetization back to the negative remanence, $-M_r$. Reapplication of the positive applied magnetic field moves the magnetization back through zero at the positive coercivity and back up to the positive saturation value. The main feature of the whole magnetization or hysteresis curve is that the change in the magnetization always lags behind the change in the applied magnetic field. The form of the whole magnetization curve and the three important parameters, M_s, M_r and $-B_{0c}$ are characteristic of a given specimen.

2.7 Magnetic Domains

The form of the magnetization curve and, in particular, the occurrence of hysteresis will now be explained. The observed behaviour arises from the existence of magnetic domains. These domains reflect the way in which regions of spontaneous magnetization are distributed throughout the ferromagnetic body. Domains are small regions typically of volume $\sim 10^{-3}$ mm^3 to ~ 1 mm^3 or larger in single crystals, each one having its own spontaneous magnetization, the direction of which is not necessarily the same in each region. The existence of such domains was first postulated by Weiss (Weiss (1907)).

In the initially unmagnetized bulk specimen the directions of magnetization of all the domains are distributed so that the specimen as a whole has no net magnetization. This state corresponds to the origin on the magnetization curve plot. It is important to be clear that magnetization *is* present, specifically, in the domains, but the domains are arranged such that throughout the whole specimen the bulk magnetization is zero. When a magnetic field is applied domains having magnetization directions parallel or nearly parallel to the field direction grow in volume at the expense of other domains having magnetizations oriented in other directions. In low fields corresponding to the first part of the initial magnetization curve these domain changes are small and reversible. At higher fields, however, the domain changes are larger and irreversible. Above the knee of the magnetization curve the domain changes are rotations of the magnetization directions within whole domains into the applied field direction. These rotations are energetically 'hard' processes and this accounts for the reduction in the gradient of the magnetization curve approaching the saturation region. In the saturation region itself one single domain exists throughout the whole specimen and this domain's magnetization is

parallel to the applied magnetic field. When the applied field is reduced from the value which produces saturation of the magnetization the domain structure does not change or 'relax' much. It requires the application of reverse fields to reduce the magnetization significantly. This accounts for the occurrence of the remanence and also of hysteresis.

The nature of domain walls or boundaries, the objects which move as domains grow, was first elucidated by Bloch (Bloch (1932)). Domain walls are not abrupt, discontinuous changes in the direction of magnetization between two different regions. Rather, they are of finite thickness and are made up through their thickness of a number of atoms, the directions of whose magnetic dipole moment vectors change gradually through the wall. The formation of a domain wall requires energy since the directions of magnetization within neighbouring domains are different. Hence, for the whole system to achieve the most stable, minimum energy configuration the formation of a domain wall in the first place requires some offsetting benefit in terms of energy reduction by some other means. This idea is of crucial importance for the existence of fine single domain particles, where, although there is enough room in the particle for a domain wall to exist, other considerations make it energetically unfavourable to set up any domain walls at all. This will be treated in greater detail later.

The structure and detailed behaviour of ferromagnetic domains is a complicated theoretical problem involving all of the energy components—magnetostatic, magnetocrystalline, and magnetostrictive—of the system. Defects and impurities present in the specimen will also affect the structure and behaviour of the domains. Numerous references exist reporting the experimental observation of domain structure and behaviour by using a variety of techniques. Examples of different techniques can be found in Bitter (1931), Parpia, Tanner and Lord (1983), and Hetherington, Jakubovics, Szpunar and Tanner (1987). Excellent treatments of the whole subject of ferromagnetic domains are given by Kittel (1949) and Craik and Tebble (1965).

2.8 Magnetic Anisotropy

An understanding of macroscopic magnetization processes and domain behaviour also requires the concept of magnetic anisotropy. Magnetic anisotropy refers to the manner in which the energy of a magnetized specimen depends upon the direction in which it is magnetized.

Magnetocrystalline anisotropy is the term used when the anisotropy arises from the crystal structure of the material. Certain crystallographic directions in a material are directions in which the magnetization may be directed in a lower energy configuration than others. For this reason the terms 'hard' and 'easy' directions of magnetization are used. The magnetocrystalline anisotropy energy is at a minimum when the magnetization lies in an easy direction. In order to make the magnetization lie in a hard direction higher applied magnetic fields need to be applied in order to overcome anisotropy energy barriers. This concept is closely tied in to the explanation of the form of the magnetization curve in terms of domain behaviour at various applied fields. All of the irreversible domain movements occur at the larger applied magnetic fields when magnetocrystalline anisotropy energy barriers are more readily overcome.

Quantitively, magnetocrystalline anisotropy energy is usually treated phenomenologically. For the simplest case, uniaxial anisotropy, where there is only one easy

axis, the magnetocrystalline anisotropy energy density, U_{ua}, is written as

$$U_{ua} = \sum_n K_n \sin^{2n} \varphi \qquad 2.22$$

Here the K_n are constants known as the magnetocrystalline anisotropy constants and φ is the angle between the magnetization direction and the easy crystallographic axis. Odd powers of $\sin \varphi$ are absent because the series must be the same for either direction along the easy axis. Usually the first one or two terms of the series are sufficient to express the magnetocrystalline anisotropy energy density accurately. An example of a material exhibiting uniaxial magnetocrystalline anisotropy is hexagonal cobalt at room temperature. The easy axis is parallel to the c-axis, that is, along the hexagonal axis.

For the case of iron and nickel which have cubic crystal structures the magnetocrystalline anisotropy is not uniaxial but is more complex. In iron the easy directions are along the three cube edges and in nickel the easy directions are along the cube diagonals. In such cases the magnetocrystalline anisotropy energy density, U_{ca}, may be written as

$$U_{ca} = K_1(\alpha_1^2\alpha_2^2 + \alpha_2^2\alpha_3^2 + \alpha_3^2\alpha_1^2) + K_2\alpha_1^2\alpha_2^2\alpha_3^2 + \ldots \qquad 2.23$$

Here $\alpha_1, \alpha_2, \alpha_3$ are direction cosines between the magnetization direction and the three cube edges.

Another form of magnetic anisotropy is that which is known as magnetostriction or magneto-elastic strain anisotropy. This anisotropy arises from the change in the magnetization of a single crystal causing a change in the dimensions of the crystal. The fractional change in a dimension, l, given by $\delta l/l$, is typically very small ($\sim 10^{-5} - 10^{-6}$). The effect of the additional strain on the crystal is to provide an additional magnetic anisotropy to the extant magnetocrystalline anisotropy. The magnetostriction is closely related to the magnetocrystalline anisotropy in that the reason the crystal deforms in the first place is to minimise the magnetocrystalline anisotropy energy. The behaviour of domains in crystals is usually strongly affected by the local stresses caused by magnetostriction.

The final form of magnetic anisotropy of interest to us is shape anisotropy. The origin of this, as the name implies, lies in the bulk shape of the specimen. When the specimen is magnetized a demagnetizing field is produced which is directed antiparallel to the magnetization direction. The demagnetizing field arises from the non-uniformity of the magnetization within the specimen and/or a discontinuity of the normal component of the magnetization at the surface of the specimen. The magnitude and direction of the demagnetizing field depend on the magnitude of the magnetization and on the specimen geometry. For simple specimen shapes (for example, approximate ellipsoids and cylinders) the demagnetizing field, $(\mathbf{B}_0)_D$, is approximately proportional to the magnetization and can be expressed as

$$(\mathbf{B}_0)_D = -D'\mu_0\mathbf{M} \qquad 2.24$$

where D' is a dimensionless constant which depends on the specimen geometry and is called the demagnetizing factor. Only for uniformly magnetized bodies (that is, ellipsoids consisting of only one domain) does equation (2.24) hold exactly. Hence, an expression for the shape anisotropy energy density, U_{Da}, can be obtained as

$$U_{Da} = \tfrac{1}{2}D'\mu_0 M^2 \qquad 2.25$$

For a specimen shape which can be roughly approximated by an infinitely long narrow cylinder (for example, an acicular magnetic tape recording particle) D' tends to zero and so U_{Da} is minimized. Thus, in such a specimen shape, or in one that is only slightly elongated in one direction (for example, a prolate ellipsoid), the magnetization vector will preferentially lie along the long axis. This effect which is essentially magnetostatic in origin will have a strong influence on domain behaviour and structure. Domains will arrange themselves in a given specimen so as to minimize the total energy, one term of which is the shape-dependent shape anisotropy energy (equation (2.25)).

2.9 Antiferromagnetism and Ferrimagnetism

The two closely related topics of antiferromagnetism and ferrimagnetism were briefly mentioned earlier. The ferrimagnet magnetite (Fe_3O_4) is often used as the solid phase of magnetic ink systems. Hence, a brief treatment of antiferromagnetism and ferrimagnetism is relevant here. (The ferrimagnetism of magnetite will be discussed in slightly more detail in the next section.)

Antiferromagnetism is the term used to describe the type of magnetic ordering in which the magnetic dipole moments are arranged in a self-compensatory way as is shown in figure 2.1(b). The simplest antiferromagnets are ionic systems such as manganese oxide (MnO), manganese fluoride (MnF_2) and nickel oxide (NiO). In such systems itinerant magnetic effects are absent and the magnetic dipole moments can be treated as localized at discrete lattice sites (the metal ions). Since the non-metal ions separate the metal ions in the crystal the direct exchange interaction is severely weakened. However, in these simple antiferromagnets superexchange occurs with the non-metal ions mediating the exchange between the metal ions.

These simple antiferromagnets can be treated theoretically by viewing the crystal as composed of two sublattices, A and B (Néel (1948)). Each sublattice has its magnetic dipole moment vectors directed in opposite directions and the magnetic dipole moments of nearest neighbours is always antiparallel. Metal antiferromagnets such as manganese (Mn) and chromium (Cr) are not amenable to such theoretical treatment in terms of sublattices. These substances need to be understood in terms of an itinerant or band model. This will not be discussed here.

The antiferromagnetic and ferrimagnetic analogue of the Curie temperature, the critical temperature below which the ordering exists, is called the Néel temperature, T_N. Above T_N in both antiferromagnets and ferrimagnets the substances behave as paramagnets.

Ferrimagnetism is similar to antiferromagnetism except that the magnetizations of the two sublattices do not cancel and a spontaneous magnetization in one direction persists (figure 2.1(c)). The exchange interaction in these ionic ferrimagnets is again superexchange. The best known class of ferrimagnets is the ferrites and these are the only substances which will be treated here.

The ferrites are a family of oxides having the general formula AOB_2O_3. The A cation is divalent and the B cation is trivalent. Of most interest in magnetic applications are those ferrites with B = Fe, the iron oxide ferrites, $AOFe_2O_3$. Common examples of such ferrites are those where A is Fe, Co, Ni, Mn, or Mg. Mixed ferrites can also be manufactured by substituting for A two or more of the divalent metal ions. This permits one to tailor the magnetic properties to some extent.

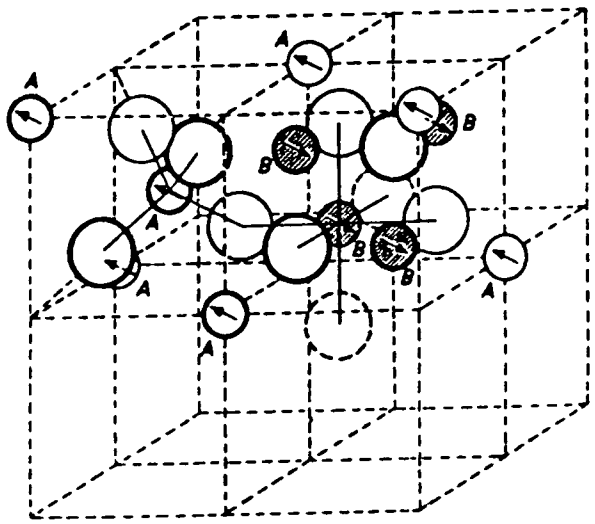

Figure 2.3 Two of the eight alternating octants in the spinel unit cell. The A and B site metal ions are in fourfold and six-fold coordination respectively with the oxygens (large circles). The oxygens are approximately half way along the body diagonals. The directions of the magnetic dipole moments for both the A and B site ions are shown and may be seen to be antiparallel (after Gorter (1955)).

The crystal structure assumed by iron oxide ferrites is called the spinel structure (from the mineral called spinel, $MgAl_2O_4$). The structure is complicated and is described with reference to figure 2.3 which shows the unit cell. The unit cell can be thought of as eight subunits (octants) consisting of two types arranged in alternating positions. Both types of octant contain four cations of type A in alternate corners and four oxygens about half way along the body diagonals. The left hand octant shown contains one type A cation at its centre in fourfold coordination with the oxygens. The right hand octant contains one B cation in the centre in six-fold coordination with the oxygens in addition to three other cations of type B. The whole structure is face-centred cubic (fcc) and contains thirty two oxygens. There are a possible sixty four A sites and thirty two B sites. However, these are not all occupied; only eight A sites and sixteen B sites are occupied. In the normal spinel structure eight A type cations occupy A sites and sixteen B type cations occupy B sites, giving the general formula $AO[B]_2O_3$. However, an inverse spinel structure also exists. Here eight of the B type cations occupy all of the A sites and the sixteen B sites are occupied by eight A and eight B sites, giving the general formula $BO[AB]O_3$. Spinels also exist having cation configurations intermediate between the normal and inverse structures.

In ferrimagnetic ferrites the A and B type cations correspond to the constituents of the two magnetic sublattices, the magnetic dipole moments of which are directed antiparallel. This is also shown in figure 2.3.

2.10 Magnetite

The rest of this part of the chapter will deal exclusively with some of the properties of magnetite. Magnetite has an inverse spinel crystal structure with the chemical formula $Fe^{3+}O[Fe^{2+}Fe^{3+}]O_3$ (Shull, Wallan and Koehler (1951)). The magnetocrystalline anisotropy is cubic, having [111] as the easy direction and [110] as the hard direction. The unit cell parameter is 8.395Å. The Néel temperature

is 847K (Pauthenet (1950)). The saturation magnetization at room temperaure is $\sim 4.71 \times 10^5 \mathrm{JT}^{-1}\mathrm{m}^{-3}$ ($\sim 90\mathrm{JT}^{-1}\mathrm{kg}^{-1}$) (Pauthenet (1950)). The first two magnetocrystalline anisotropy constants at room temperature are $K_1 = -1.35 \times 10^4 \mathrm{Jm}^{-3}$ and $K_2 = -0.44 \times 10^4 \mathrm{Jm}^{-3}$ (Banerjee and Moskowitz (1985)).

Below 118 K magnetite undergoes a structural phase transition (the Verwey transition (Verwey and Haayman (1941))) from cubic to orthorhombic. At roughly this transition temperature the first and second magnetocrystalline anisotropy constants change sign.

The most commonly found cation impurities in naturally occurring magnetite are Ti, Al, Mg and Mn (Banerjee and Moskowitz (1985)). The titanomagnetites ($Fe_{3-x}Ti_xO_4$) are important in rock magnetism (Metcalf and Fuller (1986)).

A close relation to magnetite and which in acicular particulate form has important technological applications in magnetic recording is the cation-deficient spinel, maghemite ($\gamma - Fe_2O_3$). The unit cell parameter of maghemite is 8.33Å, making it difficult to differentiate between magnetite and maghemite using X-ray techniques. Maghemite is metastable and after heating to temperatures above ~ 620 K decomposes to hematite ($\alpha - Fe_2O_3$) (Schieber (1967)).

This concludes the brief survey of most of the principle ideas of magnetism of relevance to this work. Most of the material which has been presented will be important in the second half of this chapter which deals with the magnetism of fine particles. However, the small size of these magnetic particles is of crucial importance in producing magnetic behaviour which is, in some respects, very different from that of the bulk material.

2.11 Fine Particle Magnetism

The field of fine particle magnetism is a large area of both pure and applied research. Its range encompasses, for example, magnetic liquids (ferrofluids), magnetic particulate recording media, paleomagnetism, permanent magnets, catalysis and magnetotactic microorganisms.

The most fundamental factor in the magnetic behaviour of magnetic fine particles is the particle size and the consequent domain structure within the particle. The basic idea is that, for less than a critical particle size, the lowest free energy of the particle corresponds to a state of uniform magnetization. Above this critical size a non-uniform magnetization state exists (Kittel (1949)). The uniformly magnetized particles are known as single domain (SD) particles (Morrish (1965), p340) and the non-uniformly magnetized, as multidomain (MD) particles (Bean and Jacobs (1960)). However, a third state is also identified which is intermediate between these two and which is known as the pseudo-single domain (PSD) state (Stacy and Banerjee (1974), p60, Moskowitz and Banerjee (1979)). The PSD state is characterized by particles which are of large enough size to have a MD structure, but which, nevertheless, behave more like SD particles. In particular, the coercivity and remanence of PSD particles is larger than for straightforward MD particles. The PSD state, thus, provides a gradual, rather than an abrupt change, in the magnetic properties as the particle size passes from the SD to the MD size.

Although the existence of a SD structure below a critical particle size was known of beforehand, the first realistic calculation of the critical particle size at which the transition occurs was given by Kittel (1949). Kittel first calculated the magneto-

static energy of a SD particle in zero applied field. He then calculated the total energies of configurations having postulated domain structures. In these cases, besides the magnetostatic energy, Kittel also included the exchange energy associated with the creation of domain walls. The creation of such walls increases the exchange energy in large particles, but the increase is offset by a reduction in magnetostatic energy, thus lowering the total energy. However, at a critical size the reduction in magnetostatic energy is insufficient to cancel out the increase in exchange energy from the creation of a wall. Hence, no domain wall is formed. The particle size at which this occurs is the SD transition size. Kittel calculated that for iron the SD transition occurs at a diameter of $\sim 0.02\mu$m. Most subsequent calculations have been essentially refinements of Kittel's method. More recent results for similar calculations in magnetite indicate that the PSD to SD transition occurs at diameters of $\sim 0.08 - 0.4\mu$m (Stacey and Banerjee (1974), Moskowitz and Banerjee (1979)). The PSD to MD transition occurs at a diameter of $\sim 8\mu$m (Moskowitz and Banerjee (1979)). The reasons for the uncertainties in some of these quoted values will be dealt with shortly.

Smaller-sized SD particles (typically $\sim 40 - 200$Å) exhibit superparamagnetism (SPM) (Bean and Livingston (1959)). Superparamagnetic particles are small SD ferro/ferrimagnetic particles for which the thermal energy (kT) is greater than the anisotropy energy barrier (shape and magnetocrystalline anisotropy in the main) which is preventing spontaneous reversal of the particle's magnetization. The result of this is that, within the time of the experiment, in the absence of an applied field, the thermal energy maintains a system of such particles in equilibrium with no net magnetization. The theory of SPM will be discussed in greater depth shortly.

2.12 The Field of Fine Particle Magnetism

A brief survey of the range of fine particle magnetism is given here.

Magnetic Liquids Magnetic liquids are stable lyophobic colloids of superparamagnetic ferro/ferrimagnetic particles (Rosensweig (1985)). Stability against aggregation is aided by surface treatment with surfactants. The solid phase has usually been magnetite (Rosensweig, Nestor and Timmins (1965), Kaiser and Miskolczy (1970)). However, more recently there has been some success in producing magnetic liquids containing metallic particles and magnetic 'alloy' particles (for example, Kilner, Hoon, Lambrick, Potton and Tanner (1984) and Lambrick, Mason, Hoon, Kilner and Chapman (1988)). These metallic systems have higher particle magnetizations than magnetite systems but oxidation currently remains a problem. Examples of applications in which magnetic fluids are used include rotating shaft seals and loudspeaker coils (Popplewell and Charles (1981)).

Magnetic Recording Media Contemporary particulate magnetic recording media employ acicular SD magnetic particles which are first dispersed in a non-magnetic polymer binder and then coated onto a flexible substrate. The acicular shape is desirable in order to optimise the coercivity (Wohlfarth (1981)). The most commonly used material has been maghemite, $\gamma - Fe_2O_3$. However, cobalt-modified iron oxides and metal particles have received attention more recently because of their promise of higher coercivities (Sharrock and Bodnar (1985)). In the case of metallic particles, these also promise better signal to noise characteristics because the smaller particle size permits a higher packing density.

Paleomagnetism Rock magnetism is of interest to geologists. The present day configurations of magnetic components of rocks provide insight into the past behaviour of the earth's geomagnetic field over several million years. This is because the rocks which were formed during past epochs have recorded faithfully the then prevailing geomagnetic field directions (Stacey and Banerjee (1974)).

Permanent Magnets One way of obtaining the high coercivities required in permanent magnets is to align SD particles (but not superparamagnetic particles) having high (usually shape and magnetocrystalline) anisotropy in a non-magnetic matrix. This anisotropy is usually achieved by using elongated particles (Jacobs and Luborsky (1957)). Such an arrangement suppresses the magnetization reversals necessary for demagnetization. This procedure has been particularly successful for Alnico, barium ferrite and samarium cobalt magnets.

Catalysts Fine magnetic particles play an important rôle in some chemical reactions, for example, superparamagnetic nickel particles in hydrogenation and dehydrogenation reactions (Potton, Daniell and Melville (1984)). The magnetic nature of these catalysts facilitates the determination of their function in the catalysis process since they are amenable to magnetic analysis techniques.

Magnetotactic Microorganisms The study of the rôle of biomineralization and magnetoreception in living organisms is a new but rapidly expanding area. This field studies the remarkable ability of some living organisms, for example, some bacteria (Mann (1985)), to biologically precipitate fine magnetite particles. The reasons why and the manner in which these organisms do this is not well understood.

2.13 Particle Size and Domain States

The overall magnetic properties of fine magnetic particles depend fundamentally on the particle size and the domain state. Coercivity and remanence variations with particle size are, thus, to be expected. The maximum coercivity occurs within the stable SD region. However, below this size range as the SPM region is approached the coercivity decreases and becomes zero at the SD-SPM transition. This is because the thermal fluctuation of the magnetization prevents any 'hardness' from persisting. For particle diameters greater than the SD size, that is, the PSD to the MD range of sizes, the coercivity decreases gradually. This is because the subdivision of the particle into domains renders it 'softer' (Banerjee and Moskowitz (1985), Kittel (1949), Morrish and Watt (1958)). A similar type of behaviour is found for the remanence. This has a maximum for the SD particle size range, but the peak is at a smaller particle size than for the coercivity (Kneller and Luborsky (1963)).

For SD prolate ellipsoids the coercivity mechanism can be well understood within the Stoner-Wohlfarth model (Stoner and Wohlfarth (1948)). This model minimises an individual particle's free energy in an applied field. The free energy has two components: the shape anisotropy energy and the magnetostatic energy from the applied field. (It turns out that it is not a serious omission not to include magnetocrystalline anisotropy energy and magnetoelastic strain anisotropy energy since these can both be treated in exactly the same manner as shape anisotropy and the results are essentially the same.) Values of the particle's magnetization in the direction of an applied field can be obtained and these successfully describe the qualitative features of the magnetization curve of an ensemble of such particles.

The coercivity mechanism of MD particles is a much more complex problem. This is because in real systems the response of domain walls to imposed fields is

very sensitive to particle-specific properties such as surface roughness, inclusions and particle shape. There is also frequent disagreement between experimental and theoretical estimates of the particle sizes at which the single domain/two domain and the two domain/three domain transitions occur (Stacey and Banerjee (1974), Moskowitz and Banerjee (1979)). In addition to this, there are complications about the detailed geometrical domain configuration assumed by particles in passing from the SD to the MD state. For example, Aharoni and Jakubovics have calculated that for small spheres of diameter ~ 250Å having cubic anisotropy a certain structure of cylindrical domains is a lower energy configuration than 'conventional' planar domains (Aharoni and Jakubovics (1988)).

2.14 Superparamagnetism

The term superparamagnetism, derived from the theory of classical Langevin paramagnetism, is used to describe the magnetic behaviour of an assembly of SD particles of such a small size that the thermal energy maintains the magnetization of each particle in an unstable state constantly fluctuating in a manner analogous to Brownian movement. If all the particles are the same size, then the magnetization of the assembly has a classical Langevin-type behaviour for the magnetization, M, given by (Bean and Livingston (1959))

$$M = \epsilon_v M_s \mathcal{L}\left(\frac{M_s V B_0}{kT}\right) \qquad 2.26a$$

with $\mathcal{L}$, the Langevin function, defined by

$$\mathcal{L}\left(\frac{M_s V B_0}{kT}\right) = \coth\left(\frac{M_s V B_0}{kT}\right) - \frac{kT}{M_s V B_0} \qquad 2.26b$$

Here M_s is the saturation magnetization of the particulate material, V is the particle volume, ϵ_v is the volumetric packing fraction of the magnetic material and B_0 is the applied magnetic field. Each particle has a magnetic moment $M_s V$ and each particle is magnetically saturated. The important difference between SPM and Langevin paramagnetism is that, in the former, the magnetic moment, $M_s V$, is typically more than 10^5 times larger than the single-spin magnetic moments associated with the latter. To describe real systems, equation (2.26a) must be modified to incorporate the invariably present particle size distribution of the assembly. Neglecting interparticle interactions, this modification is

$$M = \epsilon_v M_s \int_0^\infty \mathcal{L}\left(\frac{M_s V B_0}{kT}\right) n(V)\, dV \qquad 2.27$$

Here $n(V)$ is the distribution function of the particle volumes such that $n(V)\,dV$ is the number of particles having particle volumes between V and $V + dV$. (For magnetic liquids equation (2.27) is customarily expressed in terms of particle diameter rather than particle volume (for example, Chantrell, Popplewell and Charles (1978)).)

The customary definition of the critical particle volume, V_c, below which SPM occurs is (Bean and Livingston (1959))

$$V_c = 25\frac{kT}{K} \qquad 2.28$$

Here K is the anisotropy constant of the particle, the detailed origins of which are not important in the argument. The anisotropy energy barrier, KV_c, is the crucial factor in determining whether SPM occurs. For particles having volumes $V < V_c$ then the relaxation time, τ_N, of the particle magnetization vector in changing its orientation (Néel relaxation) is much less than the experimental measuring time. For particles having volumes $V > V_c$ the relaxation time is greater than the time of the experiment and the particle's magnetization is stable and is said to be 'blocked'. Thus, it is a characteristic of superparamagnetic systems that they attain thermal equilibrium within the experimental measuring time. The dependence of the relaxation time, τ_N on particle volume, in the absence of an applied field is (Néel (1949))

$$\tau_N = f_0^{-1} \exp\left(\frac{KV}{kT}\right) \qquad 2.29$$

where f_0 is approximately the Larmor precessional frequency of the magnetization vector and is of the order of 10^{-9}s^{-1}. This strong dependence of τ_N on particle size can be demonstrated by observing that an increase in particle diameter from 500Å to 740Å can change τ_N by a factor of 10^{17} (Banerjee and Moskowitz (1985)). In an assembly of particles 'frozen' into a solid configuration Néel relaxation is the only magnetization reversal process which can occur. However, in magnetic liquids at room temperature, a Brownian relaxation which involves the rotation of the whole particle can additionally occur and will predominate if its relaxation time is shorter. In an applied field, equation (2.29) is modified to become

$$\tau_N = f_0^{-1} \exp\left[\frac{KV}{kT}\left(1 - \frac{B_0}{B_{0k}}\right)^2\right] \qquad 2.30$$

where B_{0k} is the anisotropy field, $2K/M_s$.

2.15 Magnetic Viscosity in Fine Magnetic Particles

Magnetic viscosity, or time-dependent magnetization, is observed in magnetic fine particle systems. If the system is composed of particles all of the same size and whose magnetizations can only relax by one process which has a characteristic time τ, then the time-dependence of the magnetization, $M(t)$, behaves as (Street and Woolley (1949))

$$M(t) = A + C \exp\left(-\frac{t}{\tau}\right) \qquad 2.31$$

where A and C are constants. For a Néel relaxation process τ is given by equation (2.29). If some other magnetic relaxation process occurs, for example, individual domain wall jumps between pinning centres, then τ is still given by an equation of the same form as equation (2.29), but now V refers to the volume of the domain wall jump (Wohlfarth (1984)). However, for systems in which there is not one simple relaxation time, τ, but rather a distribution of such relaxation times arising from a distribution of anisotropy energy barriers, then equation (2.31) is not valid. In such cases $M(t)$ depends on the precise form of the distribution of τ. In many systems a relation of the form

$$M(t) = A - S \ln t \qquad 2.32$$

is frequently observed during a part of the measuring time (O'Grady, Chantrell, Popplewell and Charles (1981), Cayless, Hoon, Tanner, Chantrell and Kilner (1983),

O'Grady and Chantrell (1986)). It is generally argued that the '$\ln t$' behaviour arises from a summation of exponentials of the form of equation (2.31), with all of the summands incorporating all of the relevant relaxation times, τ, arising from the distribution of volumes. It is important to be clear that equation (2.32) is an approximation which is only valid for certain distributions of τ (Wohlfarth 1984). Equation (2.32) is clearly inappropriate for very small and for very large t. However, it is approximately applicable in certain ranges of t to describe a demagnetizing magnetic viscosity process in magnetic liquids, rock magnetism and spin glasses. Furthermore, '$\ln t$' behaviour has also been shown to emerge naturally from a very general theory of a spectrum of relaxation processes distributed in activation energy (Gibbs, Evetts and Leake (1983)). In equation (2.32), $S(= -dM/d\ln t)$ is called the coefficient of magnetic viscosity.

Deviations from simple '$\ln t$' behaviour have been reported. Chantrell, Hoon and Tanner (1983) have found in a Co magnetic liquid that, whilst '$\ln t$' behaviour was observed for small t, a t^{-1} behaviour was observed for $t > 250$s. Dunlop has reported a decay which is faster than $\ln t$ in a dispersion of 0.04μm magnetite particles (Dunlop (1984)).

Studies of the field-dependence of the coefficient of magnetic viscosity made by first saturating the sample in a positive saturation field and then reducing the field to a small (less than the anisotropy field) positive or negative field have shown that the maximum of S occurs in the field region very close to the negative coercivity (O'Grady, Chantrell, Popplewell and Charles (1981), Kloepper, Finkelstein and Braunstein (1984), Oseroff, Clark, Schultz and Shtrikman (1985), Chantrell, Fearon and Wohlfarth (1986)).

The temperature-dependence of the coefficient of magnetic viscosity has been investigated by Oseroff, Clark, Schultz and Shtrikman (1984) in particulate recording media. The maximum of the coefficient of magnetic viscosity exhibited a linear temperature-dependence which, surprisingly, did not extrapolate to zero at 0K. This surprising result has been explained as arising from dipolar interactions (Chantrell, Fearon and Wohlfarth (1986)). Finally, O'Grady and Chantrell (1986), in investigating a Co magnetic liquid, have found that the variation of S as a function of temperature, for their sample, displayed a maximum at $\sim$ 110K.

2.16 Conclusion

This chapter has given a brief survey of most of the important concepts in magnetism of broad relevance to this thesis. Particular emphasis has been placed on a review of fine particle magnetism because of its importance to this work. The next chapter will deal with MPI in particular. That chapter will also review flux leakage at defects.

Chapter 3

Magnetic Particle Inspection and Flux Leakage at Defects

3.1 Introduction

This chapter is devided broadly into two parts. The first part gives a review of the subject of magnetic particle inspection. This concentrates specifically on the practical aspects of MPI as a NDT technique and then goes on to review the important contributions to the extant literature concerned with magnetic inks and powders. In order to fully understand the behaviour of magnetic inks and powders during the MPI indication-formation process an understanding of magnetic leakage fields at defects is also required. Hence, the second part of the chapter gives a review of the various approaches which have been used to try to understand in detail the behaviour of leakage fields at defects, particularly with regard to their dependence both on the defect parameters and the magnetic properties of the test specimen. (In this context 'defect parameters' refers specifically to the length, width, depth and orientation of a defect.)

3.2 The Technique of MPI

The use of the MPI technique of flaw detection, since it was first developed practically about sixty years ago, has steadily increased. Today it is one of the most widely used NDT techniques for ferrous materials. Its sustained popularity is undoubtedly due to its relatively low cost and to its reliability.

The MPI technique is capable of detecting flaws or other discontinuities in the surfaces or near to the surfaces of ferromagnetic materials. The sensitivity of the technique diminishes as the distance of the flaw from the surface increases. Because the technique requires the test specimen to be magnetized, MPI can only be used on ferromagnetic materials. There are essentially two variants of the MPI technique in common usage in Europe. Both involve the application of fine ferro/ferrimagnetic particles to the region of the magnetized specimen which is under test. In one technique, the dry powder method, as the name implies, the particles are sprinkled over the surface of the test specimen in the form of a dry powder. In the second technique, the particles are suspended in a suitable carrier liquid, constituting a magnetic ink, and the suspension is applied to the surface of the test specimen.

The most commonly used materials constituting the particles are iron and magnetite (Fe_3O_4). Particle diameters are typically in the range $0.1-20\mu$m. The carrier liquids are most commonly paraffin or water. Oil is also sometimes used. When water is used, in order to wet the test specimen surface, water conditioners have to be added. In Britain a British Standard, BS 4069 (1982), specifies in detail the requirements for some of the properties of magnetic inks and powders. The requirements of the MPI testing method itself are covered by another British Standard, BS 6072 (1981).

3.3 Aids to Improved Sensitivity

Two separate methods are commonly employed to increase the sensitivity of the MPI technique. One of these which is used when the particles are darkly coloured is the use of thin coats of white contrast paints. Prior to the application of the magnetic ink or powder the test specimen is coated with a thin layer ($\sim 25\mu$m) of white contrast paint. During the test the visibility of the delineation of the flaws by the particles is enhanced by the contrast of the darkly coloured particles against the white background. Another British Standard, BS 5044 (1973), provides a specification for the properties and use of contrast aid paints. The other commonly used technique employed to improve sensitivity is the use of fluorescent particles. The fluorescent particles are coated with a pigment which fluoresces in ultraviolet radiation (wavelengths $400 - 315$nm) ('black light'). The test is conducted under 'black light' illumination and the enhanced visibility of the fluorescing particles which delineate the defect line effectively improves the sensitivity of the test. Because of the presence of the fluorescent pigment bound onto the particle, fluorescent inks and powders generally have larger median particle sizes than their non-fluorescent counterparts, although the size of the magnetic component in both types of particles may be essentially the same. The British Standard for the specification of the viewing conditions used in conjunction with fluorescent magnetic inks and powders is BS 4489 (1984).

3.4 Magnetizing Methods

The practical means of magnetizing the test specimen can be divided into two separate classes. These are current flow methods and magnetic flow methods. Magnetic flow methods involve the magnetizing of the test specimen by the application of permanent magnets or electromagnets. The region of the specimen under test becomes part of the magnetic circuit. Current flow methods achieve magnetization of the test specimen either by passing current directly through the region under test or by passing current through cables immediately adjacent to the test region. As well as dc magnetization methods, ac and half-wave rectified magnetization methods are also used. From empirical evidence these latter two methods are claimed to improve the sensitivity of the MPI method over and above the sensitivity obtained using dc methods alone (Raine (1988)). Much confusion has existed over the relative merits of the various magnetizing methods. Recently Edwards (Edwards (1986)), in an extensive investigation of the various methods, has shed some important light on the issue.

The British Standard BS 6072 (1981) is quite specific about the magnetizing level required for the test specimen. It states that the MPI method must be carried out with a magnetic flux density of at least 0.72T. It also states that for most engineering steels, which have relative permeabilities greater than 240, then this condition is satisfied if the applied field is 2.4kAm^{-1}.

3.5 Magnetic Inks and Powders

Most of the published literature on MPI has concerned itself with specific problems related to the practice of the method, for example, the geometry of the test piece (Betz (1967)) or magnetization methods (Lumb and Winship (1977)). Little has dealt with the underlying physics of the method or with the properties of the particles themselves. The important contributions to what little published literature there is will be reviewed in this section.

Betz (Betz (1967)) was the first to consider the properties of the particles themselves and their rôle in the successful use of the MPI technique. However, this treatment of the particles specifically was not very detailed and was essentially a statement of the particle properties expected to be influential in the successful use of the MPI technique.

Shelikhov and Aleksandrov (Shelikhov and Aleksandrov (1977)) were the first to give a detailed consideration to the question of how the coagulation of particles in a magnetic ink can affect the sensitivity of the method. By using optical microscopy these authors studied in detail the coagulation of particles in applied magnetic fields. This work showed that larger particles acted as 'nucleation centres' (my inverted commas) for the smaller ones and large chains were formed during the field-induced aggregation process. The largest aggregates, however, did not remain suspended but rather quickly fell to the bottom, leaving only finer chains suspended. Finally, these authors stressed the undesirability of using a magnetic ink containing very large aggregates, arguing both that their size and lack of mobility would make them insensitive even to coarse defects and that their presence would obscure the indications of finer flaws revealed by the finer particles.

The first important analysis of the effect of particle shape in relation to the MPI technique was given by Swartzendruber (Swartzendruber (1979)). Swartzendruber, in considering all of the various forces acting on MPI particles during the indication formation process, drew attention to the relationship between the shape of the particle and the magnetic force on the particle from the leakage field gradient. (All of these various forces acting on the particles during the indication formation process are discussed in Chapter 5.) Swartzendruber showed that the shape-dependent demagnetizing factor, D', of an individual particle affects the effective volume susceptibility of that particle. For particles having intrinsic volume susceptibilities very much greater than 1, then the effective volume susceptibility is essentially $(D')^{-1}$. Since the leakage field gradient force is proportional to the magnetization of the particle, M, in order to enhance this force it is desirable to have as large an effective volume susceptibility as possible, or, in other words, as low a particle demagnetizing factor as possible. The demagnetizing factor along the long axis of an elongated particle decreases with the degree of elongation. Using this argument, Swartzendruber drew attention to the desirability of using particles elongated in one direction in magnetic inks and powders. (This relationship between the demagnetizing factor and the intrinsic and effective volume susceptibilities is of importance in Chapter 7 and is treated in more detail there.)

The effect of the particle volume susceptibility was also discussed by Stadhaus (Stadhaus (1979)) who asserted that the leakage field magnetic force was proportional to the volume susceptibility. Stadhaus also claimed that the width of an indication is proportional to the particle volume susceptibility and inversely proportional to the particle density. The argument and this particular conclusion of that author are of doubtful veracity to say the least. Stadhaus did, however, include in his analysis the effects of the particle size on the MPI technique. Stadhaus performed tests which showed that the mean particle size of a magnetic powder is not important to the detectability of an indication provided that the mean particle size is considerably less than the crack width. Thus, the detectability is less when the mean particle size is too large for a given flaw. The conclusion was that, in a given test, the mean particle size should be chosen in accordance with the particular test problem.

The interrelation of the various properties of magnetic inks and powders in relation to their capabability to perform their function in the MPI method was stressed by Lovejoy (Lovejoy (1980)). Lovejoy provided no evidence for the details of some of his assertions and some of his arguments are of doubtful value, but his statement that, for overall success of the method, the importance of no one particle property can be evaluated in isolation from the others is a valid contribution.

Blakely, Simkin and Brown (Blakely, Simkin and Brown (1985)) considered the tangential leakage field magnetic force acting on a single MPI particle. Although their analysis is somewhat simplified because it neglects the normal component of the leakage field gradient which, via the particle volume susceptibility, would be expected to affect the magnetization of the particle, they identified the importance of the two specifically particle-dependent properties, the volume and the relative permeability (which is approximately equal to the volume susceptibility). Their analysis is essentially in agreement with this author's work in Chapters 5 and 7 and also with Edwards and Palmer (1986).

Although Edwards and Palmers' work did not deal with intrinsic particle properties, it will be mentioned here as it constitutes a very important contribution to the field. Apart from their contribution to the analytical approach to modelling the behaviour of the magnetic leakage fields of surface-breaking cracks which will be dealt with later in this chapter, they also considered some aspects of the behaviour of spherical MPI particles in such leakage fields. They obtained expressions for the leakage field magnetic force components on a spherical permeable MPI particle in which the leakage field gradient terms are given by the derivatives of their analytical expressions for the leakage fields. These authors then looked at the behaviour of these force components as a function of tangential displacement from the defect and showed that the maxima in the tangential force components occur near the lip of the defect. The analytical expressions for the force components enabled the rôle of gravitational forces in the indication formation process to be evaluated. Edwards and Palmer argued that, in order for an indication to be visible, the magnetic force must be greater than the gravitational force. By such a consideration of both the magnetic and the gravitational forces, Edwards and Palmer were able to estimate the magnetizing fields required to detect defects of various depths in test specimens having various relative permeabilities. One of the main conclusions from the model was that the magnetizing field specified by the British Standard, BS 6072 (1981), is adaquate for the detection of very fine cracks (widths$\sim$ 1μm) and that much lower levels of field could be used in higher permeability steels.

Whilst this review is not comprehensive, it has covered most of the important contributions to the literature that are concerned with intrinsic particle properties in magnetic inks and powders. The paucity of the published material is evident, as is the need for more work in this area. The next section deals with a very important topic in MPI but one which has not suffered the same neglect as has the investigation of the properties of the particles themselves.

3.6 Magnetic Leakage Fields at Defects

In non-rigorous and simple terms, the reason why physical discontinuities at or near to the surface of magnetized ferromagnetic specimens produce magnetic leakage fields adjacent to the discontinuity is not difficult to understand. Flaws and defects within the magnetized specimen have a relative permeability very much less than that of the test specimen itself. Hence, these objects constitute obstacles in the

magnetic circuit of which the test specimen is a component. The lines of magnetic flux density within the sample are, consequently, diverted around the discontinuity and 'squeezed' together so that the magnetic flux density increases locally. The increase in flux density constitutes the magnetic leakage field. This is represented schematically in figure 3.1.

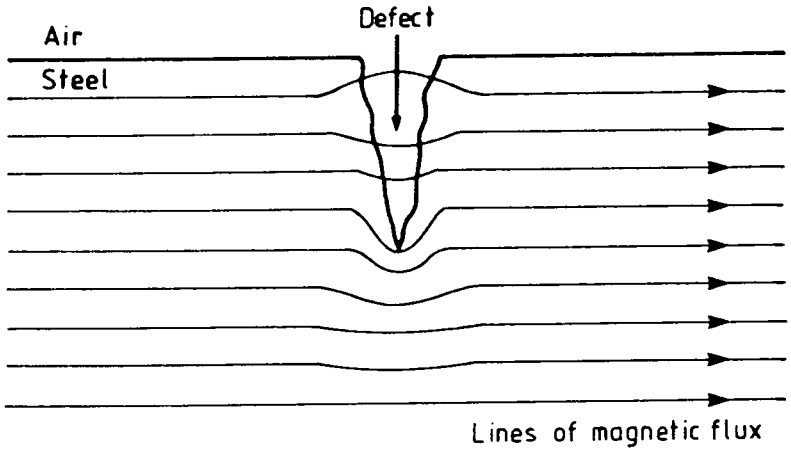

3.1 Schematic representation of the passage of lines of magnetic flux encountering a discontinuity.

Surface-breaking and slightly sub-surface defects, irrespective of the precise details of their shape, orientation and dimensions, all produce leakage field components which share common characteristic features. These are illustrated in figure 3.2. Figure 3.2*a* shows the defect in 2D, in this case a surface-breaking defect, and the x, y coordinate system used. The direction of the magnetizing field, H_0, is also shown. Figures 3.2*b*, 3.2*c* and 3.2*d* show, respectively, the x component of the leakage flux density, the y component of the leakage flux density and the total leakage flux density, $(\sqrt{B_{0x}^2 + B_{0y}^2})$, all as a function of x, on a line of constant y.

The detailed form of the curves shown in figure 3.2, for example, the location of the maximum and minimum of curve 3.2*c*, depends upon the defect parameters and the test specimen magnetic properties. The important feature is that the B_{0y} curve changes sign on either side of the defect, whilst the B_{0x} and the total leakage flux density curves do not.

Given that the leakage flux density components behave as is shown in figure 3.2, the task of all magnetic leakage flux methods of NDT is, firstly, to detect them and, secondly, having a knowledge of the specimen magnetic properties and the magnetizing conditions, to infer from them the defect parameters.

Historically, there have been two separate approaches to the study of the dependence of the magnetic leakage fields on the defect parameters and on the specimen magnetic properties. The first of these which we will discuss are a class of approaches which seek to obtain the leakage flux configuration by approximate numerical methods. These approaches are the finite element (FE) and the finite difference (FD) methods. The second class of methods of tackling the problem seeks to obtain analytical solutions for the leakage fields by approximating the defects by relatively simple geometrical shapes, and in the process rendering the analysis soluble. These

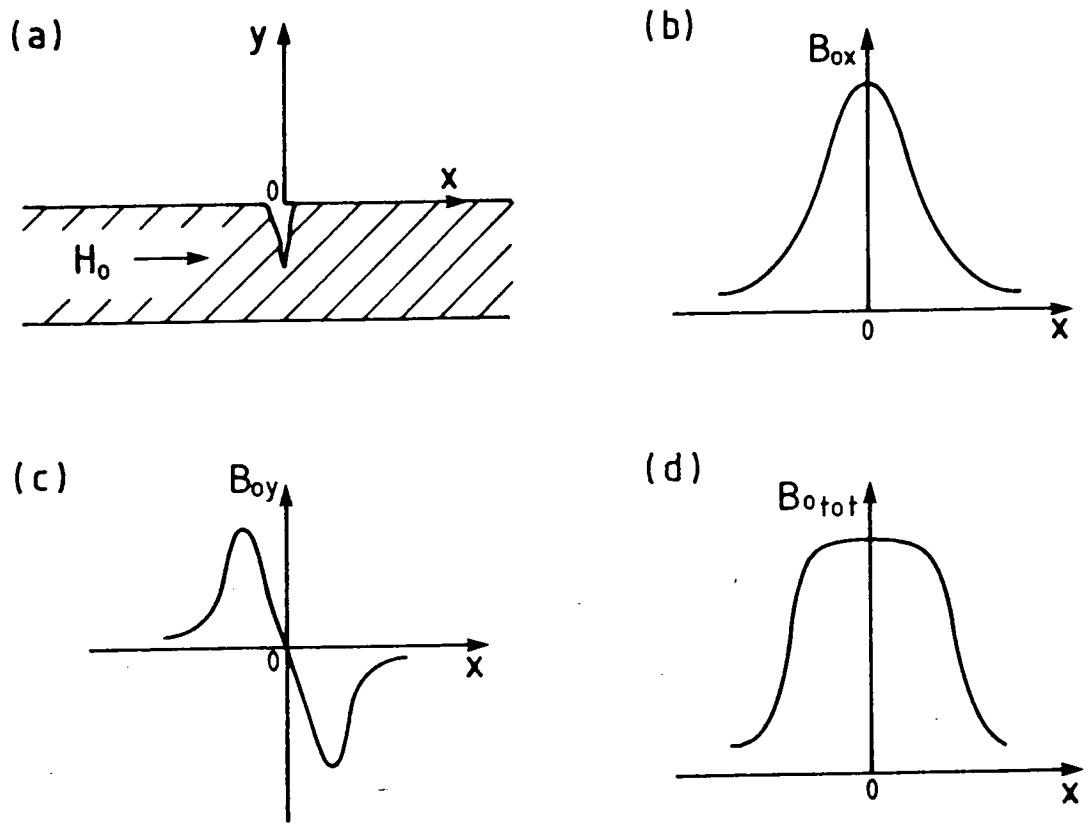

Figure 3.2 The characteristic features of the behaviour of the leakage flux density. The coordinate system is defined in (*a*). The x and y components are shown in (*b*) and (*c*) respectively. The total leakage flux density is shown in (*d*).

will be dealt with in turn.

3.7 Numerical Approximation Methods

The FE method is a very powerful tool for the determination of magnetic leakage flux densities. It is currently the most widely used method of tackling the problem and its application to electromagnetic problems, as well as to other engineering fields, is currently a very active area of research. Its biggest drawback is that, for it to be used properly, it currently demands large computing resources. Its offsetting benefits, however, are that it is capable of calculating the field distributions within structures having complex boundary geometries and nonlinear $B-H$ characteristics (non-constant relative permeability). It can, therefore, be used to model real defects more accurately than the analytical approach.

The basic idea of the FE method is to subdivide the field region into subdomains or finite elements. The field in each element is then approximated by a limited number of parameters. This approximation is usually made in terms of polynomials ('shape functions'). For a more detailed treatment of the FE method in magnetostatic problems the reader is referred to Zienkiewicz (1980).

In its specific application to NDT flux leakage problems the procedure is usually, by a process of iteration, to minimise the energy over an element using variational calculus until the process converges to stable expressions in terms of shape functions for the magnetic vector potential, **A**, in that particular element. Knowing **A** in

each element, it is then a trivial task to obtain $\mathbf{B_0}$ in each element from the relation $\mathbf{B_0} = \nabla \times \mathbf{A}$. This process is exactly the same as approximately solving Maxwell's Equations to determine $\mathbf{B_0}$ for the whole field region.

The first authors to use this method in the field of NDT flux leakage were Hwang and Lord (Hwang and Lord (1975)). These workers obtained the magnetic flux density distribution from an infinitely long ferromagnetic round bar which had an infinitely long rectangular slot of finite width and depth along its length, which was also the direction in which the dc magnetizing current was flowing. The detailed results of this modelling are given in Lord and Hwang (1977). As an illustration of the manner in which the finite elements are arranged, figure 3.3 shows the FE mesh configurations used by Lord and Hwang (1977). These two authors found that for a constant slot depth there is a linear increase in the peak to peak distance of the normal (B_{0y}) component of the leakage flux density with slot width. They also found that for a constant slot width the peak to peak distance of the B_{0y} component increases with slot depth but not in a linear manner. Rather, the peak to peak distance of the B_{0y} component saturates with increasing slot depth. This initial work of Hwang and Lord was confined to 2D modelling. However, the technique has now been extended to 3D (Ida and Lord (1983)) and so can be used to model real systems. The main drawback with the extension of this approach from 2D to 3D is the huge increase in computing resources required (Lord (1983)).

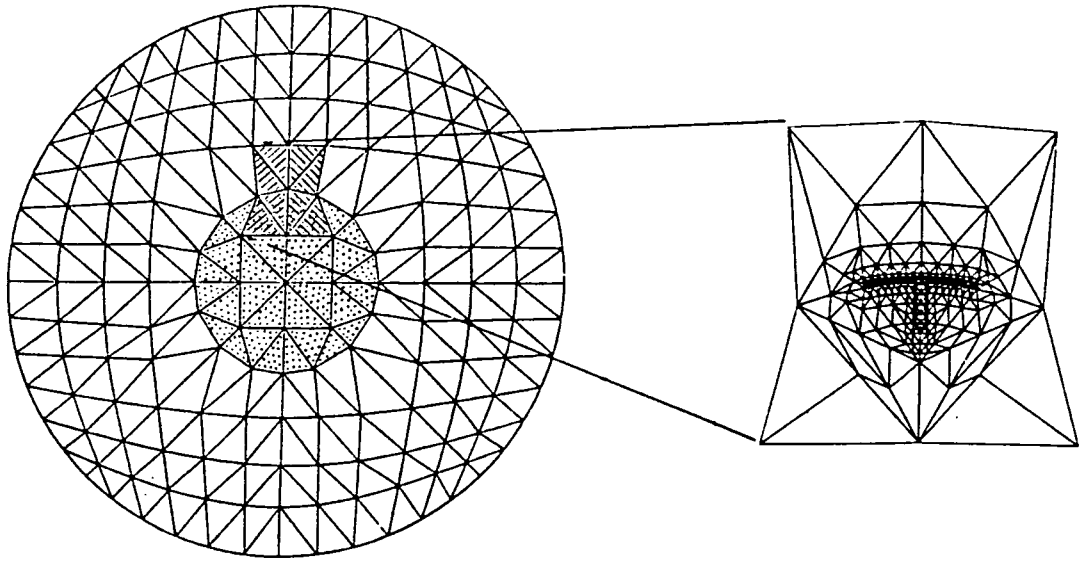

Figure 3.3 The mesh structure used by Lord and Hwang for the computation of the leakage field around a rectangular surface defect in a ferromagnetic bar magnetized in the direction perpendicular to the page. The left hand diagram shows the triangular mesh in and around the bar (the bar is shaded with dots). The right hand diagram shows an enlargement of the region of the defect. (After Lord and Hwang (1977))

The other main numerical method used for NDT flux leakage problems, the FD method, will now be discussed. This method requires less sophistication in both the mathematics and the computing resources it uses, but it is less widely applicable than the FE method. The application of the technique to electromagnetic problems

involves obtaining approximate solutions to Maxwell's Equations by subdividing the field region into a regular mesh and, at discrete points on the mesh, replacing the one partial differential equation which describes the whole magnetic flux density by many many finite difference equations, each one relevant to that particular point. The resulting set of equations are all linear and relate the potential at one point to that of its neighbouring points. Thus, the problem is reduced to a set of linear simultaneous equations (Binns and Lawrenson (1963), p251). The limitations of the method are that, in order to avoid drastically complicating the mathematical solution technique, regular meshes have to be used. This means that the discretization is less flexible than the FE method and cannot accommodate complex boundary geometries.

Brudar (Brudar (1985)) has used this method to investigate the leakage flux components at a rectangular slot in a ferromagnetic plate magnetized in the plane of the plate, perpendicular to the slot. Brudar found that for slots having depths which are less than ten times the width, the maximum value of the B_{0y} component is, to a very good approximation, proportional to the depth of the crack and is practically independent of the width. He also found that for slots having depths greater than ten times the width, the magnitudes of B_{0x} and B_{0y} become smaller and the relationship between the depth and the maximum value of B_{0y} is no longer simple. In this case the width affects the precise form of the relationship between the maximum B_{0y} value and the slot depth. It is this deviation from linearity, the saturation-type behaviour, which Lord and Hwang (1977) observed. Finally Brudar observed that the 'width' of the B_{0x} component depends on the width of the slot and not on the depth. Indeed, for wider slots the 'width' of the B_{0x} component is directly proportional to the slot width and for narrower slots the 'width' of the B_{0x} component appears to approach a certain limiting value which depends on the magnetizing field and the relative permeability of the material.

3.8 Analytical Methods

Analytical approaches to the determination of the leakage field configurations in NDT flux leakage problems are of limited value in modelling defects in realistic boundary geometries. However, their value lies in their rôle as simplified model systems which are, nevertheless, capable of providing valuable insight into what is going on in more realistic and complex systems.

Most workers in the field acknowledge the work of the two Russians, Zatsepin and Shcherbinin (Zatsepin and Shcherbinin (1966)), as being the first important contribution to the field. These two authors modelled a surface defect by a rectangular slot of infinite length in an infinite ferromagnetic half space. The direction of magnetization was parallel to the test specimen surface and perpendicular to the longitudinal direction of the slot. Provided that the depth of the slot is approximately equal to or greater than its width, these authors stated that the defect may be represented by a magnetic strip dipole in which a constant magnetic surface charge density, σ_s, is located on each face of the defect. In such a representation the distance between the two strips forming the dipole approximately equals the width of the defect and the depth of each strip approximates to the depth of the defect. Figure 3.4 shows the dimensions of the slot and the location of the magnetic surface charge density, σ_s. The cartesian coordinate system employed by Zatsepin and Shcherbinin is also shown. With the slot having a width of $2a$ and a depth of

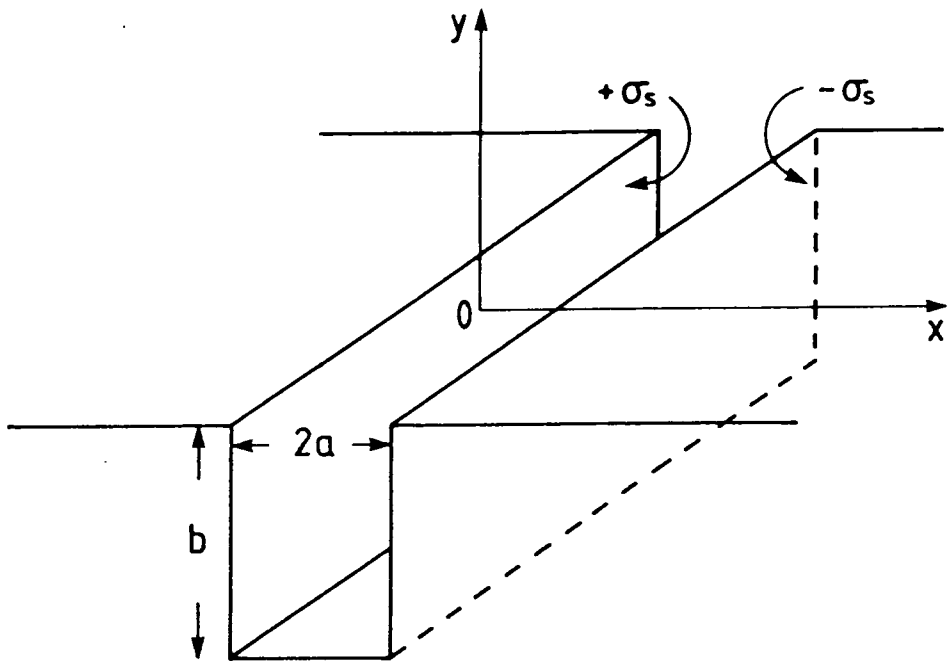

Figure 3.4 The infinite slot of depth b and width $2a$ used by Zatsepin and Shcherbinin as a model of a crack. The cartesian coordinate system relevant to equations (3.1a) and (3.1b) is also shown. σ_s is shown as located on the side faces of the slot.

b, Zatsepin and Shcherbinin obtained for the two leakage field components

$$B_{0x} = \frac{\mu_0 \sigma_s}{2\pi}\left[\tan^{-1}\frac{b(x+a)}{(x+a)^2+y(y+b)} - \tan^{-1}\frac{b(x-a)}{(x-a)^2+y(y+b)}\right] \qquad 3.1a$$

$$B_{0y} = \frac{\mu_0 \sigma_s}{4\pi}\ln\left(\frac{\left[(x+a)^2+(y+b)^2\right]\left[(x-a)^2+y^2\right]}{\left[(x+a)^2+y^2\right]\left[(x-a)^2+(y+b)^2\right]}\right) \qquad 3.1b$$

In these equations the origin of the coordinate system is at the mid line of the slot, coplanar with the test specimen surface. The notation has also been changed and SI units have been employed. In the original derivation, Zatsepin and Shcherbinin provided no justification for the assumption of a constant surface charge density. Another limitation was that the relationship between the surface charge density, σ_s, and both the magnetizing field, H_0, and the specimen relative permeability, μ_r, was not established.

Shcherbinin and Zatsepin went on to show that their expressions gave reasonable qualitative agreement with experimentally measured leakage flux components (figure 3.5) (Shcherbinin and Zatsepin (1966)). In this comparison between theory and experiment σ_s was necessarily an adjustable parameter. The work of Zatsepin and Shcherbinin has more recently been subject to criticism by Dobmann and Höller (Dobmann and Höller (1980)) who argued that Zatsepin and Shcherbinins' work does not even provide qualitative agreement in the comparison of the theoretical and experimental behaviour of residual leakage field components (that is after an active source of magnetization has been removed), the specific purpose for which originally Zatsepin and Shcherbinin recommended their analysis. Dobmann and

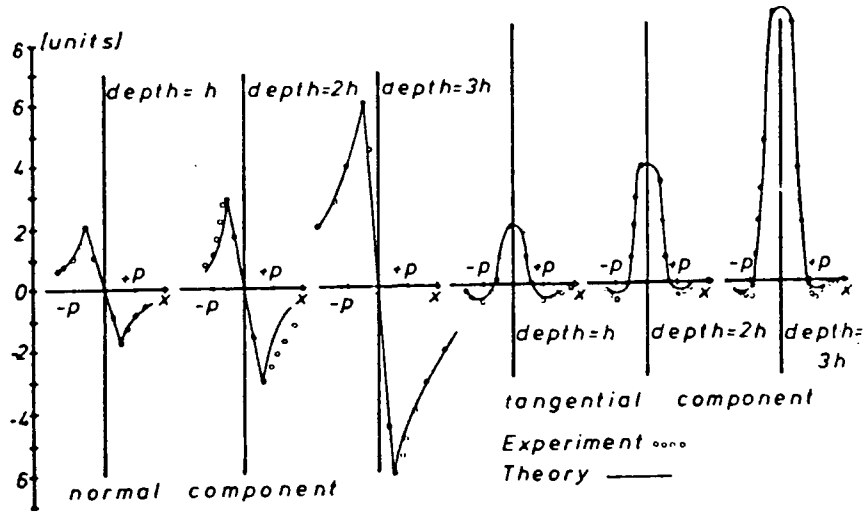

Figure 3.5 Shcherbinin and Zatsepins' comparison of experimentally measured x and y components of the leakage field with the theory given by equations (3.1a) and (3.1b). (After Dobmann and Höller (1980))

Höller also drew attention to the problem of the singular behaviour of the B_{0y} equation (equation (3.1b)) at $(x = \pm a, y = 0)$. In spite of these shortcomings, Zatsepin and Shcherbinins' work was an encouraging first attempt.

This original infinite strip dipole model was extended by Shcherbinin and Pashagin (Shcherbinin and Pashagin (1972)) to slots of finite length. Experimental data presented by Shcherbinin and Pashagin showed that for slots of constant width and depth, but varying length, at a constant magnetizing field the maximum value of the B_{0y} component was strongly dependent on the slot length. The maximum value of the B_{0y} component increased with slot length at a constant magnetizing field. These workers found also that the maximum value of the B_{0x} component showed nonlinear behaviour.

The outstanding problem of establishing the relationship between the magnetic surface charge density, σ_s, the magnetizing field, H_0, and the specimen relative permeability, μ_r, which had not been tackled by Zatsepin, Shcherbinin or Pashagin, was finally solved by Edwards and Palmer in 1986 (Edwards and Palmer (1986)). Edwards and Palmer represented a surface-breaking crack by a semi-elliptical slot of semi-minor axis (half width) a and semi-major axis (depth) b (figure 3.6). By solving Laplace's equation for a general ellipsoidal cavity in a ferromagnetic medium, these authors determined the magnetic surface charge density on the slot. σ_s was obtained as

$$\sigma_s = H_0 \frac{\pi n(\mu_r - 1)}{(n + \mu_r)\tan^{-1} n} \qquad 3.2$$

where H_0 is the magnetizing field, μ_r is the constant relative permeability of the test specimen and $n(= b/a)$ is the aspect ratio of the semi-elliptical defect. Edwards and Palmer obtained for their leakage field components exactly the same expressions as Zatsepin and Shcherbinin, but with σ_s given by equation (3.2). Thus, Edwards and

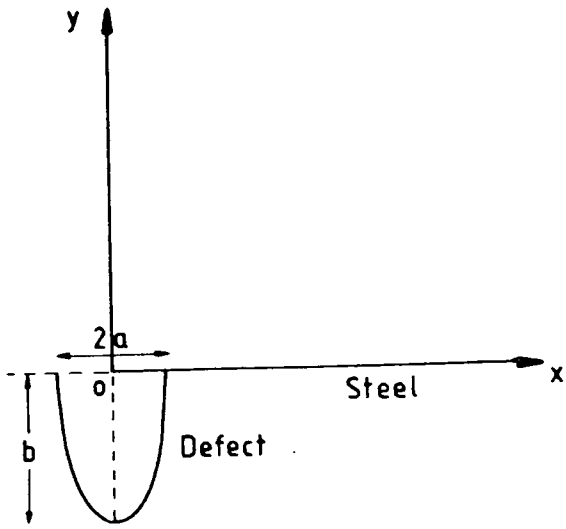

Figure 3.6 The semi-elliptical surface breaking slot used by Edwards and Palmer as a model of a surface-breaking crack. The width of the crack is $2a$ and the depth is b. The origin of the cartesian coordinate system is at the intersection of the major and minor axes.

Palmers' equations, using the coordinate system shown in figure 3.6, are

$$B_{0x} = \frac{\mu_0 H_0 n(\mu_r - 1)}{2(n + \mu_r)\tan^{-1} n}\left[\tan^{-1}\frac{b(x+a)}{(x+a)^2 + y(y+b)} - \tan^{-1}\frac{b(x-a)}{(x-a)^2 + y(y+b)}\right] \qquad 3.3a$$

$$B_{0y} = \frac{\mu_0 H_0 n(\mu_r - 1)}{4(n + \mu_r)\tan^{-1} n}\ln\left(\frac{\left[(x+a)^2 + (y+b)^2\right]\left[(x-a)^2 + y^2\right]}{\left[(x+a)^2 + y^2\right]\left[(x-a)^2 + (y+b)^2\right]}\right) \qquad 3.3b$$

Edwards and Palmer also derived the z component of the leakage field. However, they demonstrated that, provided the slot is at least twenty times as long as it is deep, then at the middle of the length of the slot, the B_{0x} and B_{0y} leakage field components are essentially the same as for a slot of infinite length, as represented by equations (3.3a) and (3.3b).

For the case $\mu_r \gg n$, equations (3.3a) and (3.3b) reveal an approximately linear relationship, at constant slot width, between the leakage field components and the slot depth. This relationship is in broad agreement with the work of Hwang and Lord and with Brudar. For real defects where n and μ_r are typically of the same order, the equations show that the leakage field components increase with μ_r, at constant H_0. Even if the test specimen is already saturated, there exists a linear relationship between the leakage field components and H_0. Edwards and Palmer went on to show that their model gave, for the B_{0y} component, excellent agreement with experimentally measured values from rectangular slots. Figure 3.7 shows the comparison between theory and experiment for several slots. The main limitation

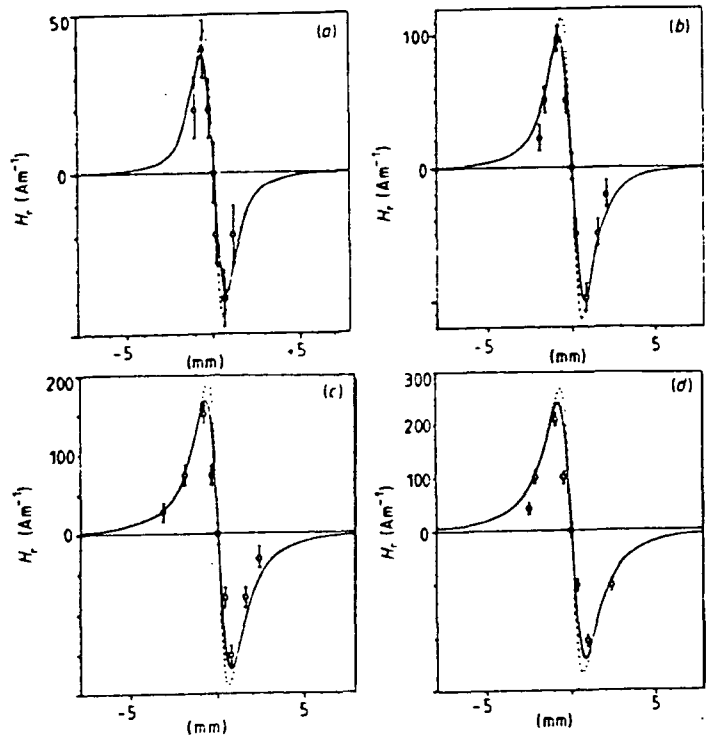

Figure 3.7 The comparison by Edwards and Palmer of experimental and measured values of the y component of the flux leakage at several rectangular slots. (Edwards and Palmer , in contrast to this work, use H rather than B_0.) The dotted lines represent the theory of equations (3.3a) and (3.3b). The full line is the same theory when averaged over the area of the Hall effect probe which was used to make the measurements. The small circles represent the experimental points. (After Edwards and Palmer (1986))

of Edwards and Palmers' model is the treatment of the relative permeability as a constant.

3.9 Summary

The latter part of this chapter has given a brief review of the main features of the behaviour of leakage field components at defects, studied by a variety of methods. It shows that there is at least a broad 'consensus' about the main details of the behaviour, although some details may vary. It is shown that the advantages of numerical approximation methods over analytical methods are that they permit the modelling of 'realistic' systems (complex boundary geometries and variable relative permeability). However, they generally require large computing resources and the simple functional relationships revealed by analytical methods are not as simply determined. Drawbacks associated with analytical models are that, currently, they do not incorporate non-constant relative permeabilities and only the simplest defect and specimen geometries are soluble.

Chapter 4

The Construction and Characterization of a 1.2T Electromagnet VSM

4.1 Introduction

This chapter gives some brief details of the construction and characterization of a 1.2T electromagnet double crank vibrating sample magnetometer (VSM). The design of this instrument is originally due to S.R. Hoon and S.N.M. Willcock and is reported elsewhere (Willcock (1985), Hoon and Willcock (1988*b*)). For this reason few details of the original design will be given here. Rather, the chapter will concentrate on specific details of the construction and characterization of this second Durham VSM. Exhaustive details and a discussion of these characterization experiments in relation to the existing literature will not be given. Again, the reason for this is because such matters have been dealt with by Willcock (1985). The final part of the chapter briefly mentions some elements of the full automation of the instrument.

4.2 Vibrating Sample Magnetometry in General

Although relatively crude instruments based on the same principle of operation as the VSM were in use beforehand, the first person to describe the VSM, as we know it today, was Foner (Foner (1956, 1959)). The principle components of Foner's VSM are illustrated in figure 4.1.

Although Foner's original design has been subsequently much improved, figure 4.1 serves to illustrate the principle of operation. The sample is vibrated at a fixed frequency in the direction perpendicular to the magnetizing field direction. At a fixed frequency and a fixed amplitude, the field-dependent magnetic moment of the sample induces an ac voltage in the sample coils with an amplitude proportional to the magnetic moment. Thus, once the calibration of the instrument is known, the magnetic field-dependence of the sample magnetic moment (and, hence, magnetization) can be determined.

In practice the calibration is usually achieved either by measuring the signal from a constant current sample coil of known magnetic moment or from a knowledge of the saturation moment of a high-purity sphere of nickel. Since Foner, who first used the technique, it is also now common practice to use phase sensitive detection techniques to enhance the signal to noise ratio of the induced ac sample coil voltage. The reference signal for the phase sensitive detector (or lock-in amplifier) is usually taken from a permanent magnet or constant current coil attached to the sample rod (but well removed from the sample detection coils) vibrating at the same frequency as the sample and inducing an in-phase signal in a nearby second coil system.

Since Foner's original design, little has changed in the design or basic principle of operation of VSMs. Most of the subsequent advances have dealt with such matters as details of the orientation and positioning of the detection coils with respect to the sample (for example, Smith (1956), Mallinson (1966), Bowden (1972), Guy (1976*a*,*b*), Nagata, Fujita, Ebisu and Taniguchi (1987), Hoon (1988)), or with

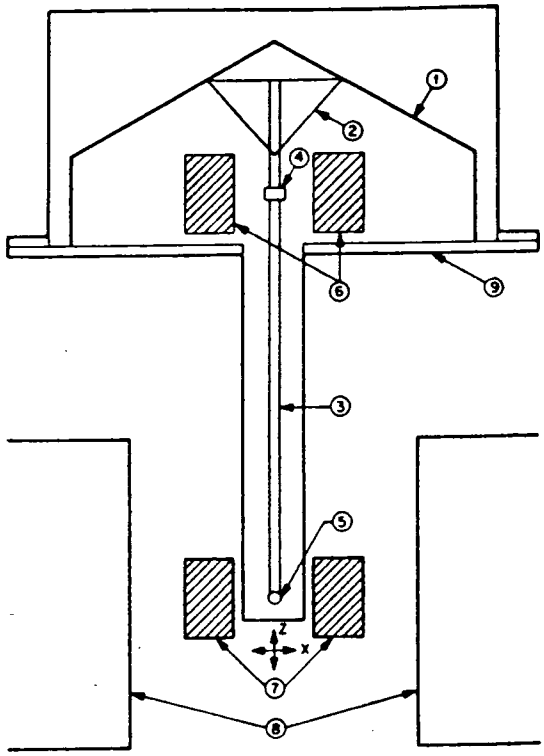

Figure 4.1 The principle elements of Foner's VSM. (1) loudspeaker transducer. (2) conical paper cup support. (3) drinking straw. (4) reference sample. (5) sample. (6) reference coils. (7) sample coils. (8) magnet poles. (9) metal container. (After Foner (1959))

details of the transducers used to vibrate the sample (for example, Hoon (1983)), or with the processing of the induced signal (for example, Gerber, Burmester and Sellmyer (1982), Josephs, Crompton and Krafft (1987)). An exhaustive review of the literature subsequent to Foner has been given by Willcock (1985).

4.3 The Sample Vibration Transducer

The sample vibration transducer is based entirely upon the design of Hoon. Hoon's crank-driven VSM transducer is an improvement on previous mechanical transducer designs because of its excellent frequency and amplitude stability with low vibrational noise and high inertial loading. These stability and low noise characteristics are achieved by a careful balancing of the masses attached to the two crank pins which themselves are separated by 180° around the central webb. The crank is driven by a low noise hysteresis induction motor (240V, 50W) running at half supply frequency. The power supply to the motor is provided by a sine wave generator producing a signal of variable frequency which is amplified up to 240Vac by means of both a Quad 50E audio amplifier and a transformer. The reference signal for the lock-in amplifier is provided by a small cylindrical permanent magnet bonded onto an extension of the crank-driving motor shaft with the long axis of the magnet perpendicular to the shaft. This permanent magnet rotates adjacent to a single coil mounted in a screened can. The signal induced in this coil has the same frequency as the detection coil signal (although, in general, the phase is different).

4.4 The Detection Coil System

The detection coil system used for the VSM was the Mallinson coil system (Mallinson (1966)). This detection coil geometry was also used on the first Durham VSM. The reason for such a choice above other possible coil systems (for example, those of Bowden (1972) or Foner (1959)) is given by Willcock (1985). Because the pole tip dimensions of the second Durham VSM are identical to those of the first, the arguments originally given by Willcock and which were applicable to the first Durham VSM are also relevant to the second. Essentially the argument is that Bowden's geometry is unsuitable because, although it is the coil geometry least sensitive to errors arising from variations in sample positioning, the task of manufacturing, inductively balancing and positioning the eight identical coils in the Durham magnet would be so difficult as to be impractical. The Foner coil geometry was rejected because, within the constraints of the available magnet air-gap, a Mallinson system could produce a larger output than a Foner system. In addition to this, in a Mallinson coil system the presence of magnetic images in the electromagnet enhances the output, whilst it reduces the output in a Foner system. The main drawback of the Mallinson system, however, is that individual Mallinson coils are sensitive to fluctuations in the field of the electromagnet. This problem does not arise, however, if the four coils are inductively balanced. Hence, it is of crucial importance when using the Mallinson geometry to take care in producing a balanced set.

Since the commissioning of the second Durham VSM, Hoon has subsequently shown, by an analysis more sophisticated than that of Willcock, the improved sensitivity of the Mallinson geometry over the Foner geometry (Hoon (1988)). Hoon has devised a modelling technique which involves the replacement of the vibrating sample moment by an equivalent set of stationary oscillating current multipolar arrays. Such an approach greatly facilitates rigourous analysis of the sensitivity of VSM detection coil systems in general. Using this method, Hoon clearly demonstrated the sensitivity advantage of the Mallinson system over the Foner system.

The detection coils themselves were wound on tufnol formers of thickness 10mm and diameter $\sim$ 64mm. The formers were then mounted onto 1mm brass cheek plates which were rigidly clamped adjacent to the magnet pole tips. The exposed sides of each Mallinson pair were protected and screened by copper covers which were fastened onto the cheek plates. Each coil was wound with 16000 turns of swg 48 enamelled copper wire. All four coils were inductively balanced *in situ* in the cheek plates by removing individual turns from those with the largest inductances. The inductances were measured at 100Hz using a Wayne Kerr LCR bridge. This balancing was done so carefully that, within experimental error, each coil had exactly the same inductance. The inductance of each coil was 12.95 ± 0.04H. This represents an improvement by a factor of 15 on the coil system of the first Durham VSM.

With the coils in position at the magnet pole tips, experiments were then performed to determine details of the sensitivity function of the coil system. The sensitivity function, $G(\mathbf{r})$, describes the detection coil output as a function of the sample position and orientation and of the detection coil configuration (Zieba and Foner (1982)). In this instance $G(\mathbf{r})$ was experimentally determined along the three principle axes. The x, y, z axes are defined as follows. The x axis is parallel to the axis of the magnet, that is, parallel to the magnetic field. The z axis is the direction

in which the sample is vibrated. The y axis is mutually orthogonal to these two directions. The sensitivity function was mapped out along the x, y, z axes by moving a constant magnetic moment mounted in the sample position on the sample rod along these three axes. The constant moment was provided by a small single layer constant current coil. Movement of the moment in the z direction was achieved by changing the amount of air in the pneumatic isolation collar which is used to prevent the propagation of mechanical vibrations from the vibrating head to the detection coil system. Movement in the x and y directions was achieved using the x-y movement mechanism which is part of the original head support design (Willcock (1985)). Figure 4.2 shows the displacement-dependence of the output from the whole detection coil system along the three principle axes. All the curves are normalized to a value of 1V at the origin.

From the measured sensitivity function it was found that a 1% change in the coil system output signal occurs for displacements of $\pm$1.5mm, $\pm$2.7mm and $\pm$2.5mm in the x, y and z directions respectively. These measured x and z displacements are exactly the same as for the first Durham VSM, but the y displacement value is an improvement on the first Durham VSM by approximately 28%.

In order to investigate the linearity of the detection coil system the constant magnetic moment which was used for the determination of the sensitivity function was again employed. The output of the detection coil system was measured as a function of the size of the constant moment coil current as this coil was vibrated at the sample position. Over three orders of magnitude of the constant coil current the deviation from linearity was determined to be less than 0.19%. This value is derived from the maximum value of the percentage difference between any measured point and a straight line fit to the data. Figure 4.3 shows the data obtained in this measurement, together with the linear fit.

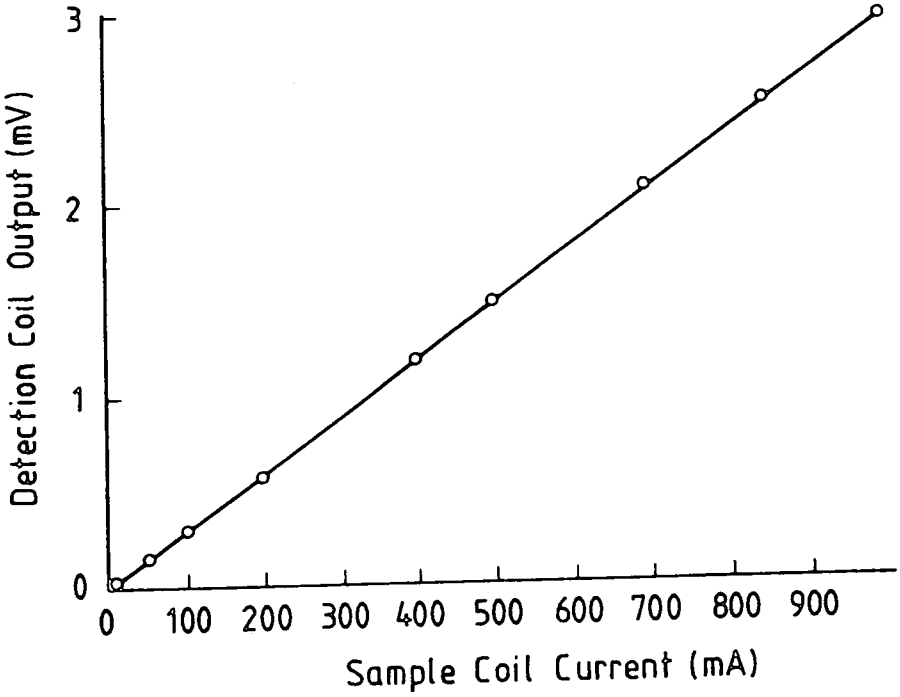

Figure 4.3 The linearity of the detection coil system. The graph shows the output from the detection coil system as a function of the constant moment current coil. Over a variation of three orders of magnitude of the current, deviations from linearity are less than 0.19%.

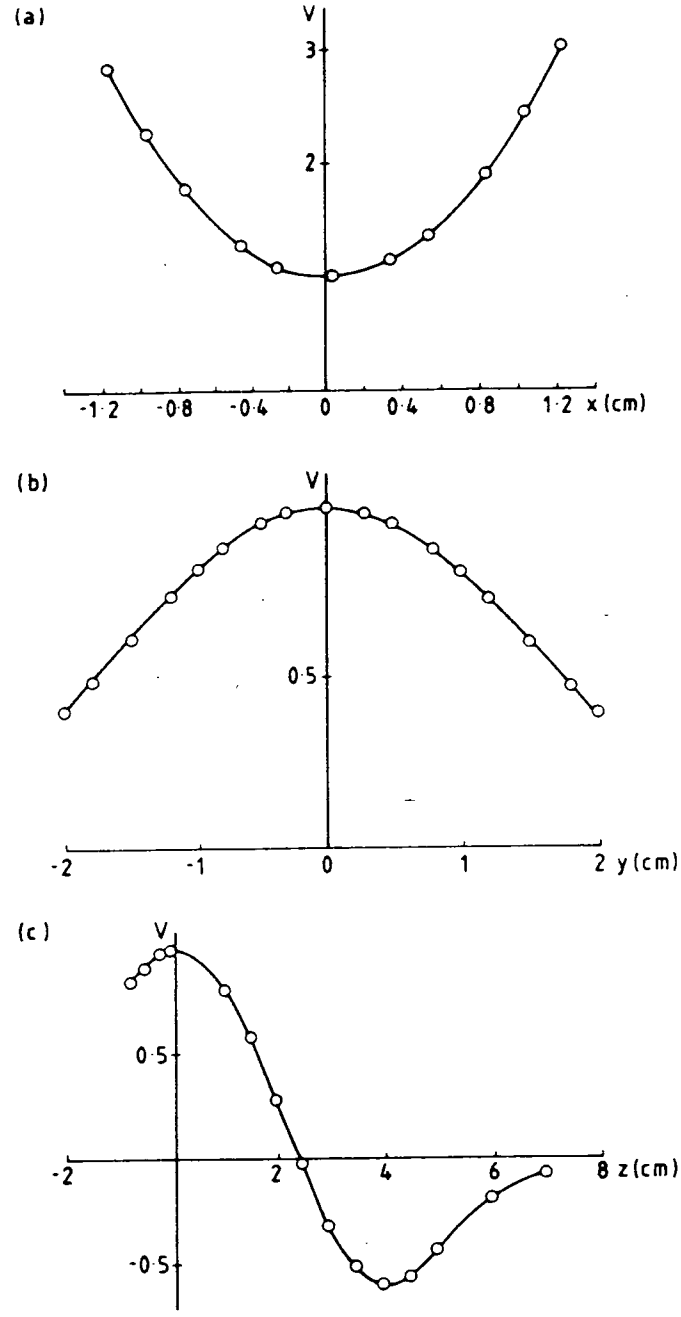

Figure 4.2 The detection coil system sensitivity function in the three principle coordinate directions. (*a*) x, (*b*) y and (*c*) z.

4.5 Field Uniformity

Over the full range of magnetic fields provided by the magnet (0 – 1.2T) the nonuniformity of the field within a 10mm radius sphere centred on the sample was found to be less than 0.38%. This value was determined by measuring the field at various positions within the 10mm sphere at field intervals spanning the full range of the magnet, facilitated by using a Hall effect probe attached to a travelling microscope which allowed accurate location of the probe in the x, y and z directions. Unfortunately this upper limit on the nonuniformity is about twice that of the first Durham VSM. There are two important consequences from measurements such as this. The first is that the 10mm radius sphere is larger than any sample likely to be

used on the VSM and so an upper limit on the spatial nonuniformity of the applied field is known. The second is that, since the field is measured by a Hall effect probe which is displaced from the sample, such nonuniformity details accurately provide information about the difference between the measured field and the field at the sample position.

4.6 Magnetic Image Experiments

Hoon and Willcock (1988*a*) have reported, for the first time, direct evidence for the existence of magnetic images in a VSM electromagnet. They found their images to have field-dependent changes of less than 0.2% over the full range of the magnet field. Since the second Durham VSM magnet is of the same type as the first Durham VSM magnet on which Hoon and Willcocks' experiments were performed, similar results would be expected in the second instrument. Such an exhaustive study as that by Hoon and Willcock was not repeated. Rather, the most important thing, and the only one which was investigated in the second Durham VSM, was to find out whether the images were significantly field-dependent.

In order to attempt to measure any image field-dependence, one part of the experiment of Hoon and Willcock was repeated. In detail, this involved using the same constant moment current coil as was used previously, but this time it was in order to determine the output of the detection coil system as a function of the magnet air-gap field. Because the sought-after field dependence may be very small, it is of the utmost importance to correct the sample moment for the diamagnetic signal produced by the coil material and holder. For a constant moment coil current the output of the coil system, as measured on the lock-in amplifier as a function of the magnet field, is given in Table 4.1.

Magnetic Field (T)	Current in Sample Coil (mA)	Lock-in Amplifier Signal (mV)
0	994.9(±0.1)	2.9283(±0.0030)
0.2009(±0.0005)	994.9(±0.1)	2.9295(±0.0030)
0.4009(±0.0010)	994.9(±0.1)	2.9255(±0.0030)
0.6087(±0.0020)	994.8(±0.1)	2.9255(±0.0030)
0.8030(±0.0020)	994.9(±0.1)	2.9245(±0.0030)
1.0020(±0.0020)	994.8(±0.1)	2.9250(±0.0030)
1.2010(±0.0020)	994.8(±0.1)	2.9280(±0.0030)

Table 4.1 The data obtained for the investigation of the field-dependence of the detection coil signal produced by a constant moment sample coil.

This data set indicates that over the magnetic field range $0 - 1.2$T the detection coil signal changes by $\sim 0.17\%$. This means that over the full range of the magnet field any field-dependence of the images produces changes less than or equal to 0.17%. Although this measured change may be caused by field-dependent images of the magnetic moment, it is impossible definitely to infer this from the precision of this experiment. Hence, this is an important null result which means that, within

the resolution of the detection coil signal measuring device (the lock-in amplifier), the images are not field-dependent. This change of less than 0.2% is in accord with Hoon and Willcock (1988*a*) and also with the work of Foner (1959) and Case and Harrington (1966). These latter two reports also referred to electromagnet VSMs. This result greatly simplifies the analysis of magnetization data obtained from the VSM. It means that the image moment contribution to the total detected signal changes in proportion to the 'real' moment signal. Had this simple relationship not existed and had the image signal been significantly field-dependent then the proportion of the image moment contribution to the total detected signal would be different at different fields and this field-dependence would have to be subtracted off prior to any meaningful analysis of the magnetization data.

4.7 Residual Noise

The procedure for residual noise subtraction from the sample data follows Willcock (1985). A least squares linear fit is fitted to the residual data enabling a subsequent subtraction of the residual signal from the sample signal. A typical residual noise data set is shown in figure 4.4. Such plots indicate that the minimum detectable moment is easily less than $10^{-9}\mathrm{JT}^{-1}$ which is more than an order of magnitude better than the first Durham VSM.

4.8 The Automation of the VSM

Full details of the general requirements for automation of VSM systems are given by Hoon and Willcock (1988*b*). In Hoon and Willcocks' approach, the controller (microcomputer), via an interdevice communication standard, is required to record the output from the lock-in amplifier and the gaussmeter and to control the ramping of the magnetic field.

On the second Durham VSM the original intention was to employ the parallel IEEE 488 interface bus standard as the interdevice communication. Although the controller, which was an Acorn BBC Model B Microcomputer and 6502 Second Processor, does not have a IEEE 488 interface fitted as standard, such an interface was provided by a CST Procyon IEEE Interface unit. This device is specially manufactured for BBC Microcomputers and operates through the 1MHz bus of the microcomputer. The Brookdeal 5206 lock-in amplifier supports the full IEEE 488 standard. The gaussmeter which is a LDJ 511rr (remote ranging) supports no interface, but its analogue output is read via a Fluke 8840A digital voltmeter which does possess the full IEEE 488 interface standard. The magnet current was controlled by a MINICAM† interface which is a modular system allowing various digital to analogue converters, stepper motor drivers, relay boards *etc.* to be incorporated and which supports the IEEE 488 standard. Unfortunately, however, the interfacing of the Brookdeal 5206 lock-in amplifier to the BBC microcomputer via the CST Procyon device proved problematical and could not be made to work reliably. Fortunately the Brookdeal 5206 also possesses a RS 232 serial interface which was used instead of the IEEE 488 interface to communicate directly with the microcomputer's RS 423 interface. Thus, by way of the two interface standards used, during the operation of the VSM, the microcomputer controls the whole system in a fully-automated manner.

The magnetic field control via the MINICAM interface is fully described by Willcock (1985) and is relevant to the second Durham VSM since exactly the same

† Manufactured by Bede Scientific Instruments, Durham, UK.

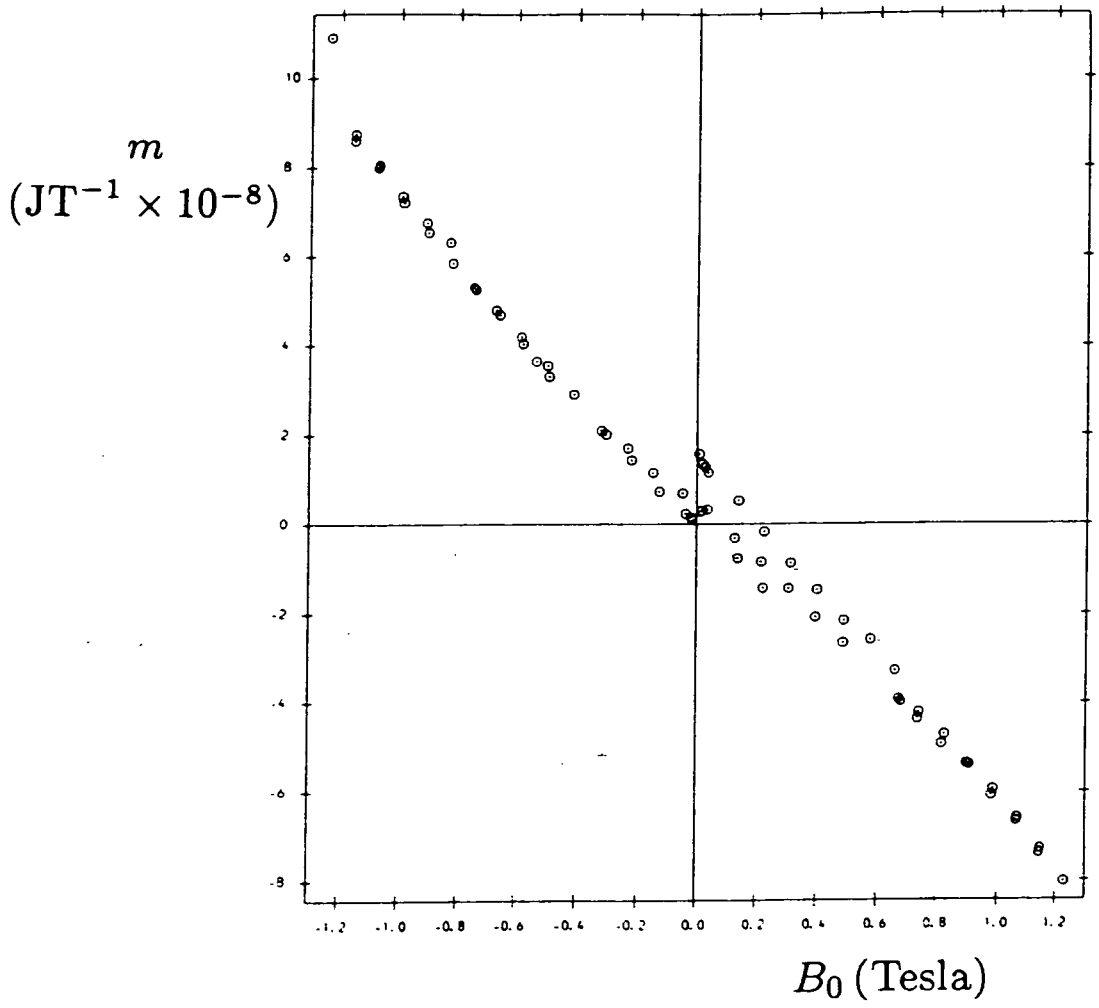

Figure 4.4 The diamagnetic residual/noise signal obtained from a DELRON sample holder.

type of power supply unit, a Newport Instruments C225 350V 30A control unit and generator, was employed. Willcock describes the conversion of this unit from a unipolar to a bipolar configuration and the necessary precautions to be considered and controlled via the MINICAM to ensure the safe reversal of the current supply to the magnet when the field changes sign. Additional hardware circuitry is also described which was added to the current control unit to prevent accidental reversal of the current at too high a current with a consequent large back emf in the magnet producing diversions of the sample under test from the magnetization curve and maybe even damaging the magnet. Following Willcock, the ramping of the current control unit is driven by a stepper-motor-controlled potentiometer via the MINICAM. This potentiometer is in parallel with a stabilized voltage source and is capable of producing a $0 - 10$V sweep corresponding to the $0 - 30$A output range of the magnet current.

One of the cards in the MINICAM crate is an 8 channel relay board. Three of the relays are used in the current control, but the other five are used to remotely autorange the gaussmeter. The range of the gaussmeter is selected by switching to

earth, via the relevant relay, one of five terminals on the gaussmeter, each one of which corresponds to a different range. This autoranging facility of the gaussmeter is not available on the first Durham VSM.

The operation of the VSM is controlled by a control program running on the microcomputer which is written in BBC BASIC. This software is user-friendly and is written as a structured set of procedures, thus enabling any user to modify it to their own particular requirements. The manner in which the software controls the instrument is based closely on the flow diagrams given by Willcock (1985) and Hoon and Willcock (1988*b*). At the start of the experiment the user is invited to enter the details of the experiment required and to set up the lock-in amplifier and gaussmeter. After this interaction the microcomputer takes over full control and conducts the experiment. When the data taking is complete the raw data set is saved on floppy disc. A suite of user-friendly data analysis programs has also been written to be used in the analysis of the data and to correct for sample demagnetizing effects and residual noise. Appendices P1 and P2 give listings of the complete VSM control program and the data analysis programs respectively.

4.9 Conclusions

Brief details of the construction, characterization and automation of the second Durham VSM have been given. There is a large area of overlap with details of the first Durham VSM and so this chapter has remained short. However, the main differences between the two Durham VSMs have been stressed and differences in details of the two characteristics have been given. Some subjects such as the calibration of the instrument have not been mentioned. This is because such topics have been treated by Willcock (1985) and his treatment is just as much relevant to the second Durham VSM as it was to the first.

Figure 4.5 gives some exemplary data obtained from the second Durham VSM. The figure shows the full magnetization curve for a polycrystalline nickel sphere at room temperature.

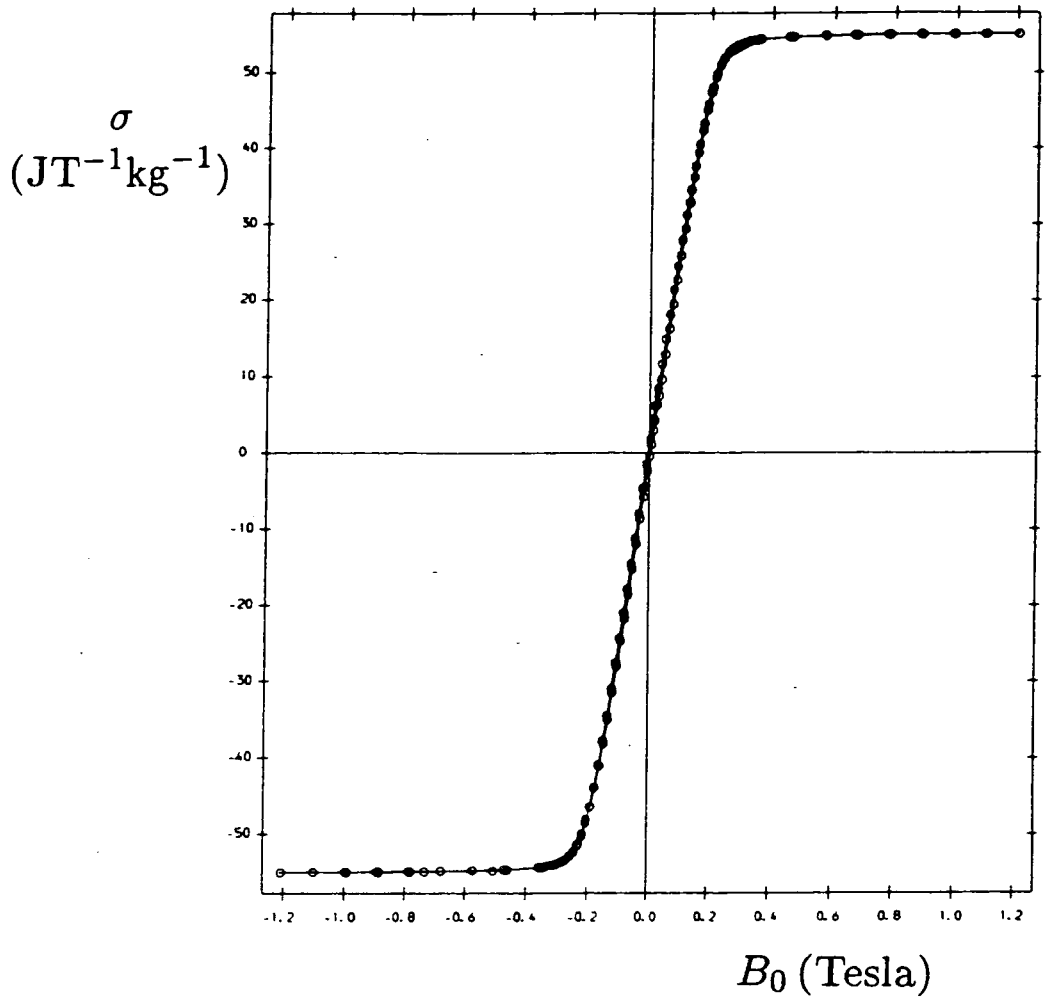

Figure 4.5 The full room temperature magnetization curve obtained from the second Durham VSM for a polycrystalline nickel sphere.

Chapter 5

The Simulation of MPI Indication Formation

I. The Formulation of the Model

5.1 Introduction

This chapter describes a simple 2-D model developed by the author to simulate the MPI indication formation process. The model is based on the simulation of the trajectories of many MPI particles moving in the magnetic leakage field of a semi-elliptical surface-breaking defect. Information about the time-evolution of the particle number density (pnd) as a function of the distance from the defect can be obtained and, consequently, the model throws important light on the MPI indication formation process.

The model employs the analytical expressions of Edwards and Palmer (Edwards and Palmer (1986)) for the leakage field of a semi-elliptical surface- breaking crack which were discussed in Chapter 3 and the first part of this chapter deals with the formulation of the equations of motion of the N-particle system in such a leakage field. The formulation involves a consideration of the complexities of the interparticle potential energy for the N-body system before we discuss the approximations and assumptions employed to make the system soluble. Other details of the model are presented together with brief computational details of the method of solution of the equations of motion. The next chapter presents the results obtained from the model. (Further details of the method used for the solution of the equations of motion can be found in Appendix A1.)

5.2 Background

Although, as discussed in Chapter 3, the study of the leakage fields of defects has received much attention, particularly over the last twenty years, the discussion of the interaction of those leakage fields with MPI particles and of any of the other forces present has suffered a relative neglect. Any discussions of the forces which affect MPI particles have tended to consider in isolation the separate contributions to the total force (for example the magnetic force only) and not touch upon the net forces and the subsequent particle trajectories.

Swartzendruber (Swartzendruber (1979)) stated that the net forces acting on MPI particles are comprised of contributions from gravitational forces, viscous forces, leakage field forces, exciting field forces, image forces and particle-particle interaction forces. Swartzendruber then presented a much simplified model of the indication formation process in dry powders which included only leakage field and gravitational forces. One important feature included by Swartzendruber was the way in which the form of the magnetic force depended on the particle susceptibility. Another conclusion from this model was that, by a consideration of the particle demagnetizing factor, particles which are elongated in one direction, for example, prolate ellipsoids, are subject to enhanced magnetic forces relative to those of spheres.

Blakely, Simkin and Brown (Blakely, Simkin and Brown (1985)), using finite

element (FE) analysis for the calculation of leakage fields, discussed the minimum threshold magnetizing fields required for a magnetic ink to form an indication. Their analysis considered only the tangential component of the magnetic force. This force, so they claimed, was proportional to the product of the particle volume, particle permeability, tangential component of the magnetizing field and the gradient of that tangential field component with respect to tangential distance. They obtained close quantitative agreement between their FE predictions of leakage fields and experimentally measured values but gave no further consideration to forces on a MPI particle in addition to that stated above.

Edwards and Palmer (Edwards and Palmer (1986)), using the gradients of their analytical expressions for the leakage field components of a surface-breaking semi-elliptical defect, were able to obtain analytical expressions for the components of the magnetic force on a spherical MPI particle. In contradistinction to Blakely *et al.* their treatment included the normal component of the magnetic force. They did not include any of the interparticle forces but argued that their expressions were valid in the early stages of the indication formation process, before the particles started to interact. They also argued that gravitational forces dominated thermal fluctuation (Brownian) forces for particles with diameters of a few micrometers. They discussed the magnitude of the magnetic force as a function of distance from the defect and related the magnetic force required to produce a visible indication to the applied magnetizing field. By considering the magnetic and gravitational forces on a MPI particle they thus inferred the threshold magnetizing fields required for the detection of defects of various sizes.

The treatment of the magnetic force in this chapter owes a great deal to the work of Edwards and Palmer. However, the author's treatment of this force also includes a consideration of the orientation of the particle's magnetization, **M**, (or magnetic dipole moment, **m**) in the magnetic field.

5.3 The Leakage Field of the Defect

The expressions of Edwards and Palmer for the leakage field components of a surface-breaking semi-elliptical defect have been thoroughly discussed in Chapter 3. It is sufficient here to recall their excellent agreement with experiment and, as a consequence, we may feel confident in employing them without reservation in the formulation of a model of indication formation in MPI. As stated previously, it is justifiable to use the 2-D approximations provided that the crack length is greater than about twenty times the crack depth. Our model only considers cases which conform to this approximation. Edwards and Palmers' approximation in this case, using the cartesian coordinate system shown in figure 5.1, is

$$B_{0x} = \frac{\mu_0 H_0 n(\mu_r - 1)}{2(n + \mu_r)\tan^{-1} n}\left[\tan^{-1}\frac{b(x+a)}{(x+a)^2 + y(y+b)} - \tan^{-1}\frac{b(x-a)}{(x-a)^2 + y(y+b)}\right] \qquad 5.1a$$

$$B_{0y} = \frac{\mu_0 H_0 n(\mu_r - 1)}{4(n + \mu_r)\tan^{-1} n}\ln\left(\frac{\left[(x+a)^2 + (y+b)^2\right]\left[(x-a)^2 + y^2\right]}{\left[(x+a)^2 + y^2\right]\left[(x-a)^2 + (y+b)^2\right]}\right) \qquad 5.1b$$

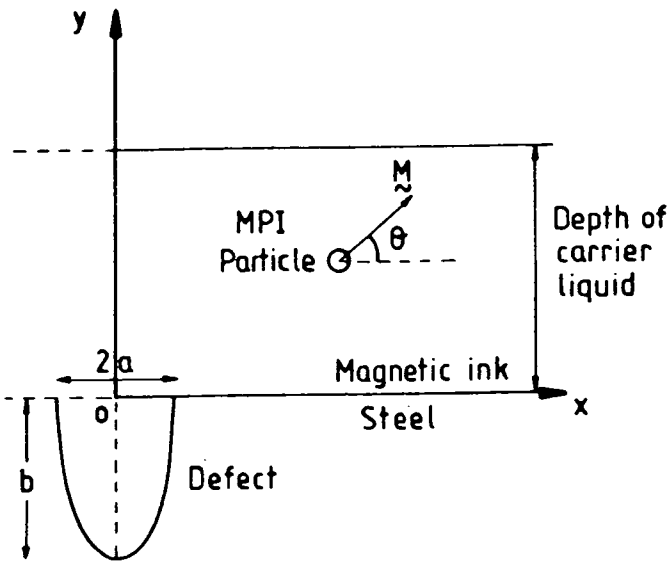

Figure 5.1 The coordinate system used by Edwards and Palmer (1986) and also by the present author.

where a and b are the defect's half-width and depth respectively, $n(= b/a)$ is the aspect ratio of the defect, μ_r is the test specimen's (constant) relative permeability and H_0 is the applied magnetizing field in the positive x direction.

5.4 The Total Energy of the N-Particle System

The most general case to consider for a magnetic ink is a system comprised of N particles, each of volume V_i $(i = 1, \ldots, N)$, where each particle is not necessarily spherical. The N particles are in the vicinity of the leakage field of a defect.

The total energy of the system, E_T, as a consequence of the assumptions and simplifications to be discussed shortly, is given by the following expression.

$$E_T = E_K + E_G + E_B \qquad 5.2$$

Here E_K is the total translational kinetic energy of all N particles, E_G is the combined gravitational and bouyancy potential energy of all of the particles and E_B is the potential energy of all of the particles' magnetic moments in the magnetic field. (Here the magnetic field refers to both the exciting field and the leakage field.) We need, however, to consider the terms we have neglected in this equation for the total energy and discuss the justification for their omission.

Particle rotational energy. Besides having translational kinetic energy the particles will also have rotational kinetic energy. The precise details of a particle's rotational motion will obviously depend on the particle's shape and orientation. Another factor to be considered, which also affects the rotational motion of the particle, is the orientation of the particle's magnetic moment vector with respect to the net magnetic field present and to the easy axis of magnetization within the particle. Thus a full treatment of this phenomenon would involve a consideration of the particle's magnetic anisotropy and of the torque this would produce. This effect is assumed to cause only a small perturbation on the translational motion and, consequently, is neglected.

Electrostatic potential energy. At the liquid-solid interface on a particle surface an electrical double layer can exist. This is an electrostatic potential caused by

the separation of charge between the phases. The whole system overall maintains electrical neutrality and the net charge is zero. The electrical double layer is comprised of the charge on the particle together with the equal and opposite charge in suspension. Because of the like charges on the surfaces of the particles this effect produces an overall interparticle repulsion. The cause of the surface charges is either the presence of surface ions produced by surface dissociation or of preferential adsorption of ions from the carrier onto the particle surface. One approximation for the interparticle electrical double layer interaction energy, E_{ij}^{E}, between two spheres i and j each of radius r and separated by a distance R_{ij} (with r being much less than 1μm) is

$$E_{ij}^{\mathrm{E}} = \frac{4\pi\epsilon_r\epsilon_0 r^2\psi_s^2}{R_{ij}} \exp\left[-\kappa(R_{ij} - 2r)\right] \qquad 5.3$$

where ϵ_r is the carrier relative permittivity, ψ_s is the double layer potential and κ is the quantity known as the reciprocal Debye-Hückel electrical double layer thickness. An idea of the magnitude of this effect is given by, for example, Fletcher and Parker (Fletcher and Parker (1984)) who calculated that in an aqueous dispersion ($\epsilon_r \simeq 80$) with $\psi_s \simeq 10$mV then 0.1μm radius particles having a differential separation of 10^{-8}m have double layer interaction energies of the order of thermal energies (kT). However, this electrical double layer interaction is only present in polar carrier liquids (for example water), or, in other words, ionizable liquids. Organic carriers such as light alkanes and paraffins are non-polar and so cannot contribute to an electrical double layer. Thus, if we limit our discussion to non-polar carrier liquids we can neglect electrical double layer interactions. (For a more complete discussion of colloidal electrical double layers and of their effect on colloidal stability the reader is referred to texts such as those by Verwey and Overbeek (1948) or by Lyklema (1982).)

London-van der Waals interaction energy. London-van der Waal's attractive interactions arise from the fluctuating electric dipoles on all of the suspended particles. These dipoles are caused by rapid fluctuations in the electric charge distributions in the atoms/molecules which compose the suspended particles. The net result for large particles composed of many atoms is that, by pairwise addition of the interactions between the atoms in each body (Hamaker (1937)), the distance-dependence of the interaction energy between two equal spheres i and j for close spheres is $\sim R_{ij}^{-1}$ and for distant spheres is $\sim R_{ij}^{-6}$. The precise details of this interaction are complex as are the various models which in different particle size regimes and concentrations are applicable. For this reason the other factors occurring in the energy of interaction equations apart from the distance-dependence mentioned above are not discussed. However, it is apparent that because of the R_{ij}^{-6} dependence this effect is always negligible, except at high particle concentrations.

Steric (entropic) repulsion energy. Some magnetic ink manufacturers add small amounts ($\sim$ 1% by volume) of stabilizing surfactant to the carrier liquid. This is to aid dispersion and to increase the time over which the suspension is stable against both sedimentation and aggregation. The theory of the repulsive interaction is the same as for magnetic liquids and conventional lyophobic colloids, involving the overlap of surfactant polymer tails of neighbouring particles. However, because such small amounts are present the effect is miniscule over the time period of indication formation and so we are justified in neglecting this contribution.

Enthalpic repulsion energy. One more interaction which is associated with the presence of stabilizing surfactants is enthalpic repulsion energy. This is an

order of magnitude smaller than the steric repulsion energy term but is mentioned here for the sake of completeness. This effect arises if the heat of solution of the surfactant molecules in the carrier liquid is exothermic. When surfactant polymer tails of neighbouring particles overlap then energy is required to increase the local concentration of surfactant (Bagchi (1972)). This effect, thus, amounts to the same thing as a repulsive interaction.

Magnetostatic interparticle interaction energy. The total magnetostatic interaction energy for N particles, each with a magnetic dipole moment $\mathbf{m}_i$ and with a position vector $\mathbf{R}_{ij}$ $(i \neq j)$ between particles i and j is given by

$$E_M = -\frac{\mu_0}{4\pi} \sum_{\substack{i=1 \\ i \neq j}}^{N} \sum_{\substack{j=1 \\ j \neq i}}^{N} \left[\frac{\mathbf{m}_i \cdot \mathbf{m}_j}{R_{ij}^3} - \frac{3(\mathbf{m}_i \cdot \mathbf{R}_{ij})(\mathbf{m}_j \cdot \mathbf{R}_{ij})}{R_{ij}^5} \right] \qquad 5.4$$

This contribution is not important unless the particles are very close together (because of the inverse cubic dependence). The mean interparticle separation is proportional to the concentration of the suspension and so it is only in high concentration suspensions that this term is important. If we consider only suspensions of low ($< 1\%$ by volume) concentration the neglect of this term is reasonable for most of the time. Obviously as a MPI indication develops in time and more and more particles become trapped adjacent to the defect and thus, increase the local concentration, this approximation becomes less and less applicable. However, this phenomenon is not included in the author's model.

5.5 The Formulation of the Model

The equations of motion are derived using classical Lagrangian mechanics. The generalized coordinates for the N-particle system are

$$(x_1, \ldots, x_N; y_1, \ldots, y_N; \theta_1, \ldots, \theta_N). \qquad 5.5$$

Here (x_i, y_i) are the cartesian position coordinates of the particle i in the coordinate system shown in figure 5.1 and pertinent to the equations of Edwards and Palmer. θ_i is the angle which the magnetic moment of particle i makes with the positive x axis.

Thus, the Lagrangian is a function of the following variables

$$L = L(x_1, \ldots, x_N; y_1, \ldots, y_N; \dot{x}_1, \ldots, \dot{x}_N; \dot{y}_1, \ldots, \dot{y}_N; \theta_1, \ldots, \theta_N). \qquad 5.6$$

The explicit form of the Lagrangian is

$$L = \tfrac{1}{2}\rho_p \sum_{i=1}^{N} V_i(\dot{x}_i^2 + \dot{y}_i^2) + \sum_{i=1}^{N} \mathbf{m}_i(\theta_i) \cdot \mathbf{B}_{0T}(x_i, y_i) - (\rho_p - \rho_w) g \sum_{i=1}^{N} V_i y_i. \qquad 5.7$$

with ρ_p the density of the particle material, ρ_w the density of the carrier liquid, $\mathbf{m}_i$ the magnetic dipole moment of particle i and g the gravitational acceleration. $\mathbf{B}_{0T}$ is the total magnetic flux density present and is composed of the contributions of both the applied magnetizing field and the leakage field components, that is, $\mathbf{B}_{0T} = \hat{\mathbf{i}}(\mu_0 H_0 + B_{0x}) + \hat{\mathbf{j}} B_{0y}$, where $\hat{\mathbf{i}}$ and $\hat{\mathbf{j}}$ are unit vectors in the x and y directions respectively. The first term on the right hand side is the total translational kinetic energy of the system which was earlier referred to as E_K in equation (5.2).

The second term is the total potential energy of all N magnetic moments in the net magnetic field, previously called E_B in equation (5.2). The third term is the combined gravitational and bouyancy potential energy of all N particles which earlier in equation (5.2) was called E_G. Here the relative permeability of the carrier fluid is taken to be unity. This is a very good approximation as a liquid does not show cooperative magnetic behaviour. A further point to note is that the particles, although having a volume V_i, are treated as having *point* position coordinates (x_i, y_i) (the 'point particle' approximation). This is the same as treating each particle as having a uniform magnetization and assuming that over the distance scale of one particle diameter the magnitude and direction of the leakage field are constant. Obviously the validity of this approximation is inversely proportional to the particle diameter. The next chapter, Chapter 6, which deals with the results also deals in greater detail with the validity of the point particle approximation.

The motion of the particles through the viscous carrier liquid produces dissipative forces on the particles. For a spherical particle i of radius r_i with position coordinates (x_i, y_i) this dissipative force, $\mathbf{F}_i^{\mathrm{D}}$, is given by Stokes' law,

$$\mathbf{F}_i^{\mathrm{D}} = 6\pi\eta r_i(\hat{\mathbf{i}}\dot{x}_i + \hat{\mathbf{j}}\dot{y}_i), \tag{5.8}$$

where η is the carrier liquid's coefficient of viscosity, $\hat{\mathbf{i}}$ and $\hat{\mathbf{j}}$ are again unit vectors in the x and y directions respectively and the dots denote differentiation with respect to time. However, since we are considering the most general case of not necessarily spherical particles Stokes' law will not necessarily be applicable. However, as an approximation and by analogy with Stokes' law, it is assumed that, whatever the shape of the particle, the dissipative force on particle i depends linearly on the carrier coefficient of viscosity and linearly on the generalized velocity $(\hat{\mathbf{i}}\dot{x}_i + \hat{\mathbf{j}}\dot{y}_i)$. It would obviously be expected, however, that the other factors and constants in the equation would not be the same as in the Stokes' law equation. This linear dependence of the generalized frictional forces on generalized velocities is found in a large class of dissipative systems (for example, damped mechanical oscillations of springs). In such cases the dissipative forces are derivable from a function $R(q, \dot{q})$ which is quadratic in the $\dot{q}$s. (Here $(q, \dot{q})$ refers to the generalized coordinates and generalized velocities respectively of *all* of the particles.) R is called the Rayleigh dissipation function. The generalization of Lagrange's equations to non-conservative systems where the generalized dissipative forces depend linearly on the generalized velocities is given by the expression

$$\frac{d}{dt}\left(\frac{\partial L}{\partial \dot{q}_i}\right) = \frac{\partial L}{\partial q_i} - \frac{\partial R}{\partial \dot{q}_i} \quad \text{for } i = 1, \ldots, 3N; \quad q_i = x_1, y_1, \theta_1, \ldots, x_N, y_N, \theta_N \tag{5.9}$$

The explicit form of the Rayleigh dissipation function in our approximation is

$$R = \eta \sum_{i=1}^{N} c_i(\dot{x}_i^2 + \dot{y}_i^2). \tag{5.10}$$

Here c_i is some factor which accommodates the deviation from sphericity (and, thus, from Stokes' law) of particle i.

Hence, by substituting equations (5.7) and (5.10) into (5.9) and using the relation $\mathbf{m}_i(\theta_i) = m_i(\hat{\mathbf{i}}\cos\theta_i + \hat{\mathbf{j}}\sin\theta_i)$, after some manipulation the following equations of motion are obtained.

$$\ddot{x}_i + \frac{2\eta c_i}{\rho_p V_i}\dot{x}_i - \frac{m_i}{\rho_p V_i}\left(\cos\theta_i \frac{\partial B_{0x}}{\partial x_i} + \sin\theta_i \frac{\partial B_{0y}}{\partial x_i}\right) = 0 \qquad 5.11a$$

$$\ddot{y}_i + \frac{2\eta c_i}{\rho_p V_i}\dot{y}_i - \frac{m_i}{\rho_p V_i}\left(\cos\theta_i \frac{\partial B_{0x}}{\partial y_i} + \sin\theta_i \frac{\partial B_{0y}}{\partial y_i}\right) + \frac{g(\rho_p - \rho_w)}{\rho_p} = 0 \qquad 5.11b$$

$$(\mu_0 H_0 + B_{0x})\sin\theta_i - B_{0y}\cos\theta_i = 0 \qquad 5.11c$$

$$\text{for } i = 1, \ldots, N$$

The partial derivative terms in equations (5.11a) and (5.11b) are given by the partial derivatives of equations (5.1a) and (5.1b), explicitly,

$$\frac{\partial B_{0x}}{\partial x_i} = \frac{\mu_0 H_0 n(\mu_r - 1)}{2(n + \mu_r)\tan^{-1} n}\left[\frac{y_i + b}{(x_i - a)^2 + (y_i + b)^2} - \frac{y_i + b}{(x_i + a)^2 + (y_i + b)^2} + \frac{y_i}{(x_i + a)^2 + y_i^2} - \frac{y_i}{(x_i - a)^2 + y_i^2}\right] \qquad 5.12a$$

$$\frac{\partial B_{0y}}{\partial x_i} = \frac{\mu_0 H_0 n(\mu_r - 1)}{2(n + \mu_r)\tan^{-1} n}\left[\frac{x_i + a}{(x_i + a)^2 + (y_i + b)^2} - \frac{x_i - a}{(x_i - a)^2 + (y_i + b)^2} + \frac{x_i - a}{(x_i - a)^2 + y_i^2} - \frac{x_i + a}{(x_i + a)^2 + y_i^2}\right] \qquad 5.12b$$

$$\text{with} \quad \frac{\partial B_{0x}}{\partial y_i} = \frac{\partial B_{0y}}{\partial x_i} \quad \text{and} \quad \frac{\partial B_{0y}}{\partial y_i} = -\frac{\partial B_{0x}}{\partial x_i} \qquad 5.12c$$

Thus, we have arrived at the equations of motion describing the system, subject to the assumptions made earlier in section 5.4. In principle, we can solve this system of equations for each (x_i, y_i, θ_i) provided that we know the volume (V_i) and the shape (essentially c_i) of each particle. The important things to note about this system of equations are firstly, that the motion of each particle i is described by three simultaneous equations, and secondly, that the three equations for each i are not coupled to any other value of i. This second point is a consequence of not including any of the interparticle interactions in the model and it means that the solution for the trajectory of each particle does not depend on the solution for any other particle, or, in other words, each particle's solution can be obtained in isolation from all of the others. It is apparent that had any of the interparticle interactions been included the resulting equations would have been a system of $3N$ simultaneous equations. This would have made the task of solving the system of equations immensely more difficult. This difficulty could be partially alleviated by, for example, introducing some means of uncoupling some of the equations by including, say, only the effects of interactions of 'nearby' particles on a particular particle's motion and ignoring the effects of more distant particles. However, the task of solution would still represent a formidable undertaking.

5.6 Further Approximations

As explained in the previous section the system of equations given by equations (5.11a), (5.11b) and (5.11c) can in principle be solved if, for each i, one knows V_i and c_i. The further simplifying approximations made here are

(1) Each particle is spherical. This means that V_i and c_i for each of the particles are given by the following equations.

$$V_i = \tfrac{4}{3}\pi r_i^3 \qquad \text{and} \qquad c_i = 3\pi r_i \tag{5.13}$$

The second equation here is simply the use of Stokes' law for the dissipative force. This approximation also means that the magnetic dipole moment of each particle, $\mathbf{m}_i$, can be expressed in terms of the particle magnetization per unit volume, $\mathbf{M}$, by means of the following equation.

$$\mathbf{m}_i = \tfrac{4}{3}\pi r_i^3 \mathbf{M} \tag{5.14}$$

(The actual numerical value of M to be used is discussed in more detail in section 5.8.)

(2) All of the particles are the same size. This means that there is no particle size distribution (psd), or, in a sense, the psd is δ-like. This is obviously not true in real fine particle systems where Gaussian or lognormal psds are usually found. For example, Granqvist and Buhrman (Granqvist and Buhrman (1976)) found that in many ultrafine (diameter < 20nm) metal particle systems produced by evaporation in an inert gas the particle size is lognormally distributed. O'Grady and Bradbury (O'Grady and Bradbury (1983)) found that, depending on the method of preparation, cobalt magnetic liquids had either gaussian or lognormal psds. Although these two examples were concerned with particles of smaller median diameter than MPI particles there is no reason to suspect that some analogous psd would not be present. However, the approximation is employed here in order to simplify matters.

Use of these approximations means that the system of equations (5.11a), (5.11b) and (5.11c) can be written in the following way.

$$\ddot{x}_i + \frac{9\eta}{2r_i^2\rho_p}\dot{x}_i - \frac{M}{\rho_p}\left(\cos\theta_i \frac{\partial B_{0x}}{\partial x_i} + \sin\theta_i \frac{\partial B_{0y}}{\partial x_i}\right) = 0 \tag{5.15a}$$

$$\ddot{y}_i + \frac{9\eta}{2r_i^2\rho_p}\dot{y}_i - \frac{M}{\rho_p}\left(\cos\theta_i \frac{\partial B_{0x}}{\partial y_i} + \sin\theta_i \frac{\partial B_{0y}}{\partial y_i}\right) + \frac{g(\rho_p - \rho_w)}{\rho_p} = 0 \tag{5.15b}$$

$$(\mu_0 H_0 + B_{0x})\sin\theta_i - B_{0y}\cos\theta_i = 0 \tag{5.15c}$$

$$\text{for } i = 1, \ldots, N$$

The magnetic force terms in the first two of these equations, (5.15a) and (5.15b), are essentially those parts having the partial derivative terms inside the large parentheses. These have some similarities to those expressions obtained by Edwards and Palmer for the magnetic force but the difference here is that our equations represent a more general case in which no assumptions are made about the dependence of $\mathbf{M}$ on $\mathbf{B}_{0T}$. Another point worthy of note is that in equations (5.15a) and (5.15b) if the coefficient of the $\dot{x}_i$ and the $\dot{y}_i$ term is zero, then the only specifically particle-dependent properties on which the subsequent particle motion depends are the particle magnetization, $\mathbf{M}$, and the particle density, ρ_p (and notably *not* the particle radius r_i). For this coefficient to be zero requires that $\eta = 0$, or, in other words, that the carrier liquid has no viscosity. An approximation of a real system in which this would be realised is the case of the dry powder technique of MPI. Here,

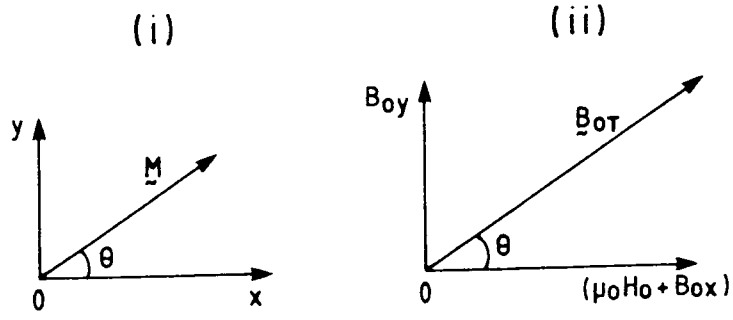

Figure 5.2 The θ_i solution (equation (5.16)) showing the parallel alignment of the particle's magnetization with the net magnetic field direction.

the carrier liquid's viscosity would be replaced by the viscosity of air which, relative to a liquid's viscosity $\simeq 0$ and also, the density of air, relative to that of the particle material, would be negligible so that $(\rho_p - \rho_w)/\rho_p \simeq 1$. Hence, the conclusion here is that in the dry powder method of MPI the only particle properties which have any bearing on the particles' motion are the magnetization and the density. However, this conclusion is only valid as long as the point particle approximation is valid. As stated earlier, the point particle approximation will be dealt with in the next chapter.

The third of these equations, (5.15c), can be solved analytically and has the simple solution

$$\theta_i = \tan^{-1}\left[\frac{B_{0y}(x_i, y_i)}{\mu_0 H_0 + B_{0x}(x_i, y_i)}\right] \qquad 5.16$$

This is the 'classical' result of the parallel alignment of the particle's magnetization with the net magnetic field direction in order to minimise the energy. This is clarified in figure 5.2.

Unfortunately, however, the author does not know of any analytical solutions for the other two equations, (5.15a) and (5.15b). Consequently, approximate solutions have to be obtained by using numerical methods. A simplifying factor in the numerical solution, however, arises from the use of the exact θ_i solution in the calculation of each point of the approximate solutions for (x_i, y_i). In other words, at any point of the (x_i, y_i) solution, by substituting the appropriate value of θ_i calculated from equation (5.16) into equations (5.15a) and (5.15b), one eliminates θ_i from equations (5.15a) and (5.15b) obtains, for each i, two simultaneous second order ordinary differential equations in (x_i, y_i).

5.7 Other Constraints

Further details incorporated into the model in order to make it 'realistic' are now discussed. The first detail concerns the fate of a particle which reaches the test specimen-carrier liquid interface (that is, the bottom of the carrier liquid) but is still some way away from the defect and has not yet been trapped. In such cases, the author's model proceeds by subsequently only solving the x coordinate equation for the particle and keeping the particle's y coordinate constant for all

subsequent trajectory calculations. This procedure corresponds to simulating the particle trajectory of a particle moving along the specimen surface. The details of such motion, in real systems, would obviously be very complicated and involve features such as the specimen's surface roughness and rheological properties. However, these complexities are not included in the author's model.

It was mentioned in Chapter 3 that contrast paint layers are sometimes applied to the test specimen to facilitate the detection of defects (BS 5044 (1973)). The effect of contrast paint layers can be investigated by taking the test specimen-carrier liquid interface to be at a non-zero y value. This offset of the interface above the line $y = 0$ essentially has the same effect as the presence of the contrast paint layer. The thickness of the paint layer would obviously be equal to the offset distance (that is, the y value of the interface). Thus, in this way, the facility for using the model to investigate the effect of varying the contrast paint layer thickness is realised.

In practice, however, a non-zero y value *must* be used because the equation for B_{0y} (equation (5.1*b*)) has a singularity at $(x = \pm a, y = 0)$. Consequently, any calculations involving the coordinates at or close to $(x = \pm a, y = 0)$ must be avoided in order to steer clear of computational problems. Avoidance is achieved by simply offsetting the specimen-carrier interface. In the author's model this offset is never less than 10μm. (The paint layer thickness is never less than 10μm.)

One last feature to be mentioned is that the solution for a particle's trajectory is terminated if $|x| \leq a$ and the particle is considered as henceforth permanently trapped. It is in the region where $|x| \simeq a$ that the increase in local concentration caused by trapped particles will start making the assumption concerning the neglect of magnetostatic interactions less and less valid. This is why the model avoids considering the details of particle trajectories if $|x| \leq a$.

5.8 Magnetization, Brownian Motion and 'Bridging'

The question now arises as to what numerical value should be used for M in the equations of motion, (5.15*a*) and (5.15*b*). If a particle were small enough to be single domain then the numerical value of M could be taken to be equal to the saturation magnetization of the particle's bulk material, M_{sb}, ($\simeq 4.714 \times 10^5$ $\mathrm{JT^{-1}m^{-3}}$ for magnetite (Fe_3O_4) and $\simeq 1.718 \times 10^6$ $\mathrm{JT^{-1}m^{-3}}$ for α-iron (α-Fe) at room temperature). This is an approximation which is only valid provided that the particles are not very small. For particle diameters less than about 100Å this approximation breaks down, as shown, for example, by Sato, IIjima, Seki and Inagaki (Sato, IIjima, Seki and Inagaki (1987)), who found that for a range of ultrafine ferrites the saturation magnetization of the particles is reduced sharply relative to the bulk saturation magnetization by an amount typically in excess of 50% for particles with diameters less than about 100Å. They thought this effect to be caused by a magnetically inactive particle surface layer or by the asymmetric environment of the atoms near the particle surface's causing some 'magnetic effects'. (This effect is not the same as the effect which produces a similar reduction in particle saturation magnetization and which is caused by the 'spin pinning' arising from the bonding of organic surfactants to particle surfaces in magnetic liquids (Berkowitz and Lahut (1973) and Berkowitz, Lahut, Jacobs, Levinson and Forester (1975))). However, only particles with diameters at least two orders of magnitude greater than those at which these effects become apparent are used in our model and besides this, our particles are too large to be single domain.

In magnetite the critical diameter between the single domain (SD) and the multidomain (MD) state occurs at $\simeq 0.4\mu$m (Stacey and Banerjee (1974), p59). In iron the critical diameter is $\simeq 200$Å (Kittel (1949)). These are only approximate values because observation and theory frequently disagree with regard to this problem. The situation is further confused by the transition from a SD to a MD state's not being an abrupt one, but a gradual one in terms of magnetic properties (particularly coercivity and remanence)(Banerjee and Moskowitz (1985)). The region of this gradual change is known as the pseudo-single domain (PSD) state. In MPI the particles or particle aggregates (which are here treated as individual particles) have median diameters above these critical diameters, and so the domain structure of the particles means that the bulk saturation magnetization, M_{sb}, of the particle material cannot be used for the value of M in equations (5.15a) and (5.15b). Thus, the situation is more complicated and the particles have a non-zero permeability, or, in other words, the value of M is a function of the total magnetic field, B_{0T}. Following Edwards and Palmer, the author's model approximates the behaviour of M by

$$\mathbf{M} = \frac{2\mathbf{B}_{0T}}{\mu_0} \qquad \text{for } M < M_{sb} \qquad 5.17a$$

or

$$\mathbf{M} = \mathbf{M}_{sb} \qquad \text{for } 2B_{0T}/\mu_0 \geq M_{sb} \qquad 5.17b$$

The effect of Brownian motion on a particle's trajectory has so far not been discussed. Edwards (Edwards (1986)) has calculated that at room temperature for particles with diameters of $\sim 0.7\mu$m the mean magnitude of Brownian displacements per unit time is equal to the gravitational displacement per unit time. Hence, for particles of that size, not to include the effects of Brownian motion would be a serious omission. However, our model only uses particles having diameters well above this critical size. The smallest particles used by the author have diameters of 4μm.

'Bridging' is the phenomenon in which the build-up of MPI particles to form an indication adjacent to a defect seriously hinders the subsequent migration of other particles to the defect. It is argued that the origin of this effect is the reduction in leakage field arising from the presence of 'bridges' across the defect formed from the built-up particles and which have a higher permeability (or a lower reluctivity) than the air/magnetic ink through which the leakage fields would otherwise have to propagate. This phenomenon is currently the subject of a great deal of debate amongst MPI operators. Some argue that the process, as described above, satisfactorily accounts for the frequently observed phenomenon in which, once an indication has formed beyond a certain particle number density, the indication size essentially saturates and stops increasing further. Others argue that the effects of 'bridging' are not sufficiently large to satisfactorily explain this phenomenon and that the explanation of this observation lies elsewhere. It will be shown later that results from our model provide an explanation, other than 'bridging', for this observation. The possible modification of the leakage field of the defect by some 'bridging' mechanism once an indication has started to evolve is not included in the our model.

5.9 The Numerical Solution of the Equations of Motion

The numerical approximations to the solutions of the equations of motion are obtained as sets of particle coordinates at discrete steps in time, with the time intervals between successive coordinate sets being very small. At each time step

complete sets of velocity components are also obtained.

The technique used in order to obtain numerical approximations to the solutions of equations (5.15*a*) and (5.15*b*) is a predictor-corrector method. As the name implies, the method proceeds by first *predicting* a value for the next point of the solution and then a different formula is used to *correct* this value. If it appears to be necessary, the corrector formula can be employed again to recorrect the approximation for this next point of the solution. There is, in principle, no limit to the number of times the process can be iterated. However, efficiency considerations make it sensible to choose a step size that avoids iterating this process a great many times.

Appendix A1 discusses in more detail the numerical solution of differential equations in general and the predictor-corrector method in particular. Only brief details about the technique of solution are given here.

The first important point to make is that a second order ordinary differential equation can be decomposed into two simultaneous first order ordinary differential equations. Thus, the second order differential equation

$$\frac{d^2\psi}{dz^2} = g\left(\frac{d\psi}{dz}, \psi, z\right) \tag{5.18}$$

can be decomposed into

$$\frac{du}{dz} = f(u, \psi, z) \quad ; \quad \frac{d\psi}{dz} = u \tag{5.19}$$

Applying this decomposition to equations (5.15*a*) and (5.15*b*) yields the following system of four simultaneous first order ordinary differential equations.

$$\dot{x} = v_x \tag{5.20a}$$

$$\dot{y} = v_y \tag{5.20b}$$

$$\dot{v}_x = -\frac{9\eta}{2r^2\rho_p}v_x + \frac{M}{\rho_p}\left[\cos\theta\frac{\partial B_{0x}}{\partial x}(x,y) + \sin\theta\frac{\partial B_{0y}}{\partial x}(x,y)\right] \tag{5.20c}$$

$$\dot{v}_y = -\frac{9\eta}{2r^2\rho_p}v_y + \frac{M}{\rho_p}\left[\cos\theta\frac{\partial B_{0x}}{\partial y}(x,y) + \sin\theta\frac{\partial B_{0y}}{\partial y}(x,y)\right] - \frac{g(\rho_p - \rho_w)}{\rho_p} \tag{5.20d}$$

Here the dots again denote differentiation with respect to time. The i subscripts are dropped and it is to be understood that these equations are applicable for any single value of i.

The predictor equation used to approximate the solution to the general equation

$$\frac{d\psi}{dz} = f(\psi, z) \tag{5.21}$$

at the point $z = z_{m+1} = z_m + h$ is given by

$$\begin{aligned}\psi_{m+1} &\simeq \psi_m + h\left(\frac{d\psi}{dz}\right)_{z=z_m} \\ &\simeq \psi_m + hf(\psi_m, z_m)\end{aligned} \tag{5.22}$$

Here ψ_{m+1} is the prediction of the approximation to the solution $\psi(z)$ at the point where $z = z_{m+1}$. h is the step size which separates neighbouring z values at which the solution is evaluated such that $z_{m+1} = z_m + h$. ψ_m is the approximation to the solution at $z = z_m$ (the previously evaluated point which is an approximation to the solution). The use of this equation to obtain the $(m+1)$th approximation to the solution, knowing the mth approximation, is known as Euler's method or a first order Runge-Kutta method.

Thus, explicitly, the four predictor equations for our system are

$$x_{m+1} = x_m + h v_{x\,m} \tag{5.23a}$$

$$y_{m+1} = y_m + h v_{y\,m} \tag{5.23b}$$

$$v_{x\,m+1} = v_{x\,m} - h\left(\frac{9\eta}{2r^2\rho_p} v_{x\,m} - \frac{M}{\rho_p}\left[\cos\theta_m \frac{\partial B_{0x}}{\partial x}(x_m, y_m) + \sin\theta_m \frac{\partial B_{0y}}{\partial x}(x_m, y_m)\right]\right) \tag{5.23c}$$

$$v_{y\,m+1} = v_{y\,m} - h\left(\frac{9\eta}{2r^2\rho_p} v_{y\,m} - \frac{M}{\rho_p}\left[\cos\theta_m \frac{\partial B_{0x}}{\partial y}(x_m, y_m) + \sin\theta_m \frac{\partial B_{0y}}{\partial y}(x_m, y_m)\right] + \frac{g(\rho_p - \rho_w)}{\rho_p}\right) \tag{5.23d}$$

These predictor equations predict the $(m+1)$th points of the solutions when the mth points are known. Here h has dimensions of time.

The corrector equation used by the author for the kth correction of the prediction of the approximation to the solution (ψ_{m+1}) of the general equation at $z = z_{m+1}$ is given by

$$\begin{aligned} \psi_{m+1}^{(k)} &= \psi_m + \frac{h}{2}\left(\frac{d\psi_m}{dz} + \frac{d\psi_{m+1}^{(k-1)}}{dz}\right) \\ &= \psi_m + \frac{h}{2}\left[f(\psi_m, z_m) + f(\psi_{m+1}^{(k-1)}, z_{m+1})\right] \end{aligned} \tag{5.24}$$

The value of the superscript in parentheses, (k), refers to the kth approximation to the solution in the iterative process. In terms of our system of equations the correctors are

$$x_{m+1}^{(k)} = x_m + \frac{h}{2}(v_{x\,m} + v_{x\,m+1}^{(k-1)}) \tag{5.25a}$$

$$y_{m+1}^{(k)} = y_m + \frac{h}{2}(v_{y\,m} + v_{y\,m+1}^{(k-1)}) \tag{5.25b}$$

$$v_{x\,m+1}^{(k)} = v_{x\,m} - \frac{h}{2}\left(\frac{9\eta}{2r^2\rho_p}[v_{x\,m} + v_{x\,m+1}^{(k-1)}] - \frac{M}{\rho_p}\left[\cos\theta_m \frac{\partial B_{0x}}{\partial x}(x_m, y_m)\right.\right.$$
$$+\cos\theta_{m+1}^{(k-1)} \frac{\partial B_{0x}}{\partial x}(x_{m+1}^{(k-1)}, y_{m+1}^{(k-1)}) + \sin\theta_m \frac{\partial B_{0y}}{\partial x}(x_m, y_m) \qquad 5.25c$$
$$\left.\left.+\sin\theta_{m+1}^{(k-1)} \frac{\partial B_{0y}}{\partial x}(x_{m+1}^{(k-1)}, y_{m+1}^{(k-1)})\right]\right)$$

$$v_{y\,m+1}^{(k)} = v_{y\,m} - \frac{h}{2}\left(\frac{9\eta}{2r^2\rho_p}[v_{y\,m} + v_{y\,m+1}^{(k-1)}] - \frac{M}{\rho_p}\left[\cos\theta_m \frac{\partial B_{0x}}{\partial y}(x_m, y_m)\right.\right.$$
$$+\cos\theta_{m+1}^{(k-1)} \frac{\partial B_{0x}}{\partial y}(x_{m+1}^{(k-1)}, y_{m+1}^{(k-1)}) + \sin\theta_m \frac{\partial B_{0y}}{\partial y}(x_m, y_m) \qquad 5.25d$$
$$\left.\left.+\sin\theta_{m+1}^{(k-1)} \frac{\partial B_{0y}}{\partial y}(x_{m+1}^{(k-1)}, y_{m+1}^{(k-1)})\right] + \frac{2g[\rho_p - \rho_w]}{\rho_p}\right)$$

The method of solution is now described. The first predictions for the next point of the solution (the $(m+1)$th) are obtained using equations 5.23*a*–5.23*d*. The first point of the solutions ($m = 1$) corresponds to the initial conditions at time $t = 0$. (The initial conditions will be dealt with in the next section, 5.10.) These four first predictions, $x_{m+1}, y_{m+1}, v_{x\,m+1}$ and $v_{y\,m+1}$ are next substituted into the right hand sides of equations 5.25*a*–5.25*d* for the first time and these values correspond to the superscript $(k-1) = (0)$, to give the first $((k) = (1))$ correction of the approximations of the solutions, that is, $x_{m+1}^{(1)}, y_{m+1}^{(1)}, v_{x\,m+1}^{(1)}$ and $v_{y\,m+1}^{(1)}$. The next iteration of the correction procedure involves substituting these values, $x_{m+1}^{(1)}, y_{m+1}^{(1)}, v_{x\,m+1}^{(1)}$ and $v_{y\,m+1}^{(1)}$, back into the right hand sides of equations 5.25*a*–5.25*d* with now $(k-1) = (1)$ to yield the (hopefully) better estimates of the solutions, $x_{m+1}^{(2)}, y_{m+1}^{(2)}, v_{x\,m+1}^{(2)}, v_{y\,m+1}^{(2)}$. It is thus apparent that all four equations are solved in parallel with the approximation of the solution of one of the equations obtained after (k) corrections being used in all four of the equations at the next, the $(k+1)$th, correction. This procedure is iterated until some convergence criterion which involves the smallness of the difference between the approximations obtained in successive iterations is satisfied. In other words, in terms of the solution of our general equation, the iterations are stopped when

$$|\psi_{m+1}^{(k+1)} - \psi_{m+1}^{(k)}| < \epsilon \quad \text{for a specified positive } \epsilon. \qquad 5.26$$

In our case the convergence criterion used involves both x and y and the iterations are stopped when both of the following conditions are satisfied

$$|x_{m+1}^{(k+1)} - x_{m+1}^{(k)}| < 1\mu\text{m} \qquad \text{and} \qquad |y_{m+1}^{(k+1)} - y_{m+1}^{(k)}| < 1\mu\text{m} \qquad 5.27$$

(Appendix A1 discusses in more detail the conditions under which this convergence criterion is satisfied, or, in other words, when the predictor-corrector process converges.) It is important here to make clear that just because the predictor-corrector process converges to some definite value does not mean that this definite value is necessarily the 'true' solution. The difference between the 'true' solution and the value to which this process converges is known as the truncation error. It can be shown (Dorn and McCracken (1972), p383) that an estimate of the truncation error, e_T, is given by the expression

$$e_T = \tfrac{1}{5}(\psi_m^{(0)} - \psi_m^{(k)}) \qquad 5.28$$

Hence, once the iterations of the corrector have stopped, one final correction to the solution can be made by estimating this truncation error and adding it to the approximate solution obtained as the value to which the predictor-corrector process has converged. This correction is duly made in our predictor-corrector algorithm. In addition to this, another interesting point to make here concerns the contrast in general between solely Runge-Kutta methods and predictor-corrector methods is the ease with which truncation error estimates can be obtained. Runge-Kutta methods are notorious for their lack of convenient truncation error estimates and for the often drastic increase in computation required to obtain good truncation error estimates. On the other hand, predictor-corrector methods produce good estimates of the truncation error which are also calculable from values readily available in the calculation. This point is dealt with in more depth in Appendix A1.

5.10 Computation Details

All of the results presented in this thesis are from systems containing 160 particles ($N = 160$) in most cases confined such that $a \leq x_i \leq 0.8$mm and 10μm $\leq y_i \leq 0.5$mm. (This lower limit on y_i represents the lowest contrast paint layer thickness used. The only time this lower limit is altered is for the investigation of the effect of varying the contrast paint layer thickness.) This number of particles was chosen as a compromise between the benefit of the reduction in computing time from using as few particles as possible and the benefit of the improved statistics from using as many particles as possible.

At time $t = 0$ all of the particles are considered as being stationary. The simulations progress by calculating the positions of each particle $(x_i(t), y_i(t))$ at subsequent times and, thus, approximating the trajectories of all of the particles. It could be argued that the initial conditions at $t = 0$, namely that all of the particles are stationary, is an arbitrary or contrived configuration of the system. This may be true. However, whatever other initial conditions were to be used instead of these, for example, assigning to each particle non-zero velocity components at $t = 0$, would be just as much arbitrary or contrived. In the absence of any precise details about how the magnetic ink is applied to the test specimen and exactly when the test specimen is magnetized (before or after the application of the magnetic ink) the initial conditions used here are as good as any. In addition to this, it would be expected that as the simulations proceed in time, the resulting configurations of the system become increasingly independent of the fine details of the initial conditions.

The starting coordinates at $t = 0$ of the particles in all of the results presented here are randomly distributed with respect to y but uniformly distributed with respect to x through the carrier fluid volume. None of the results or conclusions change if a random distribution in x is used instead of a uniform distribution, but only the uniformly distributed x coordinates will be shown here for the sake of clarity. The randomly distributed y coordinates are generated by the NAG Library subroutine G05CAF. This is a pseudo random number generator which produces pseudo random numbers taken from a uniform distribution. In all of the simulations performed the actual random distribution in y produced from this random number generator is kept the same no matter what other parameters are varied. The one exception to this condition is when the contrast paint layer thickness is varied. In this case all of the y coordinates are offset by the same distance which is equal to the paint layer thickness. Thus, although the particles' absolute y coordinates are changed, their relative displacements, one from another, are not.

Simulations for positive x coordinates only were performed. This is because the configurations of the system are symmetrical about $x = 0$.

The step size, h, used in the predictor and corrector formulae was $h = 5 \times 10^{-6}$seconds. This step size means that the number of iterations of the corrector is usually 2. Hull and Creemer (Hull and Creemer (1963)) have found strong empirical evidence to suggest that the most efficient number of iterations is usually 2. (Here efficiency means minimum computation for a given accuracy.) This appears to indicate that the chosen step size, h, is close to the optimum for maximum efficiency.

All of the simulations have been performed on the Amdahl 470/V8 computer at Durham using FORTRAN 77 code. Appendix P3 gives a listing of the program PERM which was used to run the simulations. To run a simulation which calculates the trajectories of 160 particles for 0.1 seconds takes typically 200 CPU seconds. (However, for certain values of the model parameters corresponding to small particles and high viscosity coefficients this number can go up to typically 1500 CPU seconds.) This involves for each particle 2×10^4 evaluations of a single position or velocity component. Thus, the complete trajectory calculation (two position and two velocity components) in 0.1 seconds requires 8×10^4 evaluations. The complete trajectory calculations for 160 particles in 0.1 seconds require 1.28×10^7 evaluations. As the simulations proceed the CPU time required for the evaluations falls. One of the reasons for this is that more and more particles are reaching the bottom of the carrier liquid and for these particles the number of differential equations to be solved is halved. Another reason is that more and more particles are reaching the defect and remaining stationary, requiring no further trajectory calculation. (This accounts for the large increase in CPU time required for small particles and high viscosity coefficients which was mentioned above. Both of the 'CPU-reducing' mechanisms mentioned have the least affect for this unfortunate combination of these two model parameters.) The position and velocity components of all of the particles at 0.1 second intervals are saved in files.

5.11 Conclusion

To conclude this chapter a brief summary of what has been achieved is given. It has been argued that the published literature on MPI has not addressed itself in any great detail to the behaviour of many MPI particles in defect leakage fields and the consequent formation of MPI indications. The author has presented what he believes to be the first serious attempt to model the detailed gross behaviour of such systems. Certain simplifying approximations have been employed and their inclusion has been shown to be plausible. The resulting system of equations which governs the system's behaviour has been derived, and, whilst being complex and irksome and (to the author's knowledge) not being amenable to analytical solution, the equations can, nevertheless, be solved numerically using a powerful digital computer. The method of numerical solution has been described together with some of the computation details. A limitation of the model is that the relative permeability of the steel, μ_r, is treated as a constant. This restriction is imposed in Edwards and Palmers' original derivation of their leakage field equations. Thus, any error in the model arising from this simplification will manifest itself solely in the leakage field components. The next chapter will describe in detail the results obtained from the model in the systematic study of the model parameters.

Chapter 6

The Simulation of MPI Indication Formation

II. Results From the Model

6.1 Introduction

The model presented in the previous chapter is a model of MPI indication formation. The model can be used to study the way the formation and structure of an indication depends on the model parameters. An indication is a single configuration of a many-particle system at a particular time. Thus, in the study of indication formation it is of little value to consider individual particle trajectories in isolation. Rather, one ought to consider the configuration of the many-particle system at a given time. It is a statistical consideration of the system configuration which is important. Thus, all of the simulated indications presented in this chapter are presented in terms of the particle number density (pnd) as a function of distance from the defect. The pnd is defined here as the number of particles per unit distance tangential to the test specimen surface. The pnd as a function of tangential distance from the defect at any one time can be conveniently displayed as a histogram in which the particles are placed in the relevant bin according to their distance from the defect. The height of a given bin at a fixed tangential displacement from the defect is, thus, proportional to the number of particles lying in the range of displacement which is spanned by that bin. The formation of a MPI indication corresponds to a local increase with time in the pnd close to the defect at the expense of a corresponding fall in the pnd in a region more removed from the defect.

The precise values of some of the data presented in this chapter are dependent upon the number of particles used in the simulations. Hence, little importance is to be attached to absolute values. The most important features of the results to be presented deal with *trends* and *differences*. The exact numerical values of quantities such as the pnd or contrast (to be defined shortly) are not important. The ordinate axes of many of the graphs presented in this chapter could just as well be labelled with the phrase 'arbitrary units'.

In order to satisfactorily explain every facet of the behaviour revealed by these simulations it is necessary to follow every particle's behaviour in detail. This approach is not taken in this chapter. Rather, extensive details of the reasons for specific types of particle behaviour are given only when interesting or unexpected features occur.

Figure 6.1 shows a sequence of histograms separated by 0.5s time intervals which demonstrates the manner in which the pnd for one set of the model parameters evolves with time. In this particular example there are 160 particles and the other model parameters are: particle radius, $r = 10\mu$m, $a = 100\mu$m, $b = 1$mm, $H_0 = 2.4$kAm^{-1}, $\mu_r = 1400$, $\eta = 0.5$mPas, $\rho_w = 1$gcm^{-3}, $\rho_p = 5.24$gcm^{-3} (magnetite), contrast paint thickness= 10μm, carrier liquid depth= 0.5mm.

This figure clearly shows the above-mentioned qualitative features of the time-evolution of the pnd. Such a sequence of histograms is typical of the data obtained

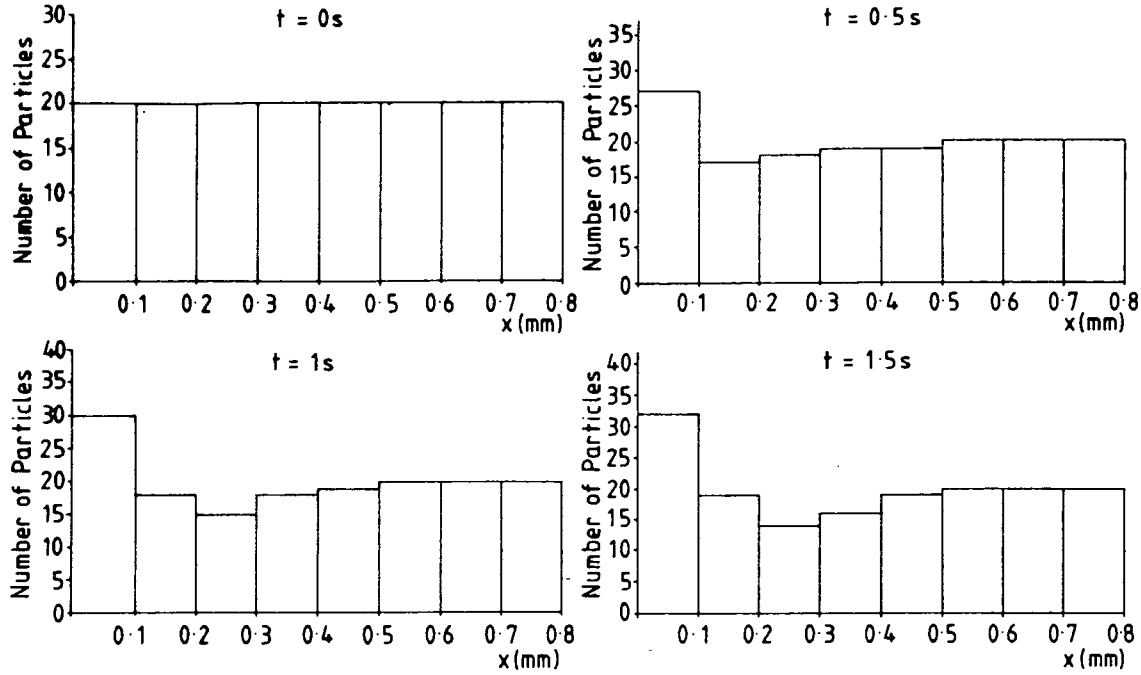

Figure 6.1 A sequence of histograms separated by 0.5s time intervals showing the time evolution of the pnd in the neighbourhood of a defect. The model parameters are given in the text.

in the systematic study of the model parameters. It may be of interest to observe that the pnds such those shown in figure 6.1 bear some resemblance to the concentration distributions employed in the the theory of high gradient magnetic separation (HGMS) (see, for example, Gerber, Takayasu and Friedlaender (1983), Gerber (1984)).

6.2 Contrast

In order to discuss some of the features of an indication quantitively, great use will be made in this chapter of the quantity called 'contrast', C. We define this dimensionless quantity to be the difference between the number of particles in the largest bin and the number of particles in the smallest bin in a pnd histogram at a given time, t. That is, at a given t,

$$C = \text{number of particles in largest bin} - \text{number of particles in smallest bin} \quad 6.1$$

It will be seen that in most cases the largest bin for $t > 0$ is the one immediately adjacent to the defect lip. However, there are cases when this does not happen and the maximum in the pnd occurs at some distance removed from the defect. In such cases the above definition of contrast is still useful and so is still employed. This is chiefly because, although the structure of the indication is more complex, the contrast present is still an important parameter with regard to the delineation of the defect to an observer.

6.3 Particle Size Effects

The effect of varying the radius of the particles was investigated. All of the other parameters were held constant. The simulations were run on a system of 160 particles. The values for the particle radii were $r = 2\mu$m, 10μm, 20μm. The other

model parameters had the following values: $a = 100\mu$m, $b = 1$mm, $H_0 = 2.4$kAm^{-1}, $\mu_r = 1400$, $\eta = 0.5$mPas, $\rho_w = 1$gcm^{-3}, $\rho_p = 5.24$gcm^{-3} (magnetite), contrast paint thickness= 10μm, carrier liquid depth= 0.5mm. Figure 6.2 shows a plot of indication contrast as a function of time for the three particle sizes.

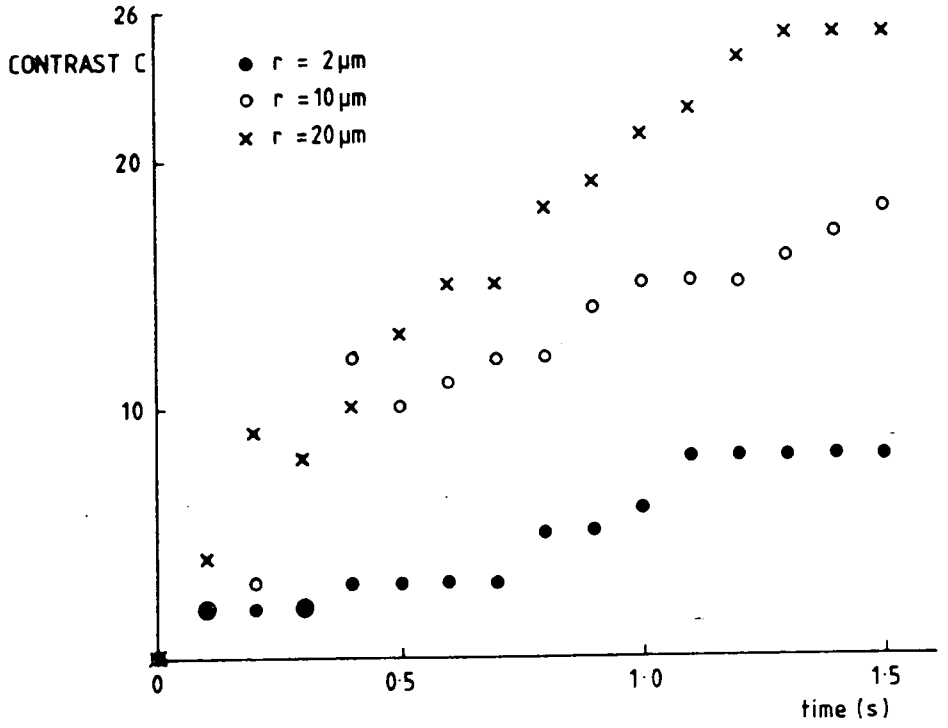

Figure 6.2 Indication contrast as a function of time for a system of 160 particles for three different particle radii. $r = 2\mu$m. $r = 10\mu$m. $r = 20\mu$m. The other model parameters are given in the text.

In the cases of the two larger particle sizes, for $t \geq 0.3$s, the contrast was always simply the difference between the number of particles in bins 1 and 3 (as numbered from left to right in figure 6.1). However, for the 2μm radius particles the maximum in the pnd occurred in bin 3 and increased with time. The minimum occurred in bin 2 and decreased with time, producing a complex indication structure. Figure 6.3 shows a sequence of histograms separated by 0.5s time intervals which represents the time evolution of the pnd for the 2μm radius particles with the maximum resulting in bin 3.

Figure 6.2 shows that for $t \geq 0.5$s, the contrast increases with particle size. Also the rate of formation of contrast increases with particle size. The similarities in the structures of the indications of the 10μm and the 20μm radius particles permits a direct comparison between the two. Figure 6.4 shows the pnd for these two particle sizes after an elapsed time of 1.5s.

From figure 6.4 it is apparent that the pnd further out from the defect than about 0.5mm does not change over a time period of 1.5s for both of these particle sizes. Indeed, for the 2μm particle radius simulation a similar result occurs, with the pnd only losing one particle from the region $x \geq 0.5$mm in a time period of 1.5s. Figure 6.5 shows the number of particles in bins 1 and 3 for the 10μmm radius and the 20μm radius particles.

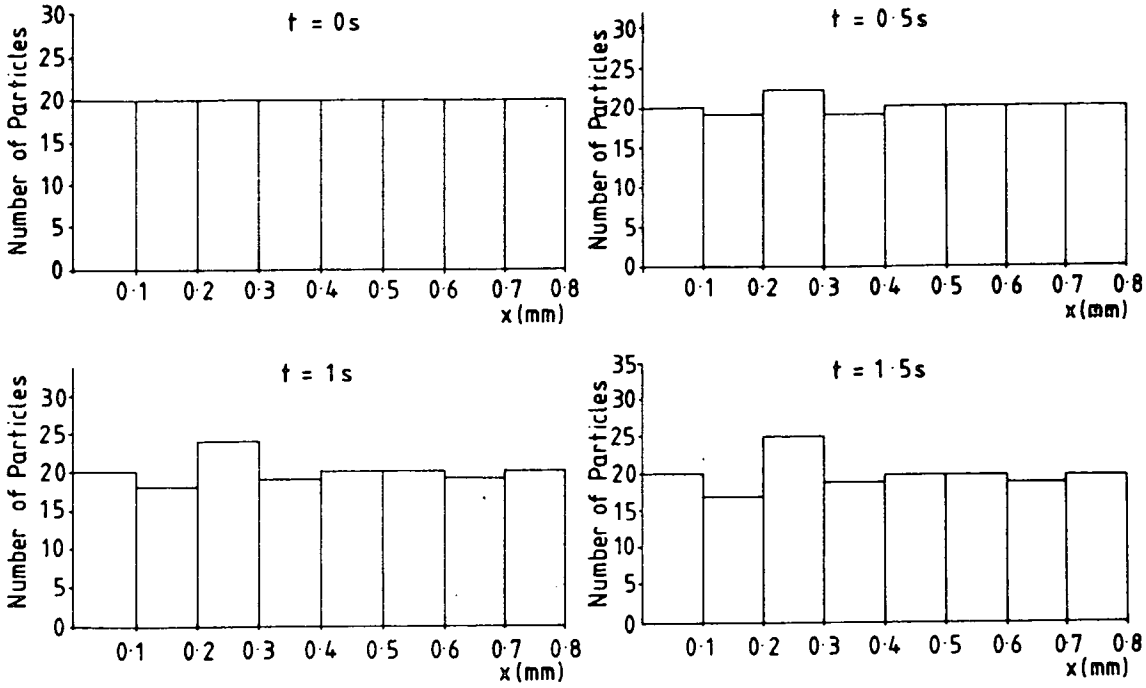

Figure 6.3 A sequence of histograms separated by 0.5s time intervals showing the time evolution of the pnd for the 2μm radius particles with the maximum occurring in bin 3.

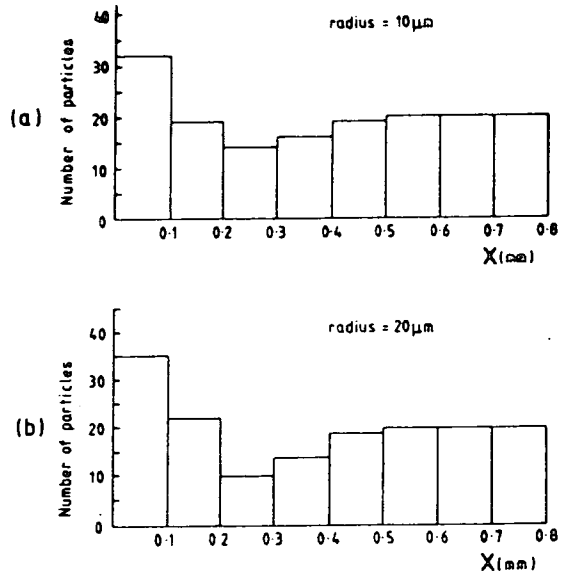

Figure 6.4 The pnds after 1.5s for (a) the 10μm radius particles. (b) the 20μm radius particles.

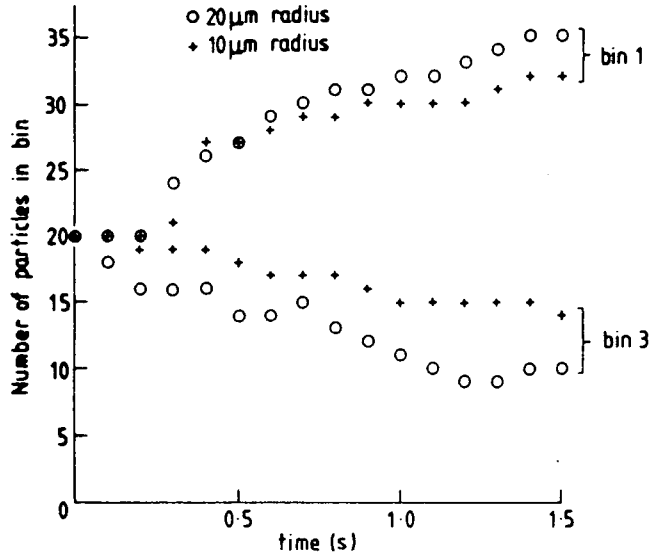

Figure 6.5 The number of particles in bins 1 and 3 as a function of time for the two particle radii. 10μm and 20μm.

Figure 6.5 is an alternative representation of some of the data in figure 6.2, but, as mentioned earlier, the comparison is more direct because of the similarities of the indication structure for the two particle sizes. Both figure 6.2 and figure 6.5 show that an indication is formed in $\sim$ 0.4s for both particle sizes and that, subsequently, the contrast of both indications improves with time.

In summary, therefore, from a practical point of view, these results suggest that it is beneficial to use larger particles in the MPI technique. The larger the particles used, the larger is the contrast formed in a given time, and also, a given contrast is attained in a shorter time. Additionally, in contradistinction to the 2μm radius particles, the maximum in the pnd occurs directly adjacent to the defect for the larger particles, rendering the precise location of the defect more perceptible to the observer. For the 2μm radius particles the maximum is slightly displaced ($\sim$ 0.25mm) from the defect.

6.4 Effects of Carrier Viscosity

The first set of data in the investigation of the effect of the carrier viscosity, η, was obtained from a series of simulations for 160 particles in which all of the parameters except η were held constant. η took the values 0.3mPas, 0.5mPas, 0.89mPas and 1.1mPas. In order to get a 'feel' for these values, observe that at room temperature, for acetone η = 0.3mPas, for water η = 0.89mPas and for acetic acid η = 1.1mPas. In this first instance, the particle radius was $r = 20\mu$m. The other model parameters had exactly the same values as in section 6.3. Explicitly, these were $a = 100\mu$m, b = 1mm, $H_0 = 2.4\text{kAm}^{-1}$, $\mu_r = 1400$, $\rho_w = 1\text{gcm}^{-3}$, $\rho_p = 5.24\text{gcm}^{-3}$ (magnetite), contrast paint thickness= 10μm and carrier liquid depth= 0.5mm. Figure 6.6 shows the contrast against time graph for these four different values of η.

One of the most striking features revealed in this graph is the lack of any significant trend with η during the formation of the indication for 0s $< t \leq$ 1s. However, for $t \geq$ 1.1s, the η-dependence of C is becoming clearer. A plot of the contrast, C, as a function of η at an elapsed time of 1.5s is shown in figure 6.7.

From figure 6.7, the maximum in the contrast occurs for η = 0.7mPas. It is

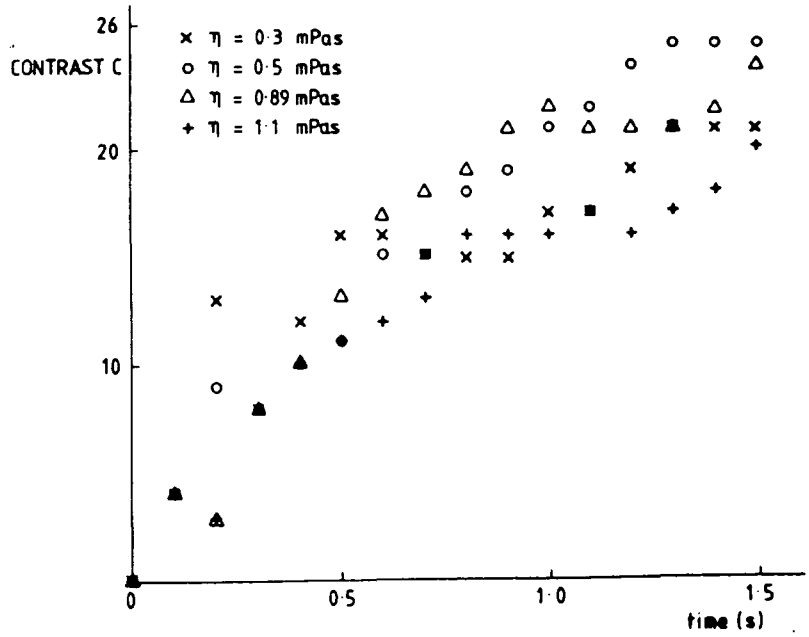

Figure 6.6 Plot of contrast as a function of time for four different values of the carrier liquid coefficient of viscosity, η, and for a particle radius of 20μm.

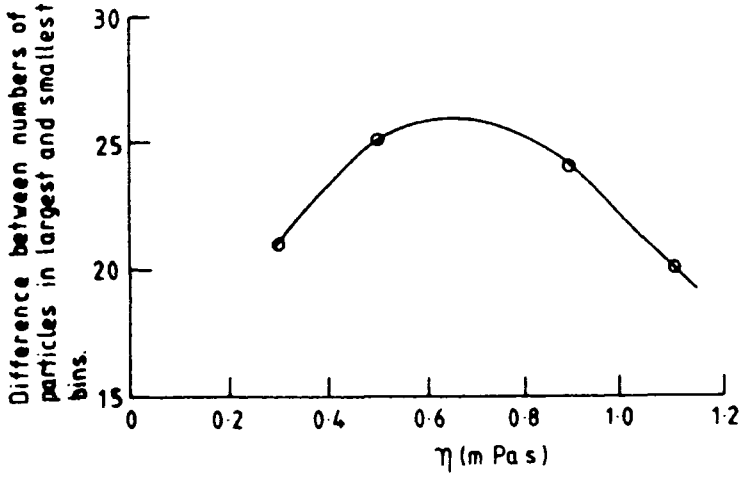

Figure 6.7 The dependence of the contrast, C, upon the carrier liquid coefficient of viscosity, η, at a time $t = 1.5$s for particles having radii of 20μm.

interesting to note that light hydrocarbons and parrafins in the temperature range $0 - 25°$C have coefficients of viscosity of approximately this same value and are widely used as the carrier liquid in commercial MPI inks. The plot also suggests that water ($\eta = 0.89$mPas) is not an optimum carrier liquid for this particle size.

This first set of simulations for the 20μm radius particles also revealed that for the cases of $\eta > 0.3$mPas, the half-width of the indication was ~ 0.5mm, the pnd remaining unchanged further away from the defect than this. However, for the case of $\eta = 0.3$mPas, the half-width of the indication stretched further from the defect, having a value of ~ 0.6mm.

Two more sets of indications were performed in order to investigate further the rôle of η. The same simulation for two more particle sizes was run. The range of the variation of η was the same ($0.3 - 1.1$mPas) and the two additional particle

radii were $r = 2\mu$m and $r = 10\mu$m. All of the other model parameters were held the same as for the first set of viscosity-variation simulations. Figure 6.8 shows the contrast against time graphs for the four different values of η and for the two further particle sizes.

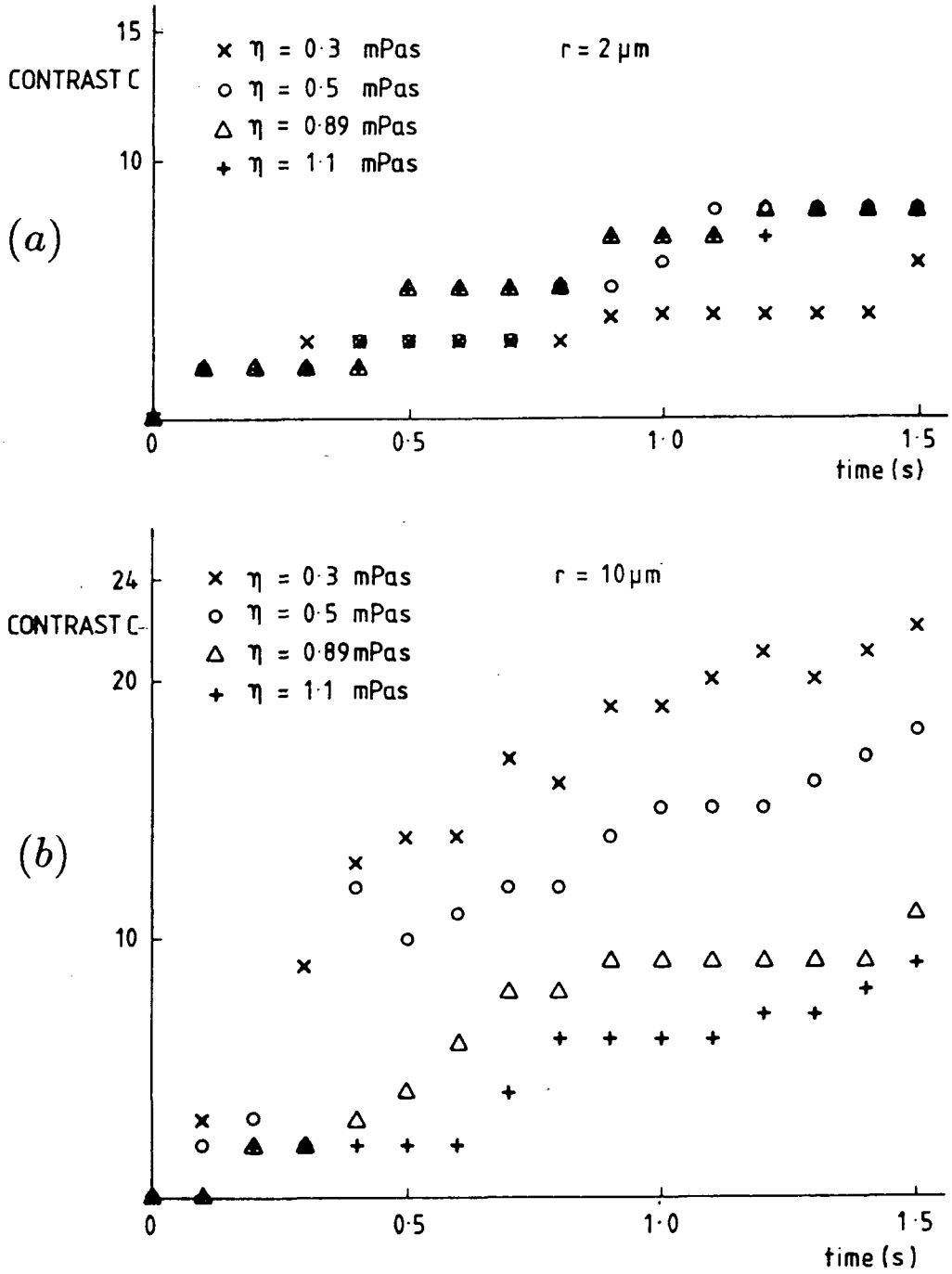

Figure 6.8 Plots of the time-dependence of the contrast, C, for four different η values and the the two particle sizes (*a*) $r = 2\mu$m. (*b*) $r = 10\mu$m.

These graphs reveal a simpler behaviour than for the 20μm radius particles. For the 2μm radius particles there is no significant difference in the behaviour of C in the range $0.5 \leq \eta \leq 1.1$mPas. However, for the lowest η value ($\eta = 0.3$mPas) both the contrast and the rate of formation of contrast are slightly reduced. For the 10μm radius particles, for $t \geq 0.4$s, there is a reduction in both the contrast and the rate of formation of contrast with η in a rather straightforward manner.

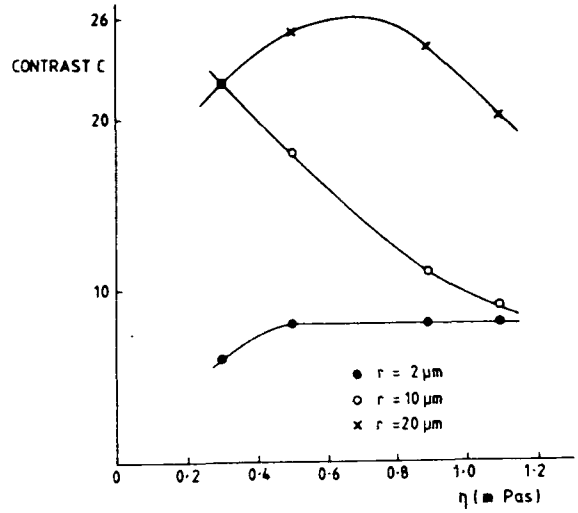

Figure 6.9 The dependence of C upon η at $t = 1.5$s for three values of the particle radius.

Additionally, the peak in the $C - \eta$ plot which was observed for the 20μm radius particles at $t = 1.5$s (figure 6.7) does not occur for the other particle sizes. The $C - \eta$ plots at $t = 1.5$s for these two additional particle sizes, together with the 20μm particle radius case, are shown in figure 6.9. For both of these additional particle sizes, for the full range of the η-variation, the half-width of the indication was never greater than 0.5mm.

In summary, it is apparent that these results indicate a complex behaviour of η, particularly in its relationship with the particle size. For the range of particle sizes investigated here there seems to be a relatively simple relationship between η and C only for the 10μm radius particles. This relationship is essentially an enhancement of the contrast and of the rate of formation of contrast with decreasing η. For the two particle sizes other than $r = 10\mu$m, one of which is larger and the other smaller, there appears to be no markedly significant differences in the dependence of C upon η. For these two particle sizes the contrast is not very sensitive to the value of η. Of course, the magnitude of the contrast is significantly better for the larger particle size considered (figure 6.9) but this result is due entirely to the effect of the particle size alone. Overall, these results suggest that for optimum contrast characteristics, it is beneficial to use a carrier liquid having a coefficient of viscosity at the lower end of the range. In real systems having a particle size distribution, it is apparent from figure 6.9 that a low viscosity would greatly increase the contrast after 1.5s for the 10μm radius particles at the expense of only a slight reduction in the contrast obtainable from both the larger (20μm radius) and the smaller (2μm radius) particles. Essentially, for the 10μm radius particles the dependence of C upon η varies rapidly over the range investigated, whilst for the other two particle sizes, the behaviour of C is less sensitive to the value of η.

6.5 Effect of Defect Size

One would expect that the size of a defect has a significant effect on the contrast, the rate of formation of the contrast and the width of the indication. These effects were investigated by running simulations for 160 particles on four different defect sizes, but such that the aspect ratio, n, was unaltered. The four sets of values for a, b were $a = 10\mu$m, $b = 100\mu$m; $a = 50\mu$m, $b = 500\mu$m; $a = 100\mu$m, $b = 1$mm and

$a = 200\mu$m, $b = 2$mm. The other model parameters were $r = 20\mu$m, $\eta = 0.5$mPas, $H_0 = 2.4\text{kAm}^{-1}$, $\mu_r = 1400$, $\rho_w = 1\text{gcm}^{-3}$, $\rho_p = 5.24\text{gcm}^{-3}$ (magnetite), contrast paint thickness= 10μm and carrier liquid depth= 0.5mm.

Unfortunately, for this set of simulations it is not meaningful to investigate the contrast-time behaviour, as was done in the previous sections, using the same bin resolution for the pnd. This is because, as a consequence of the variation in a moving the half-width of the defect across bins 1 and 2, the indication structure is highly sensitive to both the number of particles used in the simulation and the width of the bins. As an example, the region of the largest magnitudes of the flux leakage gradients for the smallest defect considered here essentially does not extend spatially beyond bin 1. Thus, the number of particles subject to this gradient is significantly reduced relative to those cases for which the width of the defect is considerably larger. Without both increasing the number of particles and increasing the resolution of the bin size, caution should be exercised in interpreting changes in contrast occurring for such a small number of particles. Because of the absence of such refinements, for the particular set of simulations reported in this section, reliable contrast-time plots are not simply derivable from the pnd distributions. This is the only set of simulations presented in this chapter for which this consideration is of relevance.

Figure 6.10 shows the pnd histograms after 1.5s for the four defect sizes investigated. The dotted line represents the relevant value of a for each defect.

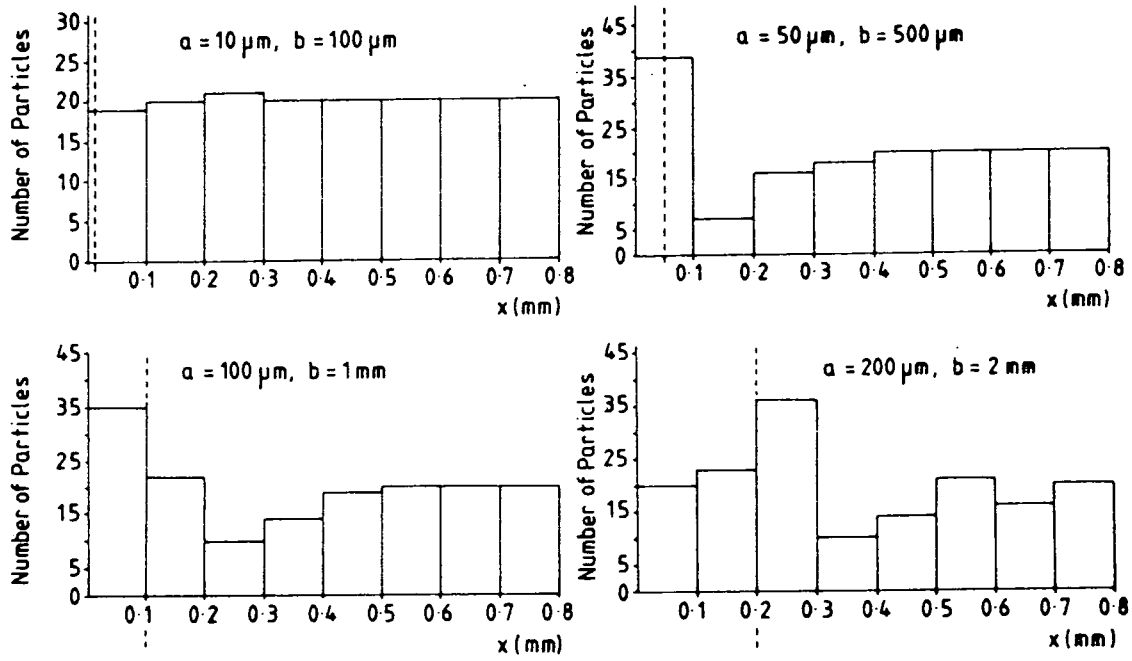

Figure 6.10 The pnd configurations after 1.5s for the four sizes of defects, each having the same aspect ratio, n. The dotted lines represent the value of a on the x-axis.

Leaving aside the problems associated with the contrast, it is apparent that the width of the indication increases with the width of the defect. This conforms

with both expectations and practical experience. Another interesting feature which is present is that for the case of the smallest defect ($a = 10\mu$m, $b = 100\mu$m) the maximum in the pnd occurs in bin 3, that is, significantly removed from the defect. Figure 6.11 shows the time evolution of the pnd for this smallest defect.

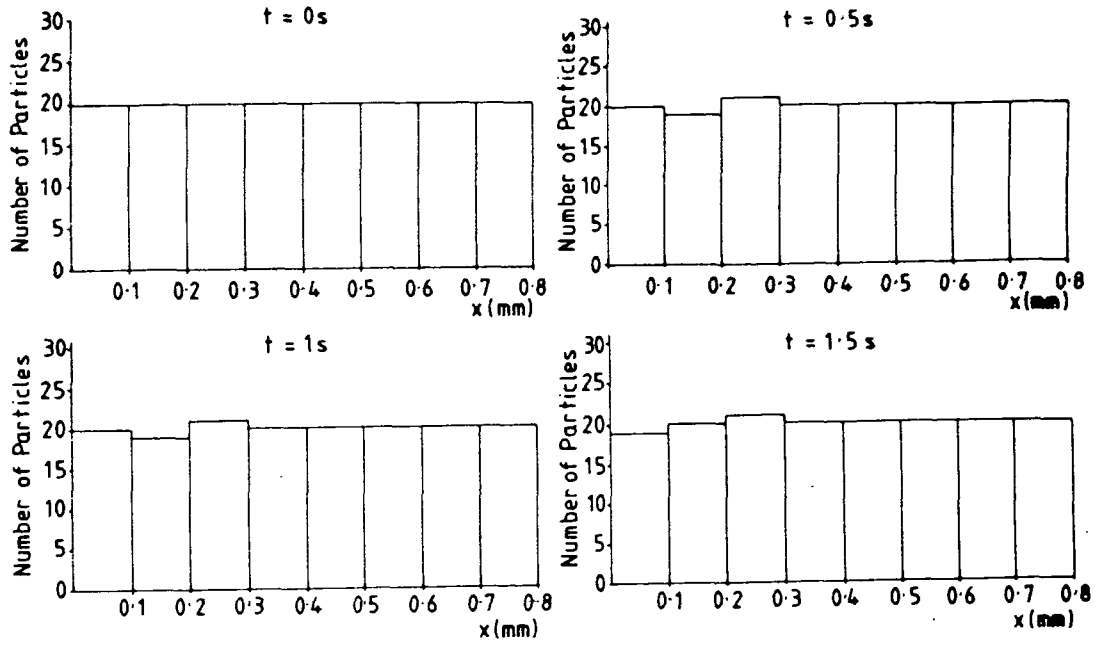

Figure 6.11 The time evolution of the pnd for the smallest defect ($a = 10\mu$m, $b = 100\mu$m), showing the maximum occurring in bin 3.

The small size of the maximum is directly attributable to the small spatial extent of the leakage flux gradients beyond bin 1. The maximum arises from the migration of one particle from bin 1, that is, *away* from the defect. Such an effect occurs because of a reversal in the sign of the leakage field gradient in passing through a stationary point of the leakage field. This effect is present in all of the simulations but is seldom so obvious because it is usually masked by superimposed particle motions from right to left occurring within the same bin in the region having an oppositely-sensed magnetic field gradient.

6.6 Effect of Magnetizing Field

In Edwards and Palmers' equations for the leakage flux components of a semi-elliptical defect the magnetizing field, H_0, appears simply as a prefactor. Also for $\mu_r \gg n$, then the leakage flux components are essentially independent of the relative permeability, μ_r. This was the régime in which the effect of the magnetizing field, H_0, was investigated. These two parameters took the values $\mu_r = 1400$, $n = 10$. It would seem reasonable to expect that the rate of formation of contrast would increase with H_0. In order to investigate this postulate, a set of simulations for 160 particles were performed in which all parameters were held constant except H_0. The other model parameters were $r = 20\mu$m, $\eta = 0.5$mPas, $a = 100\mu$m, $b = 1$mm, $\mu_r = 1400$, $\rho_w = 1\text{gcm}^{-3}$, $\rho_p = 5.24\text{gcm}^{-3}$ (magnetite), contrast paint thickness= 10μm, carrier liquid depth= 0.5mm. The values used for H_0 were

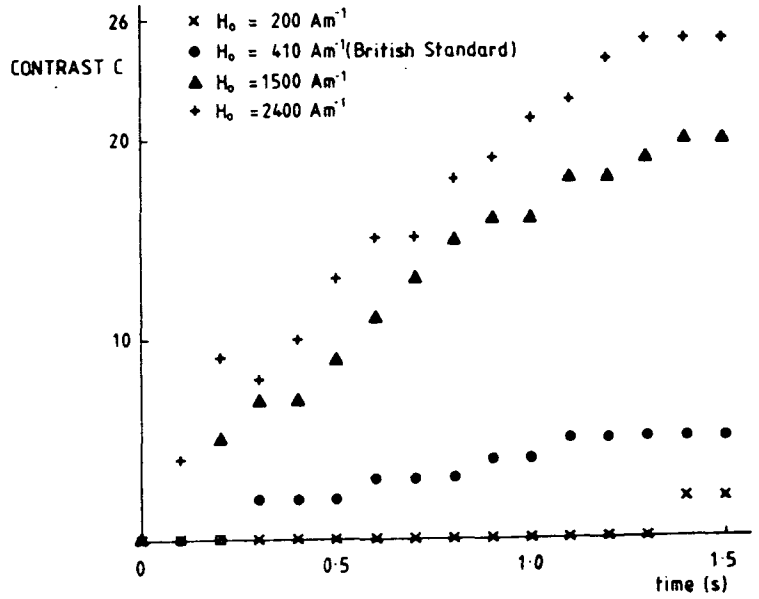

Figure 6.12 The plot of contrast as a function of time for four different values of the magnetizing field. H_0. with all of the other model parameters held constant.

$H_0 = 200\text{Am}^{-1}$, $H_0 = 410\text{Am}^{-1}$ (the British Standard minimum for the value of $\mu_r = 1400$ (BS 6072 (1981))), $H_0 = 1500\text{Am}^{-1}$ and $H_0 = 2400\text{Am}^{-1}$.

Figure 6.12 shows the contrast-time plot obtained for this investigation. The most significant feature of figure 6.12 is the clear trend of the increase in slope of the curves with H_0, as one would naïvely expect. The differences in the absolute values of the contrast attained at a given t are not significant. If the lower-field simulations were run for longer time periods they would eventually attain contrasts comparable with those of the larger-field simulations. The significant trend is the increase in the speed of the formation of the indication with magnetizing field. The simulations also showed that the rate of increase in the width of the indication with time also increases with H_0. Again, however, for the low-field indications, widths comparable with those of the larger-field simulations would result if the simulations were run for longer time periods.

6.7 Effect of Defect Aspect Ratio

For the investigation of the effect of the defect aspect ratio on the indication formation, a defect of constant half-width, a, was used. The depth, b, was varied such that $n(= b/a)$ ranged from 1 to 100. The constant value of a was $a = 100\mu$m. The values of b were $b = 100\mu$m, $b = 0.5$mm, $b = 1$mm, $b = 5$mm and $b = 10$mm. The simulations were run on systems of 160 particles and the other model parameters were $r = 20\mu$m, $\eta = 0.5$mPas, $\mu_r = 1400$, $H_0 = 2.4\text{kAm}^{-1}$, $\rho_w = 1\text{gcm}^{-3}$, $\rho_p = 5.24\text{gcm}^{-3}$ (magnetite), contrast paint thickness= 10μm, carrier liquid depth= 0.5mm.

The contrast-time plots for these data sets are shown in figure 6.13. It can be seen that the behaviour for the case $b = 100\mu$m ($n = 1$) deviates markedly from all of the others. For the other cases the behaviour can be divided into two regions. The first region corresponds to the time interval $0 < t < 0.9$s. In this region there occurs no significant trend with defect aspect ratio. The second region is the time interval $t \geq 0.9$s. It is apparent that in this region there is an increase in both the contrast and the rate of formation of contrast with defect aspect ratio.

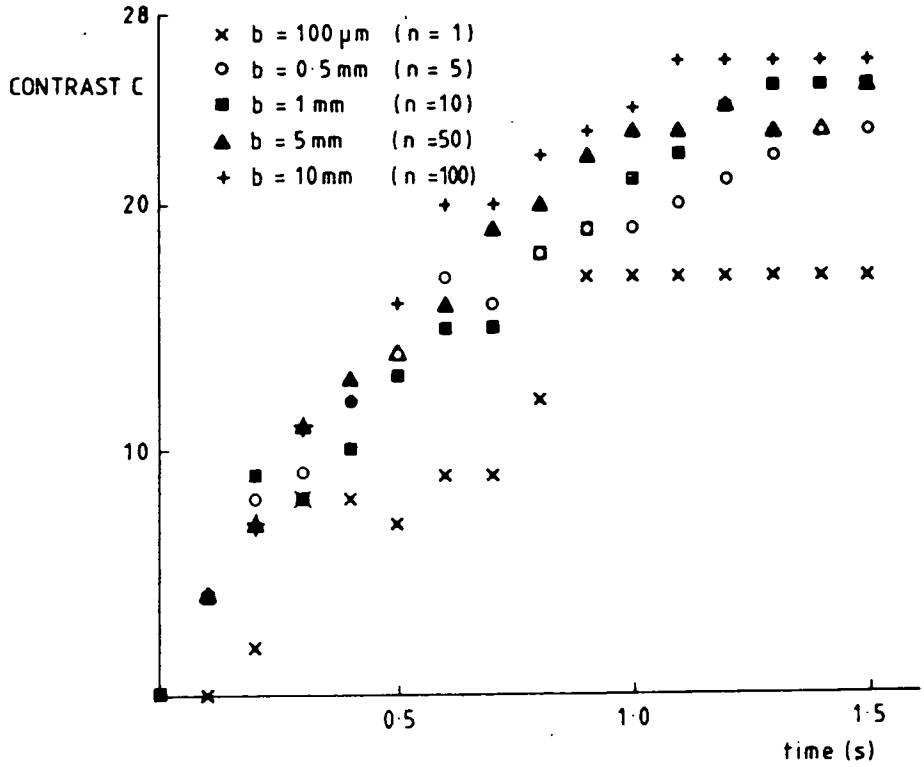

Figure 6.13 The contrast-time plot for five different values of the defect aspect ratio.

In Chapter 3 the relationship between defect width and the maximum value of the B_{0y} component of the leakage field was discussed. Between these two quantities there is an approximate proportionality. The behaviour revealed by these indication formation simulations can be broadly explained with reference to these ideas. The larger the defect depth, the larger are both the particles' magnetizations (provided they are unsaturated) and the quantity $\partial B_{0y}/\partial x$. In this way, the magnetic force attracting the particles to the defect is enhanced.

The case $b = 100\mu$m ($n = 1$) corresponds to a semi-circular defect and reveals a less straightforward type of behaviour. The maximum in the pnd for $t \geq 0.8$s, unlike all of the other cases, occurs in bin 4. This behaviour is explained simply by a reversal in the sign of the total flux gradient in the regions approximately given by $x \leq 0.09$mm and $x \geq 0.18$mm for those particles having y coordinates $\simeq 0.01$mm, or, in other words, those particles which have hit the test specimen-carrier liquid interface. The flux gradient attracts to the defect only those particles which lie between these two limits for this particular value of y. However, most particles which are not in this attractive region and for which $x < 0.4$mm hit the bottom of the carrier liquid and then move in the direction of increasing x, producing the maximum in the pnd in bin 4.

6.8 Effect of Contrast Paint Layer Thickness

The British Standard, BS 5044 (1973), recommends that the thickness of the contrast paint layer should be no greater than approximately 25μm. The reasons given are that layers thicker than this would seriously affect the sensitivity of the method and would increase the likelihood of both not detecting finer defects and of misinterpreting the indications present. The investigation reported in this section clearly shows the sound reasoning behind this particular recommendation of this

British Standard.

The simulations investigated the effect of varying the contrast paint layer thickness. The simulations were performed on systems of 160 particles and all of the other model parameters were held constant. The contrast paint layer thicknesses were 10μm, 50μm, 0.1mm and 0.2mm. The other model parameters had the values $r = 20\mu$m, $a = 100\mu$m, $b = 1$mm, $\eta = 0.5$mPas, $\mu_r = 1400$, $H_0 = 2.4\text{kAm}^{-1}$, $\rho_w = 1\text{gcm}^{-3}$, $\rho_p = 5.24\text{gcm}^{-3}$ (magnetite) and carrier liquid depth= 0.5mm. In all of the simulations, the relative displacements of all of the particles, one from another, at $t = 0$ remain unaltered. However, the absolute values of the y coordinates did vary, offset from $y = 0$ by an amount dictated by the contrast paint layer thickness.

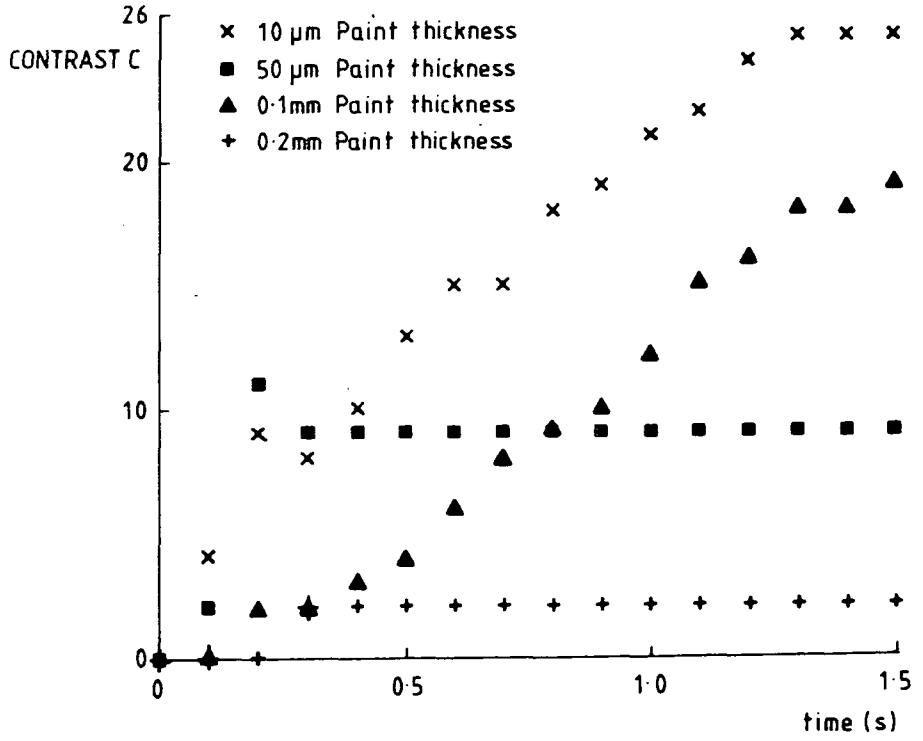

Figure 6.14 The contrast-time graphs for four different values of the contrast paint layer thickness.

The contrast-time plots for this study are shown in figure 6.14. This graph demonstrates that a complex behaviour occurs. The advantage of using the 10μm paint thickness, in terms of the enhancement of both the contrast attained and the rate of formation of contrast, is immediately perceptible. The result from the thickest paint layer-simulation, 0.2mm, is similarly straightforward: both the contrast attained and the rate of formation of contrast are drastically reduced. However, the behaviour for paint layer thicknesses between these two extremes is not simple and the trend seems confused. In increasing the paint layer thickness the maximum in the pnd becomes more and more removed from the defect—it occurs in bin 3 for the 0.2mm paint thickness-simulation. The explanation for this behaviour lies in the observation that as y increases, the effective spatial extent in the x direction of the leakage field gradient increases although the magnitude of the leakage field decreases. Also, as y increases, the maximum of the total leakage field becomes more removed from the defect. These two factors combine to produce the

maximum in the pnd at some distance displaced from the defect.

6.9 The Point Particle Approximation

The point particle approximation was mentioned in the previous chapter. The approximation centres on the treatment of the particles as having point position coordinates, despite their having volumes. It is equivalent to treating the magnetic field as having a constant magnitude and direction over the distance of one particle diameter. The results presented in this chapter should be viewed in the light of the validity or otherwise of the point particle approximation. It would be expected that as the particle size increases, so the validity of the approximation is reduced. Additionally, a further point of relevance is the magnitude of the field gradient and, specifically, whether it is justifiable, for the case of a spatially rapidly varying magnetic field, to treat the magnetic field as being constant over the distance of one particle diameter. As well as for large particles, it would be expected that the validity of the approximation diminishes for simulations involving small defects. In these cases, for large particles ($r \sim a$), there would be an appreciable variation of the field over the distance of one particle diameter and the evaluation of the magnetic force term in the equations of motion would be subject to error. In order to overcome this problem, some more sophisticated method of evaluating the magnetization which takes into account the non-constant nature of the field would have to be employed.

The result of the simulations in section 6.3 indicated that in the practice of MPI it is desirable to use particles as large as possible because of the benefits of both increased contrast and increased rate of formation of contrast. This conclusion is in contradiction to current thinking and practice in MPI. In the world of MPI there is currently a drive to use smaller and smaller particles—right down to superparamagnetic-sized particles. The reason for this is that empirical evidence suggests that the sensitivity of the technique increases with decreasing particle size. In addition to this, as was mentioned in Chapter 3, it has been argued by Shelikhov and Aleksandrov (1977) that the use of large particles is undesirable in MPI both because they are insensitive to leakage fields and because they obscure the finer indications delineated by finer particles. Hence, the reasons for this contradiction need to be clarified.

This clarification requires a detailed consideration of the applicability of the point particle approximation for large particles interacting with defect leakage fields. For those cases for which $r \sim a$, the use of the point particle approximation generally results in an over-estimation of the magnetic force on the particles. One way of visualizing this is to consider a spatially extended particle near a defect of roughly the same width as the particle diameter. Treating the leakage field as being effectively a narrow 'peak' or 'spike' highly localized at the defect, one can conceive of a large particle, one part of which overlaps the effective leakage field and the remainder of which is essentially outside of the leakage field. Such particles will only be subject to a magnetic force which is proportional to that volume of the particle which is actually located in the leakage field, and, notably not proportional to the volume of the whole particle itself. Thus, the real magnetic force is less than that calculated from the use of the point particle approximation in which the magnetic force is proportional to the volume of the *whole* particle. It is, thus, apparent how, for certain particle and defect sizes, errors can arise from the use of the point particle approximation. Although this argument has dealt with the spherical particles

used in the model, it is equally applicable to real systems for which the particles are non-spherical. The argument is in full accord with the reasoning of, for example, Shelikhov and Aleksandrov and fully explains why particles are insensitive to defects much smaller than the particle size.

We have mentioned how, currently, MPI operators are seeking to use smaller and smaller particles in the quest for the ability to increase the sensitivity of the method. The model formulated in the previous chapter provides some insight into some of the processes occurring in the MPI indication formation process when using much smaller particles than those used in either this author's model or in 'conventional large particle' magnetic inks. The previous chapter stated that Brownian motion becomes appreciable for particles having diameters less than $\sim 0.7\mu$m. Hence, particles less than this critical size, for example, superparamagnetic-sized particles, would be unsuitable in magnetic inks unless they formed into aggregates larger than the critical size of $\sim 0.7\mu$m. The reason for this is that the stochastic nature of the Brownian motion would prevent a rapid migration of single particles in the indication formation process. Thus, an aggregation formation process producing aggregates greater than $\sim 0.7\mu$m diameter would be a prerequisite in the successful use of these finer particle systems as replacements for conventional magnetic inks. In particular, a magnetic liquid which is stable against field-induced aggregation would be totally unsuitable because the necessary aggregates could not form. There may, however, be some benefit in using a highly aggregated magnetic liquid or one which is carefully manufactured to undergo an irreversible field-induced aggregation process as soon as the liquid is placed on the magnetized test specimen.

6.10 Discussion and Conclusions

In the previous chapter it was stated that some MPI operators believe that a 'saturation'-type of indication configuration, in which, after the formation of the indication, the size of the indication does not increase beyond a certain size, is caused by 'bridging'. The bridges of particles across the defect significantly reduce the magnitude of the leakage field and so prohibit the subsequent build-up of further particles at the defect. Such a mechanism for the 'saturation'-type behaviour need not be invoked if one considers the results presented in this chapter. It is clear that in several of the contrast-time plots presented, indeed, there eventually appears a saturation behaviour; the contrast remains approximately the same after an initial burst of contrast increase. Even with the absence of 'bridging' effects in the model, this feature occurs, and it is simply because of the depletion of the number of particles in the bins surrounding those bins constituting the maximum in the pnd. The number of particles available to form the initial indication is limited and so the system eventually enters an approximately time-independent configuration—particles in the furthermost bins from the defect playing a negligible rôle in the initial indication formation. Perhaps this explains the 'saturation'-type behaviour, there being no need to invoke a bridging-type process.

This chapter has presented some results obtained from the model developed in Chapter 5. Most of the results are relatively straightforward. However, it must be remembered that simplistic explanations for the results should be avoided and that the apparent simplicity often masks a diversity of effects. The results concerning the rôle of the carrier coefficient of viscosity, η, especially with regard to its relationship to the particle size, are complex and particularly interesting. One of the most important benefits of the model is the insight its development and use can

provide into the various types of particle behaviour exhibited in the interaction of the particles with the leakage fields.

Chapter 7

Experimental Observations of MPI Particles in Magnetic Field Gradients

7.1 Introduction

This chapter describes an experimental study of the behaviour of individual suspended magnetic particles in magnetic field gradients. The field gradients are essentially constant and are produced by a carefully designed coil system. The particles' motions are studied using optical microscopy.

Apart from any intrinsic value and interest associated with the study, the study is intended to constitute something of a test of the theoretical formalism developed and used in Chapters 5 and 6. The field gradients used, however, are necessarily of a simpler form than those of Edwards and Palmer (1986) which are used in the theoretical model. The complexity of designing and constructing a coil system capable of synthesizing field gradients like those of defect leakage fields would be impractical. The exercise would be further confounded by two more constraints. Firstly, there would be a real uncertainty about the coil configuration producing the field distribution it is intended to produce, bearing in mind that accurate experimental measurements would be almost impossible. Secondly, the whole coil system has to be compatible with an optical microscope operating in transmission mode—that is, the transmitted light must not be obstructed by any coil elements. A benefit of using the simpler field gradients, however, is that the equations of motion can be solved analytically. Thus, the comparison between the relevant theory and experiment is very simple and no recourse to approximate numerical solutions is necessary.

7.2 Outline of the Experiment

A brief outline of the experiment is given here. A detailed description will follow. The field gradient produced by the coil system is constant over distances of $\sim$ 0.2mm. Hence, for particles suspended in a carrier moving over distances a lot less than this the equations of motion can be formulated in which the field gradient is treated as a constant. Only one of the equations of motion is of any interest to us. This is the x-equation where x is both the direction in which the field gradient is non-zero and a direction which lies in the plane of the field of view of the microscope (orthogonal to the axis of the microscope objective). It is only in the x direction that particle motion arising directly from the field gradient can be observed by the microscope. The orthogonal direction (the y direction) would be expected to encompass gravity/bouyancy-affected and maybe field gradient-affected particle motion but since this direction is parallel to the axis of the microscope objective it cannot be 'seen' in the microscope.

Thus, the solution of the equation of motion for the particle velocity component in the x direction, v_x, gives a quantity which can be observed directly using the microscope. The analytical solution for v_x is a function of the particle volume, V, the particle magnetization, M, the field gradient in the x direction, dB_0/dx, and the carrier liquid coefficient of viscosity, η. All of these quantities are known in the

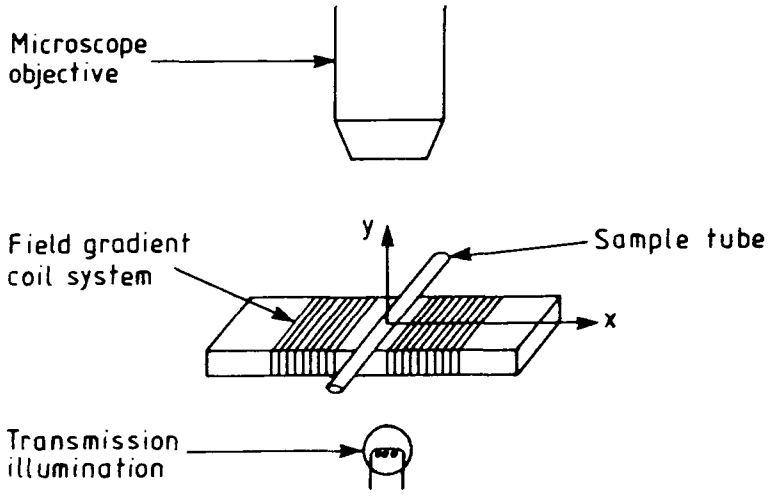

Figure 7.1 The principle components of the experimental arrangement and the coordinate system used.

experimental situation. Hence, the main idea of the experiment is to compare the experimental velocities in the x direction for individual particles with the theoretical prediction calculated from a knowledge of all of these known variables. An overview of the experimental arrangement and the coordinate system is shown in figure 7.1.

Two different samples of particles were used. The first was a sample of particles of Magnaflux 7C Concentrate and the second was of acicular particles of chromium dioxide (CrO_2) tape particles.† These tape particles nominally have length to width dimensions of $0.5 \times 0.05\,\mu$m. Later chapters will show that Magnaflux 7C Concentrate was determined by electron and X-ray diffraction to be magnetite. In both cases the carrier liquid used was distilled water.

7.3 The Equations of Motion

The derivation of the equations of motion for a single magnetic particle in the experimental field gradient closely follows the derivation of the equations of motion in Chapter 5. For this reason the present derivation is a lot more concise.

At this point it is necessary to be more specific about the components of the magnetic field. The magnetic field, $\mathbf{B}_0$, behaves as

$$\mathbf{B}_0 = \hat{\mathbf{i}} B_{0x}(x) + \hat{\mathbf{j}} B_{0y}(x) \qquad 7.1a$$

and, at a given x,

$$B_{0x} \gg B_{0y}. \qquad 7.1b$$

Therefore, $\mathbf{B}_0$ can be approximated by

$$\mathbf{B}_0 \simeq \hat{\mathbf{i}} B_{0x}(x) \qquad 7.1c$$

In other words, there are no y or z components of the field and the field gradient is non-zero only in the x direction. Later the details of the design of the coil arrangement will be presented showing how the features of this magnetic field behaviour

† Supplied by Dr. R.A. McCurrie, Bradford University, UK.

are realized. However, further justification for this form of $\mathbf{B}_0$ emerges *a posteriori*. When a particle is observed to be moving in the x direction it appears to remain travelling on a plane of constant y—that is, once focussed by the microscope, it remains in focus throughout its occupation of the whole field of view. Hence, particle motion in directions orthogonal to the x direction arising from field gradients in those directions does not appear to occur. This supports the assertion that the field gradient is non-zero only in the x direction.

Provided all of the conditions used in Chapter 5 concerning the neglect of interparticle interactions are observed the terms contributing to the particle's energy are exactly the same. The generalized coordinates for a single particle are (x, y, θ). Here (x, y, θ) have exactly the same definitions as do (x_i, y_i, θ_i) in Chapter 5 but the subscripts are now redundant. Hence, the Lagrangian for a single particle is

$$L = \tfrac{1}{2}\rho_p V(\dot{x}^2 + \dot{y}^2) + V\mathbf{M}(\theta)\cdot\mathbf{B}_0(x) - Vgy(\rho_p - \rho_w) \qquad 7.2$$

All of these symbols have the same meanings as in Chapter 5.

The Rayleigh dissipation function is

$$R = \eta c(\dot{x}^2 + \dot{y}^2) \qquad 7.3$$

where c is a constant analogous to c_i in Chapter 5.

Lagrange's equations of motion for the particle in the non-conservative (dissipative) system are

$$\frac{d}{dt}\left(\frac{\partial L}{\partial \dot{q}_i}\right) = \frac{\partial L}{\partial q_i} - \frac{\partial R}{\partial \dot{q}_i} \quad \text{for } i = 1, 2, 3, \text{ with } q_1 = x,\ q_2 = y,\ q_3 = \theta \qquad 7.4$$

Chiefly we are interested in the x equation. However, we also need to know how θ behaves, that is, the orientation of the magnetization of the particle. Substitution of equations (7.2) and (7.3) into equation (7.4) yields for the x and θ equations of motion

$$\ddot{x} + \frac{2\eta c}{\rho_p V}\dot{x} - \frac{\mathbf{M}(\theta)}{\rho_p}\cdot\frac{d\mathbf{B}_0}{dx} = 0 \qquad 7.5a$$

$$\mathbf{B}_0\cdot\frac{d\mathbf{M}}{d\theta} = 0 \qquad 7.5b$$

Using equation (7.1c) and the relation $\mathbf{M}(\theta) = M(\hat{\mathbf{i}}\cos\theta + \hat{\mathbf{j}}\sin\theta)$ in equation (7.5b) yields

$$M B_{0x}\sin\theta = 0 \qquad 7.6a$$

or

$$\theta = n\pi \quad , \quad n = 0, \pm 1, \pm 2, \ldots \qquad 7.6b$$

Put another way, $\mathbf{M}$ is always parallel to the x axis, or $\mathbf{M} = \hat{\mathbf{i}}M$. This means that the x equation of motion (7.5a) becomes

$$\ddot{x} + \frac{2\eta c}{\rho_p V}\dot{x} - \frac{M}{\rho_p}\frac{dB_0}{dx} = 0 \qquad 7.7$$

In this equation dB_0/dx is a constant which, for convenience, will be called G, that is, $(dB_0/dx) = G$.

The elementary solutions of this equation for the velocity in the x direction, $v_x(=\dot{x})$, and the position, x, respectively are

$$v_x = \frac{MVG}{2\eta c}\left[1 - E\exp\left(-\frac{2\eta ct}{\rho_p V}\right)\right] \qquad 7.8a$$

and

$$x = \frac{MVGt}{2\eta c} + \frac{MV^2G\rho_p}{(2\eta c)^2}\left[E\exp\left(-\frac{2\eta ct}{\rho_p V}\right) - F\right] \qquad 7.8b$$

Here E and F are dimensionless constants of integration. $F = E$ if $x = 0$ at $t = 0$. $F = E = 1$ if both $x = 0$ and $v_x = 0$ at $t = 0$. For simplification, the case $F = E = 1$, or $x = 0$ and $v_x = 0$ at $t = 0$, will be assumed. These solutions can be considerably simplified by virtue of the fact that, except at $t \ll 1$s, $\exp(-2\eta ct/\rho_p V) \simeq 0$. This can be demonstrated by considering the case of spheres ($V = \frac{4}{3}\pi r^3$, $c = 3\pi r$) and inserting 'typical' values. Thus, for $\eta = 0.7$mPas, $\rho_p = 5238\text{kgm}^{-3}$ and $r = 10\mu$m then $(2\eta c/\rho_p V) = (9\eta/2\rho_p r^2) = 6014\text{s}^{-1}$. This means that $\exp(-2\eta ct/\rho_p V)$ falls to $\frac{1}{100}$th of its value at $t = 0$ in 7.66×10^{-4}s. In a similar way, again for spheres, and using the further 'typical' values $G = 0.2\text{Tm}^{-1}$ and $M = \frac{1}{100} \times 4.71 \times 10^5\text{JT}^{-1}\text{m}^{-3}$ ($\frac{1}{100}$th of the saturation magnetization of magnetite) then at $t = 1$s the quantity $(MVGt/2\eta c) = 3 \times 10^{-3}$m and the quantity $[MV^2G\rho_p/(2\eta c)^2] = 5 \times 10^{-9}$m. Hence, the second term on the right hand side of equation (7.8b) is negligible in comparison with the first.

Hence, except at very small t, the solutions are essentially

$$v_x = \frac{MVG}{2\eta c} \qquad 7.9a$$

and

$$x = \frac{MVGt}{2\eta c} \qquad 7.9b$$

7.4 The Field Gradient Coil System

The coil system is essentially a modification of that used by J.E. Knowles for magnetic measurements on single γFe_2O_3 tape particles (Knowles (1980)). Indeed, the whole experimental arrangement is based on that of Knowles. Essentially, Knowles's coil system consisted of two similar coils wound on a glass former of cross-section 3.5×0.99mm, as is shown in figure 7.2.

Each coil consisted of 13 turns of 63μm wire. Between the two coils was a recess 0.2mm deep which accommodated the disposable glass tubes containing the suspended particle samples. The recess was of such a depth that the sample in the tube was coplanar with the upper surface coil windings. Knowles determined the field produced by his coil system by a calculation, presumably based on a knowledge of the current and the coil dimensions.

The coil system used in this study is essentially of the same design. However, in order to produce a field gradient, one of the coils has more turns on it than the other, and furthermore, all of the dimensions are somewhat enlarged. The coil former is derived from a glass microscope slide of cross-section 1.45×26mm. A recess of depth 0.1mm and width 1.5mm to accommodate the sample tube is

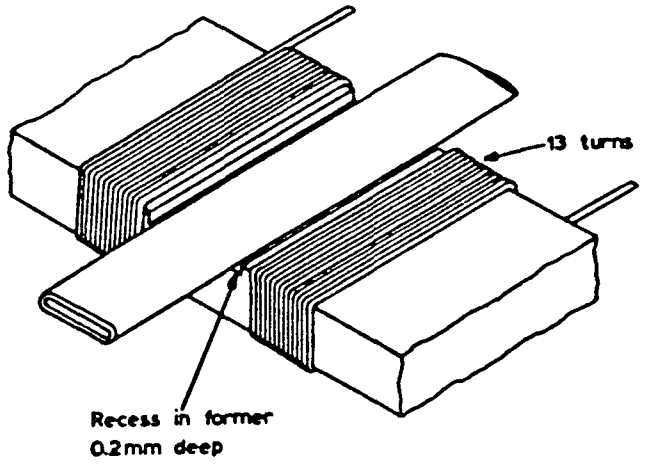

Figure 7.2 The coil system and sample tube used by Knowles (after Knowles (1980)).

provided by bonding two glass microscope cover slips of thickness 0.1mm side by side on the upper surface of the microscope slide, but separated from each other by 1.5mm. This increases the thickness of the coil former to 1.55mm. The two sets of coil windings are separated from each other by a 2mm gap and are positioned equidistantly on either side of the sample tube recess. Each set of coil windings is 3.5mm wide. The coil windings on the underside of the coil former are positioned clear of the microscope stage by means of two feet made of glass strip bonded on to the underside of the coil former outside of the coil system. Figure 7.3 illustrates the arrangement together with all the relevant dimensions.

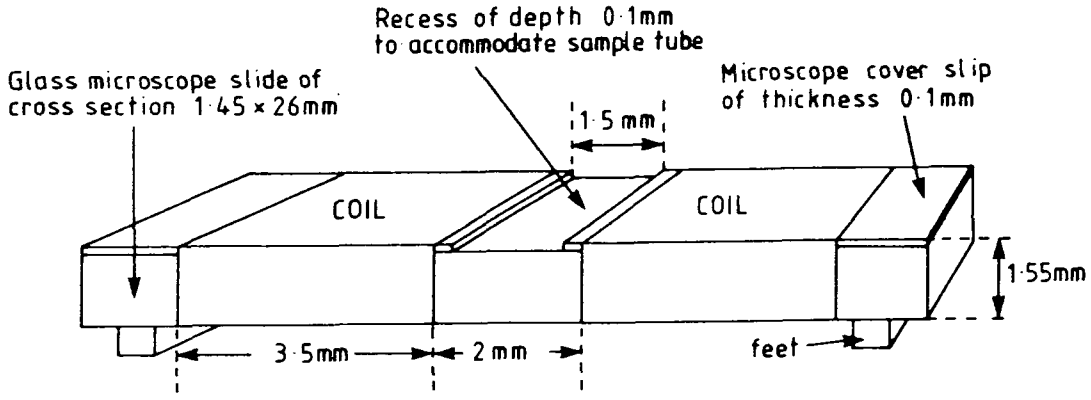

Figure 7.3 The field gradient coil system showing all the relevant dimensions.

The coils are wound from swg 40 (diameter 0.1219mm) enamelled copper wire. Each coil is wound with 40 turns arranged in 2 layers of 20 turns each, with the two coils connected in series. This coil configuration provides a constant field. To provide the field gradient one of the coils is wound with a further 40 turns, again in 2 layers of 20 turns each, on top of the existing turns. This additional gradient

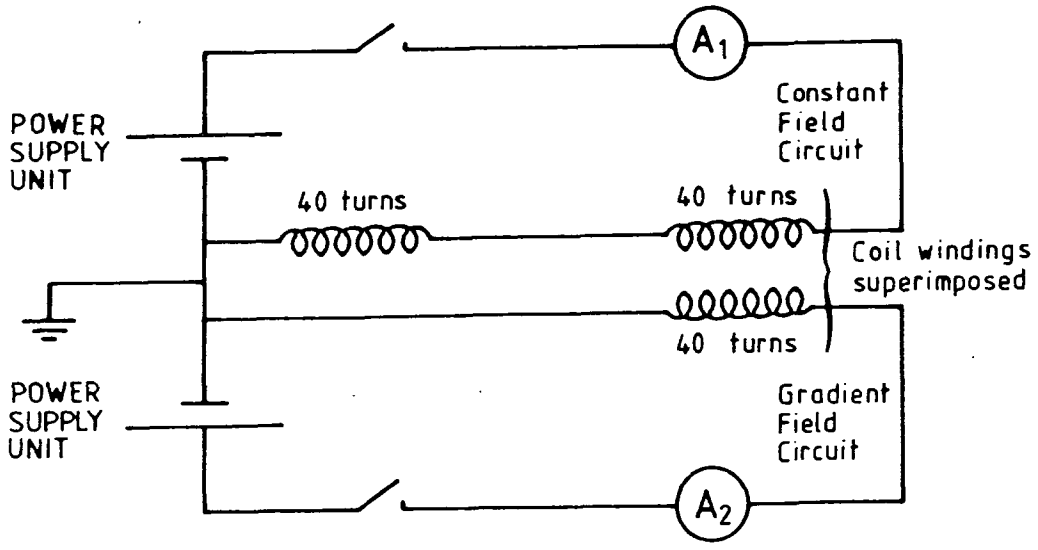

Figure 7.4 The coil system circuit showing the electrical independence of the constant and the gradient field coil components.

coil is electrically independent of the constant field coil system. By being able to vary the magnitudes of the currents in both the gradient and the constant field coil systems independently a greater variation is available in the magnitudes of the field gradients that the whole coil system can produce.

The current for the two components of the coil system is provided by two separate Farnell E30/2 stabilised power supply units. The two earths of both power supply units are connected together. The current in each of the coil circuits is measured by two separate ammeters in series with the two separate coil components. To avoid damage to the coil system the maximum current permissible in either coil is ~ 0.4A. Figure 7.4 illustrates the circuits which power the coil system.

7.5 The Calculation of the Magnetic Field

Unfortunately it is very difficult experimentally to determine the magnetic field distribution produced by the coil system described in the previous section. Conventional laboratory magnetic field-measuring devices such as a Hall effect probe would be incapable of resolving with high enough accuracy the small differences in magnetic field over the small physical dimensions of the space occupied by the sample. Knowledge of these differences is necessary for a determination of the magnitudes of field gradients. Fortunately, however, the simple geometry of the coil system (essentially a distribution of rectangular current loops) makes it possible to calculate relatively straightforwardly the field distribution produced by the coil system. Although such a calculation necessarily requires the real coil system to be approximated by an ideal system, this approach promises a more accurate determination of the field distribution than an empirical determination using readily available conventional devices.

The technique used for the calculation of the magnetic field distribution is an application of the Biot-Savart law (see, for example, Duffin (1980), p181). This elementary law relates an element of the magnetic field, $d\mathbf{B}_0$, to the current element, $I\,d\mathbf{l}$, producing it. Here $d\mathbf{l}$ is an element, having dimensions of length, of the one-

dimensional conductor which carries a current I. The Biot-Savart law is

$$d\mathbf{B}_0 = \frac{\mu_0 I\, d\mathbf{l}\times\hat{\mathbf{R}}}{4\pi R^2} \qquad 7.10$$

In this equation $\hat{\mathbf{R}}$ is a unit vector along $\mathbf{R}$ which, in turn, is the displacement of the magnetic field element, $d\mathbf{B}_0$, from the current element $I\,d\mathbf{l}$. The calculation of the magnetic field from a whole circuit or coil system requires that equation (7.10) be integrated with respect to $d\mathbf{l}$ around the whole system, that is,

$$\mathbf{B}_0(\mathbf{R}) = \oint_{\substack{Coil\\ system}} \frac{\mu_0 I\, d\mathbf{l}\times\hat{\mathbf{R}}}{4\pi R^2} \qquad 7.11$$

The method used for this integration is to model the coil system by a set of rectangular current loops, the planes of which are all mutually parallel. Hence, we will consider first one isolated rectangular current loop of length w and breadth $(u+v)$. This is shown by the current loop $ABCD$ in figure 7.5. The current, I, flows in the sense shown by the arrow.

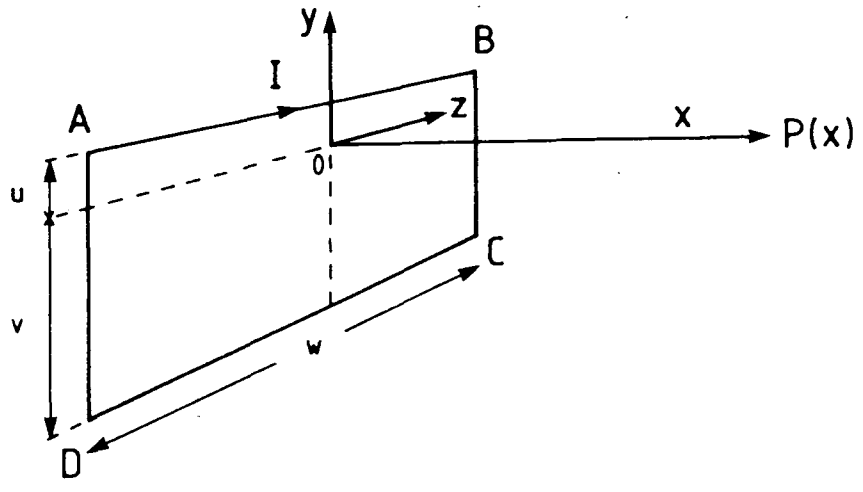

Figure 7.5 The rectangular current loop $ABCD$ showing the definitions of the coil dimensions $u.v$ and w.

In figure 7.5 an x-axis is also defined. This axis is perpendicular to the plane $ABCD$ with its origin in that plane This origin is located at the intersection of the line which bisects the conductors AB and CD with the line which cuts the conductors AD and BC in the ratio $u : v$ (that is, the intersection of the two dotted lines). Specifically, we are interested in the x component of the field produced by the whole loop at the field point $P(x)$. The details of the calculation are given in Appendix A2. It is sufficient here to state the result. The x component of the magnetic field, B_{0xi}, at the point $P(x)$ produced by the rectangular current loop is

$$B_{0xi} = -\frac{\mu_0 I w}{4\pi}\left[\frac{u}{(u^2+x^2)\sqrt{u^2+x^2+(\frac{w}{2})^2}} + \frac{v}{(v^2+x^2)\sqrt{v^2+x^2+(\frac{w}{2})^2}} + \frac{1}{[x^2+(\frac{w}{2})^2]}\left(\frac{v}{\sqrt{v^2+x^2+(\frac{w}{2})^2}} + \frac{u}{\sqrt{u^2+x^2+(\frac{w}{2})^2}}\right)\right] \qquad 7.12$$

The consideration of one isolated current loop is sufficient to show that $B_{0z} = 0$ at the point $P(x)$. From equation (7.10) the only parts of the rectangular current loop $ABCD$ which can produce magnetic field elements having non-zero z components are the conductors DA and BC. Because the current in these two conductors is flowing in opposite directions the z components of the fields they produce at the point $P(x)$ are of the same magnitude but oppositely directed and so they mutually cancel.

The practical realization of the condition $B_{0x} \gg B_{0y}$ (equation (7.1*b*)) for the coil system cannot be shown by a consideration of one isolated current loop alone. We will consider the constant field and the gradient field components of the coil system separately. For each constant field rectangular current loop $ABCD$ on one of the sets of windings there is an equivalent loop $A'B'C'D'$ symmetrically positioned with respect to the middle of the coil system in the other set of coil windings. For this pair of current loops, again from equation (7.10), the only parts which can contribute non-zero y components of the magnetic field at the middle of the coil system (the sample position) are the conductors AB and CD from one loop and $A'B'$ and $C'D'$ from the other. Again the y components of the pairs $AB, A'B'$ and $CD, C'D'$ are of equal magnitude but oppositely directed and so they mutually cancel. This demonstrates that the constant field windings provide no non-zero B_{0y} component. However, because of the asymmetric position of the gradient field coil windings with respect to the sample position, the gradient field current loops provide a small uncompensated non-zero y component of the field at the sample position. There is a non-perfect cancellation between the oppositely-directed field components produced by the AB and the CD conductors of the gradient field current loops. This y component is very small in comparison to the x component of the field at the sample position which itself has resulted from a constructive addition of the field contributions of every conductor in every current loop. Thus, it is apparent why equations (7.1*b*) and (7.1*c*) are appropriate to the coil system.

The total field produced in the x direction by the whole coil system is obtained by calculating the sum at the point $P(x)$ of all of the x component contributions from all of the rectangular current loops. Each current loop contributing to a single layer of windings will be at a different distance, x, from $P(x)$ but will have the same u,v and w. Current loops contributing to other layers of windings, besides generally having different x values, will also have different u,v and w values from those of other layers. The precise values of all of the relevant quantities necessary for this calculation were obtained from a knowledge of the wire diameter, the coil former dimensions and by careful measurements using a micrometer and a rule. The u,v,w dimensions for both of the layers of windings in both the constant field and the gradient coils are summarized in Table 7.1. All of the dimensions are given with reference to the central axis of the circularly cross-sectioned wire.

Constant Field Coil

	u(mm)	v(mm)	w(mm)
Inner 20 turns	0.16	1.51	26.12
Outer 20 turns	0.22	1.57	26.18

Gradient Field Coil

	u(mm)	v(mm)	w(mm)
Inner 20 turns	0.28	1.63	26.24
Outer 20 turns	0.34	1.69	26.31

Table 7.1 The $u.v.w$ dimensions of all of the layers of turns in the whole coil system which are required for the calculation of the total magnetic field.

The u,v,w dimensions refer to the cross-sectional area occupied by a single rectangular coil or single layer of coils. Also needed is the distance between nearest neighbour coils in the same layer of turns. The average value of this distance was determined to be 0.18mm. These measurements and indeed the whole approach to the problem assumes that any non-uniformities in the windings and any slight variations in the sizes of nominally similar windings have a negligible effect.

The calculation of the total magnetic field at the field point P by the summation of the contributions from all of the current loops, with, most generally, different currents in the constant and the gradient field components, is accomplished using a microcomputer. By moving the field point P across the space occupied by the sample the total field at the different points can be mapped out and the magnitude and behaviour of the field gradient can be determined. Figure 7.6 gives some examples of the calculated magnetic field distributions across the space occupied by the sample. The origin of distance in the x-direction is defined as the plane which bisects the axis of the two coils equidistantly from each coil. I_C and I_G refer to the currents in the constant field and the gradient field coils respectively. Appendix P4 gives a listing of the BBC BASIC program used to calculate the magnetic field distributions.

It can be seen from figure 7.6 that the field gradients are not linear over relatively large distances on the abscissa. However, over distances of $\sim$ 0.2mm a linear approximation to the gradient is excellent. Even over distances $\sim$ 0.6mm the linear approximation is good. In the experiment only particles confined to the central 0.6mm are studied and the gradient in this region is calculated by fitting a straight line to the magnetic field points. This will be dealt with in greater depth shortly.

The sensitivity to variations in u,v,w of the gradient produced by the coil system was investigated in order to ascertain the effect on the field gradient of errors in the determinations of the u,v,w dimensions. It was found that variations in the dimensions of u,v,w over distances of the order of the radius of the coil wire produced changes in the calculated field gradient of $\sim$ 5%. Any differences in u,v,w arising from non-uniformities in the windings or any errors in the determination of u,v,w are likely to have magnitudes of the order of the radius of the wire. Hence, the effect on the field gradient arising from such errors is not serious.

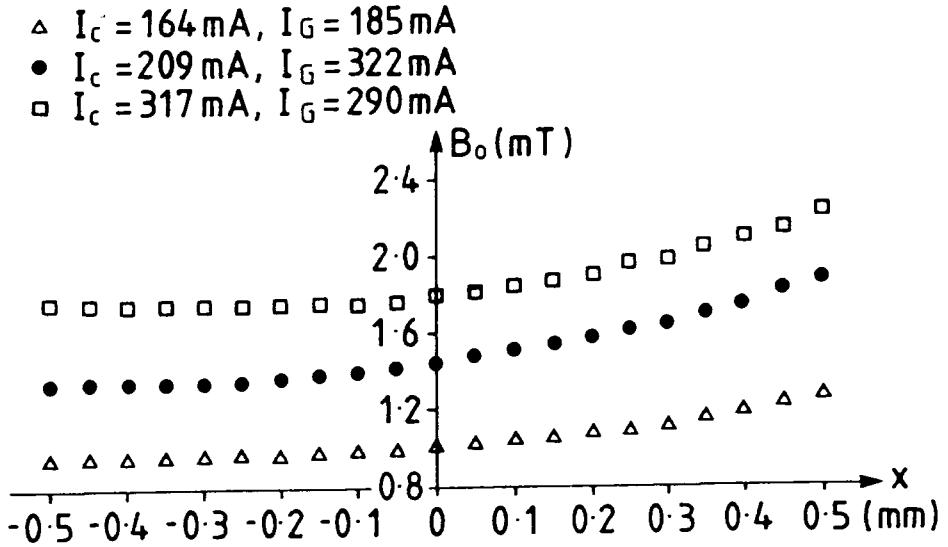

Figure 7.6 Examples of the calculated magnetic field distributions for different constant field and gradient field coil currents.

7.6 The Magnetization of the Particles

Equation (7.9*a*) states that the x component of the velocity of a particle, v_x, is proportional to the magnetization of the particle, M. Thus, a knowledge of M is important. One way of approximating the magnetization as a function of the field, B_0, was used in Chapter 5. This was

$$M = \frac{2B_0}{\mu_0} \qquad \text{for } M < M_{sb} \qquad 7.13a$$

or

$$M = M_{sb} \qquad \text{for } 2B_0/\mu_0 \geq M_{sb} \qquad 7.13b$$

This is an approximation introduced by Edwards and Palmer (1986). It is equivalent to assuming that the volume susceptibility (χ_v) equals 2 if the particle is unsaturated and it equals zero if the particle is saturated. The field at which the saturation occurs equals $\mu_0 M_{sb}/2$. Figure 7.7 illustrates the behaviour of this approximation in a graphical way.

It is important to be clear about the value of the volume susceptibility implicit in Edwards and Palmers' approximation. Edwards and Palmers' original justification for using this approximation arose from their assertion that the (assumed uniform) magnetization, **M**, of a spherical particle in a uniform magnetic field, $\mathbf{B}_0$ is given by

$$\mathbf{M} = \frac{2\mathbf{B}_0}{\mu_0}\left(\frac{\mu_r - 1}{\mu_r + 2}\right) \qquad 7.14$$

where μ_r is the *intrinsic* relative permeability of the particle material. (In this equation the author has used a slightly different notation from Edwards and Palmer and also corrected a trivial numerical error in the denomenator of the term in parenthesis.) They argued that for $\mu_r \gg 1$ (as is the case, for example, in magnetite where $\mu_r \sim 100$) equation (7.14) can be approximated by $\mathbf{M} = 2\mathbf{B}_0/\mu_0$. This does not mean that since $\mu_r \simeq \chi_v$ then also $\chi_v \gg 1$, in contradiction to its value given earlier as 2. The point here is that the value for the volume susceptibility,

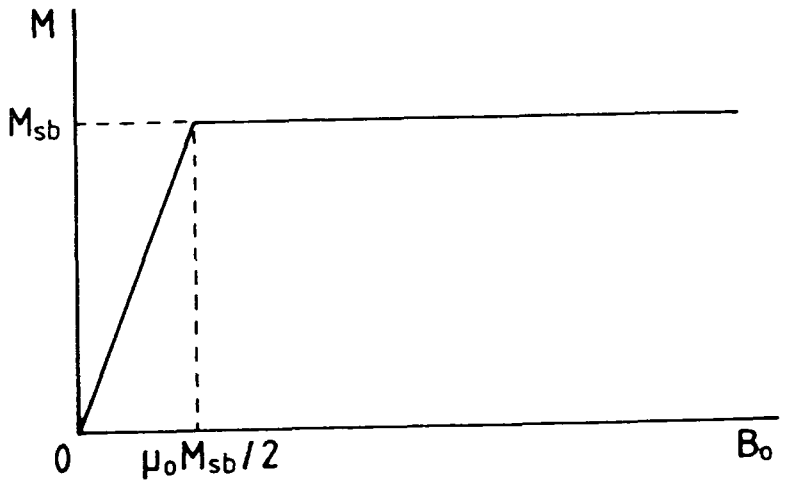

Figure 7.7 Graphical representation of the B_0-dependence of M used by Edwards and Palmer (1986) and by this author in Chapter 5.

χ_v, given as 2 does not refer to the *intrinsic* susceptibility of the particle; it refers to the *effective* susceptibility. Here effective susceptibility is to be understood to refer to the magnetization of a particle in both the applied field and the particle's demagnetizing field. The true intrinsic susceptibility is what remains after the effective susceptibility has been corrected for the demagnetizing field of the sample. In the approximation it is the intrinsic susceptibility, χ_v^{int} which satisfies the condition $\chi_v^{int} \gg 1$ and the effective susceptibility which is described by the equation $\chi_v = 2$. The relation between these two susceptibilities, assuming that the particle is uniformly magnetized, is

$$\frac{1}{\chi_v} = \frac{1}{\chi_v^{int}} + D' \qquad 7.15$$

If $\chi_v^{int} \gg 1$, then $\chi_v \simeq (D')^{-1}$, which, for a uniformly magnetized sphere ($D' = \frac{1}{3}$) yields $\chi_v \simeq 3$. If, however, one considers a spherical particle which is not uniformly magnetized, or, in other words, one which is not single domain, then equation (7.15) is no longer perfectly valid and $D' \neq \frac{1}{3}$. Hence, because of the difficulties in using equation (7.15) to infer the magnetization of a particle, it is better to use equation (7.14) and the approximation derived from it.

According to this approximation, magnetite should enter the saturation region when $B_0 = \mu_0 M_{sb}/2 = 0.296$T and iron should be saturated at $B_0 = 1.079$T. These values are well in excess of the fields the gradient coil system can produce (typically $\sim$ 2mT). In the rest of this chapter this approximation for the B_0-dependence of M and its prediction of a volume susceptibility of 2 will be referred to as Theory 1.

A second approach to the determination of M which was also used was a direct experimental method. The dry powder magnetic particles used in the experiment were set randomly aligned in an Araldite matrix in the form of discs and magnetic measurements were made on these samples using the VSM described in Chapter 4.

The dry powders were well dispersed (to achieve random alignment) in Araldite and placed in a mould made from PTFE which produced discs of diameter 5.4mm and thickness 2.9mm. Also fabricated in the mould was a disc of pure Araldite

which was used for a residual correction to the magnetic measurements. Before the magnetic measurements were performed the samples were demagnetized using the apparatus described by Lambrick (Lambrick (1986), p92). This apparatus provides a demagnetizing technique which involves spinning the discs about the normal to their planes in the 50Hz ac field of a solenoid whilst the field of this solenoid is manually reduced from 0.04T(rms) to zero over the time period of a few tens of seconds. All measurements were made at room temperature. The magnetization curve of the diamagnetic pure Araldite together with the signal produced by the sample holder (residual) was fitted by a straight line and this residual was subtracted from the two data sets for the CrO_2 and the 7C particles. No correction for the sample demagnetizing factor was made. This was deemed unnecessary because we are chiefly interested in the initial magnetization curves where M is very small. From $(1/B_0)$ extrapolations the saturation magnetizations, M^A_{sat}, of the two samples were determined and the volumetric packing fractions, ϵ_v, of the particles in the Araldite were determined from the relation $\epsilon_v = M^A_{sat}/M_{sb}$, where M_{sb} is the saturation magnetization of the bulk form of the particulate material. The bulk material saturation magnetizations were taken from Pauthenet(1950) for the 7C and from Swoboda, Arthur, Cox, Ingraham, Oppegard and Saddler (1961) for the CrO_2. The volumetric packing fractions were determined to be $\epsilon_v = 1.5 \times 10^{-3}$ for the CrO_2 in Araldite and $\epsilon_v = 5.2 \times 10^{-3}$ for the 7C in Araldite. The volumetric packing fractions enabled the initial volume susceptibilities, χ_{vi}, of the particle material alone to be determined. These are tabulated in Table 7.2.

Sample	χ_{vi}
CrO_2	1.67
7C	4.27

Table 7.2 The initial volume susceptibilities of the CrO_2 and 7C particle material.

These values can be compared to the value of the initial volume susceptibility given by Theory 1, that is $\chi_{vi} = 2$. The CrO_2 particles would appear to be represented better by Theory 1 than would the 7C particles. This is not significant, however. The agreement to within a factor of ~ 2 is the more significant result. The agreement is good bearing in mind that Theory 1 was derived for non-interacting single spherical particles, a condition of limited validity for these samples.

One would expect the effect of magnetostatic interparticle interactions and the consequent aggregation of particles to have an effect on the initial susceptibility. The initial susceptibility is enhanced by weak interparticle interactions (Menear and Bradbury (1985)). However, the aggregates formed can have two possible effects depending on their size. Studies of Monte Carlo simulations of 2D polydispersed magnetic fluids (Bradbury, Menear and Chantrell (1986)) show that if the aggregates are small (dimers or trimers) then the initial susceptibility is enhanced. Larger aggregates, however, in which flux closure can occur, tend to reduce the initial susceptibility. It would be unwise to infer anything about the size of aggregates in the 7C and CrO_2 samples solely from these measurements of the initial susceptibility and their deviation from the value of 2 because the model which predicts $\chi_{vi} = 2$ is only approximately valid for the samples. Optical and electron microscopy results to be presented later will show that the aggregates are indeed very large.

The assumption that the measured initial susceptibility of the particles in these Araldite-set samples may be used to infer the field-dependence of the magnetizations of individual suspended particles in the experiment itself is good. Provided that the particles in the set samples are randomly oriented in the matrix then they reflect both the orientation distribution in low fields and the particle size distribution of the constituents of aggregates such as those in the real experimental situation. At high fields the orientations of the components of the aggregates and the shape of the aggregates would be expected to become anisotropic and the representation of such configurations by the Araldite-set samples would be inappropriate. However, at low fields the method employed is valid.

Throughout the rest of this chapter the approach to determining the magnetizations of the particles by this direct empirical method will be called Theory 2.

In summary, therefore, the magnetizations of the suspended particles are inferred from a knowledge of the particles' initial volume susceptibilities. Two different methods are used for the estimation of χ_{vi}, called Theory 1 and Theory 2. Theory 1 is derived from Edwards and Palmers' approximation and predicts the same χ_{vi} for both the CrO_2 and 7C samples. Theory 2 has attempted to measure directly χ_{vi} for both sample types. These values are different for each sample. Theory 1 and Theory 2 agree well bearing in mind the limited applicability to the samples of some of their assumptions. In terms of the initial susceptibility equation (7.9a) can be written as the following equation with the relevant χ_{vi} given by Table 7.3.

$$v_x = \frac{\chi_{vi} B_0 V G}{2\mu_0 \eta c} \qquad 7.16$$

	CrO_2	7C
	χ_{vi}	
Theory 1	2	2
Theory 2	1.67	4.27

Table 7.3 The values of χ_{vi} relevant to equation (7.16) for both Theory 1 and Theory 2 and for both sample types.

7.7 Particle Shape and c

Typically, most of the particles observed were non-spherical. This means that there is a complication as to what is the relevant value of c, the geometrical dissipative factor, for a given particle. For spherical particles this problem does not arise and the simple relation $c = 3\pi r$ holds. Essentially the problem of the question of the generalization of Stokes' law to non-spherical particles. This problem is notoriously difficult. General solutions exist for the case of a general ellipsoid in a viscous medium (Lamb (1932), p604) and for the limiting cases of a circular cylinder and other shapes (Berry and Swain (1923)). However, these solutions are not in a readily usable form. In general these approaches address themselves to calculating an 'equivalent' radius to incorporate into the usual expression for Stokes' law. Except for a few special cases, the equations obtained are not easy to calculate.

The approach to the problem used in this Chapter is indeed the assigning of an equivalent radius, r_{equiv}, to the particles and the use of the relation $c = 3\pi r_{equiv}$,

but the values of r_{equiv} are approximated in a simple manner. Many of the particles appear to be well approximated by ellipsoids and to be moving along the line of the major axis. In such cases, r_{equiv} would be better approximated by the semi-minor axis, r_{min}, so that $r_{equiv} = r_{min}$, rather than any other dimension such as, for example, the semi-major axis or the average of the semi-minor and semi-major axes. This approach certainly gives an under-estimation of r_{equiv} but it is not clear how the estimation could be improved. One is limited by incomplete knowledge of the detailed structure of an individual particle. The approximation of the gross morphology of a particle by an ellipsoid misses out, by necessity, details of such features as the roughness of surfaces and the presence of voids in the particles. In this light it would be pretentious to assume that the way of estimating r_{equiv} could be much improved.

A few of the particles had gross shapes which could not satisfactorily be approximated by ellipsoids—for example, a few were 'L'-shaped and some were highly irregular. In the presentation of the data, these cases will be mentioned and, of course, less confidence in the accurate assigning of the correct r_{equiv} to these particles would be expected.

7.8 The Experimental Method

The sample tubes were thin-walled glass tubes (wall thickness 0.1mm) of rectangular cross section having exterior dimensions of $1.2 \times 0.3 \times 50$mm.† The sample tubes were located equidistantly between the two sets of coil windings with the tube length parallel to the z axis. The dimensions of the coil former and its sample tube recess were such that the field point $P(x)$, discussed earlier, lay on the line passing through the middle of the cross section of the sample tube. The sample tube was free to be moved along in the z direction in order to easily change the field of view.

The microscope used was a Vickers M17 Industrial Microscope operated in transmission mode and the illumination was provided by a tungsten lamp. The images from the microscope were observed in real time using a TV camera and a display monitor but were also recorded using a videocassette recorder. The TV camera was a Panasonic WV-1850/B model and the videocassette recorder was a Sony VO-5630 type. The overall magnification of the microscope-camera-TV monitor system was $\times 1887$. This magnification calibration was measured using a microscope slide graticule devided into 0.01mm divisions.

In order to reduce the presence of interparticle interactions the concentration of particles in the distilled water was very low, typically $\sim 0.1-0.05\%$ by volume. Prior to being placed in the sample tubes the suspensions were agitated by placing phials of the samples in an ultrasonic bath for various periods of time. The first reason for doing this was to facilitate homogeneous dispersion of the solid phase throughout the whole carrier liquid. The second reason was to break up the largest aggregates into smaller units of typically 10μm diameter which would remain suspended for longer periods of time.

Once in the sample tube, the very large aggregates had a tendency to sink to the bottom in a very short period of time and so these were of little use to the experiment. For this reason there is a slight biasing against the very large aggregates of the sizes of the particles observed. Only particles which stayed suspended for times of the order of a few minutes were studied.

† Supplied by Camlab, Nuffield Road, Cambridge, UK.

A further biasing, this time affecting the very small particles, resulted from taking care not to include in the data sets particles on which Brownian motion has a strong effect. Particle trajectories suffering strong Brownian motion were easily discernable during the course of the experiment and these particles were ignored.

Particles which were clearly strongly interacting with other nearby particles were also ignored. Because the carrier liquid is water, in addition to magnetostatic interactions, an electrical double layer interaction is present between nearby particles. Hence, this precaution is crucially important. Only particles separated from neighbours by at least 80μm were studied, this being the distance sufficient to treat the particle as being 'non-interacting'.

In addition to this, care was also taken to ensure that only particles in the central 0.6mm region between the two sets of coil windings were studied. This ensured that using a linear approximation to the field variation (a constant field gradient) across the coil system remained good. The constant field gradient was calculated by fitting a straight line to the points of the magnetic field against distance relationship for this 0.6mm cental region. These points were obtained as is described in section 7.5.

Particle velocities were subsequently extracted from the video images by the laborious process of approximating the displayed trajectories by straight line elements, δx, the two vertices of which were separated by a known time interval, δt. This task was greatly facilitated by securing perspex sheets onto the video monitor and employing marker pens to mark the vertices of the line segments. These measurements, after conversion for the known magnification of the system, produced for each particle an average velocity, v_x, and a standard error, σ. The dimensions of the particles were measured from the displayed images using a rule together with a knowledge of the magnification.

7.9 Results

For all particles studied the value of M used, whether in Theory 1 or Theory 2, was treated as a constant. Although the particles were moving in a varying field, the value of M calculated from the field at the mid-point of the coil system was used. Typically over the maximum distance the particles were observed to be displaced from the mid-point of the coils, M would be expected to change by $\leq 2\%$. Hence, this approximation is a negligible source of error.

7.9.i Particles in Different Field Gradients

The first data set is from a sample of CrO_2 in distilled water. Each particle is in a different gradient and each has a different magnetization. Prior to the observations the sample had been ultrasonically agitated for $\sim$ 1hour. The particles could mostly be approximated by ellipsoids. Table 7.4 presents some details of the particles and shows the two values of the velocity predicted from Theory 1 and Theory 2 (equation (7.16)). Also shown is the measured velocity and its standard error. The standard error is derived solely from the spread in the velocities obtained in the reduction of the video images to the particle velocities. The coefficient of viscosity of the carrier (water) is $\eta = 0.89$mPas.

CrO_2 in Different Gradients

Particle	Particle Shape	G (Tm^{-1})	Volume ($\times 10^{-17} m^3$)	Measured v_x (μms^{-1})	Calculated v_x (μms^{-1}) Theory 1	Calculated v_x (μms^{-1}) Theory 2
1	Ellipsoid	0.2760	12.47	0.98(±0.06)	1.25	1.04
2	Ellipsoid	0.2801	8.88	0.96(±0.15)	1.00	0.84
3	Irregular	0.3803	40.04	0.76(±0.10)	5.55	4.63
4	Ellipsoid	0.3910	2.25	0.59(±0.09)	0.61	0.51
5	Irregular	0.3979	3.05	0.58(±0.08)	0.42	0.35
6	Ellipsoid	0.4029	1.62	0.40(±0.12)	0.52	0.43
7	Ellipsoid	0.4364	2.67	0.48(±0.14)	1.10	0.92
8	Ellipsoid	0.4326	1.57	0.53(±0.20)	0.88	0.73
9	Ellipsoid	0.4363	1.50	0.52(±0.09)	0.54	0.45
10	Ellipsoid	0.4801	6.91	0.58(±0.09)	2.49	2.08

Table 7.4 The data set of 10 CrO_2 particles. all in different magnetic field gradients. The Table shows the mean measured values of v_x nd the standard error. Also shown are the calculated v_x values from Theory 1 and Theory 2.

In this sample all but two of the particles were approximated by ellipsoids and for these particles $r_{equiv} = r_{min}$ and the volumes are given by $V = \frac{4}{3}\pi r_{min}^2 r_{max}$ (that is, the volume of an ellipsoid). The other particles, having irregular shapes, had r_{equiv} and V estimated from the precise details of the shape. The ellipsoidal particles appeared to be highly globular—the aspect ratios (r_{max}/r_{min}) were all less than 3.

It can be seen from the table that for all but one of the ellipsoidal particles agreement to within a factor of ~ 2 between the measured values of v_x and those calculated from either Theory 1 or Theory 2 occurs. Bearing in mind the problems associated with determining the volumes of the particles, their volume susceptibilities and the assigning of the correct values of r_{equiv} the agreement is remarkably good.

A sample of 7C concentrate in water constitutes the second data set. Again each particle is in a different gradient and has a different magnetization. This time the sample was ultrasonically agitated for $\sim$ 3hours prior to the observations. The data is shown in Table 7.5. Again the comparison between the two theoretical and the observed values of v_x is given, together with some details of the particles themselves. Again the value of η for water is $\eta = 0.89$mPas.

7C in Different Gradients

Particle	Particle Shape	G (Tm^{-1})	Volume ($\times 10^{-17} m^3$)	Measured v_x (μms^{-1})	Calculated v_x (μms^{-1}) Theory 1	Calculated v_x (μms^{-1}) Theory 2
1	Ellipsoid	0.5103	9.42	1.57(±0.30)	6.27	13.39
2	Ellipsoid	0.5184	18.24	1.51(±0.10)	4.45	9.51
3	Ellipsoid	0.5088	282.27	3.73(±0.48)	59.66	127.37
4	Ellipsoid†	0.5148	397.36	3.47(±0.52)	22.69	48.43
5	Ellipsoid†	0.4973	38.42	4.70(±0.47)	7.26	15.50
6	Ellipsoid	0.4939	3.12	1.73(±0.19)	1.69	3.60
7	Ellipsoid	0.2659	10.21	1.34(±0.15)	2.26	4.83
8	Ellipsoid	0.3408	6.68	1.74(±0.23)	2.10	4.49
9	Ellipsoid	0.4335	5.11	2.65(±0.45)	2.23	4.77
10	Ellipsoid	0.4865	9.23	2.85(±0.72)	6.69	14.29
11	Ellipsoid	0.4984	6.88	1.09(±0.08)	2.72	5.81
12	Ellipsoid	0.4984	6.28	0.10(±0.19)	2.49	5.31

†Large visible voids in particle

Table 7.5 The data set for 12 7C particles. Details of the shape of each particle are given together with the calculated and measured values of v_x.

In this sample all of the particles appeared to be well approximated by ellipsoids, although two had large visible voids in them. For all particles $r_{equiv} = r_{min}$ and $V = \frac{4}{3}\pi r_{min}^2 r_{max}$. However, in contrast to the CrO_2 sample, these particles were significantly elongated. Most had aspect ratios in the range $5 - 10$. From Table 7.5 it can be seen that the main result is that the measured values are significantly less than the values predicted by Theory 1 and Theory 2. Even conceding the fact that one could not expect agreement to better than a factor of ~ 2, say, it is still clear that the theoretical values are over-estimating by a factor of maybe typically 3 or 4. Leaving aside error in the knowledge of the magnetization, M, or the gradient, G, it would seem that from the particle images V is being over-estimated and/or c is being under-estimated. We know already that the values of c probably tend to be under-estimates. This data set certainly supports this view. However, it is also equally probable that the volumes derived from the recorded images are over-estimates. The volume is less than it appears. This is because the size of voids and holes in particles and aggregates cannot clearly be resolved in the experimental arrangement. Although difficult to confirm, another possible explanation is that c is not at all being significantly under-estimated because all the voids and holes in the particles tend to lessen the particles' resistance to the viscous fluid. By this explanation the disagreement in the data arises mainly from over-estimates of the particle volumes. Another possibility is that the values used for χ_{vi} are greatly over-estimated. If this effect is important it would be expected to mostly affect the largest aggregates. This is because of their rotational and translational inertia and because of their being made up of entities having a spatial distribution of easy axes of magnetization, so reducing the magnetic response of the particle to an imposed magnetic field. As we shall see, this effect also appears in the rest of the data to be presented here.

7.9.ii Particles in the Same Field Gradients

The data in this section is from sets of particles of differing size (and hence, differing c) but which were all observed in the same field gradient. In addition to this, all of the particles were observed in the same average B_0 value which was used for the calculation of their magnetizations. Thus, using the approximation that χ_{vi}^{int} is the same for all of the particles, all of the particles have the same magnetization.

The first data set is for 7 particles of CrO_2 in a central coil field of $B_0 = 1.839\text{mT}$ and a field gradient of $G = 0.4357\text{Tm}^{-1}$. From the two theories the magnetizations are $M = 2927\text{JT}^{-1}\text{m}^{-3}$ (Theory 1) and $M = 2444\text{JT}^{-1}\text{m}^{-3}$ (Theory 2). Particle details and the calculated and measured values of v_x are given in Table 7.6.

CrO_2 in the Same Gradient

Particle	Particle Shape	Volume ($\times 10^{-17}\text{m}^3$)	Measured v_x (μms^{-1})	Calculated v_x (μms^{-1}) Theory 1	Calculated v_x (μms^{-1}) Theory 2
1	Irregular	65.11	0.59(±0.09)	6.91	5.77
2	Ellipsoid	140.37	0.70(±0.12)	20.13	16.81
3	Ellipsoid	47.51	0.84(±0.14)	9.07	7.58
4	Ellipsoid	93.54	0.79(±0.09)	8.95	7.47
5	Irregular	6.15	0.58(±0.17)	0.71	0.59
6	Ellipsoid	40.47	0.53(±0.07)	7.73	6.46
7	Irregular	6.16	0.80(±0.18)	0.71	0.69

Table 7.6 The data set of 7 CrO_2 particles all in the same magnetic field gradient. Shown are some details of the shapes of the particles and the measured and calculated values of v_x.

Prior to the observations this sample was ultrasonically agitated for $\sim$ 3hours. As in the previous CrO_2 data set the ellipsoidal particles in this sample all had low aspect ratios—this time they were less than 2. Similar disagreement between the calculated and measured values of v_x as was found for the 7C sample in the previous section is again evident.

Figure 7.8 shows a plot of the measured and calculated values of v_x as a function of V/c for this data set. From equation (7.16) the slopes of the theoretical curves are $\chi_{vi}B_0G/2\mu_0\eta$.

It may be thought that it is possible that the discrepancy between the measured and the theoretical values of v_x lies not in the over-estimation of V/c, but in an over-estimation of the particle susceptibility. From the measured points it is possible to obtain a value of χ_{vi} for the CrO_2. The best one-parameter (that is to say, constrained to pass through the origin) straight line fit to the measured points, using the same values for B_0 and G as are used in the theoretical curves, predicts an initial volume susceptibility, χ_{vi}, for the CrO_2 of 0.11. This is more than an order of magnitude less than the values obtained by Theory 1 or Theory 2. Although Theory 1 and Theory 2 doubtless have errors associated with them, it is unlikely that they are wrong in their values of χ_{vi} by an order of magnitude. However, errors in χ_{vi} are likely to be the cause of part of the discrepancy, as well as errors in V/c. If one assumes that the discrepancy arises solely from errors in V/c then this

data set permits a quantitative determination of the size of the over-estimation of V/c. From the value of χ_{vi} derived from the best fit to the measured v_x values the over-estimation is by slightly greater than a factor of 10.

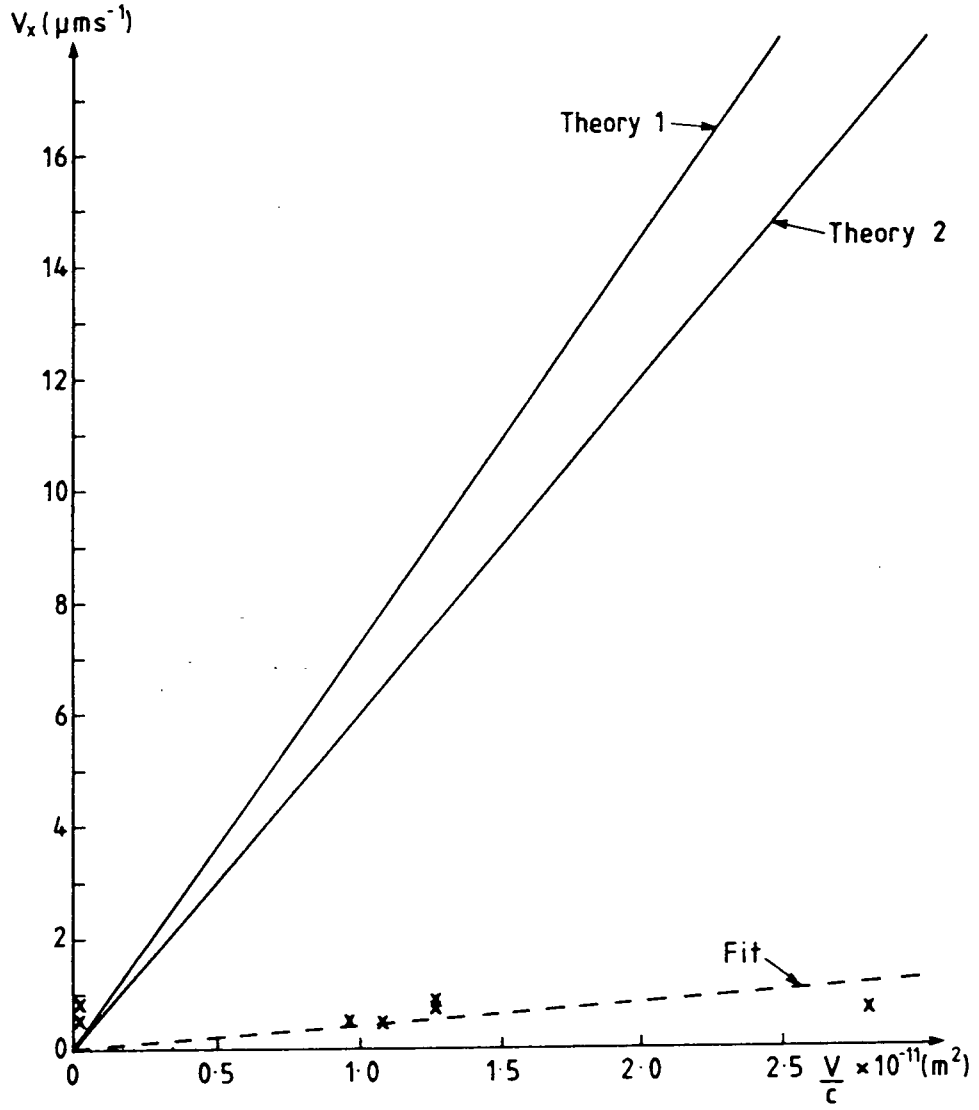

Figure 7.8 A plot of the measured and calculated values of v_x as a function of V/c for a sample of CrO_2 particles all in the same field gradient.

The next data set is a sample of 8 7C particles in the same field gradient ($G = 0.4357\text{Tm}^{-1}$) and field ($B_0 = 1.839\text{mT}$) as the previous CrO_2 sample. From the two theories the relevant magnetizations are $M = 2927\text{JT}^{-1}\text{m}^{-3}$ (Theory 1) and $M = 6250\text{JT}^{-1}\text{m}^{-3}$ (Theory 2). Again details of the particles and the measured and theoretical values of v_x are given in Table 7.7.

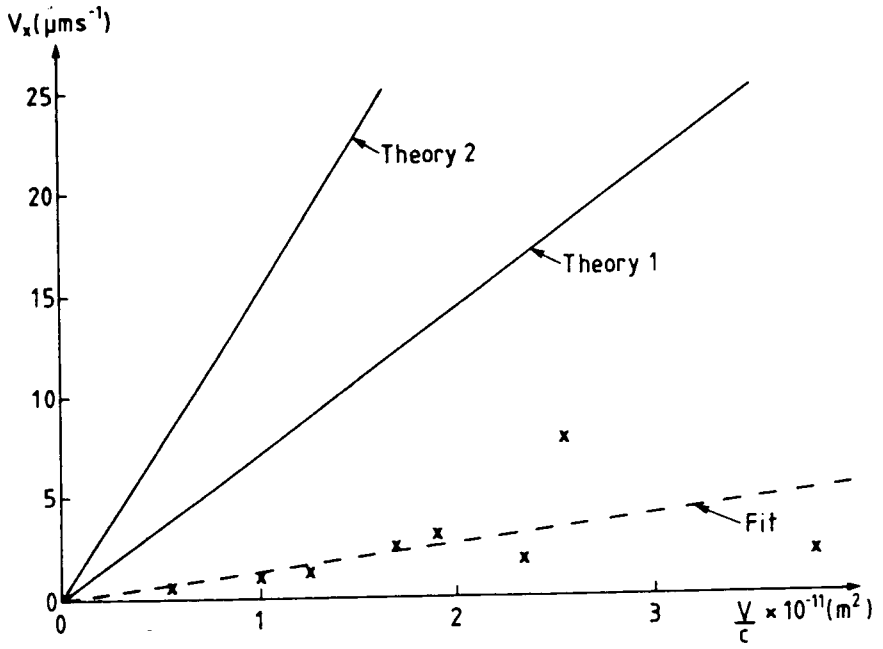

Figure 7.9 The plot of the measured and theoretical values of v_x as a function of V/c for a sample of 8 7C particles all in the same magnetic field gradient.

7C in the Same Gradient

Particle	Particle Shape	Volume ($\times 10^{-17} m^3$)	Measured v_x (μms^{-1})	Calculated v_x (μms^{-1}) Theory 1	Calculated v_x (μms^{-1}) Theory 2
1	Ellipsoid†	146.38	1.77(±0.18)	16.78	35.84
2	Irregular	106.02	2.45(±0.20)	12.16	25.96
3	Ellipsoid	9.61	0.66(±0.05)	3.93	8.39
4	Ellipsoid	130.96	1.20(±0.04)	8.95	19.10
5	Ellipsoid†	218.99	2.16(±0.23)	27.29	58.27
6	Dumbell	34.40	1.10(±0.34)	7.58	16.19
7	Ellipsoid‡	190.37	7.86(±1.19)	18.20	38.87
8	Irregular	166.46	3.02(±0.47)	13.64	29.12

†Large visible voids in particle
‡'Tail' extruding from particle

Table 7.7 A data set of 8 7C particles in the same field gradient as for the case of the CrO_2 mentioned in the previous case. Again the calculated and measured values of v_x are shown.

Prior to the experiment this sample was ultrasonically agitated for $\sim$ 3hours. Typically the aspect ratios of the ellipsoidal particles were in the range $2 - 3.5$. Again the familiar discrepancy is clear. Figure 7.9 presents a plot of v_x against V/c for the measured and theoretical values of v_x.

Again a denial of the influence of the over-estimation of V/c in causing the discrepancy, using the best fit to the measured points, yields a particle volume susceptibility, χ_{vi}, of 0.35. This is a factor of $\sim$ 6 less than the value obtained from

Theory 1 and a factor of ~ 12 less than the value obtained from Theory 2. Next if one assumes that error in V/c is the sole cause of the discrepancy then this indicates that the size of the over-estimation of V/c is by a factor of $\sim 6 - 12$.

The final data set is again from a sample of 7C particles, but this time in a lower field gradient. This set consists of 9 particles in a field gradient of $G = 0.2833\text{Tm}^{-1}$ and a central coil field of $B_0 = 1.008\text{mT}$. From Theory 1 and Theory 2 the calculated magnetizations are $M = 1604\text{JT}^{-1}\text{m}^{-3}$ (Theory 1) and $M = 3424\text{JT}^{-1}\text{m}^{-3}$ (Theory 2). Table 7.8 gives the important details of the particles.

7C in the Same Gradient

Particle	Particle Shape	Volume ($\times 10^{-17}\text{m}^3$)	Measured v_x (μms^{-1})	Calculated v_x (μms^{-1}) Theory 1	Calculated v_x (μms^{-1}) Theory 2
1	Ellipsoid	65.52	1.48($\pm$0.13)	3.94	8.40
2	Ellipsoid†	131.33	1.89($\pm$0.26)	7.46	15.92
3	Irregular	78.16	1.40($\pm$0.12)	2.66	5.69
4	Ellipsoid‡	91.50	1.07($\pm$0.15)	5.50	11.73
5	Irregular	64.31	0.68($\pm$0.07)	3.29	7.02
6	Ellipsoid	114.32	1.25($\pm$0.17)	7.78	16.61
7	Ellipsoid	28.08	0.63($\pm$0.15)	2.39	5.11
8	Ellipsoid	93.54	1.11($\pm$0.10)	4.78	10.21
9	Ellipsoid‡	45.97	2.10($\pm$0.38)	3.36	7.17

†Large visible voids in particle
‡'Tail' extruding from particle

Table 7.8 The calculated and measured values of v_x for 9 7C particles all in the same field gradient.

This sample, like the previous two, was also ultrasonically agitated for $\sim$ 3hours prior to the experiment. The aspect ratios of the ellipsoidal particles were in the range $2 - 4$. The theoretical values of v_x, based on the experimentally observed values of V/c, again appear as over-estimates. This v_x data is plotted as a function of V/c in figure 7.10.

The calculation of the 'erroneous' particle volume susceptibility, χ_{vi}, by the best straight line fit to the measured values of v_x gives a value of $\chi_{vi} = 0.50$. This is in slight disagreement with the previously measured value which was 0.35 and it indicates that for this sample, if one assumes that the discrepancy arises solely from error in V/c then the over-estimation of V/c is by a factor of $\sim 4 - 9$. This is not inconsistent with the previous data set. The possibility exists that both samples, in a statistical sense, have the same proportions of voids and interstitial holes in their particles, but that the data sets are biased in their sampling and are not large enough to reveal this.

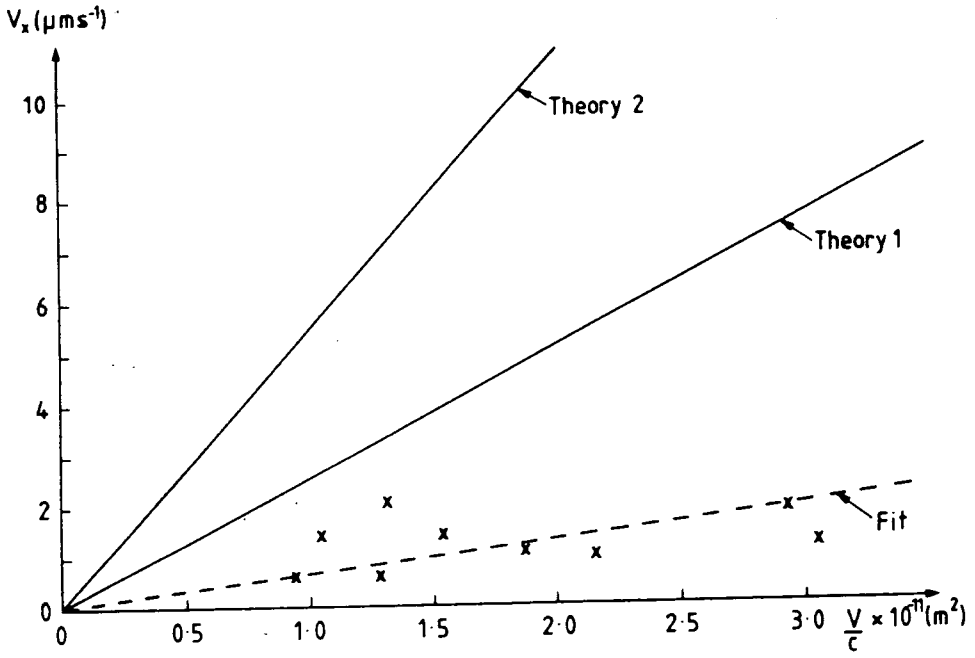

Figure 7.10 The calculated and measured values of v_x from a sample of 7C particles all in the same field gradient plotted as a function of V/c.

7.10 Discussion and Conclusions

Values of particle velocities in magnetic field gradients for CrO_2 and Magnaflux 7C Concentrate particles have been observed. At first glance they may appear to be in serious disagreement with the two theories which purport to explain their behaviour. However, it has been argued that this is not the case and that the disagreement arises chiefly from an inability to measure the volumes and susceptibilities of the particles sufficiently accurately. There is nothing wrong with the the theoretical formalism employed in this and other chapters.

An important result which has emerged is that the measured behaviour of v_x as a function of V/c (figures 7.8, 7.9 and 7.10) is indeed linear, as predicted by both Theory 1 and Theory 2, although the slopes are different. Problems associated with measuring V, c and χ_{vi} make it difficult to resolve the causes of the discrepancies in the slopes. The underlying linear relationship is, however, significant. If the discrepancy arises mainly from errors in measuring particle volumes then these errors indicate that the over-estimation of the volume can be by an order of magnitude. Uncertainty in the values of χ_{vi} and c is also probable, however, and this complicates the issue. In this case, the over-estimation of the volumes is not by such a large amount and it is a combination of uncertainties in V, c and χ_{vi} which produces the discrepancy. Voids and holes in the particles, the sizes and extents of which cannot accurately be determined using the optical microscope, are believed to be one cause of this discrepancy.

Another factor which should be remembered is that the observations were made on a narrow particle size band of the particle size distribution. The measurements made for the estimation of χ_{vi} in Theory 2 were made on particles spanning the whole particle size distribution. Hence, Theory 2's value for χ_{vi} is an 'average' for the full range of the sizes of the particles and may not be strictly accurate for the small subset of the particles studied here. Because the particles studied are at the

larger end of the particle size distribution, by the argument given at the end of section 7.9.i, they have lower susceptibilities than are given by Theory 2.

It is also significant that the best agreement between the theoretical and the measured values of v_x occurred for the first data set presented, Table 7.4. These particles were all of a more markedly smaller volume than any of the other samples. This sample, therefore, is the least affected by the presence of both voids and holes and, because of the smaller particle size, by the effect of an over-estimation of χ_{vi}.

One ought to be aware of the possible limited applicability of these results to the properties of magnetic inks in general. These experiments have found evidence for the presence of a significant volume of voids in the particles. However, since the experiment could necessarily only look at the particles which remained suspended for times of the order of a few minutes, most of the particles observed here could be merely constituting a small, non-representative subset of the whole magnetic ink system. Indeed, particles without the observed V and c characteristics could be falling out of the suspension rather quickly, leaving the small suspended residue on which this study concentrated. This observation accords with a result communicated by Wagg (1988). In preparing a system of Magnaflux 7C concentrate in water, Wagg observed an anomalously long settling time for a small proportion of larger particles. The larger particles would be the ones expected to sediment out the fastest (Shelikhov and Aleksandrov (1977)). Wagg's observation lends support to the view that it is a small subset of the whole particle size distribution which has the V and c characteristics found in this chapter, and which arise, specifically, from the presence of voids and holes.

Later chapters will present details obtained from electron microscopy of the structure of aggregates of MPI particles. These later chapters will show that voids and holes constitute a significant proportion of the apparent volume of some of the particles/aggregates. It should not be surprising, therefore, that the effects of these voids and holes manifest themselves 'macroscopically' in the study of the sets of particles which have been described in this chapter.

Chapter 8

Optical, X-ray, and Electron Analysis of Magnetic Ink Systems

8.1 Introduction

This chapter describes a series of experiments which were conducted in order to characterize in detail some 'typical' magnetic ink systems. Essentially, three types of analysis technique are reported. These are X-ray analysis, optical microscopy, and electron microscopy. Most of the analysis was performed on the black magnetic ink, Magnaflux 7HF. This system, comprised of solid particles in a kerosene carrier with a small amount ($\sim$ 1% by volume) of surfactant, was chosen as the candidate for intensive study because it is typical of a great number of commercially available non-pigmented, non-fluorescent magnetic inks. The chapter will proceed by describing in order the various investigations performed.

8.2 Optical Microscopy of the 'As-Received' and 'Dispersed' Ink

The 'as-received' Magnaflux 7HF magnetic ink system was first investigated using the optical microscope operating in transmission mode, as in Chapter 7. The microscope specimens were mounted on conventional glass optical microscope slides having shallow concave recesses to hold the liquid. The specimens were covered with conventional glass optical microscope cover slips. A typical optical micrograph is shown in figure 8.1.

It can be seen from figure 8.1 that the particles are irregularly-shaped aggregates having a wide size distribution. From a study of a large number of such micrographs an approximate value for the median aggregate diameter was obtained as $\sim 10\mu$m. An optical micrograph obtained using a higher magnification is shown in figure 8.2. This higher magnification enables one to observe that the aggregates having diameters of typically $\sim 10\mu$m are made up of apparently smaller objects having diameters of typically $1 - 3\mu$m. The fine structure of these smaller objects, however, cannot be further resolved using the optical microscope.

An initial hypothesis was that these smaller $1 - 3\mu$m diameter particles were the fundamental building blocks of the larger 10μm diameter aggregates. This hypothesis was based upon information provided by several magnetic ink manufacturers in Britain and by the current thinking of authors in the MPI field (for example, Edwards and Palmer (1986), Edwards (1986), p32). Attempts, therefore, were made at breaking up the larger aggregates into the smaller objects. The original thinking was that such a procedure could provide a simpler system which could then be used in the determination of the magnetization processes occurring in magnetic ink systems.

The most successful method for the breaking up of the larger 10μm diameter particles was found to be a simultaneous agitation and a shearing of the aggregates in the presence of both added surfactant and a decaying alternating magnetic field. The simultaneous shearing and agitation was provided by a high-shear mixer. The decaying ac field was provided by a water-cooled solenoid operating at 50Hz, the

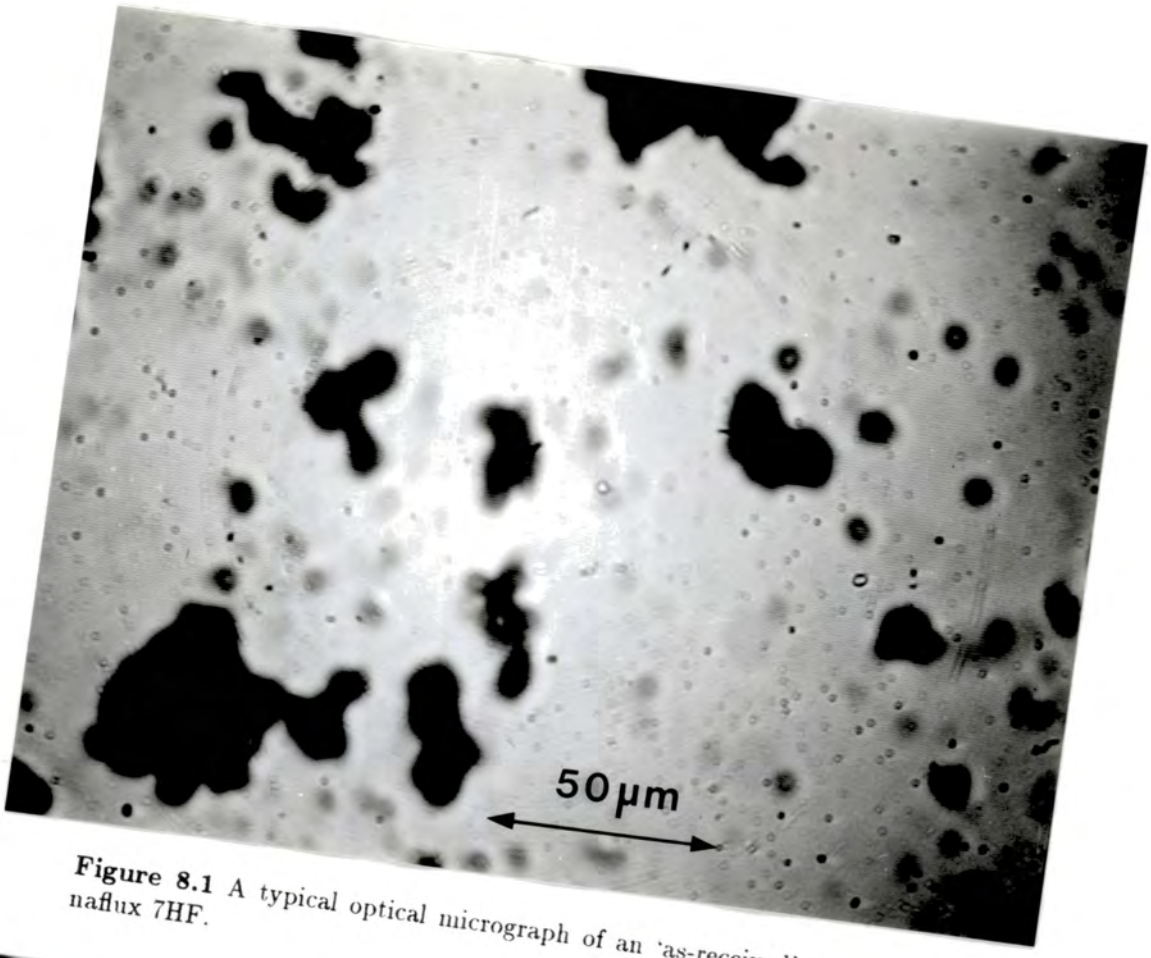

Figure 8.1 A typical optical micrograph of an 'as-received' sample of Magnaflux 7HF.

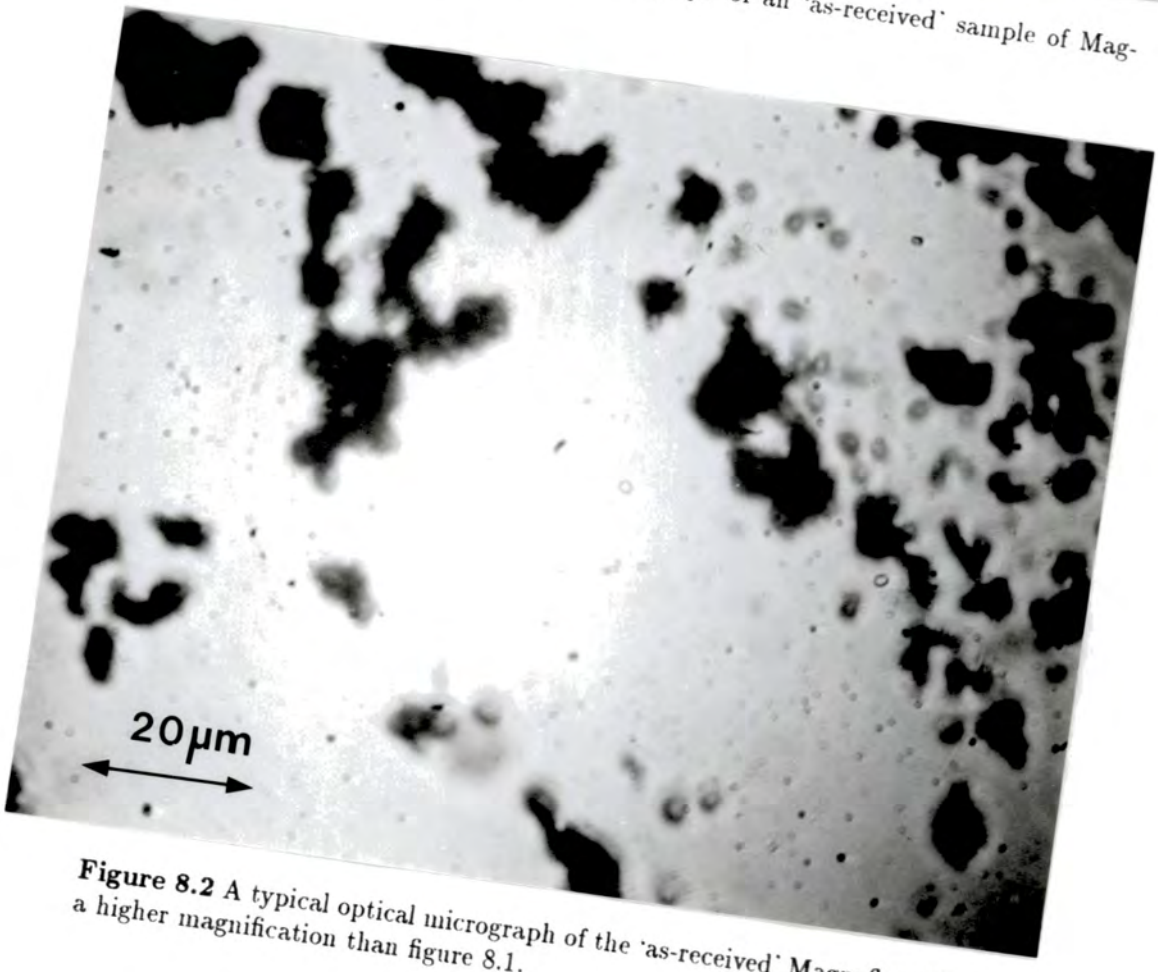

Figure 8.2 A typical optical micrograph of the 'as-received' Magnaflux 7HF at a higher magnification than figure 8.1.

field being reduced manually from its maximum value of 0.04T (rms) to zero over a time period of $\sim$ 2hours. The surfactant was $\sim$ 40% Solsperse 3000† in toluene which was added to the magnetic ink in the proportion 1 : 1 by volume. The exact chemical formula of this surfactant is withheld by ICI, but its molecular weight is approximately 3000 and it presumably has a long chain-like molecule. (Solsperse 3000 has been used successfully as a stabilizing surfactant in FeCo 'alloy' magnetic liquids (Lambrick, Mason, Harris, Russell, Hoon and Kilner (1985))). This method succeeded in breaking up the larger aggregates and produced well-dispersed systems of particles having diameters of typically $1-3\mu$m. If there are large numbers of particles very much smaller than this 'typical' size then they cannot be seen in the microscope and the possibility remains that the apparent diameter, $1-3\mu$m, is an over-estimate of the 'typical' diameter. An optical micrograph of such a dispersed system is shown in figure 8.3.

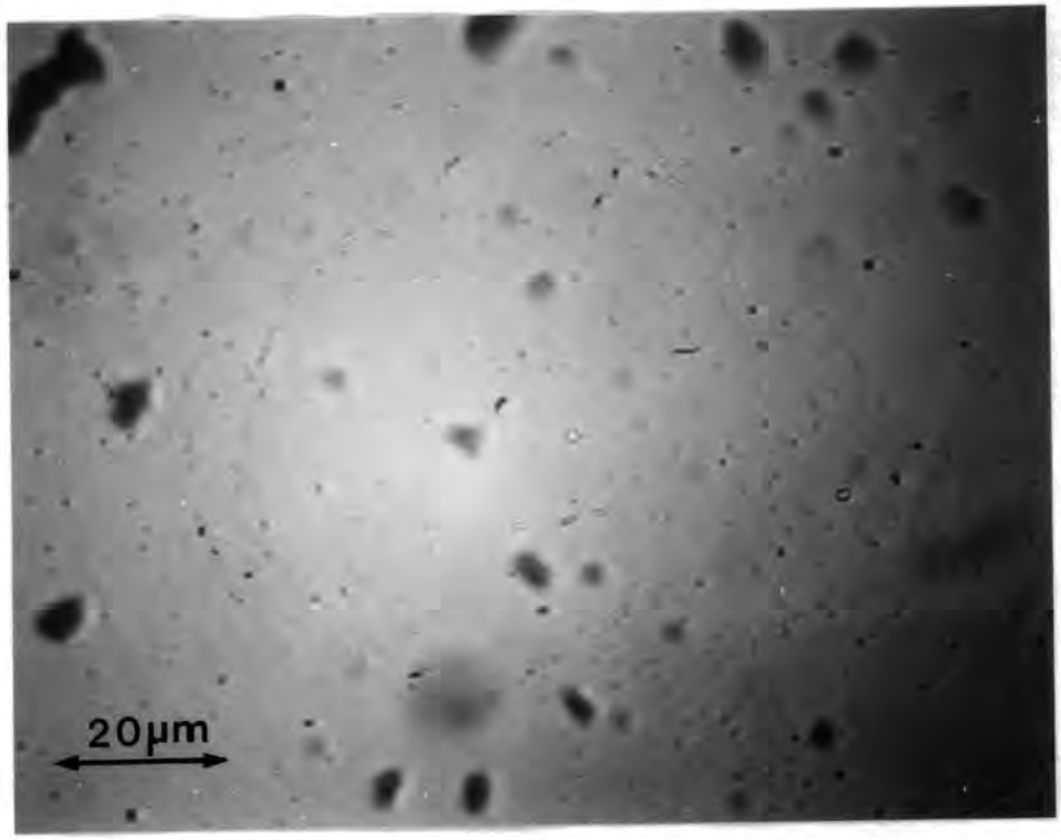

Figure 8.3 An optical micrograph of the particles in a dispersed sample of Magnaflux 7HF. The particle diameters are typically $1-3\mu$m.

Such dispersed systems were metastable with respect to reaggregation. Optical microscopy revealed that after $\sim$ 2days the dispersed systems settled out and reformed larger aggregates.

8.3 Electron Microscopy Studies

The next sections report electron microscopy studies conducted at both Durham University and Oxford University. At Durham, the electron microscopes in the School of Engineering and Applied Science were operated by the late Dr. G.J. Russell. At Oxford, the electron microscope in the Department of Metallurgy and

† Produced by ICI, UK.

Materials Science was operated by Dr. B.K. Tanner, Dr. M.G. Hetherington and Dr. J.P. Jakubovics. The generous assistance of these people is acknowledged.

8.4 Studies Using the EM7 High Voltage Electron Microscope at Oxford

In using the EM7 high-voltage electron microscope (HVEM) at Oxford, a facility for performing Lorentz microscopy on the particles was available. This technique can be used to investigate the domain structure of magnetized bodies by observing the image contrast between regions magnetized in differing directions (domains). Regions magnetized in differing directions deflect the primary beam in different directions, enabling the presence of domain walls to be determined (Craik and Tebble (1965), p312, Arii, Yatsuya, Wada and Mihama (1978)).

Samples of dispersed and reaggregated ink particles were prepared on carbon-coated grids. The instrument ran at 900keV which corresponds to a relativistic electron wavelength of 9.4×10^{-3}Å. At this energy the electrons penetrate to distances of the order of a few micrometres (Goodhew (1972), p10). Hence, full electron penetration of all of the $1 - 3\mu$m diameter dispersed particles occurs; only for the very largest aggregates is full electron penetration a problem. However, the electron microscopy study was unable to find in any of the samples the contrast arising from electron deflection in regions of differing magnetization.

Shadow transmission electron microscopy (TEM) was used to investigate the structure of the $\sim 1 - 3\mu$m diameter particles in a dispersed ink sample. This study produced the surprising result that these dispersed particles are themselves aggregates of very much smaller particles of irregular shape having diameters in the range 20 – 200nm. This is clearly shown by figure 8.4 which is an electron micrograph of a particle having a major diameter of $\sim 2.5\mu$m, but which can be seen to be constituted of much smaller particles. This result was also confirmed by the results of the TEM studies performed at Durham which will be reported shortly.

This result contradicts the previously mentioned 'conventional wisdom' with regard to the sizes of particles present in conventional commercially available magnetic ink systems. It also contradicts our earlier hypothesis about the $1 - 3\mu$m diameter particles being the basic building blocks of the particles in the ink systems.

This result has some similarities to some recent results concerning the microstructure of $\gamma - Fe_2O_3$ magnetic tape particles. Andress, Benedetti, Corradi and Fagherazzi (1986) have postulated that such tape particles are composed of a mosaic of 'islands' of much smaller crystallites than is usually thought. These crystallites are too small to be detected using conventional TEM, but the authors have obtained evidence from X-ray scattering and X-ray diffraction to support their postulate. Their postulate also explains some anomalous 'print through' values of $\gamma - Fe_2O_3$ particulate recording media. This subject, however, is still highly controversial.

Confirmation that the much smaller particles comprising the dispersed particles in the ink system were single crystallites was provided by dark-field microscopy. This technique involves permitting only one diffracted beam to form the image. This is realised either by gun-tilting, by incident beam deflection or by positioning the objective aperture off the optic axis (Van der Biest and Thomas (1976)). In this study the last of these methods was employed. Dark-field micrographs display bright image areas arising from only one crystal plane orientation. Consequently, in

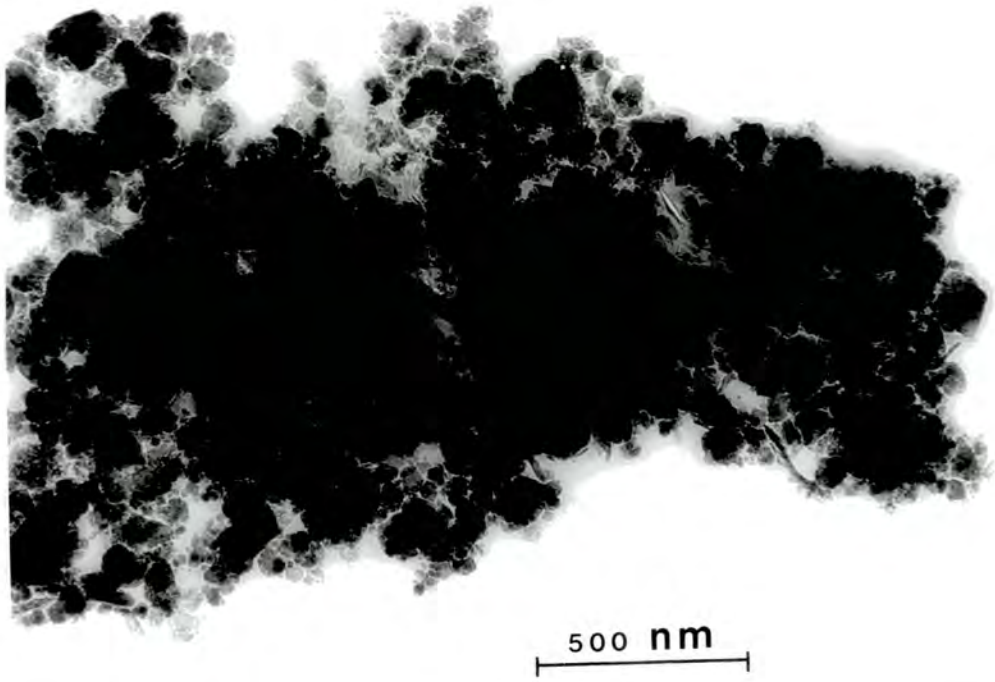

Figure 8.4 An electron micrograph at 900keV of a particle in a dispersed sample of Magnaflux 7HF.

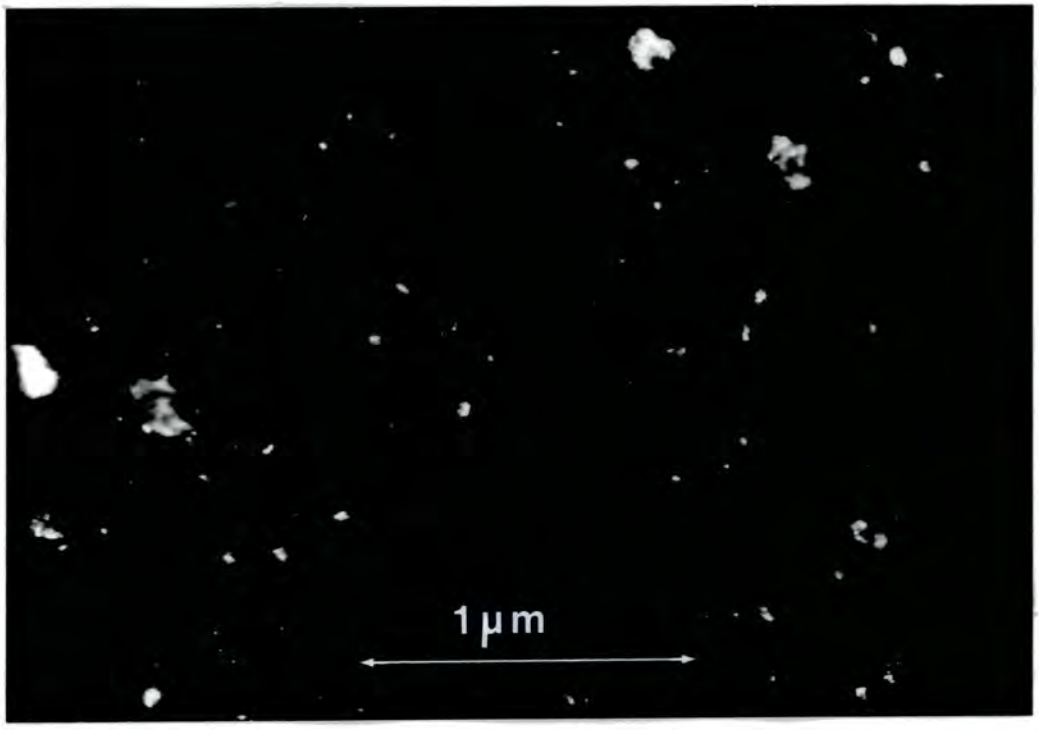

Figure 8.5 A dark-field micrograph formed by individual single crystallites which comprise a larger aggregate. The crystallite size confirms the size range (20 – 200nm) determined from the shadow TEM micrographs.

these ink particle aggregates, individual single crystallites which all have the same crystallographic orientation produce diffracted beams which enter the aperture, giving a clear indication of the sizes of individual single crystallites. Figure 8.5 shows a dark-field micrograph obtained in the study. The white areas are formed from single crystallites and confirm that the range of particle sizes is consistent with that observed in the shadow TEM micrographs.

A 300nm diameter aggregate on one of the grids was used to obtain a Laue pattern. This is shown in figure 8.6. The random orientation of the spots indicates that within the aggregate there is no preferred orientation of crystallites. The diffraction rings were indexed to a face centred cubic (fcc) crystal structure. The same pattern of diffraction rings was found for all aggregates investigated. Further details of the determination of the crystal structure and in particular the determination of the lattice parameter, using an X-ray method, will be reported later in the chapter.

Figure 8.6 Structured Laue rings from a Magnaflux 7HF aggregate. The diffraction rings reveal a fcc structure.

In summary, therefore, the investigations performed at Oxford have revealed important details about the microstructure of the particles in the magnetic ink system. Contrast associated with the presence of regions of differing magnetization and, hence, of domain walls, could not be detected. The basic building blocks of larger aggregates have been found to be small crystallites having diameters in the range 20 – 200nm. Dark-field microscopy has confirmed that these objects are indeed single crystallites in this size range. No preferred orientation of crystallites within aggregates could be found. The crystallites have a fcc crystal structure.

8.5 Studies Using the JEOL JEM 120 Transmission Electron Microscope at Durham

Shadow TEM studies of ink particles were made on the JEOL JEM 120 electron microscope at Durham. Again the samples were prepared on carbon-coated grids. The samples were comprised of the larger-sized 'as-received' ink particles and also of the dispersed particles. The instrument ran at 100keV, corresponding to an electron wavelength of 0.037Å.

The microstructure of the ink particles found in the previously-reported study at Oxford—the composite structure of many very small, irregularly-shaped crystallites having diameters in the range 20 – 200nm—was again observed. A typical micrograph of an aggregate having a major diameter of $\sim 4\mu$m is shown in figure 8.7.

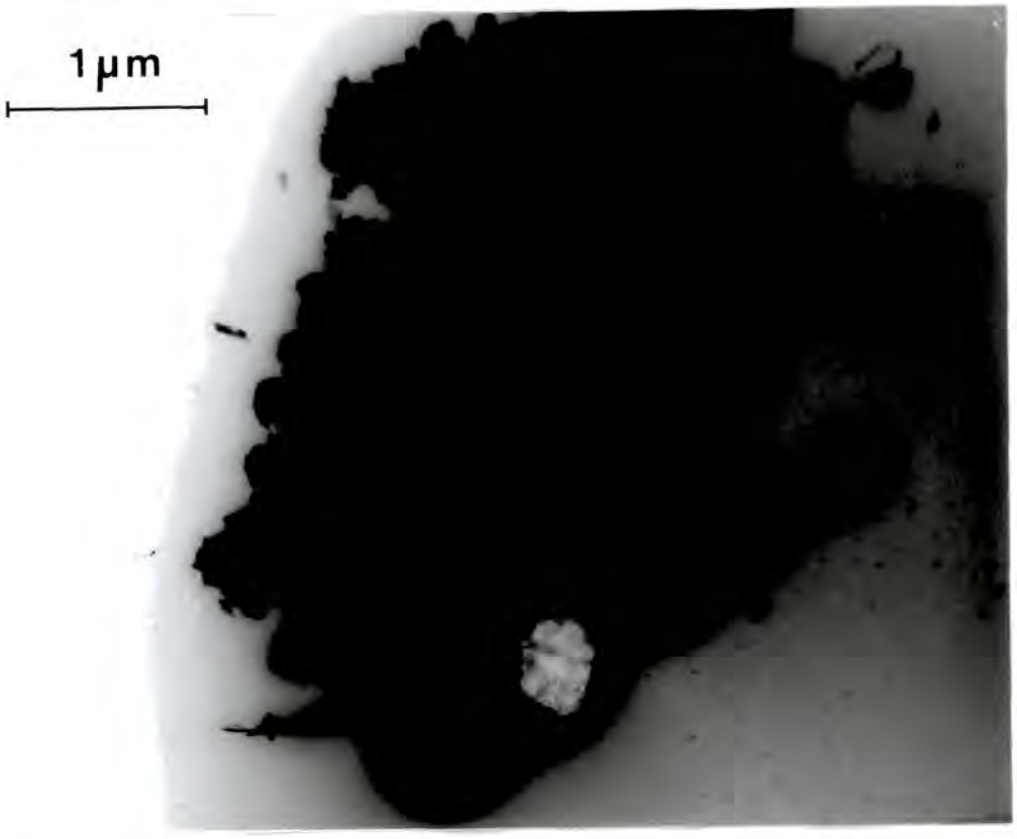

Figure 8.7 A shadow TEM micrograph of a dispersed aggregate of Magnaflux 7HF particles taken at 100keV on the Durham microscope.

The same type of microstructure was found in the 'as-received' samples. For example, figure 8.8 shows an electron micrograph of a large 'diffuse' or loosely-packed large aggregate which was found on one of the grids and through parts of which the electron beam could penetrate.

8.6 Studies Using the Cambridge Stereoscan 600 Scanning Electron Microscope at Durham

Scanning electron microscopy (SEM) is a technique in which the incident electron beam excites electromagnetic and electronic responses from a thin surface layer of the specimen. A large number of processes occur in the surface of the sample. The two processes which are of relevance to us are secondary electron emission and

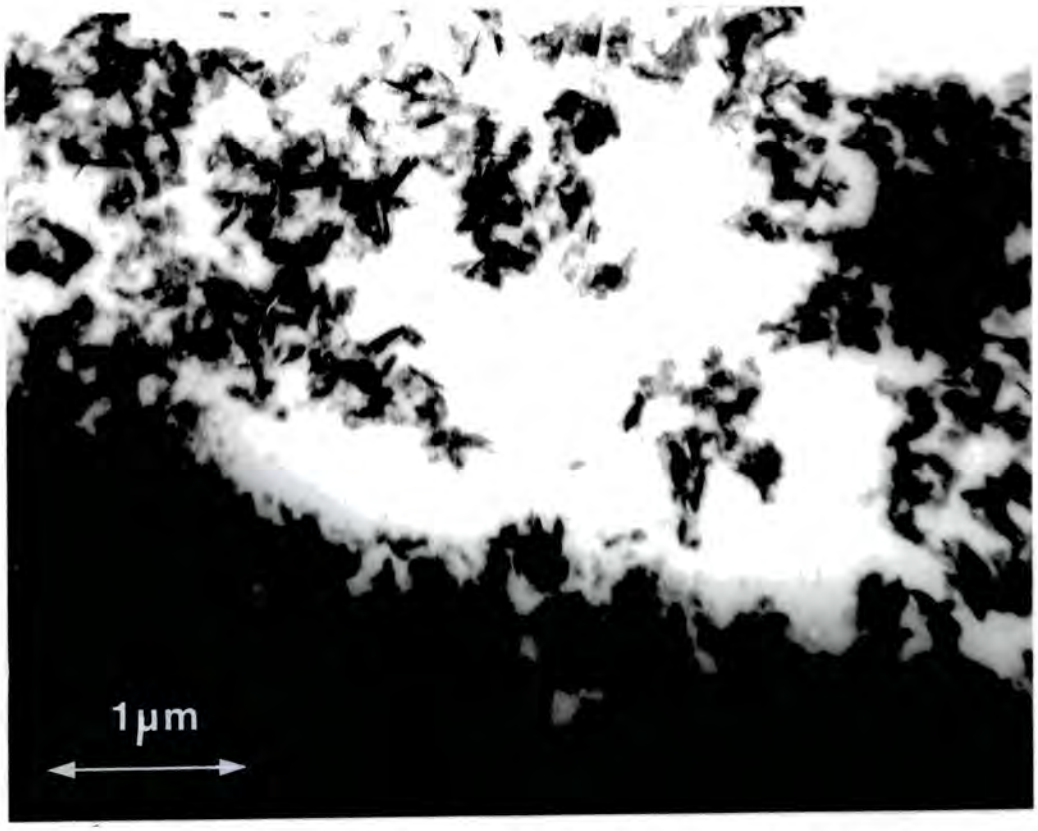

Figure 8.8 A shadow TEM micrograph of a 'diffuse' aggregate of 'as-received' Magnaflux 7HF, showing the characteristic microstructure of small irregularly-shaped crystallites.

characteristic X-ray emission. The secondary electrons originate at the surface of the sample from inelastic scattering and have energies of less than 50eV. Detection of these electrons provides information about the specimen surface topography, the imaging having a moderate resolution and a large depth of focus. Characteristic X-ray emission arises from electronic transitions. If the X-rays are detected using an energy-dispersive spectrometer then the characteristic X-ray spectrum can be used to provide localized elemental analysis. This elemental analysis is known as energy-dispersive X-ray analysis (EDAX).

For these studies the samples were first mounted on aluminium stubs. Then the samples were thinly coated with conducting coatings of gold by sputtering at very low pressure. This procedure provides an unobtrusive structure which greatly reduces the undesirable effects of diffuse back-scattering of electrons from within the specimen (Watt (1986)). The samples themselves all consisted of ink particles which had been extracted from the 'as-received' ink by a simple filtering process. The particle extract was than re-dispersed in toluene prior to mounting on the aluminium stubs. Subsequent evaporation of the toluene left only the particles themselves bonded onto the stubs.

Figure 8.9 shows a SEM micrograph of an aggregate having a major diameter of $\sim 15\mu$m. At this magnification, the aggregate appears to be composed of globular objects having diameters of typically 1μm.

At a higher magnification the fine structure of these globules could be seen. For example, figure 8.10 shows the same aggregate as in figure 8.9 but at a higher

Figure 8.9 A SEM micrograph of a 15μm aggregate from a sample of Magnaflux 7HF. At this magnification, globular structures of diameter $\sim$ 1μm are apparent.

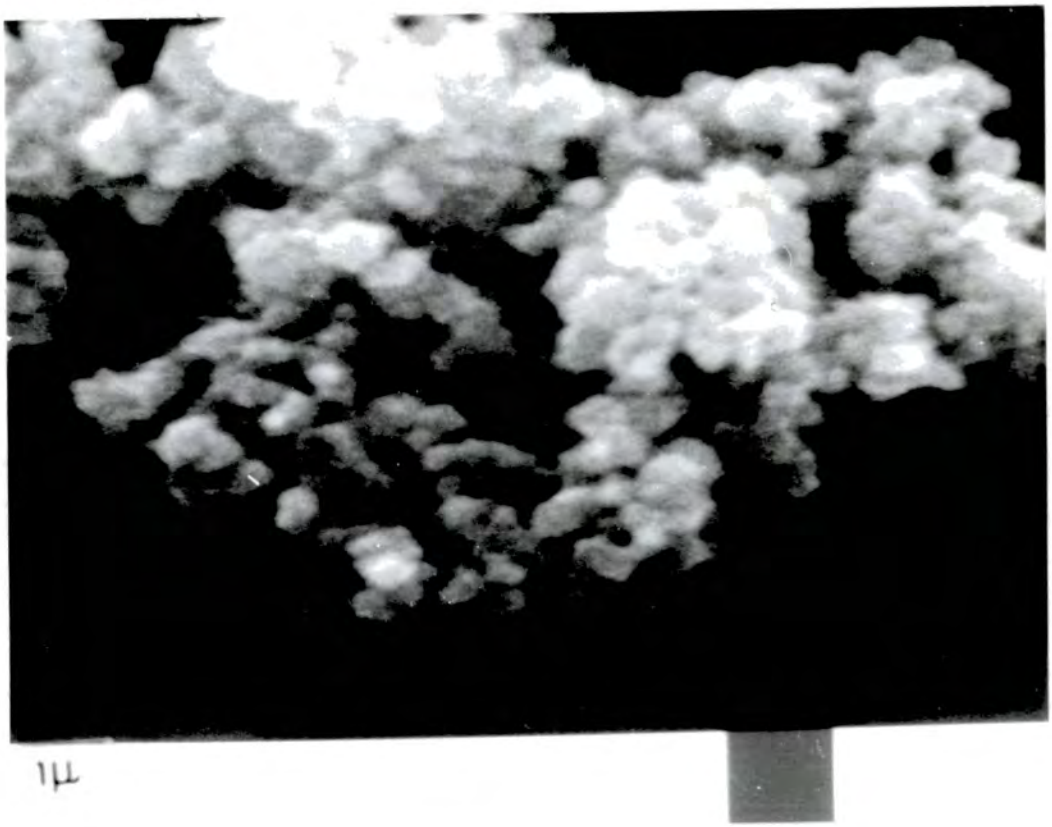

Figure 8.10 A SEM micrograph, at a higher magnification, of the same aggregate as in figure 8.9. Finer structure of the $\sim$ 1μm diameter globules is revealed.

magnification. Now the finer structure is apparent. It is believed that these $\sim 1\mu$m diameter constituents of the aggregate are to be identified with the small aggregates obtained in the dispersed ink system, mentioned in section 8.2, but which were subsequently revealed to be composed of much smaller crystallites. Micrographs such as figure 8.10 can also be used to explain why the dispersion process could not break up the large aggregates in the 'as-received' ink into anything smaller than the $1-3\mu$m diameter aggregates. There appears to be a two-level structural hierarchy in the aggregates. There are aggregates of $1-3\mu$m diameter relatively loosely bound into much larger aggregates which, themselves, can be broken up in the dispersion process. The constituents of the smaller aggregates, however, are tightly bound and are not significantly disturbed in the dispersion process. The relatively tight binding of the crystallites comprising the $1-3\mu$m aggregates is explained by the argument that the crystallites are all SD particles possessing permanent magnetic moments which arrange themselves into a configuration for which flux closure occurs. Hence, the $1-3\mu$m diameter aggregates possess negligible or very small net magnetic moments, severely weakening their bonding capability in the larger aggregate structures. Using this argument it is easy to see both how the two-levelled aggregate structure arises and how the dispersion process is only effective for one level of this aggregate structure.

The surface structure of another very large aggregate is shown in figure 8.11. The presence of $1-3\mu$m diameter globular components is apparent.

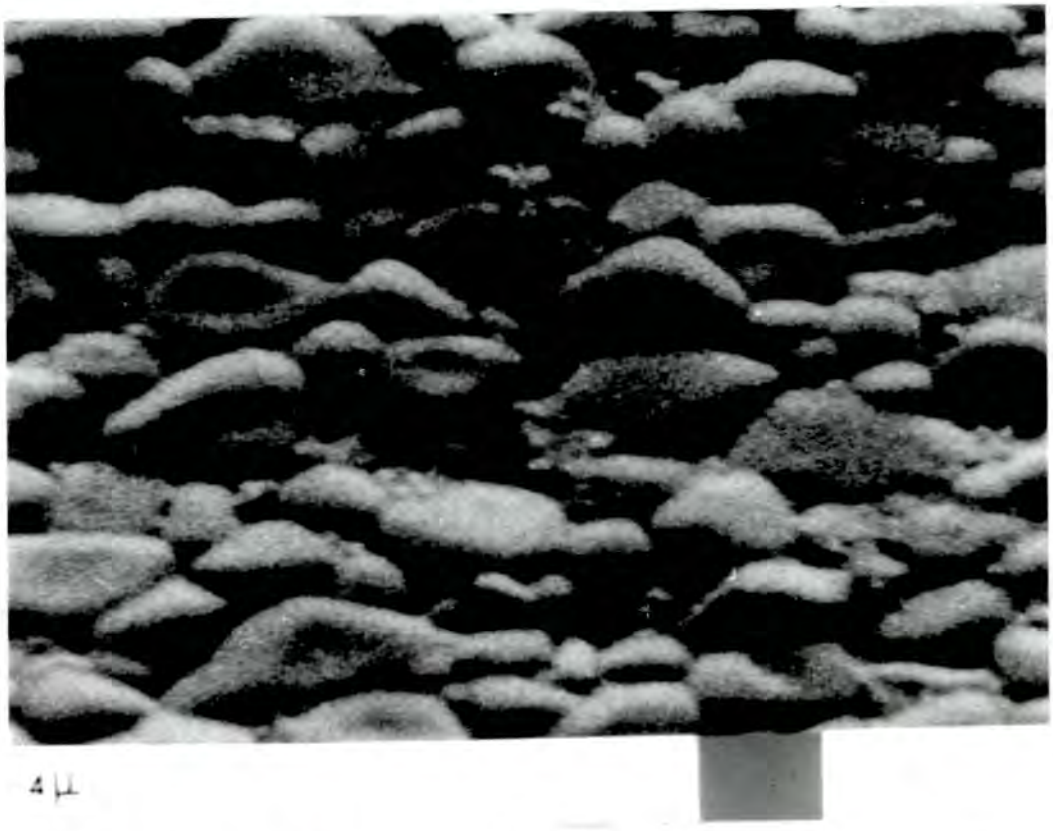

Figure 8.11 The surface structure of a large Magnaflux 7HF aggregate. $1-3\mu$m diameter globules can be clearly seen.

The microscope was fitted with a Link Systems 860 Analyser for EDAX studies. An EDAX spectrum obtained from an aggregate of Magnaflux 7HF particles is shown in figure 8.12.

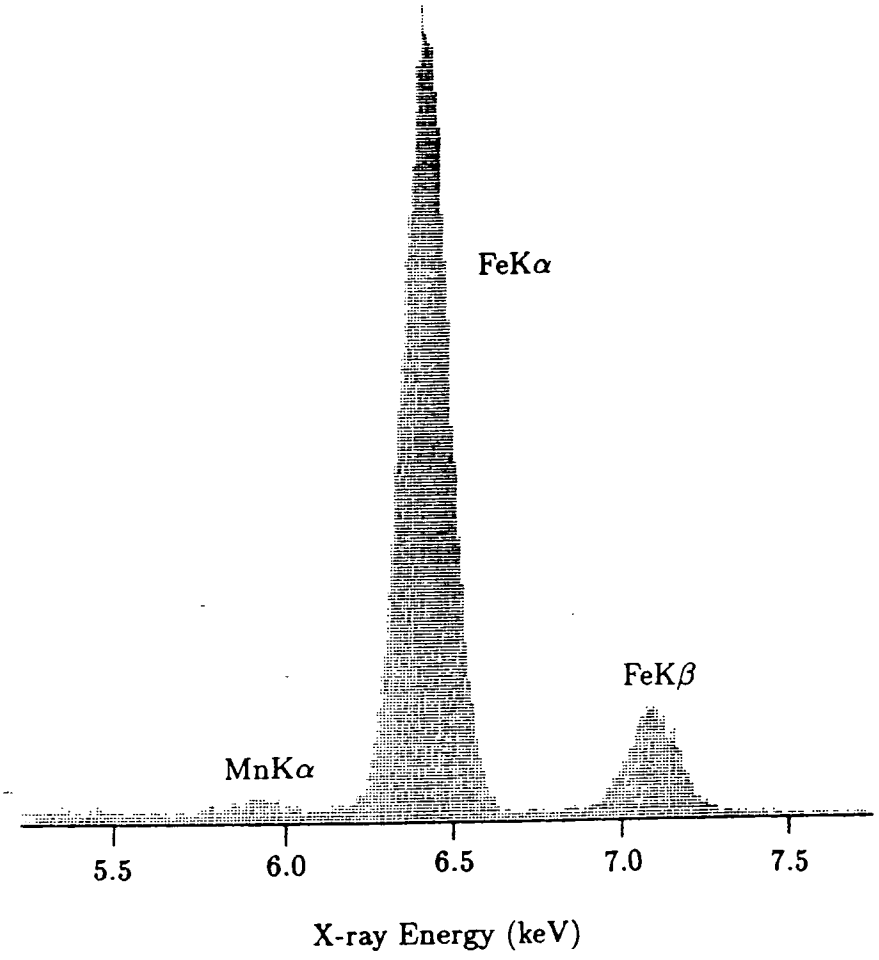

Figure 8.12 The EDAX spectrum from Magnaflux 7HF particles. The technique cannot detect elements having atomic numbers less than about 11, for example, oxygen. The Mn impurity is clearly shown.

The Fe peak is of relevance to the X-ray structure determination to be discussed in the next section. However, the presence of Mn at approximately the 1% by volume level is interesting. The X-ray structure determination will show that the particulate material is magnetite (Fe_3O_4). Mn in this abundance is consistent with the dominant impurity in naturally-occurring magnetite. Similar levels of impurities of Mn, Ti, Na, S and Cl were found also in other magnetic ink and powder systems which were also studied—both iron and magnetite ones—produced by other manufacturers.

8.7 X-ray Powder Diffraction Studies

X-ray powder diffraction was performed in order to determine the crystal structure of the particulate material in Magnaflux 7HF. The particles were filtered out from the 'as-received' ink, dried and then placed in a glass capillary tube. The sample was then inserted into a Debye-Scherrer powder camera. The X-radiation source was a Mo target. A thin foil of Zr was inserted into the beam path, prior to collimation, in order to ensure that only MoKα_1 (wavelength 0.7093Å) radiation was incident upon the sample. Details of the indexing of the diffraction lines on the film are given in Table 8.1.

(hkl)	d(Å)	a_0(Å)
(111)	4.865	8.43
(200)	missing	–
(220)	2.960	8.37
(311)	2.531	8.39
(222)	2.426	8.40
(400)	2.092	8.37
(331)	missing	–
(420)	missing	–
(422)	1.708	8.37
(511)	1.612	8.38
(440)	1.480	8.37
	Average a_0	8.385Å
	ASTM a_0	8.396Å

Table 8.1 Details of the indexing of the diffraction lines for the Magnaflux 7HF particles. The crystallographic planes, the d-spacings and the derived lattice parameter, a_0, are shown.

The indexing reveals that the material is fcc with a lattice parameter of 8.385Å. The literature value for magnetite, taken from the ASTM Tables (ASTM (1974)), is $a_0 = 8.396$Å. Thus, the material is identified as magnetite, Fe_3O_4. Additional powder diffraction studies of several other commercially available black magnetic ink systems identified the particles in those systems as being magnetite. It was mentioned in Chapter 2 that it is sometimes difficult, using X-ray techniques, to distinguish between maghemite ($\gamma - Fe_2O_3$), which has a lattice parameter of 8.33Å, and magnetite. The errors on the values of a_0 in Table 8.1 are sufficiently small to be certain that no such ambiguity arises here.

8.8 Correlation of Magnetic Behaviour with Optical Microscopy Observations of Particles in an Applied Magnetic Field

Some initial measurements of the magnetic properties of these magnetic ink systems were performed by Dr. S.N.M. Willcock on the first Durham VSM. The magnetic properties will be reported in great detail in Chapter 9. However, these initial studies revealed features which we were able to relate to optical microscopy observations of aggregates in an applied magnetic field.

The VSM measurements on 'as-received' and dispersed-then-reaggregated samples of Magnaflux 7HF revealed that the low field susceptibility of the latter samples was greater than that of the former. This result arises directly from the differing structure of the aggregates in the two systems. The aggregates in the 'as-received' system predominantly have an approximately spherical form and, for these aggregates having randomly spatially distributed magnetic moments, a flux

closure configuration of the magnetic moments of all the constituent particles occurs, resulting in a demagnetized assembly. The dispersed-then-reaggregated system, however, has predominantly chain-like aggregates formed during the reaggregation of the $1 - 3\mu$m diameter components of the dispersed system. The difference in the low field susceptibility between the two samples is explained, therefore, by observing that, in response to an imposed magnetic field, the chain aggregates can rotate relatively easily and quickly, whilst the spherical clump aggregates are relatively unresponsive and, at these low fields, would require physical deformation to exhibit the same degree of rotation as their chain-like counterparts.

These differences in response to an imposed field between chain-like aggregates and spherical clump aggregates have been observed using the optical microscope. This behaviour is shown in figure 8.13 which shows a sequence of optical micrographs for a dispersed-then-reaggregated sample of Magnaflux 7HF in which, unusually, both clump and chain-like aggregates are present. The sequence shows the changes in orientation of suspended aggregates resulting from the gradual introduction of an external dc magnetic field. It is apparent that, whilst the chain-like structures move relatively easily, the clumps remain stationary until the field is increased to $\sim 1.2\text{kAm}^{-1}$.

8.10 Discussion and Conclusions

Although the results presented in this chapter have focussed particularly on Magnaflux 7HF, because this ink is typical in its manufacture and constitution of a great many black inks, the results are of relevance to a whole class of magnetic ink systems. A dispersion process has been described which has facilitated the characterization methods. The results have indicated that the particles themselves are complex aggregates of single crystallites having typical diameters in the range $20 - 200$nm. It is to be expected that these particles are SD as they are below the SD threshold sizes for magnetite discussed in previous chapters. There appear to be two levels in the aggregate structures: tightly bound aggregates of the $20 - 200$nm diameter crystallites having diameters of typically $1 - 3\mu$m, and more loosely bound aggregates of these $1 - 3\mu$m diameter objects into much larger aggregates. The crystallite components are randomly orientated within the smaller aggregates, almost certainly producing flux closure configurations. The particle material is magnetite but a small Mn impurity has been found which suggests that the magnetite is naturally occurring rather than synthetic.

The two types of larger aggregate structure—clumps and chains—and their response to imposed fields can be related to measurements of the low field susceptibility. This result suggests that some means of stabilizing the dispersed ink may be beneficial in terms of sensitivity in defect detection.

Another important point is that measurements of aggregate size distribution are unlikely to yield data of fundamental significance since the aggregate size is strongly dependent upon the history of the magnetic ink. Unfortunately, it was not possible using the TEM micrographs to determine the particle size distribution of the $20 - 200$nm crystallites because the TEM images, such as those in figures 8.4 and 8.7, do not show the boundaries of individual crystallites sufficiently clearly. However, the presence of voids in the aggregates, such as those shown in figures 8.4 and 8.7, is of relevance to the material presented in Chapter 7. In Chapter 7 we accounted for a part of the discrepancy between the observed experimental and expected theoretical behaviour in the motions of individual MPI particles by

arguing that the particle volumes measured in the optical microscope were being over-estimated because holes and voids in the particles could not be seen. From material presented in this chapter, such as figures 8.4 and 8.7, it is clear that such voids and holes are present and account for a significant proportion of the aggregate volume.

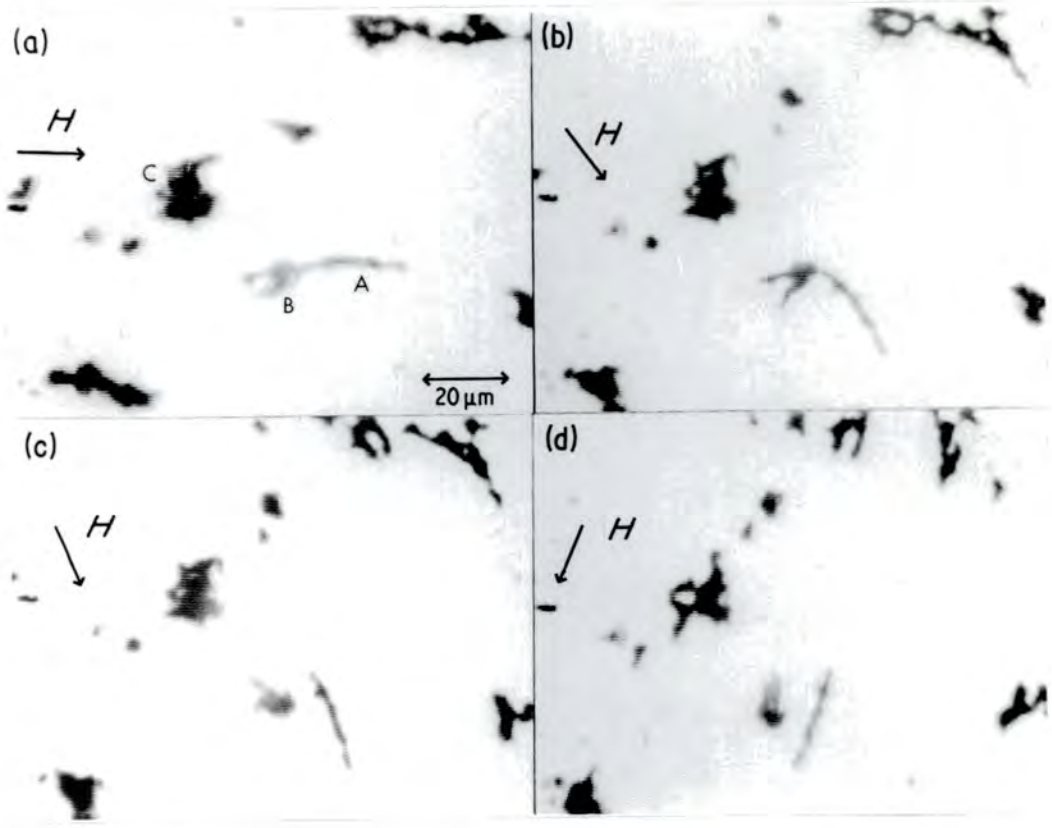

Figure 8.13 Sequence of optical micrographs of dispersed fluid under the influence of a uniform external applied field. Particular reference is made to a chained aggregate A and two clumped aggregates B and C. (a) The gradual introduction of an external field (H) results in the parallel alignment of chain aggregate A. (b) and (c) Subsequent rotation of the field vector produces the independent movement and rotation of A which eventually results in its separation from clump B. Little change is observed in the orientation of the clumped aggregates B and C. (d) Increasing the field to a maximum of 1.2kAm^{-1} results on the simultaneous deformation of the clumps to a more chain-like structure and the alignment of the same.

Chapter 9

Magnetic Properties of Magnetic Ink Systems

9.1 Introduction

This chapter reports an investigation of some of the magnetic properties displayed by magnetic ink systems. All of the magnetic measurements were obtained from the VSM which was described in Chapter 4. All of the measurements were made at either room temperature ($\sim$ 297 K) or liquid nitrogen temperature (77 K). In the case of the 77 K measurements, the sample was vibrated whilst submerged in boiling liquid nitrogen held in a small glass dewar which was rigidly secured in the magnet field gap. During the course of the 77 K measurements, as the liquid nitrogen boiled off, it was constantly replenished in order to maintain a constant volume within the dewar. The chapter begins with a treatment of the basic magnetic properties of the ink systems before it concludes with a discussion of a significant time-dependent magnetization which was discovered.

9.2 Sample Preparation

All of the VSM measurements were taken on samples which were spherical in shape and which were contained in small glass spheres. The glass spheres had an inner diameter of 5.4mm and an outer diameter of 8mm, the ink being inserted through a circular hole of approximate internal diameter 2mm by using a syringe. The hole through which the known mass of sample was inserted was subsequently sealed off using either quick-drying Araldite adhesive or, if low temperature measurements were to be made, low-temperature Araldite. Care was always taken to ensure that the adhesive material used to seal off the hole did not come into contact with the sample itself within the sphere. If this happened by accident, the sample was rejected because it is highly likely that it resulted in particles being permanently 'frozen' in the adhesive matrix.

The use of these glass spheres provides two benefits. The first is that the demagnetizing factor of the sample is known exactly ($D' = \frac{1}{3}$). The second is that the volume of the sample is known very accurately which, with a knowledge of the sample mass, enables the density of the sample to be simply inferred. When residual corrections were made to the VSM data, the residual signal was always obtained from measurements taken from an identical empty glass sphere sample holder at the same temperature as the sample proper. The subtraction of the residual signal from the proper sample signal was accomplished in the data analysis software as mentioned briefly in Chapter 4 and as listed in Appendix P2.

9.3 The Magnetization Curve

This section presents details of the magnetization curves of two samples of Magnaflux 7HF at room temperature and 77K respectively. No special importance is to be attached to the specific samples for which data is presented. More than anything else, the data is exemplary and is 'typical' of that found repeatedly in the magnetic measurements which were performed on these systems.

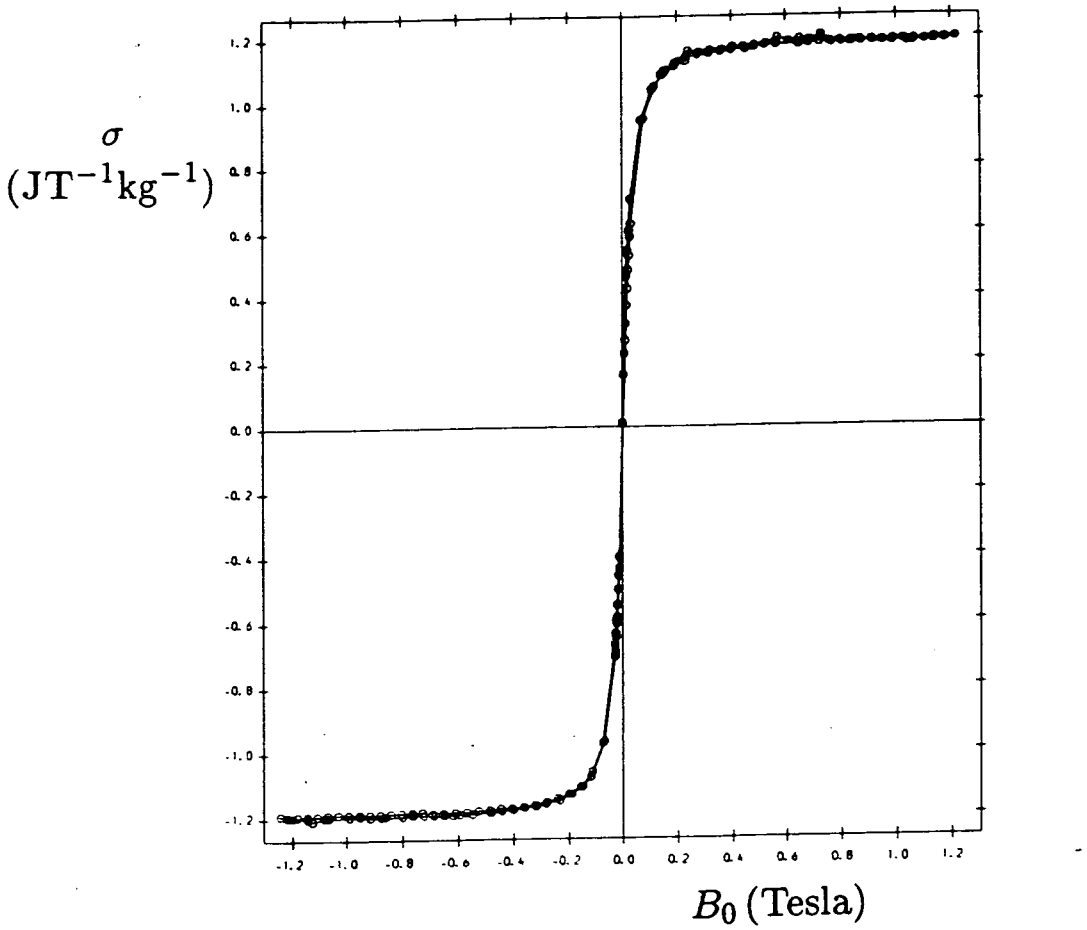

Figure 9.1 The room temperature magnetization curve for a sample of 'as-received' Magnaflux 7HF.

The room temperature magnetization curve of a sample of 'as-received' Magnaflux 7HF is shown in figure 9.1. This curve has been corrected for the VSM residual signal and for the demagnetizing field of the sample. In this particular example, the mass of the sample is 0.116g, the density is 1.407gcm^{-3} and the temperature is 295.5 K. The volumetric packing fraction, ϵ_v, is given by

$$\epsilon_v = \frac{\sigma_s \rho}{M_{sb}} \qquad 9.1$$

where σ_s is the saturation magnetization per unit mass of the sample, ρ is the density of the sample and M_{sb} is the saturation magnetization of the bulk form of the particulate material (magnetite). A $(1/B_0)$ extrapolation of the magnetization values in the saturation region of the magnetization curve given in figure 9.1, to obtain σ_s, results in a value for ϵ_v of $\epsilon_v = 3.44 \times 10^{-3}$ (= 0.344%). In equation (9.1) the value for M_{sb} is taken from Pauthenet (1950). This reference gives the temperature-dependence for magnetite of the saturation magnetization per unit mass, σ_{sb}, which is related to M_{sb} by the obvious relation

$$\sigma_{sb} = \frac{M_{sb}}{\rho_{Fe_3O_4}} \qquad 9.2$$

with $\rho_{Fe_3O_4} = 5240\text{kgm}^{-3}$.

Explicitly, Pauthenet has given the temperature-dependence of σ_{sb} for magnetite at room temperature (and below) as

$$\sigma_{sb} = \sigma_0(1 - QT^2) \qquad 9.3$$

where T is the temperature in Kelvin, $\sigma_0 = 98.48 \mathrm{JT^{-1}kg^{-1}}$ (the saturation magnetization per unit mass at absolute zero) and $Q = 8.26 \times 10^{-7}\,\mathrm{K^{-2}}$. In all of the results concerned with Magnaflux 7HF (magnetite) presented in this thesis, the method described above and the temperature-dependence given in equation (9.3) were used to obtain values of ϵ_v for the samples.

Getting back to the magnetization curve shown in figure 9.1, it is possible to see that there is a slight hysteresis. Using the facility of the VSM for a detailed coercivity study, more details of which are given in Appendix P1, enables the coercivity, B_{0c}, to be measured accurately. At room temperature, the coercivity of Magnaflux 7HF is $B_{0c} = 0.98(\pm 0.05)\mathrm{mT}$. Furthermore, this value of the coercivity, within experimental error, was found for all other samples of Magnaflux 7HF investigated at room temperature, irrespective of their differing volumetric packing fractions.

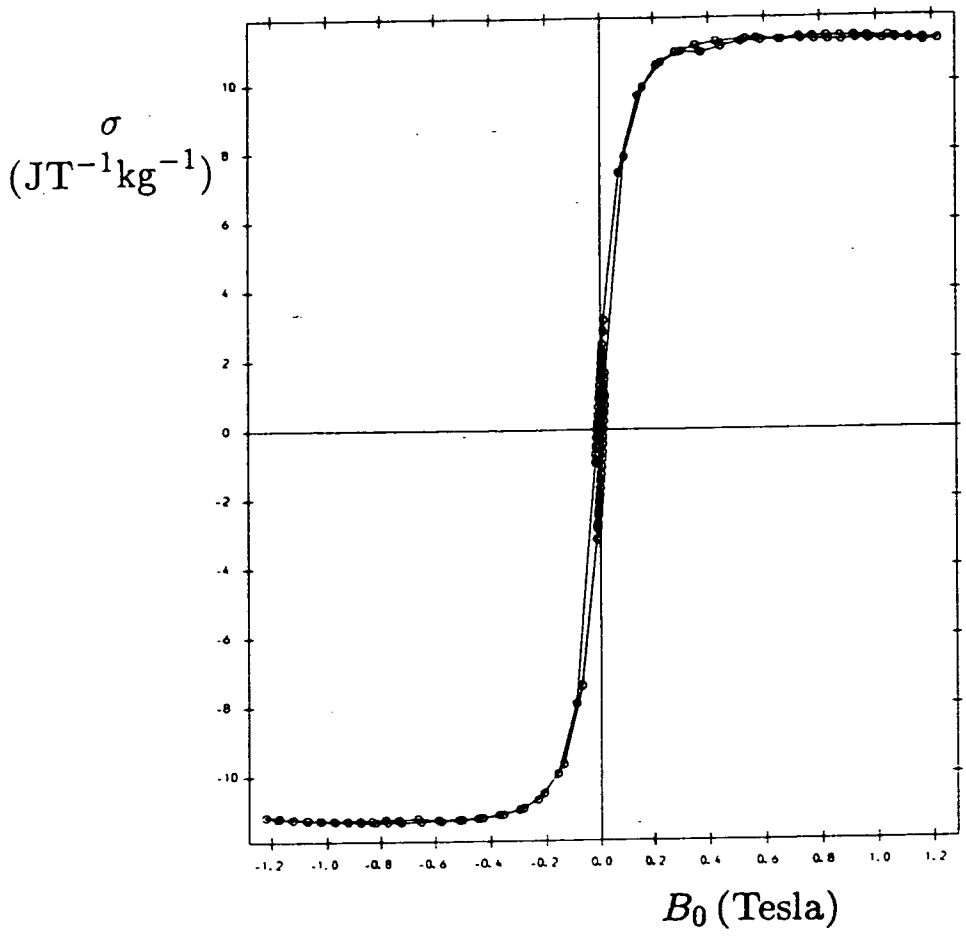

Figure 9.2 The magnetization curve at 77 K for a sample of 'as-received' Magnaflux 7HF.

The magnetization curve of another sample of 'as-received' Magnaflux 7HF, this time at 77 K, is shown in figure 9.2. Again the residual and the demagnetizing field corrections to the data have been made. This sample has a mass of 0.123g, a density of $1.496\mathrm{gcm^{-3}}$ and a volumetric packing fraction, ϵ_v, of 3.42×10^{-2} (= 3.42%). It is apparent that the hysteresis is more pronounced and that the coercivity is greater than that at room temperature. A detailed investigation of the coercivity region at 77 K for this particular sample indicated that the coercivity was $14.4(\pm 0.1)\mathrm{mT}$. This value was measured with the sample having been frozen in zero field so that the

magnetic moments of the particles were randomly oriented. It would be expected that for an aligned frozen sample the coercivity measured in the direction of the alignment would have been larger.

At 77 K a slight dependence of the coercivity upon the volumetric packing fraction was found in the very few samples for which accurate coercivity measurements were pursued. Qualitative agreement was found with the 'classical' phenomenological relationship for the coercivity of powders which is given by

$$B_{0c} = B_{00}(1 - \epsilon_v)\ldots \qquad 9.4$$

where B_{00} is the 'coercivity at infinite dilution' (Huisman (1982)). In other words, the coercivity increased with decreasing volumetric packing fraction, or, equivalently, the particle interactions reduce the coercivity. However, these changes in coercivity were typically very small ($\sim$ 0.8mT) over changes in ϵ_v of an order of magnitude. This effect may be present in the coercivity of the samples at room temperature, but the magnitude of the variation (which would be expected to be much reduced) could not be detected within the accuracy of the experiment.

9.4 Explanation for the Form of the Magnetization Curve

Explanations for the form and the characteristics of the magnetization curves given in the previous section will be presented here. Specifically, the presence of the remanence and coercivity will be related to what we know about the particles from Chapter 8. Two separate coercivity mechanisms occur, a different one dominating at each of the two different temperatures for which magnetization curves were recorded. These will be dealt with in turn.

At 77 K the particles cannot rotate in the frozen carrier. Since the crystallites comprising the particle aggregates predominantly have diameters in the range 20 – 200nm, they are above the SPM threshold size and the particles are 'blocked'. In other words, the anisotropy energy barrier for a particle having a volume V and an effective anisotropy constant K, which is given by KV, obeys the relation

$$KV > 25kT \qquad 9.5$$

and the particle magnetization is stable. This stability of the magnetization and its insensitivity to thermal disturbance is believed to be the central mechanism contributing to the occurrence of both the remanence and the coercivity at 77 K. Were the particles not to obey the inequality given by equation (9.5), they would be superparamagnetic and have their magnetic moments thermally fluctuating in a manner which prevents the 'hardness' necessary for the existence of a remanence and a coercivity. A statement equivalent to equation (9.5) is that the Néel relaxation times of the particles in most cases are hugely greater than the time of the experiment. Hence, even at zero field there is a remanence caused by particles whose magnetizations, in most cases, do not relax within the experimental measuring time.

At room temperature the cause of the coercivity is believed to be very large aggregates having large rotational inertias. In spite of the agitation of the sample provided by the VSM during measurement, these largest aggregates could be seen to remain permanently sedimented out at the bottom of the sample container. A dense packing of these largest aggregates, which would have been enhanced by a field-induced aggregation process, causes a rotational inertia of the aggregate complex which, in turn, results in a remanence and a coercivity. Also contributing to

this effect, there may be a microparticle readjustment process within aggregates. At higher fields the constituents of aggregates may preferentially readjust into elongated structures to reduce the demagnetizing energy of an aggregate and this will increase the rotational inertia of the aggregate. This type of mechanism is essentially an inhibition of the Brownian rotation-type relaxation process which occurs, for example, in magnetic liquids (Rosensweig (1985), p61).

9.5 Effect of Particle Aggregate Characteristics Upon the Initial Susceptibility

We have mentioned in Chapter 8 how observed differences in the low-field susceptibility were attributed to differences in aggregate characteristics. This section presents more results concerning this matter. Results of measurements of the initial volume susceptibility for samples having different aggregate characteristics are reported. All of the initial susceptibility data was taken at applied fields of no greater than 7mT and, in all cases, linear fits to the initial magnetization curve data points were used. Using this method, the relative errors on the coefficients of the fit were usually never greater than $\sim 1\%$.

In order to characterize fully each sample it was necessary to record the full magnetization curve. This meant that for accurate initial susceptibility measurements, each sample could only have its initial susceptibility measured once. Because of irreversible field-induced aggregation processes caused by taking the sample around the full loop, subsequent measurements of the initial susceptibility could not be relied upon to give accurate results. In order to meaningfully compare initial susceptibility values measured from different samples having different volumetric packing fractions, the reduced initial volume susceptibility, $\bar{\chi}_{vi}$, was used. This is defined by

$$\bar{\chi}_{vi} = \frac{1}{M_s}\left(\frac{dM}{dH}\right)_{H\to 0} \qquad 9.6$$

and it means that all values are normalized by the sample saturation magnetization and so can be compared with each other in a sensible way.

The first data set is a comparison between the reduced initial volume susceptibilities of four samples. The first two of these four are taken from aerosol cans of Magnaflux 7HF. One of these, the 'new' sample had been recently manufactured and was provided by the manufacturer. The other one, the 'old' sample, was approximately two years older and had remained largely undisturbed for these two years. Although prior to insertion into the VSM sample containers, both of these samples were agitated to achieve a homogeneous dispersion in the carrier liquid, it would be expected that the degree of aggregation would be significantly greater in the 'old' sample. The aggregates would be expected to be bigger and there would be a larger proportion of 'clump' rather than 'chain' aggregates. The other two samples were freshly prepared samples of 7C Concentrate in HF carrier liquid. These constituents are exactly the same as for the ready-prepared Magnaflux 7HF samples, the only difference being that the user mixes the two components together her/himself. These latter two samples will be known as 7C+HF1 and 7C+HF2. The reduced initial volume susceptibilities, $\bar{\chi}_{vi}$, and the relevant volumetric packing fractions, ϵ_v, for each sample are given in Table 9.1.

Sample	ϵ_v	$\bar{\chi}_{vi}(\mathrm{A}^{-1}\mathrm{m})$
'old'	1.21×10^{-3}	$1.09(\pm 0.05) \times 10^{-5}$
'new'	1.97×10^{-3}	$1.60(\pm 0.04) \times 10^{-5}$
7C+HF1	0.0224	$1.11(\pm 0.01) \times 10^{-5}$
7C+HF2	3.42×10^{-2}	$1.15(\pm 0.03) \times 10^{-5}$

Table 9.1 The volumetric packing fractions, ϵ_v, and the reduced initial volume susceptibilities for four different magnetic inks.

From Table 9.1, the difference between the 'old' and the 'new' sample is clear. The susceptibility difference is consistent with the argument that these two samples have different aggregate characteristics, each having differing responses to imposed fields. The difference is also in accord with the material presented in Chapter 8. For the 7C+HF1 and 7C+HF2 samples there appears to be a negligible difference in the susceptibilities. A further result is the difference in susceptibility between the 'new' sample and both of the 7C+HF samples. Since, for the practice of MPI, it is beneficial to use inks having susceptibilities as high as possible, this would suggest that the new previously-mixed ink would be better than the freshly mixed one, as well as better than the 'old' ink. Indeed, there is very little difference between the 7C+HF samples and the 'old' sample. The lower susceptibilities of the 7C+HF samples can be explained by assuming that, prior to dispersion in the carrier liquid, large aggregates were formed in the dry powder which remained even when the powder was subsequently suspended in the carrier.

So far no mention has been made of the effect of the volumetric packing fraction. In Chapter 7 we mentioned that because of the enhanced magnetostatic interparticle interactions arising from increasing the volumetric packing fraction, the initial susceptibility generally increases with ϵ_v. Hence, the data in Table 9.1 should be viewed in this light. For the two 7C+HF samples, the opposite of what is expected with ϵ_v occurs. This may indicate that the value of ϵ_v has little effect. For magnetic liquids consisting of separated single particles the initial susceptibility is proportional to ϵ_v (Chantrell, Popplewell and Charles (1978)). For the aggregates in inks having randomly spatially distributed moments it would be expected that the relationship between these two quantities is not as strong as in magnetic liquids. Hence, for the 'old' and 'new' samples, even allowing for an enhancement of $\bar{\chi}_{vi}$ caused by the $\sim 60\%$ increase in ϵ_v across the two samples, the $\sim 50\%$ increase in $\bar{\chi}_{vi}$ is unlikely to arise solely from the effect of the ϵ_v variation. This argument about large aggregates with randomly oriented moments of their constituent crystallites having susceptibilities which are not strongly dependent on ϵ_v has some elements of the argument which was given in Chapter 7 (the end of section 7.9.i). This argument said that the susceptibility of large aggregates, in general, was less than for separated particles which are at the low end of the ink particle size distribution.

Obviously, it would be more satisfactory to try to study the effect of the aggregate characteristics on the initial susceptibility in a manner for which the rôle played by ϵ_v does not present problems. The next study provides this. This experiment measured the initial susceptibility before and after an ultrasonic agitation process was performed on one sample. Hence, ϵ_v remained unaltered throughout. In this experiment the sample is again a freshly prepared sample of 7C Concentrate in HF

carrier liquid. After the initial susceptibility measurements to be reported, the full magnetization curve of the sample was recorded, allowing the volumetric packing fraction to be determined as $\epsilon_v = 0.0162$. The ultrasonic agitation process between the two measurements involved placing the sample in its spherical container into a water-filled ultrasonic bath for 1hour 45minutes. The two measurements for the reduced initial susceptibility are given in Table 9.2.

Sample	$\bar{\chi}_{vi}(\mathrm{A}^{-1}\mathrm{m})$
Freshly Prepared	$1.17(\pm 0.04) \times 10^{-5}$
After Ultrasonic Agitation	$1.64(\pm 0.03) \times 10^{-5}$

Table 9.2 The reduced initial susceptibility for a 7C+HF sample before and after ultrasonic agitation.

Table 9.2 shows clearly the enhancement of the initial susceptibility arising from the ultrasonic treatment. Not only does the agitation break up aggregates already present in the sample before the first measurement was taken, but it also apparently breaks up aggregates formed by field-induced aggregation processes *as a result* of the first measurement. This experiment provides direct evidence for the relationship we have discussed between aggregate characteristics and the initial susceptibility.

The relationship between aggregate characteristics (specifically aggregate size) and initial susceptibility was shown clearly in a further experiment. This time the samples were suspensions of magnetite particles in toluene. The magnetite was provided by Koch Light Laboratories in the form of a powder and the particles had a median diameter of approximately 1μm. An approximately 1% by volume dispersion of Fe_3O_4 in toluene was prepared and thoroughly agitated to achieve a homogeneous dispersion. The dispersion was then left to stand for about 10 minutes. After 10 minutes, two separate samples were extracted from the container holding the dispersion. The first was taken from a region near the top of the dispersion and the second from a region near the bottom. Two separate clean hypodermic syringes were used to perform these extractions and extreme care was taken not to knock the sample container by accident during the process. Because of the sedimentation occurring within the dispersion over the 10 minute time period, those particle aggregates taken from near the top had smaller diameters than those taken from near the bottom. Hence, the two extracted samples had quite different median particle sizes. Using an obvious nomenclature, these two samples will be referred to as 'top' and 'bottom'. Initial susceptibility measurements were performed on the two samples and the results, in terms of the reduced initial susceptibility, are given in Table 9.3.

Sample	ϵ_v	$\bar{\chi}_{vi}(\mathrm{A}^{-1}\mathrm{m})$
'top'	1.2×10^{-4}	$5.6(\pm 0.5) \times 10^{-6}$
'bottom'	2.5×10^{-4}	$4.0(\pm 0.2) \times 10^{-6}$

Table 9.3 The reduced initial susceptibility values for two samples of Fe_3O_4 in toluene having different median particle sizes.

The lower reduced initial susceptibility in the 'bottom' sample containing the larger aggregates is clearly demonstrated. The difference is all the more significant in view of the fact that the 'bottom' sample has about twice the volumetric packing fraction as the 'top' sample. Hence, even if there is a dependence of $\bar{\chi}_{vi}$ upon ϵ_v, for this sample, it is not as important as the dependence of $\bar{\chi}_{vi}$ upon the aggregate size.

In conclusion, therefore, these measurements have shown the important relationship which exists between magnetic properties and aggregate characteristics in magnetic ink systems. The performance of a magnetic ink in a MPI test situation would be expected to be strongly dependent upon the aggregate characteristics within the ink which, in turn, are strongly dependent upon the history of the ink. This is an important point for MPI practitioners.

In recording full magnetization curves on Magnaflux 7HF and 7C+HF samples, particularly after they had been previously saturated but were subsequently at lower fields, it soon became apparent that there was a noticeable time-dependent component to the magnetization. The investigation of this matter is described in the next section.

9.6 Magnetic Viscosity in Magnetic Ink Systems

Chapter 2 included a brief review of the main elements of the phenomenon of magnetic viscosity in magnetic fine particle systems. This section reports an investigation of a magnetic viscosity effect which was found in magnetic ink systems. In essence, it was found that, after saturation of a sample in a large positive magnetic field, in a subsequent very low field ($|B_0| \leq 35\,\mathrm{mT}$) a decay of the magnetization occurred with an approximately '$\ln t$' behaviour.

Measurements were performed at room temperature and at 77 K using the VSM. In all cases the large saturating field was defined as being positive. The magnetization decay occurred in both positive and negative low fields. In all cases the sample was subject to a saturating field of 1.25T for 10 seconds. The field was then manually rapidly reduced to the low field at which the decay measurements were made. The time $t = 0$ was defined as the time at which the lower field was attained, irrespective of the fact that the lock-in amplifier which reads the VSM detection coil output did not instantaneously settle to give a stable reading. With the lock-in amplifier running on a time constant of 3s, it took about 20 – 30s for a stable detection coil output voltage to settle, and for this reason there were no reliable data points for the magnetization in the first 20 – 30s of the decay.

The sample used for these measurements was 7C Concentrate in HF carrier liquid having a high volumetric packing fraction ($\epsilon_v = 0.0224$). Because the magnetization values at which the decays were measured were very small, the use of a sample having such a high volumetric packing fraction improves the signal to noise ratio of the measured signal. All of the data presented has been corrected for both the residual signal of the sample holder and for sample demagnetizing effects. In all cases the timing was performed by the internal clock of the microcomputer which controls the VSM.

9.6.i Measurements at Room Temperature

Decays of the magnetization were measured at room temperature in both positive and negative fields. A typical magnetization decay is shown in terms of the

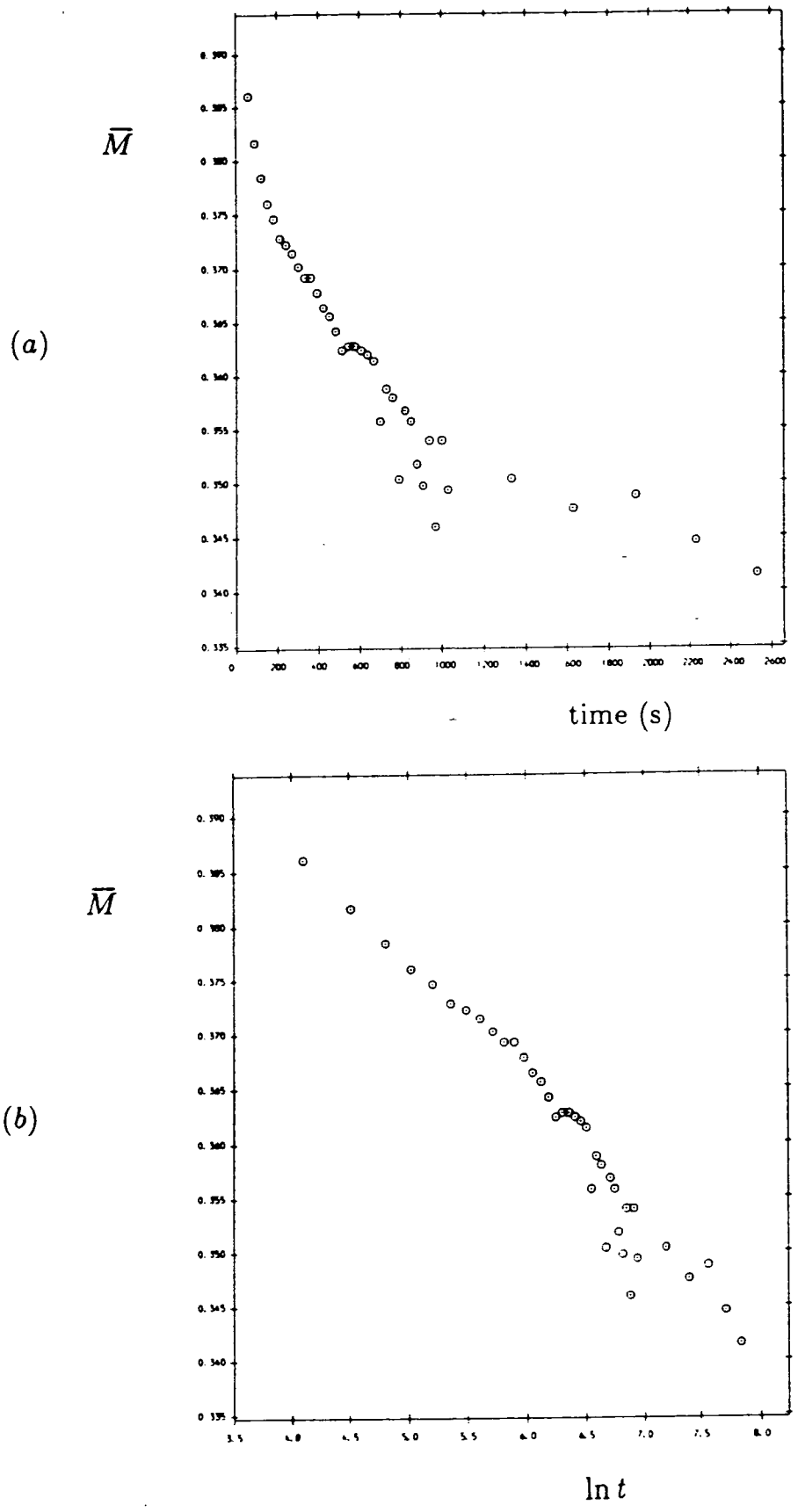

Figure 9.3 The decay of reduced magnetization, $\overline{M}$, at a magnetic field of $10.15(\pm 0.04)$mT, at room temperature, plotted (a) as a function of t, and (b) as a function of $\ln t$.

reduced magnetization, $\overline{M}(= M/M_s)$, in figure 9.3. In this figure the data is plotted both as a function of t and of $\ln t$ (with t in seconds) and the magnetic field is $10.15(\pm 0.04)$mT.

From figure 9.3 it is apparent that the decay follows reasonably closely a '$\ln t$' behaviour. The reduced coefficient of magnetic viscosity, $\bar{A}$, is defined as

$$\bar{A} = \frac{S}{M_s} = -\frac{1}{M_s}\frac{dM}{d\ln t} = -\frac{d\overline{M}}{d\ln t} \qquad 9.7$$

and can be obtained from straight line fits to data such as that shown in figure 9.3*b* (with t measured in seconds). By recording the decays of magnetization at various values of the field, the field-dependence of the reduced coefficient of magnetic viscosity was investigated. This dependence is plotted in figure 9.4.

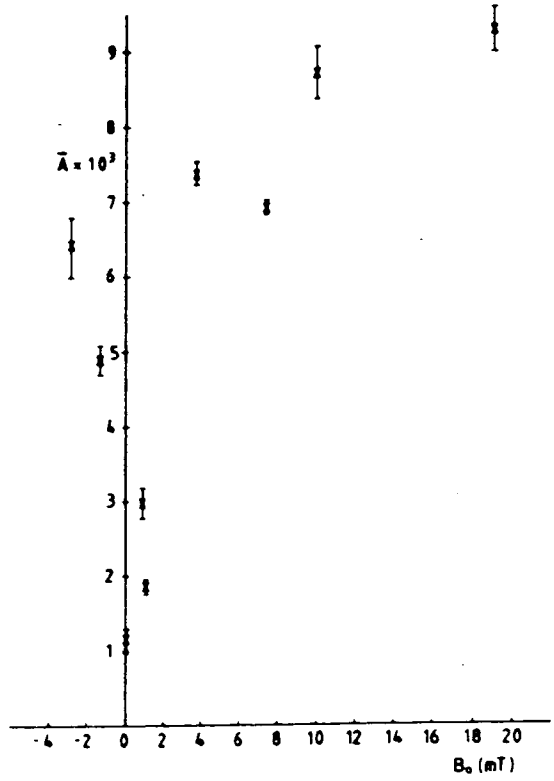

Figure 9.4 The field-dependence of the reduced coefficient of magnetic viscosity at room temperature.

It is clear that the maximum of $\bar{A}$ often found at the coercivity, which in this case is $B_{0c} = -0.98$mT, is absent. (See Chapter 2 for references concerning this result in the work of others.) There is an increase in $\bar{A}$ with the absolute value of the field. For the positive field values, this indicates that an equation such as that applicable to Néel type relaxation processes

$$\tau_N = f_0^{-1} \exp\left[\frac{KV}{kT}\left(1 - \frac{B_0}{B_{0k}}\right)^2\right], \qquad 9.8$$

is inappropriate (see Chapter 2 for the definitions of the quantities in equation (9.8)). From equation (9.8), for positive B_0 such that $B_0 < B_{0k}$, one would qualitatively expect a reduction in the relaxation times and a consequent reduction in $\bar{A}$. The

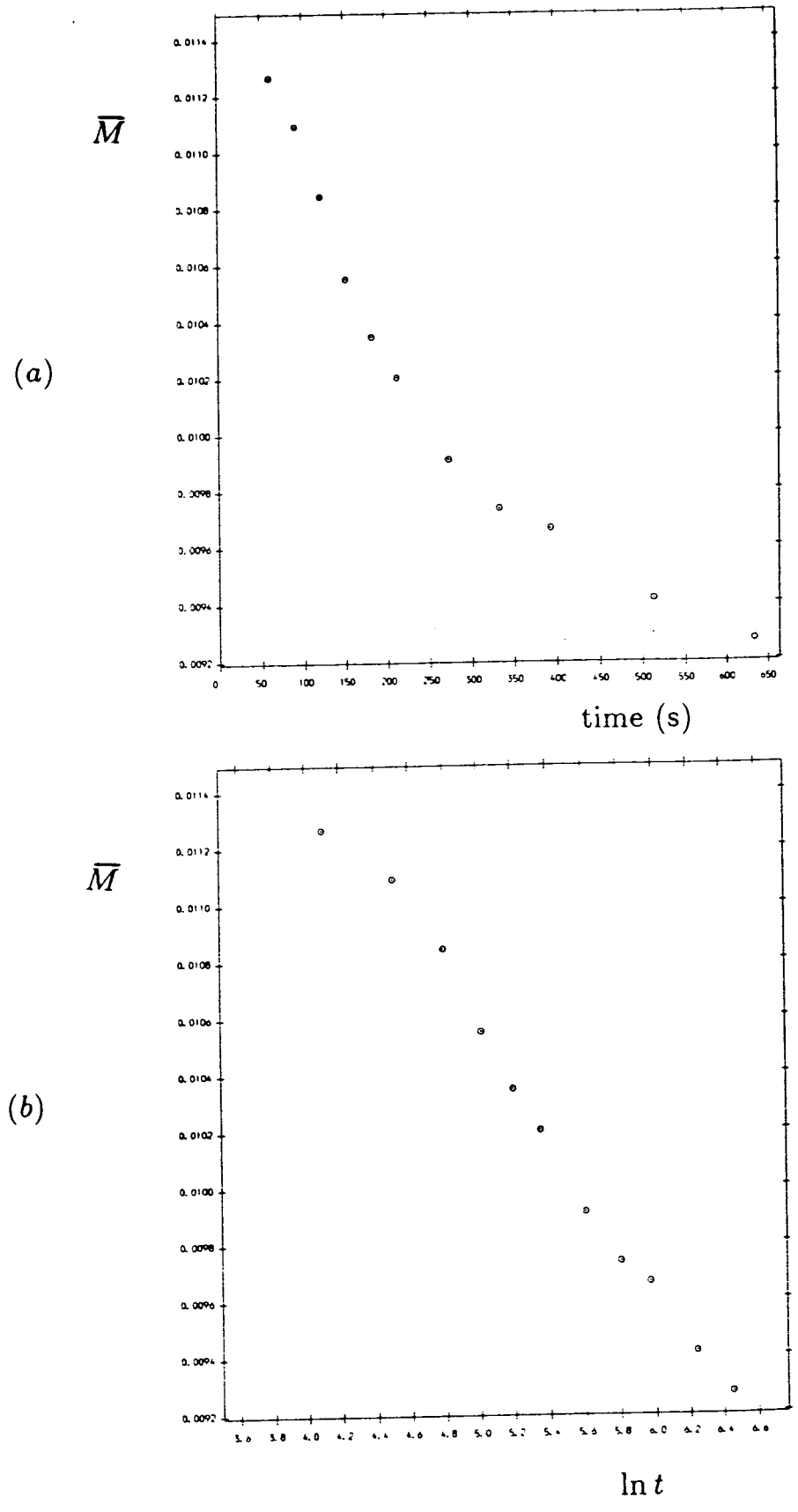

Figure 9.5 The decay of reduced magnetization, $\overline{M}$, at a magnetic field of $-12.14(\pm 0.04)$mT at 77 K plotted (a) as a function of t, and (b) as a function of $\ln t$.

reason for the form of figure 9.4 is unclear, but it may be related to the fact that the type of relaxation process is not a a Néel type process. At room temperature, as well as a Néel type process, there is a relaxation process involving the physical rotation of particles. Even if such a latter process occurs, it is still strange that $\bar{A}$ increases with positive field. Assuming that the physical rotation process accounts for the behaviour of $\bar{A}$ at room temperature, it is clear both that it is highly complex and that it dominates the Néel type process.

9.6.ii Measurements at 77 K

Decays of the magnetization were measured at 77 K. At this temperature the carrier fluid of the sample was frozen and so only a Néel type relaxation process could occur. The complication exposed in the previous section is absent. The sample was frozen in zero field before each run and then secured, whilst still frozen, to the VSM sample rod. This was to ensure that the particles were randomly oriented within the solid carrier liquid matrix.

A typical decay is shown in figure 9.5. Again the reduced magnetization is plotted as a function of both t and $\ln t$ (with t in seconds) and in this case the magnetic field is $-12.14(\pm 0.04)$mT. Again the good approximation to '$\ln t$' behaviour is apparent.

The field-dependence of $\bar{A}$ was investigated by fitting straight lines to the decays, such as that shown in figure 9.5*b*, at various fields. Reliable data could only be obtained for negative field values. This was because any decay in positive field values was so small that it was undetectable within the noise and drift of the VSM. The field-dependence of $\bar{A}$ at 77 K in negative fields is shown in figure 9.6.

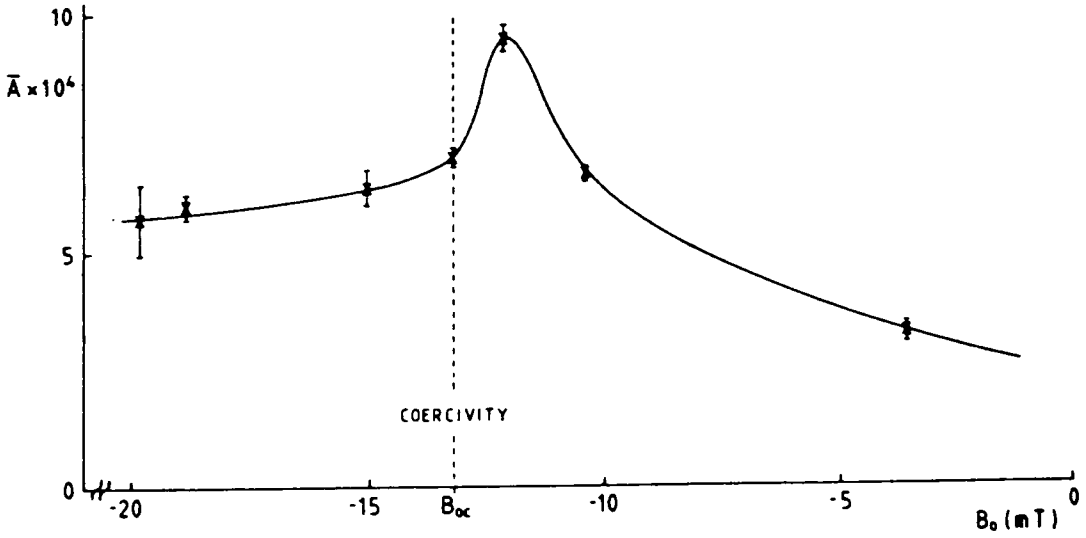

Figure 9.6 The field-dependence (in negative fields) of the reduced coefficient of magnetic viscosity at 77 K. The dotted line represents the value of the coercivity.

In figure 9.6 it is evident that a peak occurs near (but not actually *at*) the

coercivity, $B_{0c} = -13.3\text{mT}$. Such a peak has been frequently found in this type of study (O'Grady, Chantrell, Popplewell and Charles (1981), Kloepper, Finkelstein and Braunstein (1984), Oseroff, Clark, Schultz and Shtrikman (1985), Chantrell, Fearon and Wohlfarth (1986)). It also noticeable that at 77 K the values of $\bar{A}$ are typically an order of magnitude less than those at room temperature (figure 9.4). This is, perhaps, partly explicable by the effect of temperature on the Néel relaxation process, but also the presence of the previously-mentioned second type of relaxation process occurring at room temperature complicates the issue. At 77 K the only relaxation process which can occur is a Néel type process. The qualitative agreement between the form of figure 9.6 and the predictions of the models referenced above lends strong support to this assertion since all these models explicitly include a Néel relaxation process. Furthermore, the very small and, consequently, non-detectable decay at positive fields is also in qualitative agreement with expectations arising from a Néel type process and as described by equation (9.8). Unfortunately, because of both the absence of a detailed knowledge of the particle size distribution parameters and the complicating presence of strong intra-aggregate magnetostatic interactions, it is not possible to present a more quantitative analysis.

9.7 Conclusions

The fundamental magnetic properties of a magnetic ink have been presented. Two mechanisms for the coercivity have been proposed—'blocking' and the large rotational inertias of large aggregates. The initial susceptibility has explicitly and incontrovertibly been shown to depend significantly on the aggregate characteristics, which, in turn depend on the ink's history. The investigation of the time-dependent magnetization has shown that when the carrier liquid is frozen the magnetization relaxation process is almost definitely a Néel type process. At room temperature the relaxation is more complex and there appears to be a process other than the simple Néel type, perhaps involving some complex aggregate rotation or readjustment phenomenon. However, the details remain unclear. For the practice of MPI, the effect of the time-dependence of the magnetization is not important. It has a negligible effect in the time scale of the time periods in which MPI indications form.

Chapter 10

Discussion and Suggestions for Further Work

This chapter presents a general discussion of the material presented in the thesis. Inevitably, in such a discussion, there arise many opportunities for my making suggestions for further work, principally to aid in further clarification and refinement of the matters reported in this investigation. Emphasis will be placed on those suggestions for further work which I consider to be the most important.

The first part of the thesis was a review, firstly of magnetism, and then of both the topic of MPI and the detailed behaviour of magnetic leakage fields at defects. The chapter following this described the construction, characterization and automation of a VSM which was subsequently used for the magnetic measurements reported in Chapter 7 and Chapter 9. The sensitivity of this instrument, as a consequence of the care and precision taken in its design and construction, makes it capable of detecting moments of less than $10^{-9}\mathrm{JT}^{-1}$. The important factors contributing to this sensitivity are the stability of the vibration transducer, the characteristics of the detection coil system (particularly the large inductances of the coils and the noise rejection achieved by their inductive balance) and the isolation of the detection coils from mechanical vibrations originating in the vibration transducer. It is believed that this instrument represents the state-of-the-art in electromagnet VSMs. The excellence of this instrument could not have been realised without the expertise of Hoon and Willcock.

The two chapters after this described both the development of and some results obtained from a model of indication formation in MPI. Although the model, as it is reported, is a much simplified representation of the processes occurring in real systems, nevertheless, I consider it to be the first serious attempt to model the system which incorporates all of the *principal* force contributions acting on the particles. Possible refinements of the model are many, but it is hoped that the material presented in this thesis can be, at the very least, a starting point or a 'pointer in the right direction' for subsequent workers. The most obvious features to include in possible refinements of the model would be, for example, to incorporate a particle size distribution and to allow the particles to be non-spherical. A further refinement would be, when necessary, to improve upon the point particle approximation by using some more accurate means of calculating the magnetization of a particle. When particles are so large in comparison to the physical size of leakage field gradients that the validity of the point particle approximation becomes questionable, then, because the particles are situated in a non-uniform field, they will have non-uniform magnetizations. Hence, it would not be trivial to incorporate the replacement for the point particle approximation. It is likely that some numerical integration procedure would be required to calculate the correct magnetization distribution within a particle and the resulting magnetic force on such a particle would be correspondingly more complex to obtain.

There are two ways in which the effect of interparticle interactions (particularly magnetostatic interparticle interactions) could be incorporated whilst, at the same

time, not complicating the equations of motion to such a degree that they would be utterly insoluble. These will be discussed in turn. The first of these would be, for a given particle, to consider only those neighbouring particles within a specified radius as being 'interacting' whilst those further away would be 'non-interacting'. In such a scheme, the resulting equations of motion would be simultaneous, but they would be less strongly coupled than would be the case were the effect of the interactions not truncated in this manner. Hence, the equations of motion would be more difficult to solve, but the undertaking would not be impossible. The use of this cutoff radius around a particle defining a region within which particles interact and outside which they do not interact finds widespread use in Monte Carlo simulations of particle configurations in magnetic fluids (for example, Chantrell, Bradbury, Popplewell and Charles (1980)). The second way in which the effect of interparticle interactions might be included would be to incorporate them within a mean field-type scheme. This type of approach has been used to describe the magnetization of concentrated magnetic fluids (for example, Weser and Stierstadt (1985*a*,*b*)). In such a framework the external field acting on an individual particle is replaced by the local field within a cavity occupied by the whole system, and which differs from the external field by an amount proportional to the magnetization of the whole system. This approach works for magnetic liquids because the system has a homogeneous and time-independent concentration distribution (or pnd), rendering the calculation of the local field relatively straightforward. This is not the case for magnetic ink systems during the indication formation process where the indication contrast actually arises because of time-dependent concentration distribution changes. Thus, it is inevitable that a mean field-type model applied to magnetic inks would be vastly more complex and would have to employ, for example, such objects as a 'spatially variable and time-dependent mean field'.

As mentioned, the model requires powerful computing resources and the inclusion of any of the aforementioned refinements would greatly increase further the required resources. A totally different approach which would appear to demand much less in the way of computing resources is suggested by analogy with methods employed in the theory of high gradient magnetic separation (HGMS) (for example, Takayasu, Gerber and Friedlaender (1983)). These approaches consider the problem of the behaviour of the particle volume concentration, c_s, as a function of both time and of displacement from a magnetized collector. c_s satisfies a differential equation which can be solved analytically in one dimension for a simple collector geometry (a magnetized wire). Presumably, an analogous version of this differential equation for the case in which the magnetized collector corresponds to the defect could be obtained and the consequent behaviour of the particle concentration could be investigated by solving the relevant differential equation. Even if the resulting equation could not be solved analytically and so required a numerical solution, this would still represent an attractive improvement upon the computing resources demanded by the present task of solving $3N$ simultaneous equations, $2N$ of which are second order differential equations.

The results obtained from the model described in Chapter 5 were presented in Chapter 6. The first investigation which was reported concerned the effect of the particle size in the indication formation process. The model suggested that, for practical MPI, it is beneficial to use as large a particle size as possible. However, it was argued later in the same chapter that, principally because of the limited validity of the point particle approximation, this particular conclusion was questionable

and, indeed, in order to delineate the finest defects, it seems to be beneficial to use the smallest particles possible. The investigation of the rôle of the carrier liquid coefficient of viscosity revealed a complex behaviour, particularly with regard to its relationship to the particle size. Overall, however, the most important conclusion was that, for real magnetic ink systems possessing a particle size distribution, it would be beneficial, in terms of the contrast of an indication, to use carriers having coefficients of viscosity at the lower end of the $0.3 - 1.1$mPas range investigated. For the investigations of the effects of both the defect size (at constant aspect ratio) and of the magnetizing field the results were simple and agreed with intuitive expectations. The investigation of the effect of the defect aspect ratio (at constant defect width) produced results which indicated that both the contrast and the rate of formation of contrast improved with the aspect ratio (or, equivalently, with the depth) of the defect. Studies of the effect of the contrast paint layer thickness demonstrated that the recommendations of the British Standard, BS 5044 (1973), are qualitatively correct. It would be interesting to see whether the inclusion of any of the previously-mentioned refinements within the model produced significantly different results in any of these areas mentioned.

Chapter 7 described a series of experiments which measured the speeds of individual MPI particle aggregates and CrO_2 tape particle aggregates in known magnetic field gradients. It was argued that discrepancies between theoretical and experimental aggregate velocities did not arise because of serious flaws in the theoretical model, but rather, because of an inability to experimentally determine with sufficient accuracy the aggregate volumes, the aggregate susceptibilities and the aggregate geometrical dissipative factors (the latter are used in the generalization of Stokes' law to non-spherical particles). In particular the inability to measure the volume accurately was attributed to the presence of voids and holes within aggregates which constituted a significant proportion of the volume, but which could not be resolved using the optical microscope. Unfortunately, the relative weightings of the three causes of the discrepancy to the whole discrepancy could not be determined. I suggest that, in order to further refine the details of the exact rôle of these three quantities, any future work in this type of experiment should employ particle systems for which it would be much easier to determine V, c and χ_{vi}. Larger single particles (of, for example, iron or magnetite) having simple shapes (for example, spheres or prolate ellipsoids) would, perhaps, be the most promising candidates. For such larger particles it would, however, be necessary to increase the carrier viscosity, by using, for example, a lacquer, in order to keep the particles suspended for a sufficiently long time for the measurements to be performed. The use of a more viscous carrier would also require larger magnetic fields and magnetic field gradients in order to move the particles significant distances in reasonably short times. Hence, a new coil system capable of producing these specifications would probably be required.

Chapter 8 reported the methods used and the results obtained in the characterization of the particulate component of a 'typical' magnetic ink. Ultimately the particles are composed of crystallites having diameters in the range $20 - 200$nm but these crystallites are arranged into complex structures. Firstly, there appear to be flux-closure structures having diameters of typically $1 - 3\mu$m. These $1 - 3\mu$m diameter objects are then arranged into much larger, more loosely bound aggregates, having diameters of typically 10μm and greater. Two types of these latter types of aggregates were identified—chains and clumps—and differences in their low

field susceptibility were found. Reliable estimates of the particle size distribution parameters could not be obtained from the TEM micrographs of the clusters of the smallest crytallites. This was because of the lack of resolution of the individual particle boundaries. I suggest that further work in the determination of the particle size distribution parameters of the smallest crystallites would be highly rewarding, particularly to aid in the detailed understanding of some of the magnetic properties. This would require some means of breaking up the aggregates of crystallites and then again performing TEM on the dispersed system, this time, being confident that one is predominantly imaging individual crystallites clearly. One way of doing this might be to employ techniques used in the surfactant double layer stabilization of magnetic liquids (for example, Wooding, Kilner and Lambrick (1988)). Essentially, this idea involves controlling the pH of the carrier liquid so that an electric double layer charge on the particle surfaces arises and causes an interparticle repulsion which separates the particles. Once separated, the bonding of surfactants (for example, decanoic acid) onto the particle maintains stabilization even through subsequent adjustment of the carrier pH. The details of such a procedure would, however, require clarification and, furthermore, whilst this technique works for the overcoming of the magnetostatic attractions between SPM-sized particles, it may not work for the larger magnetic moments associated with the larger-sized crystallites in our problem.

Some basic magnetic properties of magnetic ink systems were presented in Chapter 9. The relationship between aggregate shape and size and initial susceptibility which was found in Chapter 8 was further elucidated. The study of the time-dependence of the magnetization provided some insight into the fundamental magnetization processes, but still some uncertainties remain. I consider that the most important problem to be solved is the explanation of the form of the field-dependence of the reduced coefficient of magnetic viscosity, $\bar{A}$, shown in figure 9.4. If the bizarre behaviour occurs because of some complex aggregate rotation or readjustment behaviour, because the systems are so 'messy' and unamenable to simple modelling schemes, it would still seem extremely difficult to gain some useful insight into the problem. A more exhaustive analysis of the field-dependence of $\bar{A}$ at 77 K would be facilitated by employing some means of dispersing the 20 – 200nm crystallites, as mentioned in the previous paragraph. Essentially, the experiment could be repeated on such a dispersed sample. With a knowledge of the particle size distribution parameters of the sample, together with the reduction of strong magnetostatic interparticle interactions, experimental data similar to that shown in figure 9.6 could be readily compared with theoretical expectations.

Appendix A1

The Numerical Solution of Differential Equations

This Appendix discusses the numerical solution of ordinary differential equations, but goes into a little more depth than did Chapter 5. The treatment considers the general first order equation

$$\frac{d\psi}{dz} = f(\psi, z) \qquad A1.1$$

with some initial condition

$$\psi(z_0) = \psi_m \qquad A1.2$$

We do not need to consider higher order equations because such equations can be reduced to systems of simultaneous first order equations.

If we have an approximation to the solution $\psi(z)$ for z in the range $z_0 \leq z \leq z_m$, then we can expand $\psi(z)$ about the point $z = z_m$ in the Taylor series

$$\psi(z) = \psi(z_m) + \left(\frac{d\psi}{dz}\right)_{z=z_m}(z - z_m) + \frac{1}{2}\left(\frac{d^2\psi}{dz^2}\right)_{z=z_m}(z - z_m)^2 + \ldots \qquad A1.3$$

How one may obtain the initial approximation to $\psi(z)$ will be discussed shortly. We can use equation (A1.3) to approximate $\psi(z)$ at the point $z = z_{m+1} = z_m + h$ by replacing, in equation (A1.3), z by $z_m + h$. Thus, equation (A1.3) becomes

$$\psi(z_{m+1}) = \psi(z_m) + h\left(\frac{d\psi}{dz}\right)_{z=z_m} + \frac{h^2}{2}\left(\frac{d^2\psi}{dz^2}\right)_{z=z_m} + \ldots \qquad A1.4$$

If we have an initial condition $\psi(z_0) = \psi_0$ it is now clear how one may have obtained one's initial approximation to the solution $\psi(z)$ in the range $z_0 \leq z \leq z_m$, as was assumed in equation (A1.3). This is simply by letting $m = 0$ in equation A1.4. In addition, with $m = 0$ in equation (A1.4), one obtains an approximation to the solution at $z = z_1$, namely $\psi(z_1) = \psi_1$. Thus, ψ_1 is the approximation to the solution at $z = z_0 + h$. In principle, now we can continue and let $m = 1$ in equation (A1.4), obtaining an approximation for ψ_2 at the z value of $z = z_2 = z_0 + 2h$. Further continuing we can obtain a whole series of approximations, $\psi_3, \psi_4, \ldots, \psi_m, \psi_{m+1}, \ldots$. However, from a practical computational point of view, because equation (A1.4) would have to be truncated at some finite term, it would be expected that at each new approximation of $\psi(z)$ the truncation error would accumulate. Hence, the problem is how to efficiently minimize the accumulated truncation errors. Thus, although the Taylor series method is of little practical use *per se* in the numerical solution of differential equations, it provides a valuable insight into the nature of the problem.

Methods other than predictor-corrector methods will not be discussed in any great depth here. However, one other popular class of techniques used for the problem will be mentioned briefly. These are the Runge-Kutta methods. This class is characterized by three features. Firstly, they are one-step methods. In other words, one first only needs to know (ψ_m, z_m) to obtain ψ_{m+1}. Secondly, different

orders of methods exist, where the order is the number of terms of the Taylor series with which they are in accord. Thirdly, they do not require any evaluations of the derivatives of $\psi(z)$, but only of ψ itself. This last point is what makes Runge-Kutta methods more attractive than methods based upon a more straightforward Taylor series type of approach. However, the disadvantage is that more than one value of (ψ_m, z_m) has to be evaluated. The other one serious drawback of Runge-Kutta methods is that the truncation error is not easy to estimate (Dorn and McCracken (1972), p376). Hence, the optimum step size, h, may be difficult to choose.

This point constitutes the major advantage of predictor-corrector methods over Runge-Kutta methods. Truncation error estimates are easily obtainable from quantities already calculated in the solution process. Typically, predictor-corrector methods employ lower order (first or second) Runge-Kutta methods as the predictor, but then successively correct the first prediction to the required accuracy.

This treatment will focus on the background to the predictor-corrector method used in Chapter 5. It is obvious that the predictor used in Chapter 5 ($\psi_{m+1} = \psi_m + hf(\psi_m, z_m)$) is the Taylor series of equation (A1.4) truncated after the first order term. It is also apparent that, without any correction, the accumulated errors—roundoff, truncation and inherent—in the use of this equation (which is a first order Runge-Kutta method or Euler's method) would soon render the technique useless for any solution other than a straight line. (A straight line solution would not require a numerical solution in the first place!) It is intended here to explain the justification for the use of the corrector formula which was employed in Chapter 5. The corrector was

$$\begin{aligned} \psi_{m+1}^{(k)} &= \psi_m + \frac{h}{2}\left(\frac{d\psi_m}{dz} + \frac{d\psi_{m+1}^{(k-1)}}{dz}\right) \\ &= \psi_m + \frac{h}{2}\left[f(\psi_m, z_m) + f(\psi_{m+1}^{(k-1)}, z_{m+1})\right] \end{aligned} \qquad A1.5$$

where the superscript in parenthesis, (k), refers to the kth iteration of the corrector in the correction process. A geometrical elucidation of the effect of equations (A1.5) will be given. The argument is presented with reference to figure (A1.1).

Figure A1.1 shows the approximation to the solution at $z = z_m$, that is (z_m, ψ_m). For $z = z_{m+1}$, the point (z_m, ψ_m) represents the previously approximated point of the solution. The line L_1 represents the slope through the point (z_m, ψ_m) which is $d\psi_m/dz$ and which is known. From the predictor we can obtain ψ_{m+1} approximately and so we know the slope approximately at the point $(z_{m+1}, \psi_{m+1}^{(0)})$, that is, $d\psi_{m+1}^{(0)}/dz$. This is given by the line L_2. The mean of the two slopes of the lines L_1 and L_2 gives the line $\bar{L}$, having a slope of $\frac{1}{2}[(d\psi_m/dz) + (d\psi_{m+1}^{(0)}/dz)]$. Hence, the approximation to the next point of the solution, $(z_{m+1}, \psi_{m+1}^{(1)})$, is obtained by constructing the line L which passes through the point (z_m, ψ_m) with the same slope as the line $\bar{L}$. The point obtained as the approximation to the solution at $z = z_{m+1}$ by this procedure is, thus, equivalent to the first iteration of the corrector, equation (A1.5). Reapplication of the corrector, by obtaining the new line L having the same gradient as $\frac{1}{2}[(d\psi_m/dz) + (d\psi_{m+1}^{(1)}/dz)]$, gives a better approximation to the solution at $z = z_{m+1}$. Hence, by iterating the correction procedure one obtains better and better approximations to the solution at $z = z_{m+1}$. The iterations are stopped when some condition involving the smallness of the difference between successive approximations is satisfied.

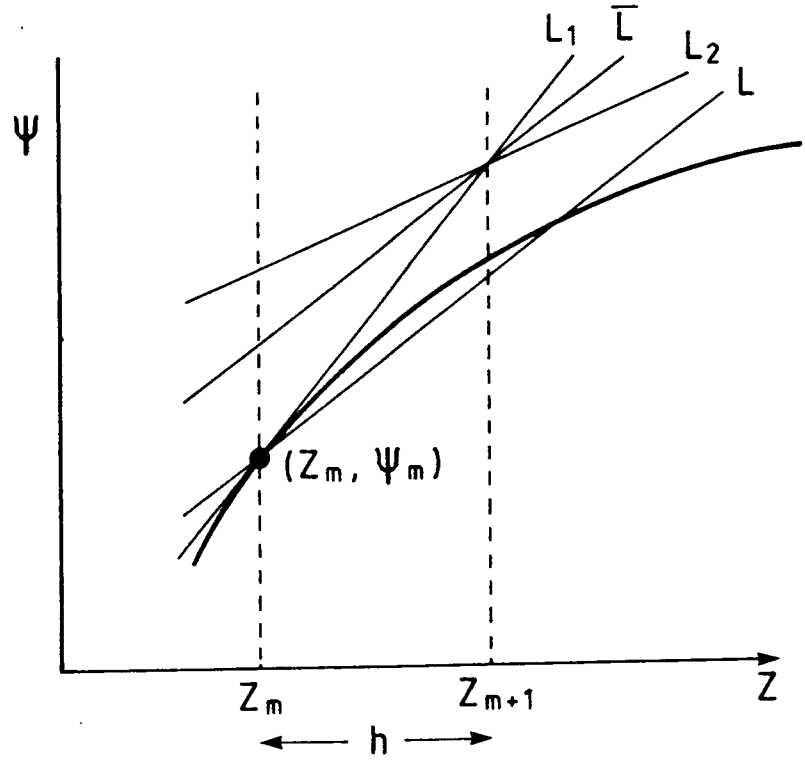

Figure A1.1 Geometrical representation of the effect of the applications of the corrector discussed in the text. The curve represents the 'true' solution.

Details of the conditions under which this process converges will now be given. Dorn and McCracken (1972) show that the crucial factor is the step size, h. The process converges if

$$h < \frac{2}{Q} \qquad A1.6$$

where Q is some upper bound on $|\partial f/\partial \psi|$ such that

$$\left|\frac{\partial f}{\partial \psi}\right| \leq Q \qquad A1.7$$

One problem here, however, is that we do not usually know what Q is. In spite of this, however, this result is in accord with a naïve intuitive expectation. The smaller h is, the faster the process will converge. However, efficiency considerations also affect the choice of h, making it desirable not to choose too small a value of h.

Appendix A2

Calculation of the x component of the Magnetic Field Produced by the Rectangular Current Loop at the Field Point $P(x)$

The rectangular current loop $ABCD$ is shown in figure A2.1. Its length is w and its breadth is $(u+v)$. A cartesian coordinate system and the field point $P(x)$ are also shown in the figure.

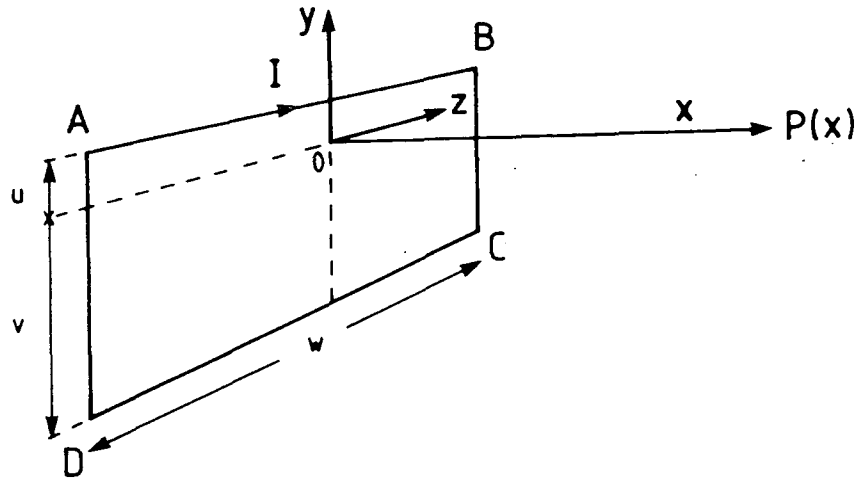

Figure A2.1 The rectangular current loop $ABCD$, showing the dimensions u,v and w, the cartesian coordinate system and the position of the field point $P(x)$.

This section gives details of the calculation of the x component at $P(x)$ of the total magnetic field produced by the current loop $ABCD$. The starting point is the Biot-Savart law,

$$d\mathbf{B}_{0i} = \frac{\mu_0 I\, d\mathbf{l}\times\hat{\mathbf{R}}}{4\pi R^2} \qquad A2.1$$

where $d\mathbf{B}_{0i}$ is an element of the magnetic field, $I\,d\mathbf{l}$ is the current element producing the magnetic field element and $\hat{\mathbf{R}}$ is a unit vector along $\mathbf{R}$, which is the position vector from the current element, $I\,d\mathbf{l}$, to the field element, $d\mathbf{B}_{0i}$. We apply equation (A2.1) in turn to each of the conductors comprising the loop $ABCD$.

Conductor AB

Since AB is parallel to the z axis the element of the conductor, dl, is simply $dl = dz$. Also the relationship $R^2 = x^2 + u^2 + z^2$ is applicable. We define the new variable, α, defined by $\cos\alpha = (\sqrt{u^2+x^2})/R$. α is the angle between $\mathbf{R}$ and the line joining $P(x)$ to the point $(0,u,0)$ (the midpoint of the conductor AB). Hence, dl can be expressed as $dl = dz = R\,d\alpha$. This means that, in a scalar form, equation (A2.1) may be written as

$$dB_{0i}^{AB} = \frac{\mu_0 I}{4\pi\sqrt{u^2+x^2}}\cos\alpha\, d\alpha \qquad A2.2$$

The extent of the range of α is from $\alpha_{min} = -\sin^{-1}[(\frac{w}{2})/\sqrt{u^2+x^2+(\frac{w}{2})^2}]$ to $\alpha_{max} = +\sin^{-1}[(\frac{w}{2})/\sqrt{u^2+x^2+(\frac{w}{2})^2}]$ and so integrating equation (A2.2) with respect to α between these two limits yields

$$\begin{aligned} B_{0i}^{AB} &= \frac{\mu_0 I}{4\pi\sqrt{u^2+x^2}} \int_{\alpha_{min}}^{\alpha_{max}} \cos\alpha \, d\alpha \\ &= \frac{\mu_0 I}{2\pi\sqrt{u^2+x^2}} \left[\frac{\frac{w}{2}}{\sqrt{u^2+x^2+(\frac{w}{2})^2}} \right] \end{aligned} \qquad A2.3$$

This gives the magnitude of the magnetic field at $P(x)$. The direction in which this acts is along the line which is perpendicular to the line joining the point $(0, u, 0)$ to $P(x)$ and lying solely in the xy plane with negative x and y components. Hence, the x component of the magnetic field, B_{0xi}^{AB}, is given by

$$B_{0xi}^{AB} = -\frac{u}{\sqrt{u^2+x^2}} B_{0i}^{AB} \qquad A2.4$$

or

$$B_{0xi}^{AB} = -\frac{\mu_0 I}{4\pi(u^2+x^2)} \left[\frac{uw}{\sqrt{u^2+x^2+(\frac{w}{2})^2}} \right] \qquad A2.5$$

Conductor CD

This situation is similar to the case of the conductor AB. However, in this case, $\cos\alpha = (\sqrt{v^2+x^2})/R$ with R given by $R^2 = x^2+v^2+z^2$. Here α is the angle between R and the line joining $P(x)$ to the point $(0, -v, 0)$. Also the relationship $dl = dz = R\,d\alpha$ still holds. Hence, the scalar Biot-Savart equation is

$$dB_{0i}^{CD} = \frac{\mu_0 I}{4\pi\sqrt{v^2+x^2}} \cos\alpha \, d\alpha \qquad A2.6$$

The extent of the range of α is from $\alpha_{min} = -\sin^{-1}[(\frac{w}{2})/\sqrt{v^2+x^2+(\frac{w}{2})^2}]$ to $\alpha_{max} = +\sin^{-1}[(\frac{w}{2})/\sqrt{v^2+x^2+(\frac{w}{2})^2}]$. The integration of equation (A2.6) with respect to α yields

$$\begin{aligned} B_{0i}^{CD} &= \frac{\mu_0 I}{4\pi\sqrt{v^2+x^2}} \int_{\alpha_{min}}^{\alpha_{max}} \cos\alpha \, d\alpha \\ &= \frac{\mu_0 I}{2\pi\sqrt{v^2+x^2}} \left[\frac{\frac{w}{2}}{\sqrt{v^2+x^2+(\frac{w}{2})^2}} \right] \end{aligned} \qquad A2.7$$

Again this is the full magnitude of the magnetic field at the field point $P(x)$. This is directed perpendicular to the line joining $P(x)$ with the point $(0, -v, 0)$ and, as in the previous case, lies in the xy plane. However, this time the x component is negative and the y component is positive. The x component, B_{0xi}^{CD}, is given by

$$B_{0xi}^{CD} = -\frac{v}{\sqrt{v^2+x^2}} B_{0i}^{CD} \qquad A2.8$$

or

$$B_{0xi}^{CD} = -\frac{\mu_0 I}{4\pi(v^2+x^2)} \left[\frac{vw}{\sqrt{v^2+x^2+(\frac{w}{2})^2}} \right] \qquad A2.9$$

Conductor BC

Conductor BC has its elements of length, dl, parallel to the y axis and so $dl = dy$. The relationship for R is $R^2 = x^2+y^2+(\frac{w}{2})^2$ and $\cos\alpha = (\sqrt{x^2+(\frac{w}{2})^2})/R$. α is the angle between R and the line which joins $P(x)$ to the point $(0,0,\frac{w}{2})$. The Biot-Savart law in scalar form is, thus,

$$dB_{0i}^{BC} = \frac{\mu_0 I}{4\pi\sqrt{x^2+(\frac{w}{2})^2}}\cos\alpha\, d\alpha \qquad A2.10$$

This time the limits for the α integration are asymmetrical with respect to $\alpha = 0$. The extent of the range of α is from from $\alpha_{min} = -\sin^{-1}[v/\sqrt{v^2+x^2+(\frac{w}{2})^2}]$ to $\alpha_{max} = \sin^{-1}[u/\sqrt{u^2+x^2+(\frac{w}{2})^2}]$. Hence, integrating equation (A2.10) with respect to α yields

$$\begin{aligned} B_{0i}^{BC} &= \frac{\mu_0 I}{4\pi\sqrt{x^2+(\frac{w}{2})^2}}\int_{\alpha_{min}}^{\alpha_{max}}\cos\alpha\, d\alpha \\ &= \frac{\mu_0 I}{4\pi\sqrt{x^2+(\frac{w}{2})^2}}\left[\frac{u}{\sqrt{u^2+x^2+(\frac{w}{2})^2}}+\frac{v}{\sqrt{v^2+x^2+(\frac{w}{2})^2}}\right] \end{aligned} \qquad A2.11$$

In a similar manner as for the previous two cases the x component is

$$B_{0xi}^{BC} = -\frac{\frac{w}{2}}{\sqrt{x^2+(\frac{w}{2})^2}}B_{0i}^{BC} \qquad A2.12$$

or

$$B_{0xi}^{BC} = -\frac{\mu_0 I\frac{w}{2}}{4\pi[x^2+(\frac{w}{2})^2]}\left[\frac{u}{\sqrt{u^2+x^2+(\frac{w}{2})^2}}+\frac{v}{\sqrt{v^2+x^2+(\frac{w}{2})^2}}\right] \qquad A2.13$$

Conductor DA

The symmetry relationship of the conductor DA with the conductor BC in respect of the x component of the magnetic field at the point $P(x)$ means that the two conductors produce exactly the same contribution. Hence,

$$B_{0xi}^{DA} = -\frac{\mu_0 I\frac{w}{2}}{4\pi[x^2+(\frac{w}{2})^2]}\left[\frac{u}{\sqrt{u^2+x^2+(\frac{w}{2})^2}}+\frac{v}{\sqrt{v^2+x^2+(\frac{w}{2})^2}}\right] \qquad A2.14$$

Thus, the total x component of the magnetic field is given by the sum of the contributions in equations (A2.5), (A2.9), (A2.13) and (A2.14). That is

$$B_{0xi} = B_{0xi}^{AB} + B_{0xi}^{BC} + B_{0xi}^{CD} + B_{0xi}^{DA} \qquad A2.15$$

Explicitly, this is

$$\begin{aligned} B_{0xi} = -\frac{\mu_0 I w}{4\pi}\Bigg[&\frac{u}{(u^2+x^2)\sqrt{u^2+x^2+(\frac{w}{2})^2}}+\frac{v}{(v^2+x^2)\sqrt{v^2+x^2+(\frac{w}{2})^2}} \\ &+\frac{1}{[x^2+(\frac{w}{2})^2]}\left(\frac{v}{\sqrt{v^2+x^2+(\frac{w}{2})^2}}+\frac{u}{\sqrt{u^2+x^2+(\frac{w}{2})^2}}\right)\Bigg] \end{aligned} \qquad A2.16$$

Appendix P1

Listings of the VSM Control Programs

The VSM Control Programs are written in BBC BASIC and run on an Acorn Model B BBC Microcomputer and 6502 Second Processor. Initially the programs invite the user to interactively set up all of the instruments. After this they allow the user to enter the details of the experiment required. There are then two experiment control programs proper. The first of these, P.VSMCP, conducts a full loop magnetization curve. The second one, P.CCIVITY, conducts a detailed study of both of the coercivity regions of the magnetization curve. For speed of execution, P.CCIVITY runs semi-interactively, requiring the user to manually ramp the field to saturate the sample at the appropriate times. The program names and some program details are given below.

P.CRIGHT : This program introduces the set of programs and asks whether the user wants to read a detailed introduction to the experiment. If the answer to this question is yes then the program LOADs and RUNs (CHAINs) P.INTRO. Otherwise, the program P.INTRO is missed out and the program P.SETUP is CHAINed directly.

P.INTRO : This program displays on the microcomputer monitor brief details of the experimental system and the manner in which the experiment is conducted. It then CHAINs P.SETUP.

P.SETUP : This program sets up all of the measuring instruments before the experiment commences. The first thing that it does is to clear the IEEE 488 bus. Then the user is asked whether the experiment is to be a detailed coercivity study or a full loop study. If the former is chosen then the program P.CCIVITY is immediately CHAINed. Otherwise the program continues and first asks for sample details, date *etc.* Then the user is asked to check that the current control unit is producing zero current, is set up in the correct logic state, and that all of the control unit-computer connections are made. The next step is to set up the 5206 lock-in amplifier. This is set to predetermined function settings, but the user is then given the option to change these if required. After this the user is asked to check that the LDJ gaussmeter and Hall effect probe are calibrated properly. The user then inputs either the gaussmeter range required for the experiment or specifies that the gaussmeter is to autorange throughout. The final stage of the set-up procedure is to enter details such as the maximum field required and the density of data points to be taken in the different regions of the magnetization curve. All of the details entered are saved in a temporary file. The program then CHAINs P.PHASE.

P.PHASE : The purpose of this program is to adjust the 5206 lock-in amplifier to have the correct phase relationship between the input and reference signals. The appropriate phase angle is that which maximizes channel 1 of the lock-in amplifier and minimizes channel 2. The

phase angle can be set either with the input signal from the sample, or if this is, perhaps, too weak, with the Ni calibration sample. In either case, the sample is first saturated (to produce the maximum input signal) and then the 5206 autofunction AUTOSET is rendered active. This function automatically alters the phase angle so that channel 1 is maximized. After this, the field is reduced to zero and then ramped up to its maximum value in the opposite direction. The field is then reduced back to zero. At this point, if the calibration sample was used to set the phase, it should now be replaced with the proper sample. Finally, the program CHAINs the next program, P.VSMCP.

P.VSMCP : This program is the one which actually controls the data taking. Both the ramping of the field and the recording of the data points at the appropriate field values (as entered in P.SETUP) are controlled in a full-loop magnetization curve. When the field is being reduced prior to a reversal, there are various checks executed to ascertain whether the current is actually low enough for the reversal to occur safely. This program accomplishes the current reversal remotely. In addition to this, when the field is increasing there are checks to make sure that the current does not get too high. For each data point recorded, ten points of lock-in output and field are measured. This gives a mean and a standard error. When the loop has been completed an alarm is sounded. The user then enters such details as the filename which is to be created for the storage of the data *etc.* Finally the 'raw' data is saved on floppy disc.

P.CCIVITY : This is the program which is CHAINed by P.SETUP if a detailed coercivity study is required. The program asks the user to set up the lock-in amplifier and the gaussmeter before the experiment starts. All of the data points recorded are close to the coercivity regions. Away from these regions, the ramping of the field, in order to saturate the sample, is performed manually. This is both to save time and to allow accurate field adjustment prior to the recording of data at the relevant parts of the magnetization curve. When the data from both coercivity regions has been saved, the program fits straight lines to the two data sets to give the two measures of the coercivity.

```
 10REM PROGRAM "P.CRIGHT"
 20REM ------------------------------------------------------------------------
 30REM ------------------------------  COPYRIGHT  ------------------------------
 40REM ------------------------------------------------------------------------
 50MODE0
 60VDU 23,1,0;0;0;0;
 70FOR N=11 TO 18
 80PRINTTAB(20,N);"=";SPC(39);"="
 90NEXT
100PRINTTAB(20,10);"-------------------------------------------------"
110PRINTTAB(24,12);"PROGRAM FOR AUTOMATED DATA TAKING"
120PRINTTAB(32,13);"ON THE VSM MARK II"
130PRINTTAB(36,15);"copyright:"
140PRINTTAB(35,16);"J.M.McCOY"
150PRINTTAB(35,17);"FEBRUARY 1986"
160PRINTTAB(20,19);"-------------------------------------------------"
170PROCspacebar(26,30,"CONTINUE")
180VDU 23,1,1;0;0;0;
190REPEAT
200PRINTTAB(3,14);"Do you wish to read the written introduction to this
                  control program (y/n)? ";
210A$=GET$
220UNTIL A$="Y" OR A$="y" OR A$="N" OR A$="n"
230IF A$="Y" OR A$="y" THEN 250 ELSE PROCdirect
240GOTO270
250VDU 23,1,0;0;0;0;
260CHAIN"P.INTRO"
270END
280:
290DEFPROCdirect
300VDU 23,1,0;0;0;0;
310CLS
320PRINTTAB(10,14);"The following section is the start of the experiment
                   proper."
330PROCspacebar(16,30,"ENTER INTO EXPERIMENT PROPER")
340CHAIN"P.SETUP"
350ENDPROC
360:
370DEFPROCspacebar(XX%,YY%,WORDS$)
380PRINTTAB(XX%,YY%);"(PRESS SPACE-BAR TO "WORDS$")"
390REPEAT:UNTIL INKEY(-99):CLS
400*FX15,0
410ENDPROC
```

```
10REM PROGRAM "P.INTRO"
20REM ------------------------------------------------------------
30REM ----------------  INITIAL WRITTEN INTRODUCTION  ----------------
40REM ------------------------------------------------------------
50MODE0
60VDU 23,1,0;0;0;0;
70PRINTTAB(34,0);"INTRODUCTION":PRINTTAB(33,1);"------------"
80PRINTTAB(11,3);"This program will control the operation of and take data
                  from"
90PRINTTAB(9,5);"the  VSM  and Newport  Power Supply  system. Before
                 continuing"
100PRINTTAB(9,7);"please make sure that you are fully familiar with the
                  operation"
110PRINTTAB(9,9);"of the  Newport Power  Supply and the other  items of
                  apparatus"
120PRINTTAB(9,11);"associated with the VSM."
130PRINTTAB(11,13);"IMPORTANT: PLEASE NOTE THAT THE MAIN REVERSING RELAY WILL
                    NOT"
140PRINTTAB(9,15);"TAKE A CURRENT OF 20 AMPS FOR MORE THAN HALF AN HOUR."
150PRINTTAB(11,18);"The program allows  the options for the LDJ  gaussmeter
                    to be"
160PRINTTAB(9,20);"either set on a  fixed range initially and to  remain
                   unaltered"
170PRINTTAB(9,22);"throughout the experiment or to autorange throughout. All
                   other"
180PRINTTAB(9,24);"peripherals are under computer control."
190PROCspacebar(26,30,"CONTINUE")
200PRINTTAB(11,3);"The operator must decide the maximum  external  field
                   (Bext)"
210PRINTTAB(9,5);"that he/she wishes to obtain and if in the non-autoranging
                  mode"
220PRINTTAB(9,7);"he/she must select the appropriate scale on the gaussmeter."
230PRINTTAB(11,9);"After   this  the   program  will   allow  the   operator
                   to"
240PRINTTAB(9,11);"split the range from 0 to Bext gauss into three regions and
                   to"
250PRINTTAB(9,13);"specify  the density  at  which  readings are taken in each
                   of"
260PRINTTAB(9,15);"these regions.  The smallest step in field available  with
                   the"
270PRINTTAB(9,17);"present system is 3 gauss."
280PRINTTAB(11,19);"The  function  settings  on  the 5206  Lock-In  amplifier
                    as"
290PRINTTAB(9,21);"selected  by  the  program  can  be  displayed  and
                   altered if"
300PRINTTAB(9,23);"required."
310PROCspacebar(26,30,"CONTINUE")
320PRINTTAB(11,3);"The M-B data will be stored on disk at the end of the
                   program"
330PRINTTAB(9,5);"so please  ensure that a suitable disk is placed  in drive
                  1 off"
340PRINTTAB(9,7);"the disk drive.  The values of M  are taken to be the
                  value of"
350PRINTTAB(9,9);"Channel 1 of the 5206 and these readings are stored on disk
                  in"
360PRINTTAB(9,11);"units of volts."
370PRINTTAB(11,13);"Before  entering  into  the  MAIN  PROGRAM  allow  the
                    LDJ"
380PRINTTAB(9,15);"gaussmeter, the  5206  Lock-In  and  the  Newport  Power
                   Supply"
```

```
390PRINTTAB(9,17);"( with generator running  under manual control ) at  least
                  half"
400PRINTTAB(9,19);"an hour to warm up."
410PRINTTAB(11,21);"Make sure that  the gaussmeter is calibrated  properly
                   and is"
420PRINTTAB(9,23);"set to the NORM setting. Also please ensure that the Hall
                  probe"
430PRINTTAB(9,25);"is  always  inserted  with  the  '+' marking  facing  the
                  coil"
440PRINTTAB(9,27);"connected to the BLACK supply lead."
450PROCspacebar(16,30,"ENTER INTO EXPERIMENT PROPER")
460CHAIN"P.SETUP"
470END
480:
490DEFPROCspacebar(XX%,YY%,WORDS$)
500PRINTTAB(XX%,YY%);"(PRESS SPACE-BAR TO "WORDS$")"
510REPEAT:UNTIL INKEY(-99):CLS
520*FX15,0
530ENDPROC
```

```
10REM PROGRAM "P.SETUP"
20REM ------------------------------------------------------------------------
30REM ------------------------  SET-UP PROGRAM  ------------------------
40REM ------------------------------------------------------------------------
50MODE0
60TIME=0
70PROCclearbus
80PROCdetails
90PROCsetzerocnt
100PROCinit
110PROCsetuplkin
120PROCsetupLDJ
130PROCfielddets
140PROCsavedets
150CHAIN"P.PHASE"
160END
170:
180DEFPROCclearbus
190REM ------------------------------------------------------------------------
200REM ------------------------  CLEAR IEEE BUS  ------------------------
210REM ------------------------------------------------------------------------
220VDU 23,1,0;0;0;0;
230PRINTTAB(9,3);"Before proceeding make sure that the CST Procyon IEEE
                 Interface"
240PRINTTAB(9,5);"is  switched on  and none of  its 3 front LEDs are
                 permanently"
250PRINTTAB(9,7);"lit up. If all is OK - "
260PROCspacebar(32,7)
270*FX15,0
280*IEEE
290REM FOLLOWING LINES CLEAR BUS
300PRINT#16,"*":REM CLEAR FLUKE
310*IFC:REM INTERFACE CLEAR
320*DISK
330ENDPROC
340:
350DEFPROCdetails
360REM ------------------------------------------------------------------------
370REM ------------------------  SAMPLE DETAILS  ------------------------
380REM ------------------------------------------------------------------------
390VDU 23,1,1;0;0;0;
400PRINTTAB(9,14);"Please enter:"
410REPEAT
420PRINTTAB(25,18);"Coercivity study required (y/n)";
430A$=GET$
440UNTIL A$="Y" OR A$="y" OR A$="N" OR A$="n"
450IF A$="Y" OR A$="y" THEN PROCchaincoerc
460INPUTTAB(25,20);"Today's date ";DA$
470INPUTTAB(25,22);"Sample type ";SA$
480INPUTTAB(25,24);"Temperature ";TEMP$
490CLS
500ENDPROC
510:
520DEFPROCchaincoerc
530CHAIN"P.CCIVITY"
540ENDPROC
550:
560DEFPROCsetzerocnt
570REM ------------------------------------------------------------------------
580REM ------------------------  SETTING ZERO CURRENT  ------------------------
```

```
590REM ----------------------------------------------------------------------
600VDU 23,1,0;0;0;0;.
610PRINTTAB(30,3);"SETTING ZERO CURRENT":PRINTTAB(29,4);
                  "-------------------------"
620A%=FNminicam("DA1",42,0,0)
630REM NN%=0 MAKES FLUKE READ VOLTAGE ACROSS SHUNT
640PROCdelay(100)
650*IEEE
660PRINT#16,"F1R1S0T0"
670*DISK
680PRINTTAB(11,6);"Adjust the lockable potentiometer on the Newport Supply
                  until"
690PRINTTAB(9,8);"a reading of less than 0.05 mV is obtained on the
                 Fluke"
700PRINTTAB(9,10);"Multimeter. Make sure that the CURRENT and LOGIC are
                  in the"
710PRINTTAB(9,12);"POSITIVE state and that all connections from the
                  Newport"
720PRINTTAB(9,14);"Control Unit to the Minicam are made. Also make sure
                  that the"
730PRINTTAB(9,16);"CONTROL MODE switch on the Newport Supply is
                  switched to"
740PRINTTAB(9,18);"'REMOTE'."
750PROCdelay(100)
760C%=FNminicam("AD1",9,0,0)
770IF ABS(C%)>1000 THEN Io$="Negative" ELSE Io$="Positive"
780PROCspacebar(26,30)
790CLS
800ENDPROC
810:
820DEFFNminicam(usr$,AD%,NN%,TT%)
830REM ----------------------------------------------------------------------
840REM ------------------------------  MINICAM  ------------------------------
850REM ----------------------------------------------------------------------
860REM ICC1 OF MINICAM HAS ADDRESS 6
870*IEEE
880*OPT 9,1
890*OPT 10,13
900STRING$=usr$+","+STR$(AD%)+","+STR$(NN%)+","+STR$(TT%)
910PRINT#6,STRING$+CHR$(13)
920INPUT#6,REPLY$
930*DISK
940=VAL(REPLY$)
950:
960DEFPROCspacebar(XX%,YY%)
970REM ----------------------------------------------------------------------
980REM ------------------------------  "SPACE-BAR"  -------------------------
990REM ----------------------------------------------------------------------
1000PRINTTAB(XX%,YY%);"(PRESS SPACE-BAR TO CONTINUE)"
1010REPEAT:UNTIL INKEY(-99)
1020ENDPROC
1030:
1040DEFPROCdelay(t)
1050REM ---------------------------------------------------------------------
1060REM ------------------------------  TIME DELAY  -------------------------
1070REM ---------------------------------------------------------------------
1080b=TIME:REPEAT:UNTIL TIME>=b+t
1090REM t IS IN 1/100s OF A SECOND
1100ENDPROC
1110:
```

```
1120DEFPROCsetuplkin
1130REM ————————————————————————————————————————————————
1140REM ————————————  SETTING UP 5206 LOCK-IN AMPLIFIER  ————————————
1150REM ————————————————————————————————————————————————
1160VDU 23,1,0;0;0;0;
1170PRINTTAB(23,3);"SETTING UP 5206 LOCK-IN AMPLIFIER"
1180PRINTTAB(22,4);"————————————————————————————————————"
1190PRINTTAB(24,6);"Give the lock-in a device-clear."
1200PROCspacebar(26,17)
1210*FX15,0
1220PRINTTAB(11,6);SPC(31)
1230PRINTTAB(26,17);SPC(29)
1240PRINTTAB(11,6);"The  5206 is being  initialised  and  set  to
                  predetermined"
1250PRINTTAB(9,8);"function settings."
1260PRINTTAB(35,17);"PLEASE WAIT"
1270PROCpnttolkin("T 4,0"):REM SETTING TIME CONSTANT & dB/OCTAVE
1280PROCdelay(100)
1290PROCpnttolkin("F 2"):REM SELECTING FREQUENCY BAND
1300PROCdelay(100)
1310PROCpnttolkin("A1 1"):REM SELECTING FREQUENCY BAND
1320PROCdelay(100)
1330PROCpnttolkin("L 14"):REM SETTING AUTO-LIMIT
1340PROCdelay(100)
1350PROCpnttolkin("W 1"):REM DISABLING FRONT KEY CONTROLS
1360L0$="CH1":L1$="Zero and off":L2$="High stab":L3$="Low":L4$="Ext. F"
1370L5$="0 degrees":L6$="1 s":L7$="12":L8$="any":L9$="Autorange":I0$="X,Y"
1380I1$="Off":I2$="100 microvolts"
1390PRINTTAB(35,17);SPC(11)
1400VDU 23,1,1;0;0;0;
1410REPEAT
1420PRINTTAB(9,17);"Do you wish to inspect these (y/n) ";
1430A$=GET$
1440UNTIL A$="Y" OR A$="y" OR A$="N" OR A$="n"
1450IF A$="N" OR A$="n" THEN ENDPROC
1460PROCsettings(L0$,L1$,L2$,L3$,L4$,L5$,L6$,L7$,L8$,L9$,I0$,I1$,I2$)
1470VDU 28,0,31,79,28:CLS
1480PRINTTAB(20,1);"If you wish to alter the settings do so now."
1490VDU 23,1,0;0;0;0;
1500PROCspacebar(26,2):CLS
1510*FX15,0
1520VDU26
1530ENDPROC
1540:
1550DEFPROCsettings(a$,b$,c$,d$,e$,f$,g$,h$,i$,j$,k$,l$,m$)
1560REM ————————————————————————————————————————————————
1570REM ————————————————  DISPLAY 5206 SETTINGS  ————————————————
1580REM ————————————————————————————————————————————————
1590CLS
1600PRINTTAB(23,2);"(1) Display        : ";a$
1610PRINTTAB(23,4);"(2) CH1 Offset     : ";b$
1620PRINTTAB(23,6);"(3) Reserve        : ";c$
1630PRINTTAB(23,8);"(4) Fband          : ";d$
1640PRINTTAB(23,10);"(5) Reference      : ";e$
1650PRINTTAB(23,12);"(6) Phase          : ";f$
1660PRINTTAB(23,14);"(7) Time constant  : ";g$
1670PRINTTAB(23,16);"(8) dB/octave      : ";h$
1680PRINTTAB(23,18);"(9) Auto-Functions : ";i$
1690PRINTTAB(22,20);"(10) Sensitivity    : ";j$
1700PRINTTAB(22,22);"(11) Output mode    : ";k$
```

```
1710PRINTTAB(22,24);"(12) Expand          : ";I$
1720PRINTTAB(22,26);"(13) Auto-limit      : ";m$
1730ENDPROC
1740:
1750DEFPROCsetupLDJ'
1760REM ------------------------------------------------------------------------
1770REM ----------------------  SETTING UP LDJ GAUSSMETER  ----------------------
1780REM ------------------------------------------------------------------------
1790VDU 23,1,0;0;0;0;
1800CLS
1810PRINTTAB(27,3);"SETTING UP LDJ GAUSSMETER"
1820PRINTTAB(26,4);"-------------------------------"
1830PRINTTAB(5,6);"1.  Set the MODE switch  to  CAL  and the range  to the 10K
                  gauss"
1840PRINTTAB(9,7);"range."
1850PRINTTAB(5,9);"2.  Let  the  LDJ  warm  up for  at  least  five  minutes
                  before"
1860PRINTTAB(9,10);"continuing."
1870PRINTTAB(5,12);"3.  Note whether  the meter reads  the calibration number
                   that is"
1880PRINTTAB(9,13);"given on the Hall probe. If it does not then adjust the
                   front"
1890PRINTTAB(9,14);"panel  CAL  adjustment using a screwdriver so that the
                   meter"
1900PRINTTAB(9,15);"displays the  probe CAL number. The instrument and probe
                   are"
1910PRINTTAB(9,16);"now calibrated."
1920PRINTTAB(5,18);"4.  Set the MODE switch to NORM."
1930PRINTTAB(5,20);"5.  For zero adjustment of the probe:"
1940PRINTTAB(9,21);"Set  the  FINE  control to midrange.  Starting  on the
                   higher"
1950PRINTTAB(9,22);"ranges  and proceeding  to the more sensitive  ranges,
                   adjust"
1960PRINTTAB(9,23);"the COARSE ZERO to give a zero meter reading. On the 10
                   gauss"
1970PRINTTAB(9,24);"range, use the FINE ZERO to zero  the meter. For more
                   details"
1980PRINTTAB(9,25);"consult the LDJ manual."
1990PROCspacebar(26,30):CLS
2000*FX15,0
2010PRINTTAB(27,3);"SETTING UP LDJ GAUSSMETER"
2020PRINTTAB(26,4);"-------------------------------"
2030VDU 23,1,1;0;0;0;
2040REPEAT
2050PRINTTAB(9,6);"Do you want the LDJ to autorange during the experiment
                  (y/n)?";
2060A$=GET$
2070UNTIL A$="Y" OR A$="y" OR A$="N" OR A$="n"
2080VDU 23,1,0;0;0;0;
2090IF A$="Y" OR A$="y" THEN PROCautoon ELSE PROCautooff
2100ENDPROC
2110:
2120DEFPROCautoon
2130NUM%=0
2140PRINTTAB(9,10);"In that case, make sure that the RANGE GAUSS switch is
                   set to"
2150PRINTTAB(9,12);"REMOTE."
2160PROCspacebar(26,30):CLS
2170*FX15,0
2180ENDPROC
```

```
2190:
2200DEFPROCautooff
2210VDU 23,1,1;0;0;0;
2220PRINTTAB(9,10);"In that case, set the  RANGE GAUSS switch to the
                   appropriate"
2230PRINTTAB(9,12);"range setting."
2240PRINTTAB(9,15);"The options for the ranges are:"
2250PRINTTAB(33,17);"1.  10   G":PRINTTAB(33,18);"2.  100  G"
2260PRINTTAB(33,19);"3.  1    KG":PRINTTAB(33,20);"4.  10  KG"
2270PRINTTAB(33,21);"5.  100 KG"
2280REPEAT
2290PRINTTAB(9,24);"Please enter the appropriate number (1-5) for the range
                   which"
2300INPUTTAB(9,26);"you have chosen. ";NUM%
2310IF NUM%<1 OR NUM%>5 THEN PRINTTAB(27,26);SPC(20)
2320UNTIL NUM%>=1 AND NUM%<=5
2330VDU 23,1,0;0;0;0;
2340ENDPROC
2350:
2360DEFPROCsavedets
2370REM ------------------------------------------------------------------------
2380REM ------------------------  SAVE DETAILS  ------------------------
2390REM ------------------------------------------------------------------------
2400X=OPENOUT":0.T.details"
2410PRINT#X,DA$,SA$,TEMP$,L9$,NUM%,lo$,hm,h2,h3,n1%,n2%,n3%
2420CLOSE#X
2430ENDPROC
2440:
2450DEFPROCfielddets
2460REM ------------------------------------------------------------------------
2470REM ------------------------  DETAILS OF FIELD  ------------------------
2480REM ------------------------------------------------------------------------
2490CLS
2500VDU23,1,1;0;0;0;
2510PRINTTAB(31,3);"DETAILS OF FIELD":PRINTTAB(30,4);"-----------------"
2520PRINTTAB(11,7);"Please enter:"
2530INPUTTAB(3,11);"Maximum Bext required (in gauss):";hm
2540INPUTTAB(3,13);"Values for boundaries between field regions 1 & 2 and 2 & 3
                   :";h2,h3
2550INPUTTAB(3,15);"No. of equally-spaced readings to be taken in regions 1,2 &
                    3:";n1%,n2%,n3%
2560REPEAT
2570PRINTTAB(18,18);"Do you wish to check this data (y/n)?";
2580A$=GET$
2590UNTIL A$="Y" OR A$="y" OR A$="N" OR A$="n"
2600IF A$="N" OR A$="n" THEN ENDPROC ELSE PROCfldetsdsp(hm,h2,h3,n1%,n2%,n3%)
2610ENDPROC
2620:
2630DEFPROCfldetsdsp(a,b,c,d%,e%,f%)
2640PRINTTAB(17,22);"Maximum Bext              : "a" gauss"
2650PRINTTAB(17,24);"Values for boundaries     : "b" & "c" gauss"
2660PRINTTAB(17,26);"No. of readings in regions : "d%" , "e%" & "f%
2670REPEAT
2680PRINTTAB(17,29);"Do you wish to alter any of these (y/n)?";
2690A$=GET$
2700UNTIL A$="Y" OR A$="y" OR A$="N" OR A$="n"
2710IF A$="N" OR A$="n" THEN ENDPROC ELSE PROCfielddets
2720ENDPROC
2730:
2740DEFPROCinit
```

```
2750REM ------------------------------------------------------------
2760REM ----------    SET UP BBC RS423 PORT & INITIALISE LOCK-IN    ----------
2770REM ------------------------------------------------------------
2780*FX156,8,227
2790*FX8,6
2800*FX7,6
2810*FX6,10
2820*FX2,2
2830*FX3,7
2840PRINT"U 0"
2850PROCdelay(50)
2860PRINT"Y 0"
2870*FX3,6
2880*FX2,2
2890*FX3,0
2900ENDPROC
2910:
2920DEFPROCpnttolkin(command$)
2930REM ------------------------------------------------------------
2940REM ----------    PRINT COMMAND TO LOCK-IN    ----------
2950REM ------------------------------------------------------------
2960*FX2,2
2970*FX3,7
2980PRINTcommand$
2990*FX3,6
3000*FX2,2
3010*FX3,0
3020ENDPROC
```

```
 10REM PROGRAM "P.PHASE"
 20REM ------------------------------------------------------------------------
 30REM ------------------------  SETTING PHASE  ------------------------
 40REM ------------------------------------------------------------------------
 50MODE0
 60TIME=0
 70PROCdetsin
 80PROCinit
 90PROCcyclic
100CHAIN"P.VSMCP"
110END
120:
130DEFFNminicam(usr$,AD%,NN%,TT%)
140REM ------------------------------------------------------------------------
150REM ------------------------  MINICAM  ------------------------
160REM ------------------------------------------------------------------------
170REM ICC1 OF MINICAM HAS ADDRESS 6
180*IEEE
190*OPT 9,1
200*OPT 10,13
210STRING$=usr$+","+STR$(AD%)+","+STR$(NN%)+","+STR$(TT%)
220PRINT#6,STRING$+CHR$(13)
230INPUT#6,REPLY$
240*DISK
250=VAL(REPLY$)
260:
270DEFPROCspacebar(XX%,YY%)
280REM ------------------------------------------------------------------------
290REM ------------------------  "SPACE-BAR"  ------------------------
300REM ------------------------------------------------------------------------
310PRINTTAB(XX%,YY%);"(PRESS SPACE-BAR TO CONTINUE)"
320REPEAT:UNTIL INKEY(-99)
330ENDPROC
340:
350DEFPROCdelay(t)
360REM ------------------------------------------------------------------------
370REM ------------------------  TIME DELAY  ------------------------
380REM ------------------------------------------------------------------------
390b=TIME:REPEAT:UNTIL TIME>=b+t
400REM t IS IN 1/100s OF A SECOND
410ENDPROC
420:
430DEFFNreadflu(command$)
440REM ------------------------------------------------------------------------
450REM ------------------------  READ FLUKE  ------------------------
460REM ------------------------------------------------------------------------
470*IEEE
480*OPT2,0
490PRINT#16,command$
500REPEAT:UNTIL PTR#1=TRUE
510INPUT#16,reading$
520PRINT#16,"N0P1"
530*DISK
540=VAL(reading$)
550:
560DEFPROCdetsin
570REM ------------------------------------------------------------------------
580REM ------------------------  READ IN DETAILS FILE  ------------------------
590REM ------------------------------------------------------------------------
600X=OPENIN":0.T.details"
```

```
610INPUT#X,DA$,SA$,TEMP$,L9$,NUM%,lo$,hm,h2,h3,n1%,n2%,n3%
620CLOSE#X
630IF NUM%=1 THEN g0=10 :REM G'METER RANGE
640IF NUM%=2 THEN g0=100
650IF NUM%=3 THEN g0=1E3
660IF NUM%=4 THEN g0=1E4
670IF NUM%=5 THEN g0=1E5
680ENDPROC
690:
700DEFPROCcyclic
710REM ------------------------------------------------------------------------
720REM ----------------------  AUTOSETTING 5206  ----------------------------
730REM ------------------------------------------------------------------------
740CLS
750VDU 23,1,0;0;0;0;
760PRINTTAB(33,3);"AUTOSETTING 5206"
770PRINTTAB(32,4);"--------------------"
780PRINTTAB(9,6);"Place the Hall probe in the field gap."
790PRINTTAB(9,9);"If the sample will produce a sufficiently strong signal by
                  which"
800PRINTTAB(9,11);"to set  the phase  then simply  place the sample  in the
                   VSM  and"
810PRINTTAB(9,13);"switch the motor on."
820PRINTTAB(9,16);"If this  is not the case then  it is necessary to  set the
                   phase"
830PRINTTAB(9,18);"using the Ni calibration  sample. If this is required then
                   place"
840PRINTTAB(9,20);"the Ni sample in the VSM and switch the motor on."
850PRINTTAB(9,23);"You  will be told  later  when  to remove the  Ni  sample
                   and to"
860PRINTTAB(9,25);"replace it with the proper sample."
870PROCspacebar(26,30)
880*FX15,0
890CLS
900PRINTTAB(33,3);"AUTOSETTING 5206"
910PRINTTAB(32,4);"--------------------"
920PRINTTAB(9,6);"Put the gaussmeter on the 10KG range."
930PROCdelay(300)
940PROCspacebar(26,10)
950*FX15,0
960CLS
970PRINTTAB(33,3);"AUTOSETTING 5206"
980PRINTTAB(32,4);"--------------------"
990PRINTTAB(27,16);"PLEASE WAIT (2-3 MINS)"
1000LDJvolts=FNreadflu("R2N16P1")
1010PROCdelay(100)
1020REPEAT
1030A%=FNminicom("DA1",42,1,0)
1040S%=FNminicom("ST1",39,150,30):REM INCREASING CURRENT
1050LDJvolts=FNreadflu("N16P1")
1060h0=LDJvolts*1E4
1070UNTIL h0>=hm
1080IF L9$="Autorange" THEN 1130
1090sts=FNreadlkin("Z")
1100PROCpnttolkin("A2 0"):REM AUTOSET OFF
1110PROCdelay(100)
1120PROCpnttolkin("A4 0"):REM AUTONORMALIZE OFF
1130PROCdelay(100)
1140sts=FNreadlkin("Z")
1150PROCdelay(100)
```

```
1160PROCpnttolkin("A1 0"):REM AUTORANGE OFF
1170PROCdelay(100)
1180PROCpnttolkin("A2 1"):REM AUTOSETTING
1190PROCdelay(1000)
1200REPEAT
1210S%=FNminicam("ST1",38,150,30):REM DECREASING CURRENT
1220A%=FNminicam("DA1",42,1,0):REM SWITCH TO READ VOLTS FROM LDJ
1230LDJvolts=FNreadflu("R2N16P1")
1240h0=LDJvolts*1E4
1250UNTIL h0<=220
1260A%=FNminicam("DA1",42,0,0):REM READ VOLTS ACROSS SHUNT
1270PROCdelay(50)
1280SHUNTvolts=FNreadflu("R1N16P1")
1290IF ABS(SHUNTvolts)>250E-3 THEN 1200
1300PROCcurrev
1310MODE0
1320VDU23,1,0;0;0;0;
1330PRINTTAB(33,3);"AUTOSETTING 5206"
1340PRINTTAB(32,4);"--------------------"
1350PRINTTAB(27,16);"PLEASE WAIT"
1360A%=FNminicam("DA1",42,1,0):REM READ LDJ
1370LDJvolts=FNreadflu("R2N16P1")
1380REPEAT
1390S%=FNminicam("ST1",39,150,30):REM INCREASING CURRENT
1400LDJvolts=FNreadflu("N16P1")
1410h0=LDJvolts*1E4
1420UNTIL ABS(h0)>=hm
1430S%=FNminicam("ST1",38,150,30):REM DECREASING CURRENT
1440LDJvolts=FNreadflu("R2N16P1")
1450h0=LDJvolts*1E4
1460IF ABS(h0)>220  THEN 1430
1470A%=FNminicam("DA1",42,0,0):REM VOLTS ACROSS SHUNT
1480SHUNTvolts=FNreadflu("R1N16P1")
1490IF ABS(SHUNTvolts)>250E-3 THEN 1430
1500PROCcurrev
1510MODE0
1520VDU23,1,0;0;0;0;
1530PRINTTAB(33,3);"AUTOSETTING 5206"
1540PRINTTAB(32,4);"--------------------"
1550PRINTTAB(9,6);"Readjust the  set-zero  potentiometer until  a reading  of
                  less"
1560PRINTTAB(9,7);"than 0.05 mV is obtained on the Fluke Multimeter."
1570PRINTTAB(9,10);"If you have had to change the range of the gaussmeter for
                    this"
1580PRINTTAB(9,11);"AUTOSETTING procedure, make sure you put it back to the
                    range"
1590PRINTTAB(9,12);"you want for the experiment."
1600PRINTTAB(9,16);"If you have set the phase using Ni now is the time to
                    replace"
1610PRINTTAB(9,17);"it with the real sample"
1620A%=FNminicam("DA1",42,0,0):REM VOLTS ACROSS SHUNT
1630SHUNTvolts=FNreadflu("R1N16P1")
1640PROCspacebar(26,30)
1650*FX15,0
1660CLS
1670IF L9$<>"Autorange" THEN ENDPROC
1680PROCpnttolkin("A1 1"):REM A'RANGE ON IF REQD
1690ENDPROC
1700:
1710:
```

```
1720DEFPROCcurrev
1730REM ————————————————————————————————————————————————
1740REM ————————————————————  CURRENT REVERSAL  ————————————————————
1750REM ————————————————————————————————————————————————
1760MODE7
1770VDU23,1,0;0;0;0;
1780PRINTTAB(4,6);CHR$(136);"REVERSING CURRENT DIRECTION"
1790PRINTTAB(32,6);CHR$(137)
1800PRINTTAB(4,7);"————————————————————————————"
1810C%=FNminicam("AD1",9,0,0)
1820IF ABS(C%)<=3 THEN lo$="Negative" ELSE lo$="Positive"
1830PRINTTAB(1,11);"Logic & current in";CHR$(136);lo$;CHR$(137);"direction"
1840PROCchangelogi
1850D%=FNminicam("AD1",9,0,0):REM CHECKING LOGIC REVERSAL
1860IF ABS(D%-C%)<=2 THEN 1840
1870C%=D%
1880A%=FNminicam("DA1",42,4,0):REM ACTIVATE MAIN POWER RELAY (5V ON)
1890PROCdelay(50)
1900A%=FNminicam("DA1",42,0,0):REM 5V OFF
1910D%=FNminicam("AD1",9,0,0)
1920IF ABS(D%-C%)<10 THEN 1960:REM CHECKING LOGIC IS UNALTERED
1930PROCchangelogi:REM RESET LOGIC IF NECESSARY
1940D%=FNminicam("AD1",9,0,0)
1950IF ABS(D%-C%)>10 THEN 1930
1960IF ABS(C%)<=3 THEN lo$="Negative" ELSE lo$="Positive"
1970PRINTTAB(1,11);SPC(2);"Now changed to";CHR$(136);lo$;CHR$(137);"direction";SPC(2)
1980PROCdelay(300)
1990ENDPROC
2000:
2010:
2020DEFPROCchangelogi
2030PROCdelay(150)
2040A%=FNminicam("DA1",42,0,0)
2050PROCdelay(100)
2060A%=FNminicam("DA1",42,2,0)
2070PROCdelay(50)
2080A%=FNminicam("DA1",42,0,0)
2090PROCdelay(100)
2100ENDPROC
2110:
2120DEFFNreadlkin(command$)
2130REM ————————————————————————————————————————————————
2140REM ————————————————————  READ LOCK-IN  ————————————————————
2150REM ————————————————————————————————————————————————
2160*FX2,2
2170*FX3,7
2180PRINT"Z"
2190*FX3,6
2200*FX2,1
2210INPUTA$
2220IF VAL(A$)<>32 THEN 2160
2230*FX2,2
2240*FX3,7
2250PRINTcommand$
2260*FX3,6
2270*FX2,1
2280INPUToutput$
2290*FX2,2
2300*FX3,0
2310=VAL(output$)
```

```
2320:
2330DEFPROCinit
2340REM ------------------------------------------------------------------------
2350REM ----------    SET UP BBC RS423 PORT & INITIALISE LOCK-IN    ----------
2360REM ------------------------------------------------------------------------
2370*FX156,8,227
2380*FX8,6
2390*FX7,6
2400*FX6,10
2410*FX2,2
2420*FX3,7
2430PRINT"U 0"
2440PROCdelay(50)
2450PRINT"Y 0"
2460*FX3,6
2470*FX2,2
2480*FX3,0
2490ENDPROC
2500:
2510DEFPROCpnttolkin(command$)
2520REM ------------------------------------------------------------------------
2530REM ----------------------    PRINT COMMAND TO LOCK-IN    ------------------
2540REM ------------------------------------------------------------------------
2550*FX2,2
2560*FX3,7
2570PRINTcommand$
2580*FX3,6
2590*FX2,2
2600*FX3,0
2610ENDPROC
```

```
10REM PROGRAM "P.VSMCP"
20REM ------------------------------------------------------------------------
30REM ----------------------  VSM CONTROL PROGRAM  ----------------------
40REM ------------------------------------------------------------------------
50DIM CH1(350):DIM B(350):DIM ECH1(350):DIM EB(350)
60DIM h9(10):DIM Q1(10):DIM FATALTEST(4)
70MODE0
80TIME=0
90NOOFPTS%=0
100PROCdetsin
110PROCfieldsteps
120PROCinit
130PROCreadTC
140PROCtakecurve
150PROCtempsaveMB
160PROCdisksaveMB
170END
180:
190DEFFNminicam(usr$,AD%,NN%,TT%)
200REM ------------------------------------------------------------------------
210REM ----------------------------  MINICAM  ----------------------------
220REM ------------------------------------------------------------------------
230REM ICC1 OF MINICAM HAS ADDRESS 6
240*IEEE
250*OPT 9,1
260*OPT 10,13
270STRING$=usr$+","+STR$(AD%)+","+STR$(NN%)+","+STR$(TT%)
280PRINT#6,STRING$+CHR$(13)
290INPUT#6,REPLY$
300*DISK
310=VAL(REPLY$)
320:
330DEFPROCspacebar(XX%,YY%)
340REM ------------------------------------------------------------------------
350REM ------------------------  "SPACE-BAR"  ------------------------
360REM ------------------------------------------------------------------------
370PRINTTAB(XX%,YY%);"(PRESS SPACE-BAR TO CONTINUE)"
380REPEAT:UNTIL INKEY(-99)
390ENDPROC
400:
410DEFPROCdelay(t)
420REM ------------------------------------------------------------------------
430REM ----------------------------  TIME DELAY  ----------------------------
440REM ------------------------------------------------------------------------
450b=TIME:REPEAT:UNTIL TIME>=b+t
460REM t IS IN 1/100s OF A SECOND
470ENDPROC
480:
490DEFFNreadflu(command$)
500REM ------------------------------------------------------------------------
510REM ----------------------------  READ FLUKE  ----------------------------
520REM ------------------------------------------------------------------------
530*IEEE
540*OPT2,0
550PRINT#16,command$
560REPEAT:UNTIL PTR#1=TRUE
570INPUT#16,reading$
580PRINT#16,"N0P1"
590*DISK
600=VAL(reading$)
```

```
610:
620DEFPROCdetsin
630REM ------------------------------------------------------------------------
640REM ----------------------  READ IN DETAILS FILE  ------------------------
650REM ------------------------------------------------------------------------
660X=OPENIN":0.T.details"
670INPUT#X,DA$,SA$,TEMP$,L9$,NUM%,lo$,hm,h2,h3,n1%,n2%,n3%
680CLOSE#X
690IF NUM%=0 THEN g0=10
700IF NUM%=0 THEN REL%=129
710IF NUM%=1 THEN g0=10 :REM G'METER RANGE
720IF NUM%=2 THEN g0=100
730IF NUM%=3 THEN g0=1E3
740IF NUM%=4 THEN g0=1E4
750IF NUM%=5 THEN g0=1E5
760IF NUM%=0 THEN PROCLDJinit
770ENDPROC
780:
790DEFPROCLDJinit
800REM ------------------------------------------------------------------------
810REM ----------------  INITIALISE LDJ IF A'RANGING  ----------------------
820REM ------------------------------------------------------------------------
830Message$="LPCI"
840A%=FNminicam("DA1",42,REL%,0)
850PROCdelay(100)
860LDJvolts=FNreadflu("F1R0S0N16P1T0")
870REPEAT
880PROCchangrange
890UNTIL LDJvolts<=1.9
900ENDPROC
910:
920DEFPROCscrnmssge(Mess$)
930REM ------------------------------------------------------------------------
940REM ---------------------  SCREEN MESSAGES  ---------------------------
950REM ------------------------------------------------------------------------
960MODE7
970VDU23,1,0;0;0;0;
980W$=" "
990IF Mess$="RMBV" THEN X%=6 ELSE X%=1
1000IF Mess$="RCD" THEN X%=5
1010IF Mess$="RMBV" THEN W$="RECORDING M AND Bo VALUES"
1020IF Mess$="LPCI" THEN W$="LOGIC POSITIVE CURRENT INCREASING"
1030IF Mess$="LNCI" THEN W$="LOGIC NEGATIVE CURRENT INCREASING"
1040IF Mess$="LPCD" THEN W$="LOGIC POSITIVE CURRENT DECREASING"
1050IF Mess$="LNCD" THEN W$="LOGIC NEGATIVE CURRENT DECREASING"
1060IF Mess$="RCD" THEN W$="REVERSING CURRENT DIRECTION"
1070X%=10
1080PRINTTAB(2,2);"Points so far: ";NOOFPTS%
1090FOR P=5 TO 7
1100PRINTTAB(X%-1,P);"-";SPC(2+LEN(W$));"-"
1110NEXT
1120FOR JJ=X%-1 TO X%+2+LEN(W$)
1130PRINTTAB(JJ,4);"-":PRINTTAB(JJ,8);"-"
1140NEXT
1150PRINTTAB(X%,6);CHR$(134);W$
1160PRINTTAB(X%+LEN(W$)+1,6);CHR$(135)
1170ENDPROC
1180:
1190DEFPROCchangrange
1200REM ------------------------------------------------------------------------
```

```
1210REM ------------------------  CHANGE LDJ RANGE  ------------------------
1220REM ------------------------------------------------------------------
1230IF (Message$="LPCI" OR Message$="LNCI") AND ABS(LDJvolts)<=0.18 THEN
                                                                    ENDPROC
1240IF (Message$="LPCD" OR Message$="LNCD") AND ABS(LDJvolts)>=1.9 THEN ENDPROC
1250IF (Message$="LPCD" OR Message$="LNCD") AND g0=10 THEN ENDPROC
1260IF (Message$="LPCI" OR Message$="LNCI") AND g0=1E5 THEN ENDPROC
1270IF (Message$="LPCD" OR Message$="LNCD") THEN PROCdownrange
1280IF (Message$="LPCI" OR Message$="LNCI") THEN PROCuprange
1290A%=FNminicam("DA1",42,REL%,0)
1300PROCdelay(100)
1310LDJvolts=FNreadflu("R2N16P1")
1320ENDPROC
1330:
1340:
1350DEFPROCuprange
1360g0=10*g0
1370IF REL%=17 THEN REL%=9
1380IF REL%=33 THEN REL%=17
1390IF REL%=65 THEN REL%=33
1400IF REL%=129 THEN REL%=65
1410ENDPROC
1420:
1430DEFPROCdownrange
1440g0=0.1*g0
1450IF REL%=65 THEN REL%=129
1460IF REL%=33 THEN REL%=65
1470IF REL%=17 THEN REL%=33
1480IF REL%=9 THEN REL%=17
1490ENDPROC
1500:
1510DEFPROCcurrev
1520REM ------------------------------------------------------------------
1530REM ------------------------  CURRENT REVERSAL  ------------------------
1540REM ------------------------------------------------------------------
1550MODE7
1560VDU23,1,0;0;0;0;
1570PROCscrnmssge("RCD")
1580C%=FNminicam("AD1",9,0,0)
1590IF ABS(C%)<=3 THEN lo$="Negative" ELSE lo$="Positive"
1600PRINTTAB(1,11);"Logic & current in";CHR$(134);lo$;CHR$(135);"direction"
1610PROCchangelogi
1620D%=FNminicam("AD1",9,0,0):REM CHECKING LOGIC REVERSAL
1630IF ABS(D%-C%)<=2 THEN 1610
1640C%=D%
1650IF NUM%<>0 THEN REL%=1
1660A%=FNminicam("DA1",42,REL%+3,0):REM ACTIVATE MAIN POWER RELAY (5V ON)
1670PROCdelay(50)
1680A%=FNminicam("DA1",42,REL%-1,0):REM 5V OFF
1690D%=FNminicam("AD1",9,0,0)
1700IF ABS(D%-C%)<10 THEN 1740:REM CHECKING LOGIC IS UNALTERED
1710PROCchangelogi:REM RESET LOGIC IF NECESSARY
1720D%=FNminicam("AD1",9,0,0)
1730IF ABS(D%-C%)>10 THEN 1710
1740IF ABS(C%)<=3 THEN lo$="Negative" ELSE lo$="Positive"
1750PRINTTAB(0,11);SPC(3);"Now changed to";CHR$(134);lo$;CHR$(135);"direction"
                                                                    ;SPC(2)
1760IF NUM%<>0 THEN 1830
1770A%=FNminicam("DA1",42,REL%,0)
1780PROCdelay(100)
```

```
1790LDJvolts=FNreadflu("R0N16P1")
1800IF lo$="Positive" THEN Message$="LPCI"
1810IF lo$="Negative" THEN Message$="LNCI"
1820IF ABS(LDJvolts)>=1.9 THEN PROCchangrange
1830PROCdelay(300)
1840ENDPROC
1850:
1860:
1870DEFPROCchangelogi
1880PROCdelay(150)
1890IF NUM%<>0 THEN REL%=1
1900A%=FNminicam("DA1",42,REL%-1,0)
1910PROCdelay(100)
1920A%=FNminicam("DA1",42,REL%+1,0)
1930PROCdelay(50)
1940A%=FNminicam("DA1",42,REL%-1,0)
1950PROCdelay(100)
1960ENDPROC
1970:
1980DEFPROCchangecnt(Message$,ss%,h)
1990REM ------------------------------------------------------------
2000REM ----------  CHANGING CURRENT TO KNOWN B VALUE  ----------
2010REM ------------------------------------------------------------
2020LDJvolts=FNreadflu("F1R2S0N16P1T0")
2030n0%=0:REM FLAG FOR DECREASING CURRENT
2040b$=""
2050IF Message$="LPCI" THEN PROCscrnmssge("LPCI")
2060IF Message$="LNCI" THEN PROCscrnmssge("LNCI")
2070IF Message$="LPCD" THEN PROCscrnmssge("LPCD")
2080IF Message$="LNCD" THEN PROCscrnmssge("LNCD")
2090IF NUM%<>0 THEN REL%=1
2100A%=FNminicam("DA1",42,REL%,0):REM READ LDJ
2110LDJvolts=FNreadflu("R2N16P1")
2120IF (ABS(LDJvolts)>=1.9 OR ABS(LDJvolts)<=0.18) AND NUM%=0 THEN
                                                    PROCchangrange
2130PRINTTAB(15,11);"Bo(gauss)":PRINTTAB(14,12);"----------"
2140VDU28,0,23,39,13
2150IF Message$="LPCI" OR Message$="LNCI" THEN SMad%=39 ELSE SMad%=38
2160S%=FNminicam("ST1",SMad%,2*ss%,30):REM CHANGING CURRENT
2170LDJvolts=FNreadflu("N16P1")
2180IF (ABS(LDJvolts)>=1.9 OR ABS(LDJvolts)<=0.18) AND NUM%=0 THEN
                                                    PROCchangrange
2190h0=LDJvolts*g0
2200PRINTTAB(19-INT(0.5*LEN(STR$(h0))));h0
2210n0%=10
2220IF Message$="LPCD" OR Message$="LNCD" THEN n0%=n0%+1
2230IF n0%=1 THEN PROCtstforcgov:REM TEST FOR WHETHER CHANGEOVER NEEDED
2240IF (Message$="LPCD" OR Message$="LNCD") AND ABS(h0)<10 THEN
                                                    PROCtstforcgov
2250IF b$="Changeover needed" THEN 2310
2260IF ABS(h0)>12900 THEN PROCwinddown
2270IF Message$="LPCI" AND h0-h<0 THEN 2140
2280IF Message$="LNCI" AND h0-h>0 THEN 2140
2290IF Message$="LPCD" AND h0>h THEN 2140
2300IF Message$="LNCD" AND h0<h THEN 2140
2310VDU26
2320F=h
2330ENDPROC
2340:
2350DEFPROCtstforcgov
```

```
2360REM ------------------------------------------------------------------------
2370REM ----------------  TEST FOR WHETHER CHANGEOVER NEEDED  ----------------
2380REM ------------------------------------------------------------------------
2390n0%=0
2400IF ABS(h0)>400 THEN ENDPROC
2410IF NUM%<>0 THEN REL%=1
2420A%=FNminicam("DA1",42,REL%-1,0)
2430PROCdelay(200)
2440SHUNTvolts=FNreadflu("R0N16P1")
2450IF ABS(SHUNTvolts)<0.05E-3 THEN b$="Changeover needed" ELSE b$="No"
2460A%=FNminicam("DA1",42,REL%,0)
2470LDJvolts=FNreadflu("R2N16P1")
2480PROCdelay(100)
2490ENDPROC
2500:
2510DEFPROCwinddown
2520REM ------------------------------------------------------------------------
2530REM ----------------------  RAMPING FIELD DOWN  ----------------------------
2540REM ------------------------------------------------------------------------
2550MODE7
2560VDU23,1,0;0;0;0;
2570VDU26
2580IF NUM%<>0 THEN REL%=1
2590A%=FNminicam("DA1",42,REL%,0):REM TEST WHETHER DANGER CONDITION IS TRUE
2600PROCdelay(100)
2610FOR J%=1 TO 4
2620LDJvolts=FNreadflu("R0N16P1")
2630h0=LDJvolts*g0
2640FATALTEST(J%)=h0
2650PROCdelay(30)
2660NEXT
2670SUMTST=0
2680FOR J%=1 TO 4
2690SUMTST=SUMTST+FATALTEST(J%)
2700IF ABS(SUMTST)<=51600 THEN ENDPROC
2710A%=FNminicam("DA1",42,REL%-1,0)
2720PROCdelay(100)
2730SHUNTvolts=FNreadflu("F1R0S0N16P1T0")
2740PRINTTAB(0,6);CHR$(136);"CURRENT TOO HIGH - RAMPING FIELD DOWN"
2750PRINTTAB(38,6);CHR$(137)
2760PROCalarm
2770PRINTTAB(7,19);"(PRESS SPACE-BAR TO END)"
2780*FX15,1
2790REPEAT
2800S%=FNminicam("ST1",38,800,30):REM DECREASING CURRENT
2810SHUNTvolts=FNreadflu("N16P1")
2820G%=INKEY(0)
2830UNTIL G%=32 OR ABS(SHUNTvolts)<0.3E-3
2840MODE0
2850PRINTTAB(23,10);"EXPERIMENT ENDED - CURRENT TOO HIGH"
2860VDU23,1,1;0;0;0;
2870REPEAT
2880PRINTTAB(7,13);"Do you want the data taken before the abandonment to be
                   saved (y/n)?";
2890A$=GET$
2900UNTIL A$="Y" OR A$="y" OR A$="N" OR A$="n"
2910IF A$="N" OR A$="n" THEN END ELSE CLS:PROCtempsaveMB:PROCdisksaveMB
2920END
2930ENDPROC
2940:
```

```
2950DEFPROCalarm
2960REM ------------------------------------------------------------------------
2970REM ------------------------  SOUND ALARM  ------------------------
2980REM ------------------------------------------------------------------------
2990ENVELOPE 2,1,2,-2,2,10,20,10,1,0,0,-1,100,100
3000SOUND 1,2,100,100
3010ENDPROC
3020:
3030DEFPROCfieldsteps
3040REM ------------------------------------------------------------------------
3050REM ------------------------  CALCULATE FIELD STEPS  ------------------------
3060REM ------------------------------------------------------------------------
3070g1=h2/n1%:g2=(h3-h2)/n2%:g3=(hm-h3)/n3%
3080s1%=INT(g1/3/10):s2%=INT(g2/3/10):s3%=INT(g3/3/10)
3090IF g1<3 THEN g1=3:IF g2<3 THEN g2=3:IF g3<3 THEN g3=3
3100IF s1%<3 THEN s1%=3:IF s2%<3 THEN s2%=3:IF s3%<3 THEN s3%=3
3110ENDPROC
3120:
3130DEFPROCreadTC
3140REM ------------------------------------------------------------------------
3150REM ------------------------  READ TIME CONST  ------------------------
3160REM ------------------------------------------------------------------------
3170TC=FNreadlkin("T"):REM READ TIME CONST
3180Tconst=FNcalcTC(TC):REM CALC TC
3190ENDPROC
3200:
3210:
3220DEFFNcalcTC(TT)
3230B=10↑(2-INT(TT/2))
3240IF TT<>(INT(TT/2)*2) THEN B=B*0.3
3250=B
3260:
3270DEFPROCtakecurve
3280REM ------------------------------------------------------------------------
3290REM ------------------------  CONTROL TAKING OF M-B CURVE  ------------------------
3300REM ------------------------------------------------------------------------
3310h1=g1:ss=s1%
3320PROCtakeMBvals
3330h=h9
3340FOR K%=1 TO 13
3350IF K%=1 THEN 3360 ELSE 3370
3360ss%=s1%:incr=g1:Message$="LPCI":GOTO 3610
3370IF K%=2 THEN 3380 ELSE 3390
3380ss%=s2%:incr=g2:Message$="LPCI":GOTO 3610
3390IF K%=3 THEN 3400 ELSE 3410
3400ss%=s3%:incr=g3:Message$="LPCI":GOTO 3610
3410IF K%=4 THEN 3420 ELSE 3430
3420ss%=s3%:incr=-g3:Message$="LPCD":GOTO 3610
3430IF K%=5 THEN 3440 ELSE 3450
3440ss%=s2%:incr=-g2:Message$="LPCD":GOTO 3610
3450IF K%=6 THEN 3460 ELSE 3470
3460ss%=s1%:incr=-g1:Message$="LPCD":GOTO 3610
3470IF K%=7 THEN 3480 ELSE 3490
3480ss%=s1%:incr=-g1:Message$="LNCI":GOTO 3610
3490IF K%=8 THEN 3500 ELSE 3510
3500ss%=s2%:incr=-g2:Message$="LNCI":GOTO 3610
3510IF K%=9 THEN 3520 ELSE 3530
3520ss%=s3%:incr=-g3:Message$="LNCI":GOTO 3610
3530IF K%=10 THEN 3540 ELSE 3550
3540ss%=s3%:incr=g3:Message$="LNCD":GOTO 3610
```

```
3550IF K%=11 THEN 3560 ELSE 3570
3560ss%=s2%:incr=g2:Message$="LNCD":GOTO 3610
3570IF K%=12 THEN 3580 ELSE 3590
3580ss%=s1%:incr=g1:Message$="LNCD":GOTO 3610
3590IF K%=13 THEN 3600 ELSE 3610
3600ss%=s2%:incr=g2:Message$="LPCI":GOTO 3610
3610REPEAT
3620h=h+incr
3630PROCchangecnt(Message$,ss%,h)
3640PROCtakeMBvals
3650IF (K%=4 OR K%=5 OR K%=6) AND b$="Changeover needed" THEN b$="" ELSE 3670
3660PROCcurrev:PROCtakeMBvals:K%=7:GOTO 3410
3670IF (K%=4 OR K%=5 OR K%=6) AND h9<g1 THEN PROCreducecnt ELSE 3690
3680GOTO 3660
3690IF (K%=10 OR K%=11 OR K%=12) AND b$="Changeover needed" THEN b$="" ELSE
                                                                    3710
3700PROCcurrev:PROCtakeMBvals:K%=13:GOTO 3470
3710IF (K%=10 OR K%=11 OR K%=12) AND h9>-g1 THEN PROCreducecnt ELSE 3730
3720GOTO 3700
3730IF K%=1 THEN 3740 ELSE 3750
3740hcon=h2:hlim=h9
3750IF K%=2 THEN 3760 ELSE 3770
3760hcon=h3:hlim=h9
3770IF K%=3 THEN 3780 ELSE 3790
3780hcon=hm:hlim=h9
3790IF K%=4 THEN 3800 ELSE 3810
3800hcon=h9:hlim=h3
3810IF K%=5 THEN 3820 ELSE 3830
3820hcon=h9:hlim=h2
3830IF K%=6 THEN 3840 ELSE 3850
3840hcon=h9:hlim=h1
3850IF K%=7 THEN 3860 ELSE 3870
3860hcon=h9:hlim=-h2
3870IF K%=8 THEN 3880 ELSE 3890
3880hcon=h9:hlim=-h3
3890IF K%=9 THEN 3900 ELSE 3910
3900hcon=h9:hlim=-hm
3910IF K%=10 THEN 3920 ELSE 3930
3920hcon=-h3:hlim=h9
3930IF K%=11 THEN 3940 ELSE 3950
3940hcon=-h2:hlim=h9
3950IF K%=12 THEN 3960 ELSE 3970
3960hcon=-h1:hlim=h9
3970IF K%=13 THEN 3980 ELSE 4000
3980hcon=2000:hlim=h9
3990IF b$="No" THEN 3620
4000UNTIL hlim>hcon
4010NEXT K%
4020IF NUM%<>0 THEN REL%=1
4030A%=FNminicam("DA1",42,REL%-1,0)
4040PROCdelay(100)
4050SHUNTvolts=FNreadflu("F1R0S0N16P1T0")
4060REPEAT
4070S%=FNminicam("ST1",38,100,30)
4080SHUNTvolts=FNreadflu("N16P1")
4090UNTIL ABS(SHUNTvolts)<0.3E-3
4100MODE0
4110VDU23,1,0;0;0;0;
4120PRINTTAB(27,14);"M-Bo data taking finished."
4130PROCalarm
```

```
4140PROCspacebar(26,30)
4150*FX15,1
4160CLS
4170ENDPROC
4180:
4190DEFPROCreducecnt
4200REM ------------------------------------------------------------------------
4210REM ----------    FOR REVERSING CURRENT IF SAFE CONDITION    ----------
4220REM ----------        HAS NOT OTHERWISE BEEN REACHED         ----------
4230REM ------------------------------------------------------------------------
4240b$=""
4250IF NUM%<>0 THEN REL%=1
4260REPEAT
4270S%=FNminicam("ST1",38,INT(g1/3),30)
4280PROCdelay(50)
4290A%=FNminicam("DA1",42,REL%,0)
4300PROCdelay(100)
4310LDJvolts=FNreadflu("R0N16P1")
4320IF LDJvolts<0 AND Message$="LPCD" THEN Message$="LNCI"
4330IF LDJvolts>=0 AND Message$="LNCD" THEN Message$="LPCI"
4340IF (ABS(LDJvolts)>=1.9 OR ABS(LDJvolts)<=0.18) AND NUM%=0 THEN
                                                        PROCchangrange
4350PROCtakeMBvals
4360A%=FNminicam("DA1",42,REL%-1,0)
4370PROCdelay(100)
4380SHUNTvolts=FNreadflu("F1R0S0N16P1T0")
4390UNTIL ABS(SHUNTvolts)<0.035E-3
4400ENDPROC
4410:
4420DEFPROCtakeMBvals
4430REM ------------------------------------------------------------------------
4440REM ----------------------    TAKE THE M & B VALUES    ----------------------
4450REM ------------------------------------------------------------------------
4460VDU23,1,0;0;0;0;
4470check%=0
4480PROCscrnmssge("RMBV")
4490IF NUM%<>0 THEN REL%=1
4500A%=FNminicam("DA1",42,REL%,0):REM READ LDJ
4510PROCdelay(50)
4520LDJvolts=FNreadflu("R2N16P1")
4530IF NOOFPTS%=0 THEN PROCdelay(2000*Tconst)
4540IF NOOFPTS%=0 THEN 4570
4550IF ABS(F)<1000 THEN PROCdelay(2000*Tconst)
4560IF ABS(F)>=1000 THEN PROCdelay(1500*Tconst)
4570PROCscrnmssge("RMBV")
4580SENS=FNreadlkin("S")
4590Z4=FNcalcsens(SENS)
4600PRINTTAB(7,11);"Bo(gauss)";SPC(10);"CH1(V)":PRINTTAB(6,12);"----------"
                    ;SPC(8);"--------"
4610VDU28,0,23,39,13
4620FOR II%=1 TO 10
4630LDJvolts=FNreadflu("N16P1")
4640h9(II%)=LDJvolts*g0
4650PROCdelay(110*Tconst)
4660Q1=FNreadlkin("Q1")
4670Q1(II%)=Q1/2000*Z4
46800%=10
4690PRINTTAB(11-INT(0.5*LEN(STR$(h9(II%)))));h9(II%);
47000%=&10410
4710PRINTTAB(25);Q1(II%)
```

```
4720NEXT
47300%=10
4740h9=0:Q1=0
4750FOR II%=1 TO 10
4760h9=h9(II%)+h9:Q1=Q1(II%)+Q1
4770NEXT
4780action$="norepeat"
4790check%=check%+1
4800ON ERROR GOTO 4570
4810FOR II%=1 TO 10:REM THIS LOOP TESTS FOR 'BUM' PTS
4820IF ABS((h9-10*h9(II%))/h9)>0.5 THEN action$="repeat"
4830IF ABS((Q1-10*Q1(II%))/Q1)>0.5 THEN action$="repeat"
4840NEXT
4850ON ERROR OFF
4860IF check%>=4 THEN 4880
4870IF action$="repeat" THEN 4570
4880Z5=Z4
4890SENS=FNreadlkin("S")
4900Z4=FNcalcsens(SENS)
4910IF Z4<>Z5 THEN 4570
4920PROCmeanstderr
4930NOOFPTS%=NOOFPTS%+1
4940CH1(NOOFPTS%)=Q1:B(NOOFPTS%)=h9:ECH1(NOOFPTS%)=EQ1:EB(NOOFPTS%)=Eh9
4950ENDPROC
4960:
4970:
4980:
4990DEFFNcalcsens(x2)
5000ZZ=x2-(INT(x2/3)*3)+1
5010IF ZZ=1 THEN ZZ=5
5020IF ZZ=3 THEN ZZ=1
5030=(10↑(-(INT(x2/3))))*ZZ
5040:
5050:
5060DEFPROCmeanstderr
5070Q1=Q1/10:h9=h9/10
5080EQ1=0:Eh9=0
5090FOR II%=1 TO 10
5100EQ1=(Q1-Q1(II%))↑2+EQ1:Eh9=(h9-h9(II%))↑2+Eh9
5110NEXT
5120EQ1=(SQR(EQ1/9))/3.Eh9=(SQR(Eh9/9))/3
5130ENDPROC
5140:
5150DEFPROCtempsaveMB
5160REM ------------------------------------------------------------------------
5170REM ----------------  SAVE VALUES IN TEMPORARY FILE  ----------------
5180REM ------------------------------------------------------------------------
5190X=OPENOUT":2.T.TEMPMB"
5200FOR J%=1 TO NOOFPTS%
5210PRINT#X,CH1(J%),B(J%),ECH1(J%),EB(J%)
5220NEXT
5230CLOSE#X
5240ENDPROC
5250:
5260DEFPROCdisksaveMB
5270REM ------------------------------------------------------------------------
5280REM ----------------  SAVE VALUES ON DISK FILE  ----------------
5290REM ------------------------------------------------------------------------
5300MODE0
5310VDU23,1,1;0;0;0;
```

```
5320PRINTTAB(27,3);"SAVE VALUES ON DISK FILE":PRINTTAB(26,4);
                   "-------------------------"
5330PRINTTAB(11,6);"The data will now be saved on a disk. Ensure that there
                    is a"
5340PRINTTAB(11,8);"suitably formatted disk in the second drive."
5350PRINTTAB(11,10);"The data will be saved in SI units."
5360PRINTTAB(11,14);"Enter the drive number:";:INPUT DR$
5370PRINTTAB(11,17);"Enter name of file to be created:";:INPUT FILE$
5380REPEAT
5390PRINTTAB(11,20);"Do you wish to store the standard errors (y/n)?";
5400A$=GET$
5410UNTIL A$="Y" OR A$="y" OR A$="N" OR A$="n"
5420IF A$="Y" OR A$="y" THEN STDERR$="YES" ELSE STDERR$="NO"
5430X=OPENIN":2.T.TEMPMB"
5440FOR J%=1 TO NOOFPTS%
5450INPUT#X,CH1(J%),B(J%),ECH1(J%),EB(J%)
5460NEXT
5470CLOSE#X
5480*DELETE":2.T.TEMPMB"
5490OSCLI("DRIVE "+DR$)
5500Y=OPENOUT FILE$
5510PRINT#Y,DA$,SA$,TEMP$,NOOFPTS%,STDERR$
5520IF STDERR$="YES" THEN PROCstderryes ELSE PROCstderrno
5530CLOSE#Y
5540ENDPROC
5550:
5560DEFPROCstderryes
5570FOR J%=1 TO NOOFPTS%
5580PRINT#Y,CH1(J%),1E-4*B(J%),ECH1(J%),1E-4*EB(J%)
5590NEXT
5600ENDPROC
5610:
5620DEFPROCstderrno
5630FOR J%=1 TO NOOFPTS%
5640PRINT#Y,CH1(J%),1E-4*B(J%)
5650NEXT
5660:
5670:
5680DEFFNreadlkin(command$)
5690REM ------------------------------------------------------------------------
5700REM ------------------------  READ LOCK-IN  ------------------------
5710REM ------------------------------------------------------------------------
5720*FX2,2
5730*FX3,7
5740PRINT"Z"
5750*FX3,6
5760*FX2,1
5770INPUTA$
5780IF VAL(A$) <>32 THEN 5720
5790*FX2,2
5800*FX3,7
5810PRINTcommand$
5820*FX3,6
5830*FX2,1
5840INPUToutput$
5850*FX2,2
5860*FX3,0
5870=VAL(output$)
5880:
5890DEFPROCinit
```

```
5900REM ------------------------------------------------------------------------
5910REM ----------- SET UP BBC RS423 PORT, INITIALISE LOCK-IN ----------
5920REM ------------------------------------------------------------------------
5930*FX156,8,227
5940*FX8,6
5950*FX7,6
5960*FX6,10
5970*FX2,2
5980*FX3,7
5990PRINT"U 0"
6000PROCdelay(50)
6010PRINT"Y 0"
6020*FX3,6
6030*FX2,2
6040*FX3,0
6050PROCdelay(50)
6060ENDPROC
```

```
 10REM PROGRAM "P.CCIVITY"
 20REM ------------------------------------------------------------------------
 30REM ----------------------  VSM COERCIVITY PROGRAM  ----------------------
 40REM ------------------------------------------------------------------------
 50DIM CH1(100):DIM B(100):DIM ECH1(100):DIM EB(100)
 60DIM h9(10):DIM Q1(10)
 70MODE0
 80VDU23,1,0;0;0;0;
 90TIME=0
100PROCinit
110PROCreadTC
120PROCintro
130PROCenterdets
140FOR K%=1 TO 2
150IF K%=1 THEN FILE$=NEGFIL$
160IF K%=2 THEN FILE$=POSFIL$
170NOOFPTS%=0
180PROCramp
190PROCcurrev
200PROCadjust
210PROClastcheck
220PROCcontrol
230PROCtempsaveMB
240PROCdisksaveMB(DR$,FILE$)
250PROCalarm
260NEXT
270FOR K%=1 TO 2
280IF K%=1 THEN FILE$=NEGFIL$
290IF K%=2 THEN FILE$=POSFIL$
300PROCinputdata
310PROCformsums
320PROCnormaleqns
330PROCstderr
340PROCprintcoer
350NEXT
360PROCaverage
370END
380:
390DEFFNminicam(usr$,AD%,NN%,TT%)
400REM ------------------------------------------------------------------------
410REM ----------------------------  MINICAM  ----------------------------
420REM ------------------------------------------------------------------------
430REM ICC1 OF MINICAM HAS ADDRESS 6
440*IEEE
450*OPT 9,1
460*OPT 10,13
470STRING$=usr$+","+STR$(AD%)+","+STR$(NN%)+","+STR$(TT%)
480PRINT#6,STRING$+CHR$(13)
490INPUT#6,REPLY$
500*DISK
510=VAL(REPLY$)
520:
530DEFPROCspacebar
540REM ------------------------------------------------------------------------
550REM ----------------------------  "SPACE-BAR"  ----------------------------
560REM ------------------------------------------------------------------------
570PRINTTAB(26,30);"(PRESS SPACE-BAR TO CONTINUE)"
580REPEAT:UNTIL INKEY(-99)
590*FX15,0
600CLS
```

```
 610ENDPROC
 620:
 630DEFPROCdelay(t)
 640REM ---------------------------------------------------------------
 650REM ------------------------  TIME DELAY  -------------------------
 660REM ---------------------------------------------------------------
 670b=TIME:REPEAT:UNTIL TIME>=b+t
 680REM t IS IN 1/100s OF A SECOND
 690ENDPROC
 700:
 710DEFFNreadflu(command$)
 720REM ---------------------------------------------------------------
 730REM ------------------------  READ FLUKE  -------------------------
 740REM ---------------------------------------------------------------
 750*IEEE
 760*OPT2,0
 770PRINT#16,command$
 780REPEAT:UNTIL PTR#1=TRUE
 790INPUT#16,reading$
 800PRINT#16,"N0P1"
 810*DISK
 820=VAL(reading$)
 830:
 840DEFPROCscrnmssge(Mess$)
 850REM ---------------------------------------------------------------
 860REM ------------------------  SCREEN MESSAGES  ----------------------
 870REM ---------------------------------------------------------------
 880MODE7
 890VDU23,1,0;0;0;0;
 900W$=" "
 910IF Mess$="RMBV" THEN X%=6 ELSE X%=5
 920IF Mess$="RMBV" THEN W$="RECORDING M AND Bo VALUES"
 930IF Mess$="RCD" THEN W$="REVERSING CURRENT DIRECTION"
 940@%=10
 950IF Mess$="RMBV" THEN PRINTTAB(2,2);"Points so far: ";NOOFPTS%
 960FOR P=5 TO 7
 970PRINTTAB(X%-1,P);"-";SPC(2+LEN(W$));"-"
 980NEXT
 990FOR JJ=X%-1 TO X%+2+LEN(W$)
1000PRINTTAB(JJ,4);"-":PRINTTAB(JJ,8);"-"
1010NEXT
1020PRINTTAB(X%,6);CHR$(134);W$
1030PRINTTAB(X%+LEN(W$)+1,6);CHR$(135)
1040ENDPROC
1050:
1060DEFPROCcurrev
1070REM ---------------------------------------------------------------
1080REM ------------------------  CURRENT REVERSAL  ---------------------
1090REM ---------------------------------------------------------------
1100MODE7
1110VDU23,1,0;0;0;0;
1120PROCscrnmssge("RCD")
1130C%=FNminicam("AD1",9,0,0)
1140IF ABS(C%)<=3 THEN lo$="Negative" ELSE lo$="Positive"
1150PRINTTAB(1,11);"Logic & current in";CHR$(134);lo$;CHR$(135);"direction"
1160PROCchangelogi
1170D%=FNminicam("AD1",9,0,0):REM CHECKING LOGIC REVERSAL
1180IF ABS(D%-C%)<=2 THEN 1160
1190C%=D%
1200A%=FNminicam("DA1",42,4,0):REM ACTIVATE MAIN POWER RELAY (5V ON)
```

```
1210PROCdelay(50)
1220A%=FNminicam("DA1",42,0,0):REM 5V OFF
1230D%=FNminicam("AD1",9,0,0)
1240IF ABS(D%-C%)<10 THEN 1280:REM CHECKING LOGIC IS UNALTERED
1250PROCchangelogi:REM RESET LOGIC IF NECESSARY
1260D%=FNminicam("AD1",9,0,0)
1270IF ABS(D%-C%)>10 THEN 1250
1280IF ABS(C%)>1000 THEN lo$="Negative" ELSE lo$="Positive"
1290PRINTTAB(0,11);SPC(3);"Now changed to";CHR$(134);lo$;CHR$(135);"direction"
                                                                    ;SPC(2)
1300PROCdelay(300)
1310ENDPROC
1320:
1330:
1340DEFPROCchangelogi
1350PROCdelay(150)
1360A%=FNminicam("DA1",42,0,0)
1370PROCdelay(100)
1380A%=FNminicam("DA1",42,2,0)
1390PROCdelay(50)
1400A%=FNminicam("DA1",42,0,0)
1410PROCdelay(100)
1420ENDPROC
1430:
1440DEFPROCalarm
1450REM ------------------------------------------------------------------------
1460REM ----------------------------  SOUND ALARM  ----------------------------
1470REM ------------------------------------------------------------------------
1480ENVELOPE 2,1,2,-2,2,10,20,10,1,0,0,-1,100,100
1490SOUND 1,2,100,100
1500ENDPROC
1510:
1520DEFPROCreadTC
1530REM ------------------------------------------------------------------------
1540REM ----------------------------  READ TIME CONST  ------------------------
1550REM ------------------------------------------------------------------------
1560TC=FNreadlkin("T"):REM READ TIME CONST
1570Tconst=FNcalcTC(TC):REM CALC TC
1580ENDPROC
1590:
1600:
1610DEFFNcalcTC(TT)
1620B=10↑(2-INT(TT/2))
1630IF TT<>(INT(TT/2)*2) THEN B=B*0.3
1640=B
1650:
1660:
1670:
1680DEFPROCtakeMBvals
1690REM ------------------------------------------------------------------------
1700REM ----------------------  TAKE THE M & B VALUES  ------------------------
1710REM ------------------------------------------------------------------------
1720VDU23,1,0;0;0;0;
1730check%=0
1740PROCscrnmssge("RMBV")
1750A%=FNminicam("DA1",42,1,0):REM READ LDJ
1760PROCdelay(50)
1770LDJvolts=FNreadflu("R0N16P1")
1780PROCdelay(2000*Tconst)
1790PROCscrnmssge("RMBV")
```

```
1800SENS=FNreadlkin("S")
1810Z4=FNcalcsens(SENS)
1820PRINTTAB(7,11);"Bo(gauss)";SPC(10);"CH1(V)":PRINTTAB(6,12);"————————"
                    ;SPC(8);"————————"
1830VDU28,0,23,39,13
1840FOR II%=1 TO 10
1850LDJvolts=FNreadflu("N16P1")
1860h9(II%)=LDJvolts*g0
1870PROCdelay(110*Tconst)
1880Q1=FNreadlkin("Q1")
1890Q1(II%)=Q1/2000*Z4
19000%=10
1910PRINTTAB(11-INT(0.5*LEN(STR$(h9(II%)))));h9(II%);
19200%=&10410
1930PRINTTAB(25);Q1(II%)
1940NEXT
19500%=10
1960h9=0:Q1=0
1970FOR II%=1 TO 10
1980h9=h9(II%)+h9:Q1=Q1(II%)+Q1
1990NEXT
2000action$="norepeat"
2010check%=check%+1
2020ON ERROR GOTO 1790
2030FOR II%=1 TO 10:REM THIS LOOP TESTS FOR 'BUM' PTS
2040IF ABS((h9-10*h9(II%))/h9)>0.5 THEN action$="repeat"
2050IF ABS((Q1-10*Q1(II%))/Q1)>0.5 THEN action$="repeat"
2060NEXT
2070ON ERROR OFF
2080IF check%>=4 THEN 2100
2090IF action$="repeat" THEN 1790
2100Z5=Z4
2110SENS=FNreadlkin("S")
2120Z4=FNcalcsens(SENS)
2130IF Z4<>Z5 THEN 1790
2140PROCmeanstderr
2150NOOFPTS%=NOOFPTS%+1
2160CH1(NOOFPTS%)=Q1:B(NOOFPTS%)=h9:ECH1(NOOFPTS%)=EQ1:EB(NOOFPTS%)=Eh9
2170ENDPROC
2180:
2190:
2200:
2210DEFFNcalcsens(x2)
2220ZZ=x2-(INT(x2/3)*3)+1
2230IF ZZ=1 THEN ZZ=5
2240IF ZZ=3 THEN ZZ=1
2250=(10↑(-(INT(x2/3))))*ZZ
2260:
2270:
2280DEFPROCmeanstderr
2290Q1=Q1/10:h9=h9/10
2300EQ1=0:Eh9=0
2310FOR II%=1 TO 10
2320EQ1=(Q1-Q1(II%))↑2+EQ1:Eh9=(h9-h9(II%))↑2+Eh9
2330NEXT
2340EQ1=(SQR(EQ1/9))/3:Eh9=(SQR(Eh9/9))/3
2350ENDPROC
2360:
2370DEFPROCtempsaveMB
2380REM ————————————————————————————————————————————————————————
```

```
2390REM ---------------  SAVE VALUES IN TEMPORARY FILE  ---------------
2400REM ------------------------------------------------------------
2410X=OPENOUT":2.T.TSAVE"
2420FOR J%=1 TO NOOFPTS%
2430PRINT#X,CH1(J%),B(J%),ECH1(J%),EB(J%)
2440NEXT
2450CLOSE#X
2460ENDPROC
2470:
2480DEFPROCdisksaveMB(DR$,FILE$)
2490REM ------------------------------------------------------------
2500REM ---------------  SAVE VALUES ON DISK FILE  ---------------
2510REM ------------------------------------------------------------
2520MODE0
2530VDU23,1,0;0;0;0;
2540PRINTTAB(25,3);"SAVING VALUES ON DISK FILE":PRINTTAB(25,4);
                  "-------------------------"
2550PRINTTAB(11,6);"The data is now being saved on a disk."
2560PRINTTAB(11,10);"The data is saved in SI units."
2570X=OPENIN":2.T.TSAVE"
2580FOR J%=1 TO NOOFPTS%
2590INPUT#X,CH1(J%),B(J%),ECH1(J%),EB(J%)
2600NEXT
2610CLOSE#X
2620OSCLI("DRIVE "+DR$)
2630Y=OPENOUT FILE$
2640PRINT#Y,NOOFPTS%,STDERR$
2650IF STDERR$="YES" THEN PROCstderryes ELSE PROCstderrno
2660CLOSE#Y
2670CLS
2680ENDPROC
2690:
2700DEFPROCstderryes
2710FOR J%=1 TO NOOFPTS%
2720PRINT#Y,CH1(J%),1E-4*B(J%),ECH1(J%),1E-4*EB(J%)
2730NEXT
2740ENDPROC
2750:
2760DEFPROCstderrno
2770FOR J%=1 TO NOOFPTS%
2780PRINT#Y,CH1(J%),1E-4*B(J%)
2790NEXT
2800:
2810:
2820DEFFNreadlkin(command$)
2830REM ------------------------------------------------------------
2840REM ---------------  READ LOCK-IN  ---------------
2850REM ------------------------------------------------------------
2860*FX2,2
2870*FX3,7
2880PRINT"Z"
2890*FX3,6
2900*FX2,1
2910INPUTA$
2920IF VAL(A$) <>32 THEN 2860
2930*FX2,2
2940*FX3,7
2950PRINTcommand$
2960*FX3,6
2970*FX2,1
```

```
2980INPUToutput$
2990*FX2,2
3000*FX3,0
3010=VAL(output$)
3020:
3030DEFPROCinit
3040REM ------------------------------------------------------------------------
3050REM ----------   SET UP BBC RS423 PORT, INITIALISE LOCK-IN   ----------
3060REM ------------------------------------------------------------------------
3070*FX156,8,227
3080*FX8,6
3090*FX7,6
3100*FX6,10
3110*FX2,2
3120*FX3,7
3130PRINT"U 0"
3140PROCdelay(50)
3150PRINT"Y 0"
3160*FX3,6
3170*FX2,2
3180*FX3,0
3190PROCdelay(50)
3200ENDPROC
3210:
3220DEFPROCintro
3230REM ------------------------------------------------------------------------
3240REM ------------------------   WRITTEN INTRODUCTION   ----------------------
3250REM ------------------------------------------------------------------------
3260PRINTTAB(30,0);"WRITTEN INTRODUCTION":PRINTTAB(29,1);"----------------
                   -------"
3270PRINTTAB(9,3);"This program will conduct a detailed study of the
                   coercivity region"
3280PRINTTAB(9,4);"once the operator has ramped the field up & down two
                   and a half"
3290PRINTTAB(9,5);"times for both calibration and test samples. The program
                   will then"
3300PRINTTAB(9,6);"take over and complete the experiment. The operator
                   should note"
3310PRINTTAB(9,7);"both the calibration & max. magnetisation voltage
                   readings. Before"
3320PRINTTAB(9,8);"the operator hands over the control to the micro
                   both the"
3330PRINTTAB(9,9);"gaussmeter & lock-in ranges for the detailed study
                   must be"
3340PRINTTAB(9,10);"established."

3350PRINTTAB(9,20);"Make sure that the logic is POSITIVE before continuing
                    and do not"
3360PRINTTAB(9,21);"allow the lock-in to autorange."
3370PROCspacebar
3380ENDPROC
3390:
3400DEFPROCenterdets
3410REM ------------------------------------------------------------------------
3420REM ------------------------   ENTER DETAILS   ------------------------------
3430REM ------------------------------------------------------------------------
3440VDU23,1,1;0;0;0;
3450PRINTTAB(9,10);"Please enter:"
3460INPUTTAB(9,14);"Range of gaussmeter ";g0
3470INPUTTAB(9,16);"Max. range of field about zero gauss(in gauss) (<170G) "
```

```
                    ;hr
3480INPUTTAB(9,18);"Field intervals between points(in gauss) ";hs
3490INPUTTAB(9,20);"Drive No. for data ";DR$
3500INPUTTAB(9,22);"Filename for negative coercivity data ";NEGFIL$
3510INPUTTAB(9,24);"Filename for positive coercivity data ";POSFIL$
3520REPEAT
3530PRINTTAB(9,26);"Do you wish to store the standard errors (y/n)?";
3540A$=GET$
3550UNTIL A$="Y" OR A$="y" OR A$="N" OR A$="n"
3560IF A$="Y" OR A$="y" THEN STDERR$="YES" ELSE STDERR$="NO"
3570ns%=INT(hs)
3580IF ns%=0 THEN ns%=1
3590VDU23,1,0;0;0;0;
3600CLS
3610ENDPROC
3620:
3630DEFPROCramp
3640REM ------------------------------------------------------------------------
3650REM ------------------------  RAMP THE FIELD  ------------------------------
3660REM ------------------------------------------------------------------------
3670C%=FNminicam("AD1",9,0,0)
3680IF ABS(C%)<=3 THEN lo$="Negative" ELSE lo$="Positive"
3690IF lo$="Positive" THEN satsign$="+1.2T"
3700IF lo$="Negative" THEN satsign$="-1.2T"
3710IF lo$="Positive" THEN remsign$="(~170 to 180G)."
3720IF lo$="Negative" THEN remsign$="(~-170 to -180G)."
3730A%=FNminicam("DA1",42,0,0)
3740PROCdelay(50)
3750SHUNTvolts=FNreadflu("R0N16P1")
3760PRINTTAB(9,6);"Switch the LDJ gaussmeter to the 10KG range and then ramp
                    the field"
3770PRINTTAB(9,7);"up to ";satsign$;" to saturate the sample."
3780PRINTTAB(9,8);"Next bring the field down again to the pole tip remanence
                    field"
3790PRINTTAB(9,9);remsign$
3800PRINTTAB(9,11);"At this stage make sure that the Fluke is displaying
                     less than"
3810PRINTTAB(9,12);"0.05mV."
3820PRINTTAB(9,13);"Finally switch the gaussmeter back to the required range."
3830PROCspacebar
3840ENDPROC
3850:
3860DEFPROCadjust
3870REM ------------------------------------------------------------------------
3880REM ----------------  ADJUST STARTING FIELD VALUE  -------------------------
3890REM ------------------------------------------------------------------------
3900A%=FNminicam("DA1",42,1,0)
3910PROCdelay(100)
3920LDJvolts=FNreadflu("F1R0S0N16P1T0")
3930IF ABS(LDJvolts*g0)<0.9*hr THEN ENDPROC
3940REPEAT
3950S%=FNminicam("ST1",39,3,20):REM INCREASE CNT,REDUCE FIELD
3960PROCdelay(80)
3970LDJvolts=FNreadflu("N16P1")
3980UNTIL ABS(LDJvolts*g0)<0.9*hr
3990ENDPROC
4000:
4010DEFPROClastcheck
4020REM ------------------------------------------------------------------------
4030REM ----------  LAST CHECK BEFORE HANDING OVER TO COMPUTER  -----------------
```

```
4040REM ------------------------------------------------------------------------
4050MODE0
4060VDU23,1,0;0;0;0;
4070PRINTTAB(9,6);"Make sure the gaussmeter is on the correct range, the
                   lock-in is not"
4080PRINTTAB(9,8);"autoranging and the Hall probe is properly positioned."
4090PRINTTAB(9,12);"Henceforth the computer is in control."
4100PROCspacebar
4110ENDPROC
4120:
4130DEFPROCcontrol
4140REM ------------------------------------------------------------------------
4150REM ----------------------  CONTROL TAKING POINTS  ----------------------
4160REM ------------------------------------------------------------------------
4170PROCtakeMBvals
4180REPEAT
4190S%=FNminicom("ST1",39,ns%,20)
4200PROCtakeMBvals
4210UNTIL ABS(h9)>hr
4220ENDPROC
4230:
4240DEFPROCinputdata
4250REM ------------------------------------------------------------------------
4260REM ----------------------------  INPUT DATA  ----------------------------
4270REM ------------------------------------------------------------------------
4280OSCLI("DRIVE "+DR$)
4290X=OPENIN FILE$
4300INPUT#X,NOOFPTS%,STDERR$
4310IF STDERR$="YES" THEN PROCinputerrY ELSE PROCinputerrN
4320CLOSE#X
4330*DRIVE 0
4340ENDPROC
4350:
4360DEFPROCinputerrY
4370FOR F%=1 TO NOOFPTS%
4380INPUT#X,CH1(F%),B(F%),ECH1(F%),EB(F%)
4390NEXT
4400ENDPROC
4410:
4420DEFPROCinputerrN
4430FOR F%=1 TO NOOFPTS%
4440INPUT#X,CH1(F%),B(F%)
4450NEXT
4460ENDPROC
4470:
4480DEFPROCformsums
4490SUMX=0:SUMY=0:SUMXY=0:SUMXX=0
4500FOR F%=1 TO NOOFPTS%
4510SUMY=CH1(F%)+SUMY
4520SUMX=B(F%)+SUMX
4530SUMXY=B(F%)*CH1(F%)+SUMXY
4540SUMXX=(B(F%)↑2)+SUMXX
4550NEXT
4560ENDPROC
4570:
4580DEFPROCnormaleqns
4590DENOM=(NOOFPTS%*SUMXX)-SUMX↑2
4600a=((NOOFPTS%*SUMXY)-(SUMX*SUMY))/DENOM
4610b=((SUMY*SUMXX)-(SUMX*SUMXY))/DENOM
4620coer=-1*b/a
```

```
4630IF K%=1 THEN negc=coer
4640ENDPROC
4650:
4660DEFPROCstderr
4670SUMRESSQU=0
4680FOR F%=1 TO NOOFPTS%
4690SUMRESSQU=SUMRESSQU+(CH1(F%)-a*B(F%)-b)↑2
4700NEXT
4710aSTDERR=SQR(NOOFPTS%*SUMRESSQU/((NOOFPTS%-2)*DENOM))
4720bSTDERR=aSTDERR*SQR(SUMXX/NOOFPTS%)
4730cSTDERR=(SQR((b*aSTDERR/a)↑2+bSTDERR↑2))/a
4740IF K%=1 THEN negcSTDERR=cSTDERR
4750ENDPROC
4760:
4770DEFPROCprintcoer
4780IF K%=1 THEN sign$="Negative "
4790IF K%=2 THEN sign$="Positive "
4800PRINTTAB(35,1);"RESULTS":PRINTTAB(34,2);"---------"
4810PRINTTAB(9,4+(K%-1)*12);"In the relationship 'CH1=a*Bo+b',a & b are given
                            by:"
4820PRINTTAB(20,6+(K%-1)*12);"a= ";a" (+/-) ";aSTDERR" V/T"
4830PRINTTAB(20,8+(K%-1)*12);"b= ";b" (+/-) ";bSTDERR" V"
4840PRINTTAB(9,10+(K%-1)*12);sign$;"coercivity(-b/a)= ";coer" (+/-) ";cSTDERR
                            " tesla"
4850ENDPROC
4860:
4870DEFPROCaverage
4880avcoer=0.5*(ABS(negc)+ABS(coer))
4890avcSTDERR=0.5*(negcSTDERR+cSTDERR)
4900PRINTTAB(11,28);"AVERAGE COERCIVITY= ";avcoer" (+/-) ";avcSTDERR" tesla"
4910ENDPROC
```

Appendix P2

Listings of the VSM Data Analysis Programs

The suite of VSM Data Analysis Programs is written in BBC BASIC and runs on an Acorn Model B BBC Microcomputer. There are eight analysis programs which, for convenience, are accessible through one menu program, P.MENU. The names and some details of all of the programs are given below.

P.MENU : This displays on the microcomputer monitor a menu of the available analysis programs. It CHAINs the option chosen.

P.SCNPLT1 : This plots on the microcomputer monitor a graph of the 'raw' VSM data, that is, values of signal voltage against applied field. It then offers the user the option of screen-dumping the graph onto either a dedicated printer or the local area network (Clearway) printer, in either case by CHAINing the screen-dump program, P.EPATALL.

P.SCNPLT2 : This is exactly the same as the previous program, P.SCNPLT1, except that it plots the corrected data, that is, values of the specific magnetization, σ, against *internal* field. The screen-dumping options are exactly the same as for the previous case.

P.LNPNT1 : This lists the 'raw' VSM data on the microcomputer minitor and then offers the option of having the same data sent to one of the two printers.

P.LNPNT2 : This is exactly the same as the previous program, except that it offers the facilities for the corrected VSM data.

P.PIXY : This program plots a hard copy of the corrected VSM data on the high quality PIXY3 plotter.

P.RES : This program subtracts a least squares linear fit to the residual/sample holder data from the 'raw' data set prior to converting this data into magnetization data. The calibration for the conversion is derived from the signal obtained from a saturated high-purity polycrystalline Ni sphere at known temperature. The program also provides a facility for subtracting the effect of the sample demagnetizing field.

P.MSAT : This program enables the saturation magnetization to be calculated from a $(1/B_0)$ extrapolation of the magnetization values in the saturation region. The number of points to include in the extrapolation is chosen interactively, based upon a graphical display of the relevant data.

P.INITSUS : This program fits a straight line to the initial magnetization curve to give the initial susceptibility. The number of points to include in the fit is chosen interactively, based upon a graphical display of the relevant data.

```
10REM PROGRAM "P.MENU"
20REM ------------------------------------------------------------------------
30REM ------------------------  MENU PROGRAM  ------------------------
40REM ------------------------------------------------------------------------
50MODE7
60PRINTTAB(6,0);CHR$(134);"VSM DATA FACILITIES MENU"
70PRINTTAB(5,1);CHR$(134);"-----------------------------"
80PRINTTAB(2,3);" (1) PLOT 'RAW' VSM DATA (VOLTS) ON"
90PRINTTAB(7,4);"SCREEN (+SCREEN DUMP)"
100PRINTTAB(2,5);" (2) PLOT CORRECTED VSM DATA (J/T/kg)"
110PRINTTAB(7,6);"ON SCREEN (+SCREEN DUMP)"
120PRINTTAB(2,7);" (3) LIST 'RAW' VSM DATA (VOLTS) ON"
130PRINTTAB(7,8);"SCREEN AND/OR EPSON"
140PRINTTAB(2,9);" (4) LIST CORRECTED VSM DATA (J/T/kg)"
150PRINTTAB(7,10);"ON SCREEN AND/OR EPSON"
160PRINTTAB(2,11);" (5) PLOT CORRECTED VSM DATA (J/T/kg)"
170PRINTTAB(7,12);"ON PIXY"
180PRINTTAB(2,13);" (6) RESIDUAL SUBTRACTION AND"
190PRINTTAB(7,14);"CONVERSION OF VOLTS TO J/T/kg"
200PRINTTAB(7,15);"(+DEMAG CORRECTIONS)"
210PRINTTAB(2,16);" (7) 1/Bo PLOT AND SATURATION"
220PRINTTAB(7,17);"MAGNETISATION EXTRAPOLATION"
230PRINTTAB(2,18);" (8) INITIAL SUSCEPTIBILITY"
240PRINTTAB(7,19);"CALCULATION"
250PRINTTAB(2,20);" (9) EXIT"
260REPEAT
270PRINTTAB(6,24);CHR$(134);CHR$(136);"Enter option (1-9):";CHR$(137);
280A%=GET
290UNTIL A%>48 AND A%<58
300CLS
310IF A%=49 THEN PROCrawsplot
320IF A%=50 THEN PROCcorsplot
330IF A%=51 THEN PROCrawlist
340IF A%=52 THEN PROCcorlist
350IF A%=53 THEN PROCchainpixy
360IF A%=54 THEN PROCchainres
370IF A%=55 THEN PROCchainsat
380IF A%=56 THEN PROCchainisus
390IF A%=57 THEN END
400END
410:
420DEFPROCrawsplot
430CHAIN":0B.P.SCNPLT1"
440ENDPROC
450:
460DEFPROCcorsplot
470CHAIN":0B.P.SCNPLT2"
480ENDPROC
490:
500DEFPROCrawlist
510CHAIN":0B.P.LNPNT1"
520ENDPROC
530:
540DEFPROCchainpixy
550CHAIN":0B.P.PIXY"
560ENDPROC
570:
580DEFPROCcorlist
590CHAIN":0B.P.LNPNT2"
600ENDPROC
```

```
610:
620DEFPROCchainres
630CHAIN":0B.P.RES"
640ENDPROC
650:
660DEFPROCchainsat
670CHAIN":0B.P.MSAT"
680ENDPROC
690:
700DEFPROCchainisus
710CHAIN":0B.P.INITSUS"
720ENDPROC
```

```
 5REM PROGRAM "P.SCNPLT1"
10REM ------------------------------------------------------------------------
20REM ----------------  PROGRAM TO PLOT VSM DATA ON SCREEN  ----------------
30REM ------------------------------------------------------------------------
40MODE0
50DIM Bo(350):DIM CH1(350)
60DIM EBo(350):DIM ECH1(350)
70VDU23,1,0;0;0;0;
80PROCtitle
90PROCdetails
100PROCtitle
110PROCfileinput
120PROCconvert:REM CONVERT V TO uV
130PROChighest
140PROClowest
150PROCtitle
160PROCintervalsX
170PROCtitle
180PROCintervalsY
190IF STDERR$="NO" THEN 220
200PROCtitle
210PROCerrbars
220PROCdrawaxes
230PROClabelaxes
240PROCplotintsY
250PROCplotintsX
260PROCplotdata
270IF REPLY$="Y" OR REPLY$="y" THEN PROCplotbars
280PROCwritecomms
290PROCoptions
300END
310:
320DEFPROCtitle
330PRINTTAB(22,3);"PROGRAM TO PLOT VSM DATA ON SCREEN"
340PRINTTAB(21,4);"----------------------------------------"
350ENDPROC
360:
370DEFPROCfileinput
380OSCLI("DRIVE "+DR$)
390X=OPENIN FILE$
400INPUT#X,DA$,SA$,TEMP$,NOOFPTS%,STDERR$
410IF STDERR$="YES" THEN PROCinputerrY ELSE PROCinputerrN
420CLOSE#X
430*DRIVE 0
440ENDPROC
450:
460DEFPROCinputerrY
470FOR F%=1 TO NOOFPTS%
480INPUT#X,CH1(F%),Bo(F%),ECH1(F%),EBo(F%)
490NEXT
500ENDPROC
510:
520DEFPROCinputerrN
530FOR F%=1 TO NOOFPTS%
540INPUT#X,CH1(F%),Bo(F%)
550NEXT
560ENDPROC
570:
580DEFPROClowest
590LOWCH1=CH1(1)
```

```
600LOWBo=Bo(1)
610FOR I%=1 TO NOOFPTS%
620IF CH1(I%)<LOWCH1 THEN LOWCH1=CH1(I%)
630IF Bo(I%)<LOWBo THEN LOWBo=Bo(I%)
640NEXT
650ENDPROC
660:
670DEFPROChighest
680HIGHCH1=CH1(1)
690HIGHBo=Bo(1)
700FOR I%=1 TO NOOFPTS%
710IF CH1(I%)>HIGHCH1 THEN HIGHCH1=CH1(I%)
720IF Bo(I%)>HIGHBo THEN HIGHBo=Bo(I%)
730NEXT
740ENDPROC
750:
760DEFPROCconvert
770IF STDERR$="YES" THEN PROCconvY ELSE PROCconvN
780ENDPROC
790:
800DEFPROCconvY
810FOR F%=1 TO NOOFPTS%
820CH1(F%)=1E6*CH1(F%):ECH1(F%)=1E6*ECH1(F%)
830NEXT
840ENDPROC
850:
860DEFPROCconvN
870CH1(F%)=1E6*CH1(F%)
880NEXT
890ENDPROC
900:
910DEFPROCdetails
920VDU23,1,1;0;0;0;
930PRINTTAB(9,7);"Please enter:"
940INPUTTAB(23,9);"Drive No. for data file ";DR$
950INPUTTAB(25,11);"Filename of data file ";FILE$
960PRINTTAB(9,14);"Options to plot are:":PRINTTAB(30,16);"(1) Smooth curve"
970PRINTTAB(30,17);"(2) Single points":PRINTTAB(30,18);"(3) Triangles"
980REPEAT
990PRINTTAB(30,20);"Enter option (1-3):";
1000A%=GET
1010UNTIL A%=49 OR A%=50 OR A%=51
1020IF A%=49 THEN K%=5
1030IF A%=50 THEN K%=69
1040IF A%=51 THEN K%=85
1050VDU23,1,0;0;0;0;
1060CLS
1070ENDPROC
1080:
1090DEFPROCdrawaxes
1100CLS
1110VDU24,0;100;1279;1023;
1120VDU28,0,31,79,29
1130YUNIT=0.95*922/ABS(HIGHCH1-LOWCH1)
1140XUNIT=0.95*1280/ABS(HIGHBo-LOWBo)
1150YORIG1=(922*0.975)-ABS(HIGHCH1*YUNIT)+101
1160XORIG1=(1280*0.975)-ABS(HIGHBo*XUNIT)
1170YORIG2=(0.025*922)+ABS(LOWCH1*YUNIT)+101
1180XORIG2=(1280*0.025)+ABS(LOWBo*XUNIT)
1190XORIG=(XORIG1+XORIG2)/2
```

```
1200YORIG=(YORIG1+YORIG2)/2
1210MOVE XORIG,YORIG-ABS(LOWCH1*YUNIT)
1220PLOT 5,XORIG,YORIG+ABS(HIGHCH1*YUNIT)
1230MOVE XORIG-ABS(LOWBo*XUNIT),YORIG
1240PLOT 5,XORIG+ABS(HIGHBo*XUNIT),YORIG
1250ENDPROC
1260:
1270DEFPROClabelaxes
1280VDU5
1290MOVE XORIG+10,YORIG+ABS(HIGHCH1*YUNIT)+22:PRINT"CH1(uV)"
1300MOVE XORIG+ABS(HIGHBo*XUNIT)-65,YORIG+35
1310IF GAPX<=5E-2 THEN PRINT"Bo(mT)" ELSE PRINT"Bo(T)"
1320VDU4
1330ENDPROC
1340:
1350DEFPROCintervalsX
1360PRINTTAB(9,7);"The values of Bo(tesla) range from "LOWBo" to "HIGHBo
1370PRINTTAB(9,10);"The options for Bo-axis intervals are:"
1380PRINTTAB(30,12);"(1) Every   1mT":PRINTTAB(30,13);"(2) Every   5mT"
1390PRINTTAB(30,14);"(3) Every  10mT":PRINTTAB(30,15);"(4) Every  50mT"
1400PRINTTAB(30,16);"(5) Every  0.1T":PRINTTAB(30,17);"(6) Every  0.5T"
1410PRINTTAB(30,18);"(7) Every    1T"
1420REPEAT
1430PRINTTAB(28,20);"Enter option (1-7):";
1440A%=GET
1450UNTIL A%>48 AND A%<56
1460IF A%=49 THEN GAPX=1E-3
1470IF A%=50 THEN GAPX=5E-3
1480IF A%=51 THEN GAPX=1E-2
1490IF A%=52 THEN GAPX=5E-2
1500IF A%=53 THEN GAPX=0.1
1510IF A%=54 THEN GAPX=0.5
1520IF A%=55 THEN GAPX=1
1530CLS
1540ENDPROC
1550:
1560DEFPROCintervalsY
1570PRINTTAB(9,7);"The values of CH1(uV) range from "LOWCH1" to "HIGHCH1
1580PRINTTAB(9,10);"The options for CH1-axis intervals are:"
1590PRINTTAB(30,12);"(1) Every  0.1uV":PRINTTAB(30,13);"(2) Every    1uV"
1600PRINTTAB(30,14);"(3) Every   10uV"
1610REPEAT
1620PRINTTAB(28,18);"Enter option (1-3):";
1630A%=GET
1640UNTIL A%=49 OR A%=50 OR A%=51
1650IF A%=49 THEN GAPY=0.1
1660IF A%=50 THEN GAPY=1
1670IF A%=51 THEN GAPY=10
1680CLS
1690ENDPROC
1700:
1710DEFPROCerrbars
1720VDU23,1,1;0;0;0;
1730REPEAT
1740PRINTTAB(16,11);"Do you want +/- standard errors plotted (y/n)?";
1750REPLY$=GET$
1760UNTIL REPLY$="Y" OR REPLY$="y" OR REPLY$="N" OR REPLY$="n"
1770VDU23,1,0;0;0;0;
1780CLS
1790ENDPROC
```

```
1800:
1810DEFPROCplotintsY
1820VDU5
1830YINT=YUNIT*GAPY
1840NNTOP%=ABS(HIGHCH1*YUNIT) DIV YINT
1850MOVE XORIG,YORIG
1860FOR I%=1 TO NNTOP%
1870IF I%=NNTOP% AND ABS(HIGHCH1)-NNTOP%*GAPY<0.3*GAPY THEN 1950
1880MOVE XORIG,YORIG+I%*YINT
1890PLOT 5,XORIG+5,YORIG+I%*YINT
1900IF GAPY=0.1 THEN @%=&00005
1910IF GAPY=1 THEN @%=&00003
1920IF GAPY=10 THEN @%=&00004
1930MOVE XORIG-100,YORIG+I%*YINT+15
1940PRINT GAPY*I%
1950NEXT
1960MOVE XORIG,YORIG+ABS(HIGHCH1*YUNIT)
1970PLOT 5,XORIG+5,YORIG+ABS(HIGHCH1*YUNIT)
1980IF HIGHCH1<100 THEN @%=&20104
1990IF HIGHCH1<10 THEN @%=&20104
2000IF HIGHCH1<1 THEN @%=&20206
2010IF HIGHCH1<0.1 THEN @%=&20205
2020MOVE XORIG-100,YORIG+ABS(HIGHCH1*YUNIT)+15
2030PRINT HIGHCH1
2040NNBOT%=ABS(LOWCH1*YUNIT) DIV YINT
2050MOVE XORIG,YORIG
2060FOR J%=1 TO NNBOT%
2070IF J%=NNBOT% AND ABS(LOWCH1)-NNBOT%*GAPY<0.3*GAPY THEN 2150
2080MOVE XORIG,YORIG-J%*YINT
2090PLOT 5,XORIG+5,YORIG-J%*YINT
2100IF GAPY=0.1 THEN @%=00005
2110IF GAPY=1 THEN @%=00003
2120IF GAPY=10 THEN @%=00004
2130MOVE XORIG-100,YORIG-J%*YINT+15
2140PRINT (-1)*GAPY*J%
2150NEXT
2160MOVE XORIG,YORIG-ABS(LOWCH1*YUNIT)
2170PLOT 5,XORIG+5,YORIG-ABS(LOWCH1*YUNIT)
2180@%=&20104
2190MOVE XORIG-85,YORIG-ABS(LOWCH1*YUNIT)+15
2200PRINT LOWCH1
2210VDU4
2220ENDPROC
2230:
2240DEFPROCplotintsX
2250VDU5
2260XINT=XUNIT*GAPX
2270NNL%=ABS(LOWBo*XUNIT) DIV XINT
2280MOVE XORIG,YORIG
2290FOR I%=1 TO NNL%
2300IF I%=NNL% AND ABS(LOWBo)-NNL%*GAPX<0.3*GAPX THEN 2420
2310MOVE XORIG-I%*XINT,YORIG
2320PLOT 5,XORIG-I%*XINT,YORIG-5
2330MOVE (XORIG-60)-I%*XINT,YORIG-15
2340IF GAPX=1E-3 THEN @%=&20004
2350IF GAPX=5E-3 THEN @%=&20106
2360IF GAPX=1E-2 THEN @%=&20107
2370IF GAPX=5E-2 THEN @%=&20107
2380IF GAPX=0.1 THEN @%=&20104
2390IF GAPX=0.5 THEN @%=&20104
```

```
2400IF GAPX=1 THEN @%=&20104
2410IF GAPX<=5E-2 THEN PRINT (-1)*GAPX*I%*1000 ELSE PRINT ((-1)*GAPX*I%)
2420NEXT
2430IF ABS(LOWBo)>10000 THEN @%=&20104
2440IF ABS(LOWBo)<10000 THEN @%=&20103
2450IF ABS(LOWBo)<1000 THEN @%=&20103
2460IF ABS(LOWBo)<500 THEN @%=&00005
2470IF ABS(LOWBo)<100 THEN @%=&00003
2480IF ABS(LOWBo)<10 THEN @%=&20103
2490MOVE XORIG-ABS(LOWBo*XUNIT),YORIG
2500PLOT 5,XORIG-ABS(LOWBo*XUNIT),YORIG-5
2510MOVE XORIG-ABS(LOWBo*XUNIT)-30,YORIG-15
2520IF GAPX<=5E-2 THEN PRINT LOWBo*1000 ELSE PRINT LOWBo
2530NNR%=ABS(HIGHBo*XUNIT) DIV XINT
2540MOVE XORIG,YORIG
2550FOR I%=1 TO NNR%
2560IF I%=NNR% AND ABS(HIGHBo)-NNR%*GAPX<0.3*GAPX THEN 2680
2570MOVE XORIG+I%*XINT,YORIG
2580PLOT 5,XORIG+I%*XINT,YORIG-5
2590MOVE (XORIG-60)+I%*XINT,YORIG-15
2600IF GAPX=1E-3 THEN @%=&20004
2610IF GAPX=5E-3 THEN @%=&20106
2620IF GAPX=1E-2 THEN @%=&20107
2630IF GAPX=5E-2 THEN @%=&20107
2640IF GAPX=0.1 THEN @%=&20104
2650IF GAPX=0.5 THEN @%=&20104
2660IF GAPX=1 THEN @%=&20104
2670IF GAPX<=5E-2 THEN PRINT GAPX*I%*1000 ELSE PRINT (GAPX*I%)
2680NEXT
2690IF ABS(HIGHBo)>10000 THEN @%=&20104
2700IF ABS(HIGHBo)<10000 THEN @%=&20103
2710IF ABS(HIGHBo)<1000 THEN @%=&20103
2720IF ABS(HIGHBo)<500 THEN @%=&00003
2730IF ABS(HIGHBo)<100 THEN @%=&00003
2740IF ABS(HIGHBo)<10 THEN @%=&20103
2750MOVE XORIG+ABS(HIGHBo*XUNIT),YORIG
2760PLOT 5,XORIG+ABS(HIGHBo*XUNIT),YORIG-5
2770MOVE XORIG+ABS(HIGHBo*XUNIT)-30,YORIG-15
2780IF GAPX<=5E-2 THEN PRINT HIGHBo*1000 ELSE PRINT HIGHBo
2790VDU4
2800ENDPROC
2810:
2820DEFPROCplotdata
2830MOVE XORIG+(Bo(1)*XUNIT),YORIG+(CH1(1)*YUNIT)
2840FOR F%=2 TO NOOFPTS%
2850PLOT K%,XORIG+(Bo(F%)*XUNIT),YORIG+(CH1(F%)*YUNIT)
2860NEXT
2870ENDPROC
2880:
2890DEFPROCplotbars
2900FOR F%=1 TO NOOFPTS%
2910MOVE XORIG+(Bo(F%)*XUNIT),YORIG+((CH1(F%)+ECH1(F%))*YUNIT)
2920PLOT 5,XORIG+(Bo(F%)*XUNIT),YORIG+((CH1(F%)-ECH1(F%))*YUNIT)
2930MOVE XORIG+((Bo(F%)+EBo(F%))*XUNIT),YORIG+(CH1(F%)*YUNIT)
2940PLOT 5,XORIG+((Bo(F%)-EBo(F%))*XUNIT),YORIG+(CH1(F%)*YUNIT)
2950NEXT
2960ENDPROC
2970:
2980DEFPROCwritecomms
2990@%=10
```

```
3000VDU5
3010MOVE XORIG-ABS(LOWBo*XUNIT),YORIG+ABS(HIGHCH1*YUNIT):PRINT"Filename :";FILE$
3020MOVE XORIG-ABS(LOWBo*XUNIT),YORIG+ABS(HIGHCH1*YUNIT)-35:PRINT"Date     :";DA$
3030MOVE XORIG-ABS(LOWBo*XUNIT),YORIG+ABS(HIGHCH1*YUNIT)-70:PRINT"Sample   :";SA$
3040MOVE XORIG-ABS(LOWBo*XUNIT),YORIG+ABS(HIGHCH1*YUNIT)-105:PRINT"Temp     :";TEMP$
3050MOVE XORIG-ABS(LOWBo*XUNIT),YORIG+ABS(HIGHCH1*YUNIT)-140:PRINT"No of pts:";NOOFPTS%
3060VDU4
3070ENDPROC
3080:
3090DEFPROCoptions
3100PRINT"Options are: (1) Screen dump on printer. (2)Exit to menu."
3110REPEAT
3120PRINT"Enter number:";
3130A%=GET
3140UNTIL A%=49 OR A%=50
3150PRINT
3160IF A%=49 THEN PROCchaindump
3170IF A%=50 THEN PROCchainmenu
3180ENDPROC
3190:
3200DEFPROCchaindump
3210PRINT"Options are: (1) Dedicated printer. (2) Clearway printer."
3220REPEAT
3230PRINT"Enter number:";
3240A%=GET
3250UNTIL A%=49 OR A%=50
3260PRINT
3270IF A%=49 THEN PROCdedicated
3280IF A%=50 THEN PROCclearway
3290PRINT"DUMPING"
3300CHAIN":0B.P.EPATALL"
3310ENDPROC
3320:
3330DEFPROCchainmenu
3340VDU26
3350CHAIN":0B.P.MENU"
3360ENDPROC
3370:
3380DEFPROCdedicated
3390*FX5,1
3400*FX6,0
3410*FX8,7
3420*FX7,7
3430ENDPROC
3440:
3450DEFPROCclearway
3460*FX5,2
3470*FX6,0
3480*FX8,7
3490*FX7,7
3500ENDPROC
```

```
 5REM PROGRAM "P.SCNPLT2"
10REM ------------------------------------------------------------
20REM ----------    PROGRAM TO PLOT VSM DATA ON SCREEN    ----------
30REM ------------------------------------------------------------
40MODE0
50DIM Bo(350):DIM SIG(350)
60DIM EBo(350):DIM ESIG(350)
70VDU23,1,0;0;0;0;
80PROCtitle
90PROCdetails
100PROCtitle
110PROCfileinput
120PROChighest
130PROClowest
140PROCtitle
150PROCintervalsX
160PROCtitle
170PROCintervalsY
180IF STDERR$="NO" THEN 210
190PROCtitle
200PROCerrbars
210PROCdrawaxes
220PROClabelaxes
230PROCplotintsY
240PROCplotintsX
250PROCplotdata
260IF REPLY$="Y" OR REPLY$="y" THEN PROCplotbars
270PROCwritecomms
280PROCoptions
290END
300:
310DEFPROCtitle
320PRINTTAB(22,3);"PROGRAM TO PLOT VSM DATA ON SCREEN"
330PRINTTAB(21,4);"----------------------------------------"
340ENDPROC
350:
360DEFPROCfileinput
370OSCLI("DRIVE "+DR$)
380X=OPENIN FILE$
390INPUT#X,DA$,SA$,TEMP$,NOOFPTS%,STDERR$
400IF STDERR$="YES" THEN PROCinputerrY ELSE PROCinputerrN
410CLOSE#X
420*DRIVE 0
430ENDPROC
440:
450DEFPROCinputerrY
460FOR F%=1 TO NOOFPTS%
470INPUT#X,SIG(F%),Bo(F%),ESIG(F%),EBo(F%)
480NEXT
490ENDPROC
500:
510DEFPROCinputerrN
520FOR F%=1 TO NOOFPTS%
530INPUT#X,SIG(F%),Bo(F%)
540NEXT
550ENDPROC
560:
570DEFPROClowest
580LOWSIG=SIG(1)
590LOWBo=Bo(1)
```

```
600FOR I%=1 TO NOOFPTS%
610IF SIG(I%)<LOWSIG THEN LOWSIG=SIG(I%)
620IF Bo(I%)<LOWBo THEN LOWBo=Bo(I%)
630NEXT
640ENDPROC
650:
660DEFPROChighest
670HIGHSIG=SIG(1)
680HIGHBo=Bo(1)
690FOR I%=1 TO NOOFPTS%
700IF SIG(I%)>HIGHSIG THEN HIGHSIG=SIG(I%)
710IF Bo(I%)>HIGHBo THEN HIGHBo=Bo(I%)
720NEXT
730ENDPROC
740:
750DEFPROCdetails
760VDU23,1,1;0;0;0;
770PRINTTAB(9,7);"Please enter:"
780INPUTTAB(23,9);"Drive No. for data file ";DR$
790INPUTTAB(25,11);"Filename of data file ";FILE$
800PRINTTAB(9,14);"Options to plot are:":PRINTTAB(30,16);"(1) Smooth curve"
810PRINTTAB(30,17);"(2) Single points":PRINTTAB(30,18);"(3) Triangles"
820REPEAT
830PRINTTAB(30,20);"Enter option (1-3):";
840A%=GET
850UNTIL A%=49 OR A%=50 OR A%=51
860IF A%=49 THEN K%=5
870IF A%=50 THEN K%=69
880IF A%=51 THEN K%=85
890VDU23,1,0;0;0;0;
900CLS
910ENDPROC
920:
930DEFPROCdrawaxes
940CLS
950VDU24,0;100;1279;1023;
960VDU28,0,31,79,29
970YUNIT=0.95*922/ABS(HIGHSIG-LOWSIG)
980XUNIT=0.95*1280/ABS(HIGHBo-LOWBo)
990YORIG1=(922*0.975)-ABS(HIGHSIG*YUNIT)+101
1000XORIG1=(1280*0.975)-ABS(HIGHBo*XUNIT)
1010YORIG2=(0.025*922)+ABS(LOWSIG*YUNIT)+101
1020XORIG2=(1280*0.025)+ABS(LOWBo*XUNIT)
1030XORIG=(XORIG1+XORIG2)/2
1040YORIG=(YORIG1+YORIG2)/2
1050MOVE XORIG,YORIG-ABS(LOWSIG*YUNIT)
1060PLOT 5,XORIG,YORIG+ABS(HIGHSIG*YUNIT)
1070MOVE XORIG-ABS(LOWBo*XUNIT),YORIG
1080PLOT 5,XORIG+ABS(HIGHBo*XUNIT),YORIG
1090ENDPROC
1100:
1110DEFPROClabelaxes
1120VDU5
1130MOVE XORIG+10,YORIG+ABS(HIGHSIG*YUNIT)+22:PRINT"sigma"
1140MOVE XORIG+10,YORIG+ABS(HIGHSIG*YUNIT)-15:PRINT"(J/T/kg)"
1150MOVE XORIG+ABS(HIGHBo*XUNIT)-65,YORIG+35
1160IF GAPX<=5E-2 THEN PRINT"Bo(mT)" ELSE PRINT"Bo(T)"
1170VDU4
1180ENDPROC
1190:
```

```
1200DEFPROCintervalsX
1210PRINTTAB(9,7);"The values of Bo(tesla) range from "LOWBo" to "HIGHBo
1220PRINTTAB(9,10);"The options for Bo-axis intervals are:"
1230PRINTTAB(30,12);"(1) Every   1mT":PRINTTAB(30,13);"(2) Every   5mT"
1240PRINTTAB(30,14);"(3) Every  10mT":PRINTTAB(30,15);"(4) Every  50mT"
1250PRINTTAB(30,16);"(5) Every  0.1T":PRINTTAB(30,17);"(6) Every  0.5T"
1260PRINTTAB(30,18);"(7) Every    1T"
1270REPEAT
1280PRINTTAB(28,20);"Enter option (1-7):";
1290A%=GET
1300UNTIL A%>48 AND A%<56
1310IF A%=49 THEN GAPX=1E-3
1320IF A%=50 THEN GAPX=5E-3
1330IF A%=51 THEN GAPX=1E-2
1340IF A%=52 THEN GAPX=5E-2
1350IF A%=53 THEN GAPX=0.1
1360IF A%=54 THEN GAPX=0.5
1370IF A%=55 THEN GAPX=1
1380CLS
1390ENDPROC
1400:
1410DEFPROCintervalsY
1420PRINTTAB(9,7);"The values of sigma(J/T/kg) range from "LOWSIG" to "HIGHSIG
1430PRINTTAB(9,10);"The options for sigma-axis intervals are:"
1440PRINTTAB(30,12);"(1) Every  1 J/T/kg":PRINTTAB(30,13);"(2) Every 10 J/T/kg"
1450REPEAT
1460PRINTTAB(28,15);"Enter option (1-2):";
1470A%=GET
1480UNTIL A%=49 OR A%=50
1490IF A%=49 THEN GAPY=1
1500IF A%=50 THEN GAPY=10
1510CLS
1520ENDPROC
1530:
1540DEFPROCerrbars
1550VDU23,1,1;0;0;0;
1560REPEAT
1570PRINTTAB(16,11);"Do you want +/- standard errors plotted (y/n)?";
1580REPLY$=GET$
1590UNTIL REPLY$="Y" OR REPLY$="y" OR REPLY$="N" OR REPLY$="n"
1600VDU23,1,0;0;0;0;
1610CLS
1620ENDPROC
1630:
1640DEFPROCplotintsY
1650VDU5
1660YINT=YUNIT*GAPY
1670NNTOP%=ABS(HIGHSIG*YUNIT) DIV YINT
1680MOVE XORIG,YORIG
1690FOR I%=1 TO NNTOP%
1700IF I%=NNTOP% AND ABS(HIGHSIG)-NNTOP%*GAPY<0.3*GAPY THEN 1770
1710MOVE XORIG,YORIG+I%*YINT
1720PLOT 5,XORIG+5,YORIG+I%*YINT
1730IF GAPY=1 THEN @%=&00003
1740IF GAPY=10 THEN @%=&00004
1750MOVE XORIG-100,YORIG+I%*YINT+15
1760PRINT GAPY*I%
1770NEXT
1780MOVE XORIG,YORIG+ABS(HIGHSIG*YUNIT)
1790PLOT 5,XORIG+5,YORIG+ABS(HIGHSIG*YUNIT)
```

```
1800IF HIGHSIG<100 THEN @%=&20104
1810IF HIGHSIG<10 THEN @%=&20104
1820MOVE XORIG-100,YORIG+ABS(HIGHSIG*YUNIT)+15
1830PRINT HIGHSIG
1840NNBOT%=ABS(LOWSIG*YUNIT) DIV YINT
1850MOVE XORIG,YORIG
1860FOR J%=1 TO NNBOT%
1870IF J%=NNBOT% AND ABS(LOWSIG)-NNBOT%*GAPY<0.3*GAPY THEN 1940
1880MOVE XORIG,YORIG-J%*YINT
1890PLOT 5,XORIG+5,YORIG-J%*YINT
1900IF GAPY=1 THEN @%=00003
1910IF GAPY=10 THEN @%=00004
1920MOVE XORIG-70,YORIG-J%*YINT+15
1930PRINT (-1)*GAPY*J%
1940NEXT
1950MOVE XORIG,YORIG-ABS(LOWSIG*YUNIT)
1960PLOT 5,XORIG+5,YORIG-ABS(LOWSIG*YUNIT)
1970@%=&20104
1980MOVE XORIG-100,YORIG-ABS(LOWSIG*YUNIT)+15
1990PRINT LOWSIG
2000VDU4
2010ENDPROC
2020:
2030DEFPROCplotintsX
2040VDU5
2050XINT=XUNIT*GAPX
2060NNL%=ABS(LOWBo*XUNIT) DIV XINT
2070MOVE XORIG,YORIG
2080FOR I%=1 TO NNL%
2090IF I%=NNL% AND ABS(LOWBo)-NNL%*GAPX<0.3*GAPX THEN 2210
2100MOVE XORIG-I%*XINT,YORIG
2110PLOT 5,XORIG-I%*XINT,YORIG-5
2120MOVE (XORIG-60)-I%*XINT,YORIG-15
2130IF GAPX=1E-3 THEN @%=&20004
2140IF GAPX=5E-3 THEN @%=&20106
2150IF GAPX=1E-2 THEN @%=&20107
2160IF GAPX=5E-2 THEN @%=&20107
2170IF GAPX=0.1 THEN @%=&20104
2180IF GAPX=0.5 THEN @%=&20104
2190IF GAPX=1 THEN @%=&20104
2200IF GAPX<=5E-2 THEN PRINT (-1)*GAPX*I%*1000 ELSE PRINT ((-1)*GAPX*I%)
2210NEXT
2220IF ABS(LOWBo)>10000 THEN @%=&20104
2230IF ABS(LOWBo)<10000 THEN @%=&20103
2240IF ABS(LOWBo)<1000 THEN @%=&20103
2250IF ABS(LOWBo)<500 THEN @%=&00005
2260IF ABS(LOWBo)<100 THEN @%=&00003
2270IF ABS(LOWBo)<10 THEN @%=&20103
2280MOVE XORIG-ABS(LOWBo*XUNIT),YORIG
2290PLOT 5,XORIG-ABS(LOWBo*XUNIT),YORIG-5
2300MOVE XORIG-ABS(LOWBo*XUNIT)-30,YORIG-15
2310IF GAPX<=5E-2 THEN PRINT LOWBo*1000 ELSE PRINT LOWBo
2320NNR%=ABS(HIGHBo*XUNIT) DIV XINT
2330MOVE XORIG,YORIG
2340FOR I%=1 TO NNR%
2350IF I%=NNR% AND ABS(HIGHBo)-NNR%*GAPX<0.3*GAPX THEN 2470
2360MOVE XORIG+I%*XINT,YORIG
2370PLOT 5,XORIG+I%*XINT,YORIG-5
2380MOVE (XORIG-60)+I%*XINT,YORIG-15
2390IF GAPX=1E-3 THEN @%=&20004
```

```
2400IF GAPX=5E-3 THEN @%=&20106
2410IF GAPX=1E-2 THEN @%=&20107
2420IF GAPX=5E-2 THEN @%=&20107
2430IF GAPX=0.1 THEN @%=&20104
2440IF GAPX=0.5 THEN @%=&20104
2450IF GAPX=1 THEN @%=&20104
2460IF GAPX<=5E-2 THEN PRINT GAPX*I%*1000 ELSE PRINT (GAPX*I%)
2470NEXT
2480IF ABS(HIGHBo)>10000 THEN @%=&20104
2490IF ABS(HIGHBo)<10000 THEN @%=&20103
2500IF ABS(HIGHBo)<1000 THEN @%=&20103
2510IF ABS(HIGHBo)<500 THEN @%=&00003
2520IF ABS(HIGHBo)<100 THEN @%=&00003
2530IF ABS(HIGHBo)<10 THEN @%=&20103
2540MOVE XORIG+ABS(HIGHBo*XUNIT),YORIG
2550PLOT 5,XORIG+ABS(HIGHBo*XUNIT),YORIG-5
2560MOVE XORIG+ABS(HIGHBo*XUNIT)-30,YORIG-15
2570IF GAPX<=5E-2 THEN PRINT HIGHBo*1000 ELSE PRINT HIGHBo
2580VDU4
2590ENDPROC
2600:
2610DEFPROCplotdata
2620MOVE XORIG+(Bo(1)*XUNIT),YORIG+(SIG(1)*YUNIT)
2630FOR F%=2 TO NOOFPTS%
2640PLOT K%,XORIG+(Bo(F%)*XUNIT),YORIG+(SIG(F%)*YUNIT)
2650NEXT
2660ENDPROC
2670:
2680DEFPROCplotbars
2690FOR F%=1 TO NOOFPTS%
2700MOVE XORIG+(Bo(F%)*XUNIT),YORIG+((SIG(F%)+ESIG(F%))*YUNIT)
2710PLOT 5,XORIG+(Bo(F%)*XUNIT),YORIG+((SIG(F%)-ESIG(F%))*YUNIT)
2720MOVE XORIG+((Bo(F%)+EBo(F%))*XUNIT),YORIG+(SIG(F%)*YUNIT)
2730PLOT 5,XORIG+((Bo(F%)-EBo(F%))*XUNIT),YORIG+(SIG(F%)*YUNIT)
2740NEXT
2750ENDPROC
2760:
2770DEFPROCwritecomms
2780@%=10
2790VDU5
2800MOVE XORIG-ABS(LOWBo*XUNIT),YORIG+ABS(HIGHSIG*YUNIT):PRINT"Filename :";FILE$
2810MOVE XORIG-ABS(LOWBo*XUNIT),YORIG+ABS(HIGHSIG*YUNIT)-35:PRINT"Date     :";DA$
2820MOVE XORIG-ABS(LOWBo*XUNIT),YORIG+ABS(HIGHSIG*YUNIT)-70:PRINT"Sample   :";SA$
2830MOVE XORIG-ABS(LOWBo*XUNIT),YORIG+ABS(HIGHSIG*YUNIT)-105:PRINT"Temp     :";TEMP$
2840MOVE XORIG-ABS(LOWBo*XUNIT),YORIG+ABS(HIGHSIG*YUNIT)-140:PRINT"No of pts:";NOOFPTS%
2850VDU4
2860ENDPROC
2870:
2880DEFPROCoptions
2890PRINT"Options are: (1) Screen dump on printer. (2)Exit to menu."
2900REPEAT
2910PRINT"Enter number:";
2920A%=GET
2930UNTIL A%=49 OR A%=50
2940PRINT
2950IF A%=49 THEN PROCchaindump
2960IF A%=50 THEN PROCchainmenu
2970ENDPROC
2980:
2990DEFPROCchaindump
```

```
3000PRINT"Options are: (1) Dedicated printer. (2) Clearway printer."
3010REPEAT
3020PRINT"Enter number:";
3030A%=GET
3040UNTIL A%=49 OR A%=50
3050PRINT
3060IF A%=49 THEN PROCdedicated
3070IF A%=50 THEN PROCclearway
3080PRINT"DUMPING"
3090CHAIN":0B.P.EPATALL"
3100ENDPROC
3110:
3120DEFPROCchainmenu
3130VDU26
3140CHAIN":0B.P.MENU"
3150ENDPROC
3160:
3170DEFPROCdedicated
3180*FX5,1
3190*FX6,0
3200*FX8,7
3210*FX7,7
3220ENDPROC
3230:
3240DEFPROCclearway
3250*FX5,2
3260*FX6,0
3270*FX8,7
3280*FX7,7
3290ENDPROC
```

```
  5REM PROGRAM "P.LNPNT1"
 10REM ------------------------------------------------------------
 20REM ----------------------  PROGRAM TO LIST VSM DATA  ----------------------
 30REM ------------------------------------------------------------
 40MODE0
 50VDU23,1,0;0;0;0;
 60DIM X(350):DIM Y(350)
 70DIM EX(350):DIM EY(350)
 80PROCtitle
 90PROCdetails
100PROCtitle
110PROCfileinput
120PROChighest
130PROClowest
140CLS
150VDU14
160PROCprntdets
170PROCprntdata
180PROCoptions
190IF B$="AGAIN" THEN CLS:GOTO 80
200END
210:
220DEFPROCfileinput
230OSCLI("DRIVE "+DR$)
240X=OPENIN FILE$
250INPUT#X,DA$,SA$,TEMP$,NOOFPTS%,STDERR$
260IF STDERR$="YES" THEN PROCinputerrY ELSE PROCinputerrN
270CLOSE#X
280*DRIVE 0
290ENDPROC
300:
310DEFPROCtitle
320PRINTTAB(27,3);"PROGRAM TO LIST VSM DATA"
330PRINTTAB(26,4);"-------------------------"
340ENDPROC
350:
360DEFPROCinputerrY
370FOR F%=1 TO NOOFPTS%
380INPUT#X,Y(F%),X(F%),EY(F%),EX(F%)
390NEXT
400ENDPROC
410:
420DEFPROCinputerrN
430FOR F%=1 TO NOOFPTS%
440INPUT#X,Y(F%),X(F%)
450NEXT
460ENDPROC
470:
480DEFPROCdetails
490VDU23,1,1;0;0;0;
500PRINTTAB(9,7);"Please enter:"
510INPUTTAB(23,9);"Drive No. for data file ";DR$
520INPUTTAB(25,11);"Filename of data file ";FILE$
530VDU23,1,0;0;0;0;
540CLS
550ENDPROC
560:
570DEFPROClowest
580LOWY=Y(1)
590LOWX=X(1)
```

```
600FOR I%=1 TO NOOFPTS%
610IF Y(I%)<LOWY THEN LOWY=Y(I%)
620IF X(I%)<LOWX THEN LOWX=X(I%)
630NEXT
640ENDPROC
650:
660DEFPROChighest
670HIGHY=Y(1)
680HIGHX=X(1)
690FOR I%=1 TO NOOFPTS%
700IF Y(I%)>HIGHY THEN HIGHY=Y(I%)
710IF X(I%)>HIGHX THEN HIGHX=X(I%)
720NEXT
730ENDPROC
740:
750DEFPROCprntdets
760PRINTTAB(35);"VSM DATA"
770PRINTTAB(34);"----------"
780PRINT
790PROCprintaline(2,78)
800PRINT:PRINT
810PRINTTAB(5);"Filename :";FILE$
820PRINTTAB(5);"Date     :";DA$
830PRINTTAB(5);"Sample   :";SA$
840PRINTTAB(5);"Temp     :";TEMP$
850PRINTTAB(5);"No of pts:";NOOFPTS%
860PRINT:PRINT
870PRINTTAB(5);"Max. CH1 value(V):";HIGHY
880PRINTTAB(5);"Min. CH1 value(V):";LOWY
890PRINTTAB(5);"Max. Bo value(T)  :";HIGHX
900PRINTTAB(5);"Min. Bo value(T)  :";LOWX
910PRINT:PRINT
920PROCprintaline(2,78)
930IF STDERR$="YES" THEN PROChdingssteY ELSE PROChdingssteN
940ENDPROC
950:
960DEFPROChdingssteY
970PRINTTAB(2);"|";SPC(18);"|";SPC(18);"|";SPC(18);"|";SPC(18);"|"
980PRINTTAB(2);"|";SPC(6);"Bo(T)";SPC(7);"|";SPC(3);"Bostderr(T)";SPC(4);"|";SPC(6);
              "CH1(V)";SPC(6);"|";SPC(3);"CH1stderr(V)";SPC(3);"|"
990PRINTTAB(2);"|";SPC(18);"|";SPC(18);"|";SPC(18);"|";SPC(18);"|"
1000PROCprintaline(2,78)
1010ENDPROC
1020:
1030DEFPROChdingssteN
1040PRINTTAB(21);"|";SPC(18);"|";SPC(18);"|"
1050PRINTTAB(21);"|";SPC(6);"Bo(T)";SPC(7);"|";SPC(6);"CH1(V)";SPC(6);"|"
1060PRINTTAB(21);"|";SPC(18);"|";SPC(18);"|"
1070PROCprintaline(21,59)
1080ENDPROC
1090:
1100DEFPROCprntdata
1110IF STDERR$="YES" THEN PROCsteYformat ELSE PROCsteNformat
1120PRINT:PRINT
1130@%=10
1140ENDPROC
1150:
1160DEFPROCoptions
1170PRINTTAB(15);"Options are:"
1180PRINTTAB(20);"(1) List data on printer. (2) Return to menu."
```

```
1190PRINTTAB(20);"(3) Repeat execution."
1200REPEAT
1210PRINTTAB(24);"Enter number:";
1220A%=GET
1230UNTIL A%=49 OR A%=50 OR A%=51
1240IF A%=49 THEN PROCsetuppntr
1250IF A%=50 THEN PROCchainmenu
1260IF A%=51 THEN B$="AGAIN"
1270ENDPROC
1280:
1290DEFPROCprintaline(L%,R%)
1300FOR I%=L% TO R%
1310PRINTTAB(I%);"-";
1320NEXT
1330ENDPROC
1340:
1350DEFPROCsteYformat
1360PRINTTAB(2);"|";SPC(18);"|";SPC(18);"|";SPC(18);"|";SPC(18);"|"
1370@%=&0000A
1380FOR F%=1 TO NOOFPTS%
1390PRINTTAB(");"|";SPC(2);X(F%);:PRINTTAB(21);"|";SPC(2);EX(F%);:PRINTTAB(40);"|";SPC(2);
                Y(F%);:PRINTTAB(59);"|";SPC(2);EY(F%);:PRINTTAB(78);"|"
1400NEXT
1410PRINTTAB(2);"|";SPC(18);"|";SPC(18);"|";SPC(18);"|";SPC(18);"|"
1420PROCprintaline(2,78)
1430ENDPROC
1440PRINTTAB(21);"|";SPC(4);X(F%);:PRINTTAB(40);"|";SPC(4);Y(F%);:PRINTTAB(57);"|"
1450DEFPROCsteNformat
1460PRINTTAB(21);"|";SPC(18);"|";SPC(18);"|"
1470@%=&0000A
1480FOR F%=1 TO NOOFPTS%
1490PRINTTAB(21);"|";SPC(4);X(F%);:PRINTTAB(40);"|";SPC(2);Y(F%);:PRINTTAB(59);"|"
1500NEXT
1510PRINTTAB(21);"|";SPC(18);"|";SPC(18);"|"
1520PROCprintaline(21,59)
1530ENDPROC
1540:
1550DEFPROCchainmenu
1560CHAIN":0B.P.MENU"
1570ENDPROC
1580:
1590DEFPROCsetuppntr
1600PRINT
1610PRINTTAB(15);"Options are:"
1620PRINTTAB(20);"(1) Dedicated printer."
1630PRINTTAB(20);"(2) Clearway printer."
1640REPEAT
1650PRINTTAB(24);"Enter number:";
1660A%=GET
1670UNTIL A%=49 OR A%=50
1680PRINT
1690IF A%=49 THEN PROCdedicated
1700IF A%=50 THEN PROCclearway
1710VDU2
1720VDU15
1730VDU12
1740PROCprntdets
1750PROCprntdata
1760VDU12
1770VDU3
```

```
1780PROCoptions
1790ENDPROC
1800:
1810DEFPROCdedicated
1820*FX5,1
1830*FX6,0
1840*FX8,7
1850*FX7,7
1860ENDPROC
1870:
1880DEFPROCclearway
1890*FX5,2
1900*FX6,0
1910*FX8,7
1920*FX7,7
1930ENDPROC
```

```
  5REM PROGRAM "P.LNPNT2"
 10REM ------------------------------------------------------------------------
 20REM ----------------------  PROGRAM TO LIST VSM DATA  ----------------------
 30REM ------------------------------------------------------------------------
 40MODE0
 50VDU23,1,0;0;0;0;
 60DIM Bo(350):DIM SIG(350)
 70DIM EBo(350):DIM ESIG(350)
 80PROCtitle
 90PROCdetails
100PROCtitle
110PROCfileinput
120PROChighest
130PROClowest
140CLS
150VDU14
160PROCprntdets
170PROCprntdata
180PROCoptions
190IF B$="AGAIN" THEN CLS:GOTO 80
200END
210:
220DEFPROCfileinput
230OSCLI("DRIVE "+DR$)
240X=OPENIN FILE$
250INPUT#X,DA$,SA$,TEMP$,NOOFPTS%,STDERR$
260IF STDERR$="YES" THEN PROCinputerrY ELSE PROCinputerrN
270CLOSE#X
280*DRIVE 0
290ENDPROC
300:
310DEFPROCtitle
320PRINTTAB(27,3);"PROGRAM TO LIST VSM DATA"
330PRINTTAB(26,4);"--------------------------"
340ENDPROC
350:
360DEFPROCinputerrY
370FOR F%=1 TO NOOFPTS%
380INPUT#X,SIG(F%),Bo(F%),ESIG(F%),EBo(F%)
390NEXT
400ENDPROC
410:
420DEFPROCinputerrN
430FOR F%=1 TO NOOFPTS%
440INPUT#X,SIG(F%),Bo(F%)
450NEXT
460ENDPROC
470:
480DEFPROCdetails
490VDU23,1,1;0;0;0;
500PRINTTAB(9,7);"Please enter:"
510INPUTTAB(23,9);"Drive No. for data file ";DR$
520INPUTTAB(25,11);"Filename of data file ";FILE$
530VDU23,1,0;0;0;0;
540CLS
550ENDPROC
560:
570DEFPROClowest
580LOWSIG=SIG(1)
590LOWBo=Bo(1)
```

```
600FOR I%=1 TO NOOFPTS%
610IF SIG(I%)<LOWSIG THEN LOWSIG=SIG(I%)
620IF Bo(I%)<LOWBo THEN LOWBo=Bo(I%)
630NEXT
640ENDPROC
650:
660DEFPROChighest
670HIGHSIG=SIG(1)
680HIGHBo=Bo(1)
690FOR I%=1 TO NOOFPTS%
700IF SIG(I%)>HIGHSIG THEN HIGHSIG=SIG(I%)
710IF Bo(I%)>HIGHBo THEN HIGHBo=Bo(I%)
720NEXT
730ENDPROC
740:
750DEFPROCprntdets
760PRINTTAB(35);"VSM DATA"
770PRINTTAB(34);"----------"
780PRINT
790PROCprintaline(2,78)
800PRINT:PRINT
810PRINTTAB(5);"Filename :";FILE$
820PRINTTAB(5);"Date     :";DA$
830PRINTTAB(5);"Sample   :";SA$
840PRINTTAB(5);"Temp     :";TEMP$
850PRINTTAB(5);"No of pts:";NOOFPTS%
860PRINT:PRINT
870PRINTTAB(5);"Max. sigma value(J/T/kg):";HIGHSIG
880PRINTTAB(5);"Min. sigma value(J/T/kg):";LOWSIG
890PRINTTAB(5);"Max. Bo value(T)        :";HIGHBo
900PRINTTAB(5);"Min. Bo value(T)        :";LOWBo
910PRINT:PRINT
920PROCprintaline(2,78)
930IF STDERR$="YES" THEN PROChdingssteY ELSE PROChdingssteN
940ENDPROC
950:
960DEFPROChdingssteY
970PRINTTAB(2);"|";SPC(18);"|";SPC(18);"|";SPC(18);"|";SPC(18);"|"
980PRINTTAB(2);"|";SPC(6);"Bo(T)";SPC(7);"|";SPC(3);"Bostderr(T)";SPC(4);"|";SPC(2);
              "sigma(J/T/kg)";SPC(3);"|";SPC(1);"sigstderr(J/T/kg)";"|"
990PRINTTAB(2);"|";SPC(18);"|";SPC(18);"|";SPC(18);"|";SPC(18);"|"
1000PROCprintaline(2,78)
1010ENDPROC
1020:
1030DEFPROChdingssteN
1040PRINTTAB(21);"|";SPC(18);"|";SPC(18);"|"
1050PRINTTAB(21);"|";SPC(6);"Bo(T)";SPC(7);"|";SPC(2);"sigma(J/T/kg)";SPC(3);"|"
1060PRINTTAB(21);"|";SPC(18);"|";SPC(18);"|"
1070PROCprintaline(21,59)
1080ENDPROC
1090:
1100DEFPROCprntdata
1110IF STDERR$="YES" THEN PROCsteYformat ELSE PROCsteNformat
1120PRINT:PRINT
1130@%=10
1140ENDPROC
1150:
1160DEFPROCoptions
1170PRINTTAB(15);"Options are:"
1180PRINTTAB(20);"(1) List data on printer. (2) Return to menu."
```

```
1190PRINTTAB(20);"(3) Repeat execution."
1200REPEAT
1210PRINTTAB(24);"Enter number:";
1220A%=GET
1230UNTIL A%=49 OR A%=50 OR A%=51
1240IF A%=49 THEN PROCsetuppntr
1250IF A%=50 THEN PROCchainmenu
1260IF A%=51 THEN B$="AGAIN"
1270ENDPROC
1280:
1290DEFPROCprintaline(L%,R%)
1300FOR I%=L% TO R%
1310PRINTTAB(I%);"-";
1320NEXT
1330ENDPROC
1340:
1350DEFPROCsteYformat
1360PRINTTAB(2);"|";SPC(18);"|";SPC(18);"|";SPC(18);"|";SPC(18);"|"
1370@%=&0000A
1380FOR F%=1 TO NOOFPTS%
1390PRINTTAB(2);"|";SPC(2);Bo(F%);:PRINTTAB(21);"|";SPC(2);EBo(F%);:PRINTTAB(40);"|";SPC(2)
                ;SIG(F%);:PRINTTAB(59);"|";SPC(2);ESIG(F%);:PRINTTAB(78);"|"
1400NEXT
1410PRINTTAB(2);"|";SPC(18);"|";SPC(18);"|";SPC(18);"|";SPC(18);"|"
1420PROCprintaline(2,78)
1430ENDPROC
1440:
1450DEFPROCsteNformat
1460PRINTTAB(21);"|";SPC(18);"|";SPC(18);"|"
1470@%=&0000A
1480FOR F%=1 TO NOOFPTS%
1490PRINTTAB(21);"|";SPC(4);Bo(F%);:PRINTTAB(40);"|";SPC(2);SIG(F%);:PRINTTAB(59);"|"
1500NEXT
1510PRINTTAB(21);"|";SPC(18);"|";SPC(18);"|"
1520PROCprintaline(21,59)
1530ENDPROC
1540:
1550DEFPROCchainmenu
1560CHAIN":0B.P.MENU"
1570ENDPROC
1580:
1590DEFPROCsetuppntr
1600PRINT
1610PRINTTAB(15);"Options are:"
1620PRINTTAB(20);"(1) Dedicated printer."
1630PRINTTAB(20);"(2) Clearway printer."
1640REPEAT
1650PRINTTAB(24);"Enter number:";
1660A%=GET
1670UNTIL A%=49 OR A%=50
1680PRINT
1690IF A%=49 THEN PROCdedicated
1700IF A%=50 THEN PROCclearway
1710VDU2
1720VDU15
1730VDU12
1740PROCprntdets
1750PROCprntdata
1760VDU12
1770VDU3
```

```
1780PROCoptions
1790ENDPROC
1800:
1810DEFPROCdedicated
1820*FX5,1
1830*FX6,0
1840*FX8,7
1850*FX7,7
1860ENDPROC
1870:
1880DEFPROCclearway
1890*FX5,2
1900*FX6,0
1910*FX8,7
1920*FX7,7
1930ENDPROC
```

```
  5REM PROGRAM "P.PIXY"
 10REM ------------------------------------------------------------------------
 20REM ----------------  PROGRAM TO PLOT VSM DATA ON PIXY  ----------------
 30REM ------------------------------------------------------------------------
 40MODE0
 50DIM Bo(350):DIM SIG(350)
 60DIM EBo(350):DIM ESIG(350)
 70VDU23,1,0;0;0;0;
 80PROCtitle
 90PROCdetails
100PROCtitle
110PROCfileinput
120PROChighest
130PROClowest
140PROCtitle
150PROCintervalsX
160PROCtitle
170PROCintervalsY
180PROCtitle
190PROCsetuppixy
200PROCdrawaxes
210PROClabelaxes
220PROCplotintsY
230PROCplotintsX
240PROCplotdata
250PROCwritecomms
260PROCoptions
270IF B$="AGAIN" THEN 70
280END
290:
300DEFPROCtitle
310PRINTTAB(23,3);"PROGRAM TO PLOT VSM DATA ON PIXY"
320PRINTTAB(22,4);"--------------------------------------"
330ENDPROC
340:
350DEFPROCfileinput
360OSCLI("DRIVE "+DR$)
370X=OPENIN FILE$
380INPUT#X,DA$,SA$,TEMP$,NOOFPTS%,STDERR$
390IF STDERR$="YES" THEN PROCinputerrY ELSE PROCinputerrN
400CLOSE#X
410*DRIVE 0
420ENDPROC
430:
440DEFPROCinputerrY
450FOR F%=1 TO NOOFPTS%
460INPUT#X,SIG(F%),Bo(F%),ESIG(F%),EBo(F%)
470NEXT
480ENDPROC
490:
500DEFPROCinputerrN
510FOR F%=1 TO NOOFPTS%
520INPUT#X,SIG(F%),Bo(F%)
530NEXT
540ENDPROC
550:
560DEFPROClowest
570LOWSIG=SIG(1)
580LOWBo=Bo(1)
590FOR I%=1 TO NOOFPTS%
```

```
 600IF SIG(I%)<LOWSIG THEN LOWSIG=SIG(I%)
 610IF Bo(I%)<LOWBo THEN LOWBo=Bo(I%)
 620NEXT
 630ENDPROC
 640:
 650DEFPROChighest
 660HIGHSIG=SIG(1)
 670HIGHBo=Bo(1)
 680FOR I%=1 TO NOOFPTS%
 690IF SIG(I%)>HIGHSIG THEN HIGHSIG=SIG(I%)
 700IF Bo(I%)>HIGHBo THEN HIGHBo=Bo(I%)
 710NEXT
 720ENDPROC
 730:
 740DEFPROCdetails
 750VDU23,1,1;0;0;0;
 760PRINTTAB(9,7);"Please enter:"
 770INPUTTAB(23,9);"Drive No. for data file ";DR$
 780INPUTTAB(25,11);"Filename of data file ";FILE$
 790PRINTTAB(9,14);"Options to plot are:":PRINTTAB(30,16);"(1) Smooth curve"
 800PRINTTAB(30,17);"(2) Single points":PRINTTAB(30,18);"(3) Triangles"
 810PRINTTAB(30,19);"(4) Squares":PRINTTAB(30,20);"(5) Crosses"
 820REPEAT
 830PRINTTAB(30,22);"Enter option (1-5):";
 840K%=GET
 850UNTIL K%=49 OR K%=50 OR K%=51 OR K%=52 OR K%=53
 860VDU23,1,0;0;0;0;
 870CLS
 880ENDPROC
 890:
 900DEFPROCdrawaxes
 910YUNIT=0.95*1800/ABS(HIGHSIG-LOWSIG)
 920XUNIT=0.95*2450/ABS(HIGHBo-LOWBo)
 930YORIG1=(1800*0.975)-ABS(HIGHSIG*YUNIT)
 940XORIG1=(2450*0.975)-ABS(HIGHBo*XUNIT)
 950YORIG2=(0.025*1800)+ABS(LOWSIG*YUNIT)
 960XORIG2=(2450*0.025)+ABS(LOWBo*XUNIT)
 970XORIG=(XORIG1+XORIG2)/2
 980YORIG=(YORIG1+YORIG2)/2
 990*FX3,7
1000PRINT"J1"
1010PRINT"S3"
1020PRINT"T1"
1030PRINT"M";XORIG",";YORIG-ABS(LOWSIG*YUNIT)
1040PRINT"D";XORIG",";YORIG+ABS(HIGHSIG*YUNIT)
1050PRINT"M";XORIG-ABS(LOWBo*XUNIT)",";YORIG
1060PRINT"D";XORIG+ABS(HIGHBo*XUNIT)",";YORIG
1070PRINT"T10"
1080ENDPROC
1090:
1100DEFPROClabelaxes
1110PRINT"S5"
1120PRINT"M";XORIG-320",";YORIG+ABS(HIGHSIG*YUNIT)-10:PRINT"K r"
1130PRINT"M";XORIG-450",";YORIG+ABS(HIGHSIG*YUNIT)-90:PRINT"P (J/T/kg)"
1140PRINT"M";XORIG+ABS(HIGHBo*XUNIT)-200",";YORIG+35
1150IF GAPX<=5E-2 THEN PRINT"P Bo(mT)" ELSE PRINT"P Bo(T)"
1160PRINT"S3"
1170ENDPROC
1180:
1190DEFPROCintervalsX
```

```
1200PRINTTAB(9,7);"The values of Bo(tesla) range from "LOWBo" to "HIGHBo
1210PRINTTAB(9,10);"The options for Bo-axis intervals are:"
1220PRINTTAB(30,12);"(1) Every   1mT":PRINTTAB(30,13);"(2) Every   5mT"
1230PRINTTAB(30,14);"(3) Every  10mT":PRINTTAB(30,15);"(4) Every  50mT"
1240PRINTTAB(30,16);"(5) Every  0.1T":PRINTTAB(30,17);"(6) Every  0.5T"
1250PRINTTAB(30,18);"(7) Every    1T"
1260REPEAT
1270PRINTTAB(28,20);"Enter option (1-7):";
1280A%=GET
1290UNTIL A%>48 AND A%<56
1300IF A%=49 THEN GAPX=1E-3
1310IF A%=50 THEN GAPX=5E-3
1320IF A%=51 THEN GAPX=1E-2
1330IF A%=52 THEN GAPX=5E-2
1340IF A%=53 THEN GAPX=0.1
1350IF A%=54 THEN GAPX=0.5
1360IF A%=55 THEN GAPX=1
1370CLS
1380ENDPROC
1390:
1400DEFPROCintervalsY
1410PRINTTAB(9,7);"The values of sigma(J/T/kg) range from "LOWSIG" to "HIGHSIG
1420PRINTTAB(9,10);"The options for sigma-axis intervals are:"
1430PRINTTAB(30,12);"(1) Every  1 J/T/kg":PRINTTAB(30,13);"(2) Every 10 J/T/kg"
1440REPEAT
1450PRINTTAB(28,15);"Enter option (1-2):";
1460A%=GET
1470UNTIL A%=49 OR A%=50
1480IF A%=49 THEN GAPY%=1
1490IF A%=50 THEN GAPY%=10
1500CLS
1510ENDPROC
1520:
1530DEFPROCplotintsY
1540YINT=YUNIT*GAPY%
1550NNTOP%=ABS(HIGHSIG*YUNIT) DIV YINT
1560PRINT"M";XORIG",";YORIG
1570FOR I%=1 TO NNTOP%
1580IF I%=NNTOP% AND ABS(HIGHSIG)-NNTOP%*GAPY%<0.3*GAPY% THEN 1650
1590PRINT"M";XORIG",";YORIG+I%*YINT
1600PRINT"D";XORIG+15",";YORIG+I%*YINT
1610IF GAPY%=1 THEN @%=&00003
1620IF GAPY%=10 THEN @%=&00004
1630PRINT"M";XORIG-70",";YORIG+I%*YINT
1640PRINT"P";GAPY%*I%
1650NEXT
1660PRINT"M";XORIG",";YORIG+ABS(HIGHSIG*YUNIT)
1670PRINT"D";XORIG+15",";YORIG+ABS(HIGHSIG*YUNIT)
1680IF HIGHSIG<100 THEN @%=&20104
1690IF HIGHSIG<10 THEN @%=&20104
1700PRINT"M";XORIG-70",";YORIG+ABS(HIGHSIG*YUNIT)+15
1710PRINT"P";HIGHSIG
1720NNBOT%=ABS(LOWSIG*YUNIT) DIV YINT
1730PRINT"M";XORIG",";YORIG
1740FOR J%=1 TO NNBOT%
1750IF J%=NNBOT% AND ABS(LOWSIG)-NNBOT%*GAPY%<0.3*GAPY% THEN 1820
1760PRINT"M";XORIG",";YORIG-J%*YINT
1770PRINT"D";XORIG+15",";YORIG-J%*YINT
1780IF GAPY%=1 THEN @%=00003
1790IF GAPY%=10 THEN @%=00004
```

```
1800PRINT"M";XORIG-90",";YORIG-J%*YINT
1810PRINT"P";(-1)*GAPY%*J%
1820NEXT
1830PRINT"M";XORIG",";YORIG-ABS(LOWSIG*YUNIT)
1840PRINT"D";XORIG+15",";YORIG-ABS(LOWSIG*YUNIT)
1850@%=&20104
1860PRINT"M";XORIG-100",";YORIG-ABS(LOWSIG*YUNIT)
1870PRINT"P";LOWSIG
1880ENDPROC
1890:
1900DEFPROCplotintsX
1910XINT=XUNIT*GAPX
1920NNL%=ABS(LOWBo*XUNIT) DIV XINT
1930PRINT"M";XORIG",";YORIG
1940FOR I%=1 TO NNL%
1950IF I%=NNL% AND ABS(LOWBo)-NNL%*GAPX<0.3*GAPX THEN 2070
1960PRINT"M";XORIG-I%*XINT",";YORIG
1970PRINT"D";XORIG-I%*XINT",";YORIG-15
1980PRINT"M";(XORIG-30)-I%*XINT",";YORIG-55
1990IF GAPX=1E-3 THEN @%=&20004
2000IF GAPX=5E-3 THEN @%=&20106
2010IF GAPX=1E-2 THEN @%=&20107
2020IF GAPX=5E-2 THEN @%=&20107
2030IF GAPX=0.1 THEN @%=&20104
2040IF GAPX=0.5 THEN @%=&20104
2050IF GAPX=1 THEN @%=&20104
2060IF GAPX<=5E-2 THEN PRINT"P";(-1)*GAPX*1000*I% ELSE PRINT"P";((-1)*GAPX*I%)
2070NEXT
2080IF ABS(LOWBo)>10000 THEN @%=&20104
2090IF ABS(LOWBo)<10000 THEN @%=&20103
2100IF ABS(LOWBo)<1000 THEN @%=&20103
2110IF ABS(LOWBo)<500 THEN @%=&00005
2120IF ABS(LOWBo)<100 THEN @%=&00003
2130IF ABS(LOWBo)<10 THEN @%=&20103
2140PRINT"M";XORIG-ABS(LOWBo*XUNIT)",";YORIG
2150PRINT"D";XORIG-ABS(LOWBo*XUNIT)",";YORIG-15
2160PRINT"M";XORIG-ABS(LOWBo*XUNIT)-30",";YORIG-55
2170IF GAPX<=5E-2 THEN PRINT"P";LOWBo*1000 ELSE PRINT"P";LOWBo
2180NNR%=ABS(HIGHBo*XUNIT) DIV XINT
2190PRINT"M";XORIG",";YORIG
2200FOR I%=1 TO NNR%
2210IF I%=NNR% AND ABS(HIGHBo)-NNR%*GAPX<0.3*GAPX THEN 2330
2220PRINT"M";XORIG+I%*XINT",";YORIG
2230PRINT"D";XORIG+I%*XINT",";YORIG-15
2240PRINT"M";(XORIG-30)+I%*XINT",";YORIG-55
2250IF GAPX=1E-3 THEN @%=&20004
2260IF GAPX=5E-3 THEN @%=&20106
2270IF GAPX=1E-2 THEN @%=&20107
2280IF GAPX=5E-2 THEN @%=&20107
2290IF GAPX=0.1 THEN @%=&20104
2300IF GAPX=0.5 THEN @%=&20104
2310IF GAPX=1 THEN @%=&20104
2320IF GAPX<=5E-2 THEN PRINT"P";GAPX*I%*1000 ELSE PRINT"P";(GAPX*I%)
2330NEXT
2340IF ABS(HIGHBo)>10000 THEN @%=&20104
2350IF ABS(HIGHBo)<10000 THEN @%=&20103
2360IF ABS(HIGHBo)<1000 THEN @%=&20103
2370IF ABS(HIGHBo)<500 THEN @%=&00003
2380IF ABS(HIGHBo)<100 THEN @%=&00003
2390IF ABS(HIGHBo)<10 THEN @%=&20103
```

```
2400PRINT"M";XORIG+ABS(HIGHBo*XUNIT)",";YORIG
2410PRINT"D";XORIG+ABS(HIGHBo*XUNIT)",";YORIG-15
2420PRINT"M";XORIG+ABS(HIGHBo*XUNIT)-30",";YORIG-55
2430IF GAPX<=5E-2 THEN PRINT"P";HIGHBo*1000 ELSE PRINT"P";HIGHBo
2440ENDPROC
2450:
2460DEFPROCplotdata
2470PRINT"M";XORIG+(Bo(1)*XUNIT)",";YORIG+(SIG(1)*YUNIT)
2480IF K%=49 THEN PROCsmthcrve
2490IF K%=50 THEN PROCshape(1)
2500IF K%=51 THEN PROCshape(4)
2510IF K%=52 THEN PROCshape(3)
2520IF K%=53 THEN PROCshape(7)
2530ENDPROC
2540:
2550DEFPROCsmthcrve
2560FOR F%=2 TO NOOFPTS%
2570PRINT"D";XORIG+(Bo(F%)*XUNIT)",";YORIG+(SIG(F%)*YUNIT)
2580NEXT
2590ENDPROC
2600:
2610DEFPROCshape(NN%)
2620FOR F%=2 TO NOOFPTS%
2630PRINT"M";XORIG+(Bo(F%)*XUNIT)",";YORIG+(SIG(F%)*YUNIT)
2640PRINT"N";NN%
2650NEXT
2660ENDPROC
2670:
2680DEFPROCwritecomms
2690@%=10
2700PRINT"M";XORIG-ABS(LOWBo*XUNIT)",";YORIG+ABS(HIGHSIG*YUNIT):PRINT"PFilename :";FILE$
2710PRINT"M";XORIG-ABS(LOWBo*XUNIT)",";YORIG+ABS(HIGHSIG*YUNIT)-35:PRINT"PDate     :";DA$
2720PRINT"M";XORIG-ABS(LOWBo*XUNIT)",";YORIG+ABS(HIGHSIG*YUNIT)-70:PRINT"PSample   :";SA$
2730PRINT"M";XORIG-ABS(LOWBo*XUNIT)",";YORIG+ABS(HIGHSIG*YUNIT)-105:PRINT"PTemp     :";TEMP$
2740PRINT"M";XORIG-ABS(LOWBo*XUNIT)",";YORIG+ABS(HIGHSIG*YUNIT)-140:PRINT"PNo of pts:";NOOFPTS%
2750PRINT"J0"
2760PRINT"M0,0"
2770*FX3,0
2780PRINTTAB(35,12);SPC(8):PRINTTAB(34,13);SPC(10)
2790ENDPROC
2800:
2810DEFPROCoptions
2820PRINTTAB(12,12);"Options are: (1) Repeat execution. (2)Exit to menu."
2830REPEAT
2840PRINT"Enter number:";
2850A%=GET
2860PRINT
2870UNTIL A%=49 OR A%=50
2880IF A%=49 THEN B$="AGAIN":CLS
2890IF A%=50 THEN PROCchainmenu
2900ENDPROC
2910:
2920DEFPROCchainmenu
2930VDU26
2940CHAIN":0B.P.MENU"
2950ENDPROC
2960:
2970DEFPROCsetuppixy
2980PRINTTAB(12,7);"Set up the Pixy- paper etc. then press SPACE-BAR to continue."
2990REPEAT:UNTIL INKEY(-99)
```

```
3000*FX15,0
3010PRINTTAB(12,7);SPC(62)
3020PRINTTAB(35,12);"PLOTTING":PRINTTAB(34,13);"----------"
3030ENDPROC
```

```
 5REM PROGRAM "P.RES"
20REM ------------------------------------------------------------------------
20REM ----------    PROGRAM TO SUBTRACT RESIDUAL NOISE, CONVERT    ----------
30REM ----------    VOLTS TO  MAGNETISATION VALUES AND  CORRECT    ----------
40REM ----------           FOR DEMAGNETIZATION FACTORS             ----------
50REM ----------         Copyright J.M.McCoy,June 1986             ----------
60REM ------------------------------------------------------------------------
70MODE0
80DIM Bo(350):DIM CH1(350)
90DIM EBo(350):DIM ECH1(350)
100VDU23,1,0;0;0;0;
110B$="":C$=""
120PROCtitle
130PROCintro
140PROCtitle
150PROCreference
160PROCtitle
170PROCquestone
180IF B$="NORES" THEN 270
190PROCtitle
200PROCresdetsin
210PROCtitle
220PROCfileinput
230PROCformsums
240PROCnormaleqns
250PROCstderr
260PROCprintab
270PROCtitle
280PROCdatadetsin
290PROCtitle
300PROCfileinput
310IF B$="NORES" THEN 330
320PROCsubtract
330PROCconvert
340PROCquesttwo
350PROCdemag
360PROCtitle
370PROCdatadetsou
380PROCfileoutput
390CHAIN":0B.P.MENU"
400END
410:
420DEFPROCtitle
430PRINTTAB(26,3);"PROGRAM TO CORRECT VSM DATA"
440PRINTTAB(25,4);"--------------------------------"
450ENDPROC
460:
470DEFPROCfileinput
480OSCLI("DRIVE "+DR$)
490X=OPENIN FILE$
500INPUT#X,DA$,SA$,TEMP$,NOOFPTS%,STDERR$
510IF STDERR$="YES" THEN PROCinputerrY ELSE PROCinputerrN
520CLOSE#X
530*DRIVE 0
540ENDPROC
550:
560DEFPROCinputerrY
570FOR F%=1 TO NOOFPTS%
580INPUT#X,CH1(F%),Bo(F%),ECH1(F%),EBo(F%)
590NEXT
```

```
600ENDPROC
610:
620DEFPROCinputerrN
630FOR F%=1 TO NOOFPTS%
640INPUT#X,CH1(F%),Bo(F%)
650NEXT
660ENDPROC
670:
680DEFPROCquestone
690VDU23,1,1;0;0;0;
700REPEAT
710PRINTTAB(9,7);"Do you want residual data subtracted from the 'true' data (y/n)?";
720A$=GET$
730UNTIL A$="Y" OR A$="y" OR A$="N" OR A$="n"
740IF A$="N" OR A$="n" THEN B$="NORES"
750VDU23,1,0;0;0;0;
760CLS
770ENDPROC
780:
790DEFPROCreference
800VDU23,1,1;0;0;0;
810PRINTTAB(9,7);"Please enter:"
820INPUTTAB(23,9);"Mass of Ni reference sample (in grams) :";mcal
830INPUTTAB(11,11);"Voltage of psd o/p at start for Ni at 1.1T (in mV) :";Vcs
840INPUTTAB(13,13);"Voltage of psd o/p at end for Ni at 1.1T (in mV) :";Vce
850INPUTTAB(1,15);"Start temperature of Ni run (in Kelvin) (input 77 for lq N1) :";Temp1
860INPUTTAB(3,17);"End temperature of Ni run (in Kelvin) (input 77 for lq Ni) :";Temp2
870INPUTTAB(31,19);"Mass of real sample (in grams) :";msamp
880INPUTTAB(27,21);"Density of real sample (in g/cmt3) :";rho
890VDU23,1,0;0;0;0;
900CLS
910ENDPROC
920:
930DEFPROCresdetsin
940VDU23,1,1;0;0;0;
950PRINTTAB(9,7);"Please enter:"
960INPUTTAB(23,9);"Drive No. for residual file ";DR$
970INPUTTAB(25,11);"Filename of residual file ";FILE$
980VDU23,1,0;0;0;0;
990CLS
1000ENDPROC
1010:
1020DEFPROCintro
1030PRINTTAB(9,6);"The program reads in the residual data and, assuming a diamagnetic"
1040PRINTTAB(9,7);"nature, solves the normal equations to give a linear least squares"
1050PRINTTAB(9,8);"fit to the  data of the form y=ax+b ."
1060PRINTTAB(11,9);"The program then inputs the 'true' raw data set and from its CH1"
1070PRINTTAB(9,10);"values  subtracts the appropriate  value for the  residual at that"
1080PRINTTAB(9,11);"point calculated from the least squares fit."
1090PRINTTAB(11,12);"The magnetisation  data which is in volts is then converted into"
1100PRINTTAB(9,13);"units of  J/T/kg (sigma).  After this the Bo values  are corrected"
1110PRINTTAB(9,14);"for the demagnetisation factor  of a sphere (1/3) to give the true"
1120PRINTTAB(9,15);"field in the sample."
1130PRINTTAB(11,16);"Finally, the new corrected data is output onto disc."
1140PROCspacebar
1150ENDPROC
1160:
1170DEFPROCspacebar
1180PRINTTAB(26,30);"(PRESS SPACE-BAR TO CONTINUE)"
1190REPEAT:UNTIL INKEY(-99):CLS
```

```
1200*FX15,0
1210ENDPROC
1220:
1230DEFPROCformsums
1240SUMY=0:SUMX=0:SUMXY=0:SUMXX=0
1250FOR F%=1 TO NOOFPTS%
1260SUMY=CH1(F%)+SUMY
1270SUMX=Bo(F%)+SUMX
1280SUMXY=Bo(F%)*CH1(F%)+SUMXY
1290SUMXX=(Bo(F%)↑2)+SUMXX
1300NEXT
1310ENDPROC
1320:
1330DEFPROCnormaleqns
1340DENOM=(NOOFPTS%*SUMXX)-SUMX↑2
1350a=((NOOFPTS%*SUMXY)-(SUMX*SUMY))/DENOM
1360b=((SUMY*SUMXX)-(SUMX*SUMXY))/DENOM
1370ENDPROC
1380:
1390DEFPROCstderr
1400SUMRESSQU=0
1410FOR F%=1 TO NOOFPTS%
1420SUMRESSQU=SUMRESSQU+(CH1(F%)-a*Bo(F%)-b)↑2
1430NEXT
1440aSTDERR=SQR(NOOFPTS%*SUMRESSQU/((NOOFPTS%-2)*DENOM))
1450bSTDERR=aSTDERR*SQR(SUMXX/NOOFPTS%)
1460ENDPROC
1470:
1480DEFPROCprintab
1490PRINTTAB(9,6);"For the assumed linear relationship of the form CH1=a*Bo+b (y=ax+b)"
1500PRINTTAB(9,8);"yields for a and b:"
1510PRINTTAB(20,11);"a= ";a" (+/-) ";aSTDERR"  V/T"
1520PRINTTAB(20,13);"b= ";b" (+/-) ";bSTDERR"  V"
1530PROCspacebar
1540ENDPROC
1550:
1560DEFPROCdatadetsin
1570VDU23,1,1;0;0;0;
1580PRINTTAB(9,7);"Please enter:"
1590INPUTTAB(23,9);"Drive No. for data file ";DR$
1600INPUTTAB(25,11);"Filename of data file ";FILE$
1610VDU23,1,0;0;0;0;
1620CLS
1630ENDPROC
1640:
1650DEFPROCsubtract
1660FOR F%=1 TO NOOFPTS%
1670RES=a*Bo(F%)+b
1680CH1(F%)=CH1(F%)-RES
1690NEXT
1700ENDPROC
1710:
1720DEFPROCconvert
1730sigmasat1=55.2-((Temp1-288)*0.024)
1740sigmasat2=55.2-((Temp2-288)*0.024)
1750IF Temp1=77 OR Temp1=77.344 THEN sigmasat1=58.537
1760IF Temp2=77 OR Temp2=77.344 THEN sigmasat2=58.537
1770const1=sigmasat1*mcal*1000/(msamp*Vcs)
1780const2=sigmasat2*mcal*1000/(msamp*Vce)
1790IF STDERR$="YES" THEN PROCconvY ELSE PROCconvN
```

```
1800ENDPROC
1810:
1820DEFPROCconvY
1830FOR F%=1 TO NOOFPTS%
1840const=const1+(F%*(const2-const1)/NOOFPTS%)
1850CH1(F%)=const*CH1(F%)
1860ECH1(F%)=const*ECH1(F%)
1870NEXT
1880ENDPROC
1890:
1900DEFPROCconvN
1910FOR F%=1 TO NOOFPTS%
1920const=const1+(F%*(const2-const1)/NOOFPTS%)
1930CH1(F%)=const*CH1(F%)
1940NEXT
1950ENDPROC
1960:
1970DEFPROCdatadetsou
1980VDU23,1,1;0;0;0;
1990PRINTTAB(9,7);"Please enter:"
2000INPUTTAB(23,9);"Drive No. for new data file output ";DR$
2010INPUTTAB(25,11);"Name of data file to be created ";FILE$
2020VDU23,1,0;0;0;0;
2030CLS
2040ENDPROC
2050:
2060DEFPROCfileoutput
2070OSCLI("DRIVE "+DR$)
2080X=OPENOUT FILE$
2090PRINT#X,DA$,SA$,TEMP$,NOOFPTS%,STDERR$
2100IF STDERR$="YES" THEN PROCoutputerrY ELSE PROCoutputerrN
2110CLOSE#X
2120*DRIVE 0
2130ENDPROC
2140:
2150DEFPROCoutputerrY
2160FOR F%=1 TO NOOFPTS%
2170PRINT#X,CH1(F%),Bo(F%),ECH1(F%),EBo(F%)
2180NEXT
2190ENDPROC
2200:
2210DEFPROCoutputerrN
2220FOR F%=1 TO NOOFPTS%
2230PRINT#X,CH1(F%),Bo(F%)
2240NEXT
2250ENDPROC
2260:
2270DEFPROCdemag
2280coeff=(rho*1000*4*3.14159265*1E-7)*demag
2290FOR F%=1 TO NOOFPTS%
2300Bo(F%)=Bo(F%)-coeff*CH1(F%)
2310NEXT
2320ENDPROC
2330:
2340DEFPROCquesttwo
2350VDU23,1,1;0;0;0;
2360INPUTTAB(2,7);"Input demag factor (1/3 for sphere)(input '0' for no demag corrections)";demag
2370VDU23,1,0;0;0;0;
2380CLS
2390ENDPROC
```

```
  5REM PROGRAM "P.MSAT"
 10REM ------------------------------------------------------------------------
 20REM ----------    PROGRAM TO CALCULATE SATURATION MAGNETISATION    ----------
 30REM ----------       FROM EXTRAPOLATION OF SATURATION VALUES       ----------
 40REM ------------------------------------------------------------------------
 50MODE0
 60DIM Bo(350):DIM SIG(350)
 70DIM EBo(350):DIM ESIG(350)
 80DIM BB(100):DIM SSIG(100)
 90VDU23,1,0;0;0;0;
100PROCtitle
110PROCdetails
120PROCtitle
130PROCfileinput
140PROCtitle
150PROCcutoff
160PROCrecip
170PROChighest
180PROClowest
190PROCdrawaxes
200PROCaxesints
210PROClabelaxes
220PROCplotdata
230PROCspacebar
235PROCtitle
240PROCcontinue
250IF A%=49 THEN 140
260PROCformsums
270PROCnormaleqns
280PROCtitle
290PROCstderr
300PROCprintac
310PROCoptions
320IF D%=49 THEN 90
330IF D%=50 THEN 140
340VDU23,1,1;0;0;0;
350CHAIN":0B.P.MENU"
360END
370:
380DEFPROCtitle
390PRINTTAB(19,3);"PROGRAM TO CALCULATE SATURATION MAGNETISATION"
400PRINTTAB(18,4);"----------------------------------------------------"
410ENDPROC
420:
430DEFPROCfileinput
440OSCLI("DRIVE "+DR$)
450X=OPENIN FILE$
460INPUT#X,DA$,SA$,TEMP$,NOOFPTS%,STDERR$
470IF STDERR$="YES" THEN PROCinputerrY ELSE PROCinputerrN
480CLOSE#X
490*DRIVE 0
500ENDPROC
510:
520DEFPROCinputerrY
530FOR F%=1 TO NOOFPTS%
540INPUT#X,SIG(F%),Bo(F%),ESIG(F%),EBo(F%)
550NEXT
560ENDPROC
570:
580DEFPROCinputerrN
```

```
590FOR F%=1 TO NOOFPTS%
600INPUT#X,SIG(F%),Bo(F%)
610NEXT
620ENDPROC
630:
640DEFPROClowest
650LOWSSIG=SSIG(1)
660LOWBB=BB(1)
670FOR I%=1 TO P%-1
680IF SSIG(I%)<LOWSSIG THEN LOWSSIG=SSIG(I%)
690IF BB(I%)<LOWBB THEN LOWBB=BB(I%)
700NEXT
710ENDPROC
720:
730DEFPROChighest
740HIGHSSIG=SSIG(1)
750HIGHBB=BB(1)
760FOR I%=1 TO P%-1
770IF SSIG(I%)>HIGHSSIG THEN HIGHSSIG=SSIG(I%)
780IF BB(I%)>HIGHBB THEN HIGHBB=BB(I%)
790NEXT
800ENDPROC
810:
820DEFPROCdetails
830VDU23,1,1;0;0;0;
840PRINTTAB(9,7);"Please enter:"
850INPUTTAB(23,9);"Drive No. for data file ";DR$
860INPUTTAB(25,11);"Filename of data file ";FILE$
870VDU23,1,0;0;0;0;
880CLS
890ENDPROC
900:
910DEFPROCcutoff
920PRINTTAB(9,8);"Having studied the data, what is the cut-off value of Bo in tesla"
930PRINTTAB(9,9);"below which  the data will be excluded ? (Enter lowest field value"
940INPUTTAB(9,10);"of positive saturation region of curve) ";Bcutoff
950P%=1
960FOR I%=1 TO NOOFPTS%
970IF Bo(I%)>Bcutoff THEN BB(P%)=Bo(I%) ELSE 1000
980SSIG(P%)=SIG(I%)
990P%=P%+1
1000NEXT
1010ENDPROC
1020:
1030DEFPROCrecip
1040FOR I%=1 TO P%-1
1050BB(I%)=1/BB(I%)
1060NEXT
1070ENDPROC
1080:
1090DEFPROCdrawaxes
1100CLS
1110VDU24,0;100;1279;1023
1120VDU28,0,31,79,29
1130YUNIT=0.9*922/ABS(HIGHSSIG-LOWSSIG)
1140XUNIT=0.9*1280/ABS(HIGHBB-LOWBB)
1150XORIG=0.05*1280
1160YORIG=0.05*922+101
1170MOVE XORIG,YORIG
1180PLOT 5,XORIG+(HIGHBB-LOWBB)*XUNIT,YORIG
```

```
1190MOVE XORIG,YORIG
1200PLOT 5,XORIG,YORIG+(HIGHSSIG-LOWSSIG)*YUNIT
1210ENDPROC
1220:
1230DEFPROCaxesints
1240XINT=(HIGHBB-LOWBB)*XUNIT/10
1250YINT=(HIGHSSIG-LOWSSIG)*YUNIT/10
1260MOVE XORIG,YORIG
1270FOR I%=1 TO 10
1280MOVE XORIG+I%*XINT,YORIG
1290PLOT 5,XORIG+I%*XINT,YORIG-10
1300NEXT
1310MOVE XORIG,YORIG
1320FOR I%=1 TO 10
1330MOVE XORIG,YORIG+I%*YINT
1340PLOT 5,XORIG-5,YORIG+I%*YINT
1350NEXT
1360VDU5
1370?&FE07=&20205
1380FOR I%=0 TO 10 STEP 1
1390MOVE XORIG-60+I%*XINT,YORIG-20
1400PRINTLOWBB+I%*(HIGHBB-LOWBB)/10
1410NEXT
1420FOR I%=0 TO 10 STEP 1
1430MOVE 5,YORIG+10+I%*YINT
1440PRINTLOWSSIG+I%*(HIGHSSIG-LOWSSIG)/10
1450NEXT
1460VDU4
1470ENDPROC
1480:
1490DEFPROClabelaxes
1500VDU5
1510MOVE XORIG+100,950
1520PRINT"sigma(J/T/kg)"
1530MOVE 1100,YORIG+60
1540PRINT"1/Bo(Tt-1)"
1550VDU4
1560ENDPROC
1570:
1580DEFPROCplotdata
1590MOVE XORIG+(BB(1)-LOWBB)*XUNIT,YORIG+(SSIG(1)-LOWSSIG)*YUNIT
1600FOR I%=2 TO P%-1
1610PLOT 69,XORIG+(BB(I%)-LOWBB)*XUNIT,YORIG+(SSIG(I%)-LOWSSIG)*YUNIT
1620NEXT
1630ENDPROC
1640:
1650DEFPROCspacebar
1655VDU23,1,0;0;0;0;
1660PRINTTAB(26);"(PRESS SPACE-BAR TO CONTINUE)"
1670REPEAT:UNTIL INKEY(-99)
1680CLS
1690VDU26
1700*FX15,0
1710ENDPROC
1720:
1730DEFPROCcontinue
1740VDU23,1,1;0;0;0;
1750PRINTTAB(9,8);"Does the cut-off give a sufficiently linear data set for"
1760PRINTTAB(9,9);"extrapolation ?"
1762PRINTTAB(11,11);"Options are:"
```

```
1764PRINTTAB(22,13);"(1) Change cut-off value"
1765PRINTTAB(22,14);"(2) Continue with linear fit"
1770REPEAT
1780PRINTTAB(27,16);"Enter number (1-2):";
1790A%=GET
1800UNTIL A%=49 OR A%=50
1810CLS
1820VDU23,1,0;0;0;0;
1830VDU26
1840ENDPROC
1850:
1860DEFPROCformsums
1870SUMX=0:SUMY=0:SUMXY=0:SUMXX=0
1880FOR I%=1 TO P%-1
1890SUMX=BB(I%)+SUMX
1900SUMY=SSIG(I%)+SUMY
1910SUMXY=BB(I%)*SSIG(I%)+SUMXY
1920SUMXX=(BB(I%)↑2)+SUMXX
1930NEXT
1940ENDPROC
1950:
1960DEFPROCnormaleqns
1970DENOM=((P%-1)*SUMXX)-SUMX↑2
1980a=(((P%-1)*SUMXY)-(SUMX*SUMY))/DENOM
1990c=((SUMY*SUMXX)-(SUMX*SUMXY))/DENOM
2000ENDPROC
2010:
2020DEFPROCstderr
2030SUMRESSQU=0
2040FOR F%=1 TO P%-1
2050SUMRESSQU=SUMRESSQU+(SSIG(F%)-a*BB(F%)-c)↑2
2060NEXT
2070aSTDERR=SQR((P%-1)*SUMRESSQU/((P%-3)*DENOM))
2080cSTDERR=aSTDERR*SQR(SUMXX/(P%-1))
2090ENDPROC
2100:
2110DEFPROCprintac
2120P%=10
2130PRINTTAB(9,6);"The assumed linear relationship of the form 'sigma=a*(1/Bo)+c'"
2140PRINTTAB(9,8);"yields for a and c"
2150PRINTTAB(20,11);"a= ";a" (+/-) ";aSTDERR"  J/kg"
2160PRINTTAB(20,13);"c= ";c" (+/-) ";cSTDERR"  J/T/kg"
2170PRINTTAB(30,16);"No of pts used= ";P%-1
2180PRINTTAB(30,18);"Cut-off field= ";Bcutoff;" tesla"
2190PRINTTAB(20,20);"sigmasat= ";c" (+/-) ";cSTDERR"  J/T/kg"
2200ENDPROC
2210:
2220DEFPROCoptions
2230VDU23,1,1;0;0;0;
2240PRINTTAB(7,23);"Options are:"
2250PRINTTAB(9,24);"(1) Repeat execution with new data file"
2260PRINTTAB(9,25);"(2) Change cut-off value and repeat execution with same data file"
2270PRINTTAB(9,26);"(3) Return to menu"
2280REPEAT
2290PRINTTAB(26,28);"Enter number (1-3):";
2300D%=GET
2310UNTIL D%=49 OR D%=50 OR D%=51
2320IF D%=49 OR D%=50 THEN CLS
2330ENDPROC
```

```
 5REM PROGRAM "P.INITSUS"
10REM ------------------------------------------------------------------------
20REM ----------    PROGRAM TO CALCULATE INITIAL SUSCEPTIBILITY    ----------
30REM ------------------------------------------------------------------------
40MODE0
50DIM Bo(350):DIM SIG(350)
60DIM EBo(350):DIM ESIG(350)
70VDU23,1,0;0;0;0;
80D%=0
90PROCtitle
100PROCinputtype
110PROCtitle
120PROCnoofpts
130IF D%=50 THEN 150
140PROCinputdata
150PROChighest
160PROCdrawaxes
170PROCaxesints
180PROClabelaxes
190PROCplotdata
200PROCspacebar
210PROCtitle
220PROCformsums
230PROCnormaleqns
240PROCtitle
250PROCstderr
260PROCprintac
270PROCoptions
280IF D%=49 THEN 90
290IF D%=50 THEN 110
300IF D%=51 THEN 320
310VDU23,1,1;0;0;0;
320CHAIN":0B.P.MENU"
330END
340:
350DEFPROCtitle
360PRINTTAB(19,3);"PROGRAM TO CALCULATE INITIAL SUSCEPTIBILITY"
370PRINTTAB(18,4);"----------------------------------------------"
380ENDPROC
390:
400DEFPROCinputtype
410VDU23,1,1;0;0;0;
420PRINTTAB(15,6);"Options for type of input are:"
430PRINTTAB(28,8);"(1) Data file"
440PRINTTAB(28,9);"(2) 'By hand'"
450REPEAT
460PRINTTAB(26,11);"Enter option (1-2):";
470C%=GET
480UNTIL C%=49 OR C%=50
490VDU23,1,0;0;0;0;
500CLS
510ENDPROC
520:
530DEFPROCnoofpts
540VDU23,1,1;0;0;0;
550PRINTTAB(18,11);"(Input more than you need the first time)"
560INPUTTAB(20,10);"How many data points are to be used ";n%
570VDU23,1,0;0;0;0;
580CLS
590ENDPROC
```

```
600:
610DEFPROCinputdata
620IF C%=50 THEN 630 ELSE 650
630PROCtitle
640PROCtypeindata:ENDPROC
650PROCtitle
660PROCdetails
670PROCtitle
680PROCfileinput
690ENDPROC
700:
710DEFPROCfileinput
720OSCLI("DRIVE "+DR$)
730X=OPENIN FILE$
740INPUT#X,DA$,SA$,TEMP$,NOOFPTS%,STDERR$
750IF STDERR$="YES" THEN PROCinputerrY ELSE PROCinputerrN
760CLOSE#X
770*DRIVE 0
780ENDPROC
790:
800DEFPROCinputerrY
810FOR F%=1 TO n%
820INPUT#X,SIG(F%),Bo(F%),ESIG(F%),EBo(F%)
830NEXT
840ENDPROC
850:
860DEFPROCinputerrN
870FOR F%=1 TO n%
880INPUT#X,SIG(F%),Bo(F%)
890NEXT
900ENDPROC
910:
920DEFPROChighest
930HIGHSIG=SIG(1)
940HIGHBo=Bo(1)
950FOR I%=1 TO n%
960IF SIG(I%)>HIGHSIG THEN HIGHSIG=SIG(I%)
970IF Bo(I%)>HIGHBo THEN HIGHBo=Bo(I%)
980NEXT
990ENDPROC
1000:
1010DEFPROCdrawaxes
1020CLS
1030VDU24,0;100;1279;1023
1040VDU28,0,31,79,29
1050XUNIT=0.9*1280/ABS(HIGHBo)
1060YUNIT=0.9*922/ABS(HIGHSIG)
1070XORIG=0.05*1280
1080YORIG=0.05*922+101
1090MOVE XORIG,YORIG
1100PLOT 5,XORIG+HIGHBo*XUNIT,YORIG
1110MOVE XORIG,YORIG
1120PLOT 5,XORIG,YORIG+HIGHSIG*YUNIT
1130ENDPROC
1140:
1150DEFPROCaxesints
1160XINT=HIGHBo*XUNIT/10
1170YINT=HIGHSIG*YUNIT/10
1180MOVE XORIG,YORIG
1190FOR I%=1 TO 10
```

```
1200MOVE XORIG+I%*XINT,YORIG
1210PLOT 5,XORIG+I%*XINT,YORIG-10
1220NEXT
1230MOVE XORIG,YORIG
1240FOR I%=1 TO 10
1250MOVE XORIG,YORIG+I%*YINT
1260PLOT 5,XORIG-5,YORIG+I%*YINT
1270NEXT
1280VDU5
1290?&FE=&20205
1300FOR I%=0 TO 10
1310MOVE XORIG-60+I%*XINT,YORIG-20
1320PRINT1000*I%*HIGHBo/10
1330NEXT
1340FOR I%=1 TO 10
1350MOVE 5,YORIG+10+I%*YINT
1360PRINT I%*HIGHSIG/10
1370NEXT
1380VDU4
1390ENDPROC
1400:
1410DEFPROClabelaxes
1420VDU5
1430MOVE XORIG+100,950
1440PRINT"sigma(J/T/kg)"
1450MOVE 1100,YORIG+60
1460PRINT"Bo(mT)"
1470VDU4
1480ENDPROC
1490:
1500DEFPROCplotdata
1510MOVE XORIG+Bo(1)*XUNIT,YORIG+SIG(1)*YUNIT
1520FOR F%=1 TO n%
1530PLOT 69,XORIG+Bo(F%)*XUNIT,YORIG+SIG(F%)*YUNIT
1540NEXT
1550ENDPROC
1560:
1570DEFPROCspacebar
1580VDU23,1,0;0;0;0;
1590PRINTTAB(26);"(PRESS SPACE-BAR TO CONTINUE)"
1600REPEAT:UNTIL INKEY(-99)
1610VDU26
1620*FX15,0
1630CLS
1640ENDPROC
1650:
1660DEFPROCdetails
1670VDU23,1,1;0;0;0;
1680PRINTTAB(9,7);"Please enter:"
1690INPUTTAB(23,9);"Drive No. for data file ";DR$
1700INPUTTAB(25,11);"Filename of data file ";FILE$
1710VDU23,1,0;0;0;0;
1720CLS
1730ENDPROC
1740:
1750DEFPROCtypeindata
1760VDU23,1,1;0;0;0;
1770PRINTTAB(13,8);"Please type in the following data:"
1780FOR F%=1 TO n%
1790PRINTTAB(19,9+F%);"Bo(";F%;") ";:INPUTTAB(26,9+F%);Bo(F%)
```

```
1800PRINTTAB(50,9+F%);"sigma(";F%;") ";:INPUTTAB(60,9+F%);SIG(F%)
1810NEXT
1820CLS
1830ENDPROC
1840:
1850DEFPROCformsums
1860SUMX=0:SUMY=0:SUMXY=0:SUMXX=0
1870FOR I%=1 TO n%
1880SUMX=Bo(I%)+SUMX
1890SUMY=SIG(I%)+SUMY
1900SUMXY=Bo(I%)*SIG(I%)+SUMXY
1910SUMXX=(Bo(I%)↑2)+SUMXX
1920NEXT
1930ENDPROC
1940:
1950DEFPROCnormaleqns
1960DENOM=(n%*SUMXX)-SUMX↑2
1970a=((n%*SUMXY)-(SUMX*SUMY))/DENOM
1980c=((SUMY*SUMXX)-(SUMX*SUMXY))/DENOM
1990ENDPROC
2000:
2010DEFPROCstderr
2020SUMRESSQU=0
2030FOR I%=1 TO n%
2040SUMRESSQU=SUMRESSQU+(SIG(I%)-a*Bo(I%)-c)↑2
2050NEXT
2060aSTDERR=SQR(n%*SUMRESSQU/((n%-2)*DENOM))
2070cSTDERR=aSTDERR*SQR(SUMXX/n%)
2080ENDPROC
2090:
2100DEFPROCprintac
2110@%=10
2120PRINTTAB(9,6);"The assumed linear relationship of the form 'sigma=a*Bo+c'(Bo->0)"
2130PRINTTAB(9,8);"yields for a and c"
2140PRINTTAB(8,11);"a= ";a" (+/-) ";aSTDERR"  J/T↑2/kg"
2150PRINTTAB(8,13);"c= ";c" (+/-) ";cSTDERR"  J/T/kg"
2160PRINTTAB(8,15);"No of pts used= ";n%
2170PRINTTAB(8,17);"initial mass susceptibility= ";a" (+/-) ";aSTDERR"  J/T↑2/kg"
2180PRINTTAB(8,19);"offset from zero= ";c" (+/-) ";cSTDERR"  J/T/kg"
2190ENDPROC
2200:
2210DEFPROCoptions
2220VDU23,1,1;0;0;0;
2230PRINTTAB(10,25);"Options are:"
2240PRINTTAB(23,26);"(1) Repeat execution with new data"
2250PRINTTAB(23,27);"(2) Change number of points"
2260PRINTTAB(23,28);"(3) Return to menu"
2270REPEAT
2280PRINTTAB(26,31);"Enter number (1-3):";
2290D%=GET
2300UNTIL D%=49 OR D%=50 OR D%=51
2310CLS
2320ENDPROC
```

Appendix P3

Listing of the Program to Solve the Equations of Motion for the Indication-Formation Simulation

This Appendix gives a listing of the program PERM which solves the equations of motion of all of the 160 particles in the MPI indication-formation simulation. The program is written in FORTRAN 77 and runs on the Amdahl 470/V8 computer at the University of Durham.

At the beginning of the program the position and velocity coordinates of all of the particles, together with all of the other model parameters, are read in. If a particle is still suspended and is capable of moving in both the x and the y directions then the subroutine PRCOXY solves for the subsequent trajectory using a predictor-corrector method. If the particle reaches the test specimen-carrier liquid interface then it can only subsequently move in the x direction and the subroutine PRCOX is then invoked to solve for the trajectory. If the initial particle coordinates indicate that the particle is already at the test specimen-carrier liquid interface then the subroutine PRCOX is used directly for the subsequent trajectory calculation.

The final position and velocity coordinates after the trajectories of all of the particles have been followed for 0.1 seconds are then written to an output file. This output data can then be used as input data in a subsequent re-running of the simulation for a further 0.1 seconds.

During the execution of the program, at any value of x and y, the particle's magnetization, M, and the angle this makes with the x axis, θ, are evaluated using respectively the two FUNCTIONs, MAG and THET, both of which take the particle position coordinates as arguments. The two FUNCTIONs, DHXBDX and DHYBDX, evaluate the functional parts of two of the four field gradient components, both of which are functions of x and y. However, by equation (5.12c), with these evaluations, one also obtains the functional parts of the other two field gradient components.

```
      PROGRAM PERM
      DIMENSION X(1000),Y(1000),VX(1000),VY(1000),T(1000)
      DIMENSION XB(1000),YB(1000),VXB(1000),VYB(1000)
      DOUBLE PRECISION X,Y,VX,VY,T,XB,YB,VXB,VYB
      COMMON ALPHA,BETA,ASPECT,GAMMA,DELTA,H,A,B,RADIUS,HO,MU,PNTTHK
      REAL MU,MAG
      H=5.0E-6
      PNTTHK=1.0E-5
C
C
C INPUT SYSTEM PARAMETERS AND INITIAL PARTICLE COORDINATES AND VELOCITIES
C
      READ(7,*),RADIUS,RHOP,RHOC,ETA,HO,BDEF,ADEF,MU,NPARTS
      READ(7,*)(XB(I),YB(I),VXB(I),VYB(I),I=1,160)
C
C
      NEVAL=20
C
C EVALUATE CLUSTERS OF CONSTANTS IN DIFFERENTIAL EQUATIONS
C
      ASPECT=B/A
      ALPHA=(9.0*ETA)/(2.0*RHOP*RADIUS**2)
      BETA=4.0*3.14159265*1.0E-7*HO*ASPECT*(MU-1.0)
      BETA=BETA/(2.0*RHOP*ATAN(ASPECT)*(ASPECT+MU))
      GAMMA=9.80665*(RHOP-RHOC)/RHOP
C
C SOLVE TRAJECTORY FOR EACH PARTICLE, ONE AT A TIME
C
      DO 600 L=1,160
          A=ADEF
          B=BDEF
          X(1)=XB(L)
          Y(1)=YB(L)
          VX(1)=VXB(L)
          VY(1)=VYB(L)
          T(1)=0.0
C
C
C CALL PREDICTOR-CORRECTOR SUBROUTINE TO SOLVE BOTH X,Y DIFFERENTIAL EQUATIONS
C
          IF (Y(1).LT.PNTTHK) THEN
              JJ=1
              GOTO 50
          ENDIF
          JJ=NEVAL
          IFAIL=0
          CALL PRCOXY(X,Y,VX,VY,T,JJ,IFAIL)
          IF (JJ.GE.NEVAL) THEN
              NEVAL=JJ
              GOTO 60
          ENDIF
C
C CALL PREDICTOR CORRECTOR TO SOLVE X DIFFERENTIAL EQUATION ONLY
C
  50      IFAIL=0
          CALL PRCOX(X,Y,VX,VY,T,JJ,NEVAL,IFAIL)
  60      XB(L)=X(NEVAL)
          YB(L)=Y(NEVAL)
          VXB(L)=VX(NEVAL)
          VYB(L)=VY(NEVAL)
```

```
 600 CONTINUE
C
C WRITE DATA TO OUTPUT FILE
C
      WRITE(10,*),RADIUS,RHOP,RHOC,ETA,HO,BDEF,ADEF,MU,160
      WRITE(10,*)(XB(I),YB(I),VXB(I),VYB(I),I=1,160)
      STOP
      END
C
C
      FUNCTION THET(XX,YY,AA,BB)
C
C CALCULATES THE ANGLE THETA AT AN INPUT X,Y ARGUMENT
C
      DOUBLE PRECISION C1,C2,C3,C4
      COMMON ALPHA,BETA,ASPECT,GAMMA,DELTA,H,A,B,RADIUS,HO,MU,PNTTHK
      C1=ATAN(BB*(XX+AA)/((XX+AA)**2+YY*(YY+BB)))
      C2=ATAN(BB*(XX-AA)/((XX-AA)**2+YY*(YY+BB)))
      HX=HO*ASPECT*(MU-1.0)*(C1-C2)/(2.0*ATAN(ASPECT)*(ASPECT+MU))
      C3=((XX+AA)**2+(YY+BB)**2)*((XX-AA)**2+YY**2)
      C4=((XX+AA)**2+YY**2)*((XX-AA)**2+(YY+BB)**2)
      HY=HO*ASPECT*(MU-1.0)*(LOG(C3/C4))/(4.0*ATAN(ASPECT)*(ASPECT+MU))
      THET=ATAN(HY/(HX+HO))
      RETURN
      END
C
C
      FUNCTION MAG(XX,YY,AA,BB)
C
C CALCULATES PARTICLE MAGNETIZATION AT AN INPUT X,Y ARGUMENT
C
      DOUBLE PRECISION C1,C2,C3,C4
      COMMON ALPHA,BETA,ASPECT,GAMMA,DELTA,H,A,B,RADIUS,HO,MU,PNTTHK
      C1=ATAN(BB*(XX+AA)/((XX+AA)**2+YY*(YY+BB)))
      C2=ATAN(BB*(XX-AA)/((XX-AA)**2+YY*(YY+BB)))
      HX=HO*ASPECT*(MU-1.0)*(C1-C2)/(2.0*ATAN(ASPECT)*(ASPECT+MU))
      C3=((XX+AA)**2+(YY+BB)**2)*((XX-AA)**2+YY**2)
      C4=((XX+AA)**2+YY**2)*((XX-AA)**2+(YY+BB)**2)
      HY=HO*ASPECT*(MU-1.0)*(LOG(C3/C4))/(4.0*ATAN(ASPECT)*(ASPECT+MU))
      MAG=2.0*SQRT(HY**2+(HO+HX)**2)
      IF (ABS(MAG).GE.4.7138E5) THEN
      MAG=4.7138E5
      ENDIF
      RETURN
      END
C
C
      FUNCTION DHXBDX(XX,YY,AA,BB)
C
C CALCULATES THE FUNCTIONAL PART OF ONE OF THE FIELD GRADIENT EXPRESSIONS
C
      DOUBLE PRECISION C1,C2,C3,C4
      XX=1.0E6*XX
      YY=1.0E6*YY
      AA=1.0E6*AA
      BB=1.0E6*BB
      C1=(YY+BB)/((XX-AA)**2+(YY+BB)**2)
      C2=(YY+BB)/((XX+AA)**2+(YY+BB)**2)
      C3=YY/((XX+AA)**2+YY**2)
      C4=YY/((XX-AA)**2+YY**2)
```

```
      XX=1.0E-6*XX
      YY=1.0E-6*YY
      AA=1.0E-6*AA
      BB=1.0E-6*BB
      DHXBDX=(C1-C2+C3-C4)*1.0E6
      RETURN
      END
C
C
      FUNCTION DHYBDX(XX,YY,AA,BB)
C
C CALCULATES THE FUNCTIONAL PART OF THE OTHER FIELD GRADIENT EXPRESSION
C
      DOUBLE PRECISION C1,C2,C3,C4
      XX=1.0E6*XX
      YY=1.0E6*YY
      AA=1.0E6*AA
      BB=1.0E6*BB
      C1=(XX+AA)/((XX+AA)**2+(YY+BB)**2)
      C2=(XX-AA)/((XX-AA)**2+(YY+BB)**2)
      C3=(XX-AA)/((XX-AA)**2+YY**2)
      C4=(XX+AA)/((XX+AA)**2+YY**2)
      XX=1.0E-6*XX
      YY=1.0E-6*YY
      AA=1.0E-6*AA
      BB=1.0E-6*BB
      DHYBDX=(C1-C2+C3-C4)*1.0E6
      RETURN
      END
C
C
      SUBROUTINE PRCOXY(X,Y,VX,VY,T,JJ,IFAIL)
C
C SOLVES BOTH X AND Y EQUATIONS
C
      DIMENSION X(1000),Y(1000),VX(1000),VY(1000),T(1000)
      DIMENSION XX(1001),YY(1001),VXX(1001),VYY(1001),TT(1001)
      DOUBLE PRECISION X,Y,VX,VY,T,XX,YY,VXX,VYY,TT,CX1,CY1,CVX1,CVY1
      COMMON ALPHA,BETA,ASPECT,GAMMA,DELTA,H,A,B,RADIUS,HO,MU,PNTTHK
      CX1=0.0
      CY1=0.0
      CVX1=0.0
      CVY1=0.0
      XX(1)=X(1)
      YY(1)=Y(1)
      VXX(1)=VX(1)
      VYY(1)=VY(1)
      TT(1)=T(1)
      JJ=JJ-1
C
      DO 95 N=1,JJ
        DO 90 M=1,1000
C
C PREDICT X,Y,VX,VY
C
          XX(M+1)=XX(M)+H*VXX(M)
          YY(M+1)=YY(M)+H*VYY(M)
          E1=DHXBDX(XX(M),YY(M),A,B)
          E2=DHYBDX(XX(M),YY(M),A,B)
          ANG=THET(XX(M),YY(M),A,B)
```

```
          FLD=MAG(XX(M),YY(M),A,B)
          U1=FLD*(E1*COS(ANG)+E2*SIN(ANG))
          U2=FLD*(E1*SIN(ANG)-E2*COS(ANG))
          VXX(M+1)=VXX(M)+H*(-1.0*ALPHA*VXX(M)+BETA*U1)
          VYY(M+1)=VYY(M)+H*(-1.0*ALPHA*VYY(M)-BETA*U2-GAMMA)
C
C STORE FIRST PREDICTIONS OF X,Y,VX,VY FOR USE IN TRUNCATION ERROR ESTIMATE
C
          FIRSX=XX(M+1)
          FIRSY=YY(M+1)
          FIRSVX=VXX(M+1)
          FIRSVY=VYY(M+1)
          ITN=1
C
C CORRECT X,Y,VX,VY
C
 100      CX1=XX(M)+0.5*H*(VXX(M)+VXX(M+1))
          CY1=YY(M)+0.5*H*(VYY(M)+VYY(M+1))
          E3=DHXBDX(XX(M+1),YY(M+1),A,B)
          E4=DHYBDX(XX(M+1),YY(M+1),A,B)
          ANG=THET(XX(M+1),YY(M+1),A,B)
          FLD=MAG(XX(M+1),YY(M+1),A,B)
          U3=FLD*(E3*COS(ANG)+E4*SIN(ANG))
          U4=FLD*(E3*SIN(ANG)-E4*COS(ANG))
          CVX1=VXX(M)-0.5*H*(ALPHA*(VXX(M+1)+VXX(M))-BETA*(U3+U1))
          CVY1=VYY(M)-H*(ALPHA*(VYY(M+1)+VYY(M))+BETA*(U2+U4)+2.0*GAMMA)/2.0
C
C IF CORRECTOR HAS NOT PRODUCED CONVERGENCE,INCREASE ITERATION COUNTER
C CHECK FOR LIMIT ON ITERATIONS,AND IF OK RETURN TO CORRECTOR
C
          Q1=ABS(XX(M+1)-CX1)
          Q2=ABS(YY(M+1)-CY1)
            IF (Q1.LT.1.0E-6.AND.Q2.LT.1.0E-6)THEN
C
C CORRECT USING TRUNCATION ERROR ESTIMATE
C
              XX(M+1)=CX1+0.2*(FIRSX-CX1)
              YY(M+1)=CY1+0.2*(FIRSY-CY1)
              VXX(M+1)=CVX1+0.2*(FIRSVX-CVX1)
              VYY(M+1)=CVY1+0.2*(FIRSVY-CVY1)
              TT(M+1)=TT(M)+H
                IF(YY(M+1).LT.PNTTHK.OR.ABS(XX(M+1)).LT.A) THEN
                  XX(1001)=XX(M+1)
                  YY(1001)=YY(M+1)
                  VXX(1001)=VXX(M+1)
                  VYY(1001)=VYY(M+1)
                  TT(1001)=TT(M+1)
                  GOTO 91
                ENDIF
              GOTO 90
            ELSE
              ITN=ITN+1
            ENDIF
            IF (ITN.GE.10) THEN
              IFAIL=1
              X(N+1)=X(N)
              Y(N+1)=Y(N)
              VX(N+1)=VX(N)
              VY(N+1)=VY(N)
              NPTS=N+1
```

```
            GOTO 99
          ELSE
            XX(M+1)=CX1
            YY(M+1)=CY1
            VXX(M+1)=CVX1
            VYY(M+1)=CVY1
          ENDIF
C
C ELSE RECORRECT
C
          GOTO 100
  90    CONTINUE
  91  X(N+1)=XX(1001)
      Y(N+1)=YY(1001)
      VX(N+1)=VXX(1001)
      VY(N+1)=VYY(1001)
      T(N+1)=TT(1001)
      XX(1)=XX(1001)
      YY(1)=YY(1001)
      VXX(1)=VXX(1001)
      VYY(1)=VYY(1001)
      TT(1)=TT(1001)
      NPTS=N+1
C
C IF PARTICLE HAS HIT INTERFACE OR IS TRAPPED AT DEFECT THEN RETURN
C
      IF (Y(N+1).LT.PNTTHK.OR.ABS(X(N+1)).LE.A) THEN
        NPTS=N+1
        GOTO 99
      ENDIF
  95  CONTINUE
  99  JJ=NPTS
      RETURN
      END
C
C
      SUBROUTINE PRCOX(X,Y,VX,VY,T,JJ,NEVAL,IFAIL)
C
C SOLVES X EQUATION, KEEPING Y CONSTANT
C
      DIMENSION X(1000),Y(1000),VX(1000),VY(1000),T(1000)
      DIMENSION XX(1001),YY(1001),VXX(1001),VYY(1001),TT(1001)
      DOUBLE PRECISION X,Y,VX,VY,T,XX,YY,VXX,VYY,TT,CX1,CY1,CVX1,CVY1
      DOUBLE PRECISION YYCST,VYYCST
      COMMON ALPHA,BETA,ASPECT,GAMMA,DELTA,H,A,B,RADIUS,HO,MU,PNTTHK
      CX1=0.0
      CY1=0.0
      CVX1=0.0
      CVY1=0.0
      XX(1)=X(JJ)
      YY(1)=Y(JJ)
      VXX(1)=VX(JJ)
      VYY(1)=0.0
      TT(1)=T(JJ)
      YYCST=Y(JJ)
      VYYCST=0.0
      IF (Y(1).LT.PNTTHK.OR.ABS(XX(1)).LT.A) THEN
        NPTS=1
        GOTO 207
      ENDIF
```

```
      NEVAL=NEVAL-1
C
      DO 195 N=JJ,NEVAL
        DO 190 M=1,1000
C
C PREDICT X,Y,VX,VY
C
        XX(M+1)=XX(M)+H*VXX(M)
        YY(M+1)=YYCST
        VYY(M+1)=0.0
        E1=DHXBDX(XX(M),YYCST,A,B)
        E2=DHYBDX(XX(M),YYCST,A,B)
        ANG=THET(XX(M),YYCST,A,B)
        FLD=MAG(XX(M),YYCST,A,B)
        U1=FLD*(E1*COS(ANG)+E2*SIN(ANG))
        U2=FLD*(E1*SIN(ANG)-E2*COS(ANG))
        VXX(M+1)=VXX(M)+H*(-1.0*ALPHA*VXX(M)+BETA*U1)
C
C STORE FIRST PREDICTIONS OF X,VX FOR USE IN TRUNCATION ERROR ESTIMATE
C
        FIRSX=XX(M+1)
        FIRSVX=VXX(M+1)
        ITN=1
C
C CORRECT X,VX
C
 200    CX1=XX(M)+0.5*H*(VXX(M)+VXX(M+1))
        E3=DHXBDX(XX(M+1),YYCST,A,B)
        E4=DHYBDX(XX(M+1),YYCST,A,B)
        ANG=THET(XX(M+1),YYCST,A,B)
        FLD=MAG(XX(M+1),YYCST,A,B)
        U3=FLD*(E3*COS(ANG)+E4*SIN(ANG))
        U4=FLD*(E3*SIN(ANG)-E4*COS(ANG))
        CVX1=VXX(M)-0.5*H*(ALPHA*(VXX(M+1)+VXX(M))-BETA*(U3+U1))
C
C IF CORRECTOR HAS NOT PRODUCED CONVERGENCE,INCREASE ITERATION COUNTER
C CHECK FOR LIMIT ON ITERATIONS, AND IF OK RETURN TO CORRECTOR
C
        Q1=ABS(XX(M+1)-CX1)
        IF (Q1.LT.1.0E-6) THEN
C
C CORRECT USING TRUNCATION ERROR ESTIMATE
C
          XX(M+1)=CX1+0.2*(FIRSX-CX1)
          VXX(M+1)=CVX1+0.2*(FIRSVX-CVX1)
          TT(M+1)=TT(M)+H
            IF (ABS(XX(M+1)).LT.A) THEN
              XX(1001)=XX(M+1)
              YY(1001)=YYCST
              VXX(1001)=VXX(M+1)
              VYY(1001)=0.0
              TT(1001)=TT(M+1)
              GOTO 191
            ENDIF
          GOTO 190
      ELSE
          ITN=ITN+1
      ENDIF
        IF (ITN.GE.10) THEN
          IFAIL=1
```

```
          X(N+1)=X(N)
          Y(N+1)=Y(N)
          VX(N+1)=VX(N)
          VY(N+1)=VY(N)
          NPTS=N+1
          GOTO 209
        ELSE
C
C ELSE RECORRECT
C
          XX(M+1)=CX1
          VXX(M+1)=CVX1
        ENDIF
        GOTO 200
  190 CONTINUE
  191 X(N+1)=XX(1001)
      Y(N+1)=YYCST
      VX(N+1)=VXX(1001)
      VY(N+1)=0.0
      T(N+1)=TT(1001)
      XX(1)=XX(1001)
      YY(1)=YYCST
      VXX(1)=VXX(1001)
      VYY(1)=0.0
      TT(1)=TT(1001)
      NPTS=N+1
      IF (ABS(X(N+1)).LT.A) THEN
        NPTS=N+1
        GOTO 199
      ENDIF
  195 CONTINUE
  199 IF (ABS(X(NPTS)).LT.A) THEN
C
C IF PARTICLE IS TRAPPED AT DEFECT TAKE LAST VALUE AND RETURN
C
  207   NEVAL=NEVAL-1
        DO 201 I=NPTS,NEVAL
          X(I+1)=X(NPTS)
          Y(I+1)=YYCST
          VX(I+1)=0.0
          VY(I+1)=0.0
          T(I+1)=T(I)+(1.0E3*H)
  201   CONTINUE
        NEVAL=NEVAL+1
      ENDIF
  209 RETURN
      END
```

Appendix P4

Listing of the Program to Calculate the Field Distribution for the Coil-Gradient System

This is a BBC BASIC program which runs on an Acorn Model B BBC Microcomputer. At a field point $P(x)$ which lies on the x axis (as defined in Chapter 7) it calculates the total x component of the magnetic field due to all of the rectangular current loops comprising the coil system. The total x component of the field at $P(x)$ is calculated as $P(x)$ is moved in steps along the x axis, enabling the whole field in the x direction to be mapped out for subsequent calculation of the field gradient.

```
10REM GRADIENT FIELD DISTRIBUTION CALCULATION
20DIM U(4):DIM V(4):DIM W(4)
30DIM XL(21):DIM XR(21)
40U(1)=0.161E-3:W(1)=26.122E-3:V(1)=1.511E-3
50U(2)=0.222E-3:W(2)=26.183E-3:V(2)=1.572E-3
60U(3)=0.283E-3:W(3)=26.244E-3:V(3)=1.633E-3
70U(4)=0.344E-3:W(4)=26.305E-3:V(4)=1.694E-3
80MUNOUGHT=4*PI*1E-7
90INPUTTAB(5);"PLEASE ENTER THE CONST FIELD CURRENT (AMPS):";IC
100INPUTTAB(5);"PLEASE ENTER THE GRAD FIELD CURRENT (AMPS):";IG
110VDU 2
120PRINTTAB(5);"CONST FIELD CURRENT = ";IC;" AMPS"
130PRINTTAB(5);"GRAD FIELD CURRENT = ";IG;" AMPS"
140PRINT
150FOR G=-0.5 TO 0.55 STEP 0.05
160PARL=0:PARR=0:PARG=0
170XMID=1.0875
180FOR F%=1 TO 20
190XL(F%)=XMID+G+(F%-1)*0.175
200XR(F%)=XMID-G+(F%-1)*0.175
210NEXT
220FOR F%=1 TO 20
230XL(F%)=1E-3*XL(F%)
240XR(F%)=1E-3*XR(F%)
250NEXT
260FOR F%=1 TO 2
270FOR K%=1 TO 20
280AL=(W(F%)*U(F%))/(((U(F%)↑2)+(XL(K%)↑2))*SQR((U(F%)↑2)+(XL(K%)↑2)+((0.5*W(F%))↑2)))
290AR=(W(F%)*U(F%))/(((U(F%)↑2)+(XR(K%)↑2))*SQR((U(F%)↑2)+(XR(K%)↑2)+((0.5*W(F%))↑2)))
300AG=(W(F%+2)*U(F%+2))/(((U(F%+2)↑2)+(XR(K%)↑2))*SQR((U(F%+2)↑2)+(XR(K%)↑2)+((0.5*W(F%+2))↑2)))
310BL=(W(F%)*V(F%))/(((V(F%)↑2)+(XL(K%)↑2))*SQR((V(F%)↑2)+(XL(K%)↑2)+((0.5*W(F%))↑2)))
320BR=(W(F%)*V(F%))/(((V(F%)↑2)+(XR(K%)↑2))*SQR((V(F%)↑2)+(XR(K%)↑2)+((0.5*W(F%))↑2)))
330BG=(W(F%+2)*V(F%+2))/(((V(F%+2)↑2)+(XR(K%)↑2))*SQR((V(F%+2)↑2)+(XR(K%)↑2)+((0.5*W(F%+2))↑2)))
340CL=W(F%)/((XL(K%)↑2)+((0.5*W(F%))↑2))
350CR=W(F%)/((XR(K%)↑2)+((0.5*W(F%))↑2))
360CG=W(F%+2)/((XR(K%)↑2)+((0.5*W(F%+2))↑2))
370DL=V(F%)/(SQR((XL(K%)↑2)+(V(F%)↑2)+((0.5*W(F%))↑2)))
380DR=V(F%)/(SQR((XR(K%)↑2)+(V(F%)↑2)+((0.5*W(F%))↑2)))
390DG=V(F%+2)/(SQR((XR(K%)↑2)+(V(F%+2)↑2)+((0.5*W(F%+2))↑2)))
400EL=U(F%)/(SQR((XL(K%)↑2)+(U(F%)↑2)+((0.5*W(F%))↑2)))
410ER=U(F%)/(SQR((XR(K%)↑2)+(U(F%)↑2)+((0.5*W(F%))↑2)))
420EG=U(F%+2)/(SQR((XR(K%)↑2)+(U(F%+2)↑2)+((0.5*W(F%+2))↑2)))
430PARL=PARL+AL+BL+(CL*(DL+EL))
440PARR=PARR+AR+BR+(CR*(DR+ER))
450PARG=PARG+AG+BG+(CG*(DG+EG))
460NEXT K%
470NEXT F%
480BL=(MUNOUGHT*IC/(4*PI))*PARL*1E3
490BR=(MUNOUGHT*IC/(4*PI))*PARR*1E3
500BG=(MUNOUGHT*IG/(4*PI))*PARG*1E3
510PRINTTAB(5);"X-COORD = "G " mm"
520PRINTTAB(5);"Bo(LEFT)(mT) =";BL
530PRINTTAB(5);"Bo(RIGHT)(mT) =";BR
540PRINTTAB(5);"Bo(L+R)(mT)=Boconst =";BL+BR
550PRINTTAB(5);"BoGRAD(mT) =";BG
560PRINTTAB(5);"Bo(GRAD+L+R)(mT)=Botot =";BG+BL+BR
570PRINT:PRINT
580NEXT G
590VDU3
600END
```

References

Aharoni, A. and Jakubovics, J.P. *Cylindrical Domains in Small Ferromagnetic Spheres with Cubic Anisotropy* IEEE Trans. Magn. **MAG-24**, 1892 (1988)

American Society for Testing and Materials (ASTM) *Selected Powder Diffraction Data for Minerals* Joint Committee on Powder Diffraction Standards, Swarthmore, Pennsylvania (1974)

Andress, S.J., Benedetti, A., Corradi, A.R. and Fagherazzi, G. *The Microstructure of* $\gamma - Fe_2O_3$ *and Its Effects on the Magnetization Properties* IEEE Trans. Magn. **MAG-22**, 1341 (1986)

Arii, T., Yatsuya, S., Wada, N. and Mihama, K. *Ferromagnetic Domains in F.C.C. Cobalt Fine Particles Observed by Lorentz Electron Microscopy* Japan. J. Appl. Phys. **17**, 259 (1978)

Bagchi, P. *Enthalpic Repulsion between Two Identical Spherical Particles Coated with a Polymeric Adsorption Layer* J. Coll. Int. Sci. **41**, 380 (1972)

Banerjee, S.K. and Moskowitz, B.M. *Ferrimagnetic Properties of Magnetite* in *Magnetite Biomineralization and Magnetoreception in Organisms*, Ed. J.L. Kirschvink, D.S. Jones and B.J. Macfadden, Plenum, New York, p17 (1985)

Bean, C.P. and Livingston, J.D. *Superparamagnetism* J. Appl. Phys. **30**, 120S (1959)

Bean, C.P. and Jacobs, I.S. *Magnetization of a Dilute Suspension of a Multidomain Ferromagnet* J. Appl. Phys. **31**, 1228 (1960)

Berkowitz, A.E. and Lahut, J.A. *Superparamagnetic ferrite particles produced by milling* in *Magnetism and Magnetic Materials-1972* AIP Conference Proceedings No. 10, Ed. C.D. Graham Jr. and J.J. Rhyne, American Institute of Physics, New York, p966 (1973)

Berkowitz, A.E., Lahut, J.A., Jacobs, I.S., Levinson, L.M. and Forester, D.W. *Spin Pinning at Ferrite-Organic Interfaces* Phys. Rev. Lett. **34**, 594 (1975)

Berry, A. and Swain, L.M. *On the Steady Motion of a Cylinder through Infinite Viscous Fluid* Proc. Roy. Soc. A **102**, 766 (1923)

Betz, C.E. *Principles of Magnetic Particle Testing* Magnaflux Corporation, Chicago, Illinois (1967)

Binns, K.J. and Lawrenson, P.J. *Analysis and Computation of Electric and Magnetic Field Problems* Pergamon Press, New York (1963)

Bitter, F. *On Inhomogeneities in the Magnetization of Ferromagnetic Materials* Phys. Rev. **38**, 1903 (1931)

Blakely, P.J., Simkin, J. and Brown, S.T. *Validation of Finite Element Analysis of the Magnetic Fields Around Fine Cracks* IEEE Trans. Magn. **MAG-21**, 2420 (1985)

Bleaney, B.I. and Bleaney, B. *Electricity and Magnetism, 3rd Edition* Oxford University Press (1976)

Bloch, F. *Zur Theorie des Austauschproblems und der Remanenzerscheinung der Ferromagnetika* Z. Phys. **74**, 295 (1932)

Bowden, G.J. *Detection coil systems for vibrating sample magnetometers* J. Phys. E: Sci. Instrum. **5**, 1115 (1972)

Bradbury, A., Menear, S. and Chantrell, R.W. *A Monte Carlo Calculation of the Magnetic Properties of a Ferrofluid Containing Interacting Polydispersed Particles* J. Magn. Magn. Mat. **54-57**, 745 (1986)

British Standards Institution *Specification for contrast aid paints used in magnetic particle flaw detection* BS 5044 (1973)

British Standards Institution *Magnetic particle flaw detection* BS 6072 (1981)

British Standards Institution *Magnetic flaw detection inks and powders* BS 4069 (1982)

British Standards Institution *Measurement of UV-A radiation (black light) used in non-destructive testing* BS 4489 (1984)

Brudar, B. *Magnetic leakage fields calculated by the method of finite differences* NDT International **18**, 353 (1985)

Case, W.E. and Harrington, R.D. *Calibration of Vibrating-Sample Magnetometers* J. Res. Nat. Bur. Stand. **70C**, 255 (1966)

Cayless, A.T., Hoon, S.R., Tanner, B.K., Chantrell, R.W. and Kilner, M. *High Sensitivity Measurements of Néel Relaxation in Fine Particle Ferromagnetic Systems* J. Magn. Magn. Mat. **30**, 303 (1983)

Chantrell, R.W., Popplewell, J. and Charles, S.W. *Measurements of Particle Size Distribution Parameters in Ferrofluids* IEEE Trans. Magn. **MAG-14**, 975 (1978)

Chantrell, R.W., Bradbury, A., Popplewell, J. and Charles, S.W. *Particle cluster configuration in magnetic fluids* J. Phys. D: Appl. Phys. **13**, L119 (1980)

Chantrell, R.W., Hoon, S.R. and Tanner, B.K. *Time-Dependent Magnetization in Fine-Particle Ferromagnetic Systems* J. Magn. Magn. Mat. **38**, 133 (1983)

Chantrell, R.W., Fearon, M. and Wohlfarth, E.P. *The Time-Dependent Magnetic Behaviour of Fine Particle Systems* phys. stat. sol. (*a*) **97**, 213 (1986)

Chikazumi, S. *Physics of Magnetism* John Wiley, New York (1964)

Craik, D.J. and Tebble, R.S. *Ferromagnetism and Ferromagnetic Domains* North Holland, Amsterdam (1965)

Crangle, J. *The Magnetic Properties of Solids* Edward Arnold, London (1977)

Dobmann, G. and Höller, P. *Physical Analysis Methods of Magnetic Flux Leakage* in *Research Techniques in Nondestructive Testing Vol. IV* Ed. R.S. Sharpe, Academic Press, New York, p39 (1980)

Dorn, W.S. and McCracken, D.D. *Numerical Methods with Fortran IV Case Studies* John Wiley, New York (1972)

Duffin, W.J. *Electricity and Magnetism, 3rd Edition* McGraw-Hill, London (1980)

Dunlop, D.J. *Temperature, Time and Interaction Effects in Rock Magnetism* J. Magn. Magn. Mat. **45**, 107 (1984)

Edwards, C. *A Study of Magnetic Particle Inspection* Ph.D. Thesis, University of Hull (1986)

Edwards, C. and Palmer, S.B. *The magnetic leakage field of surface-breaking cracks* J. Phys. D: Appl. Phys. **19**, 657 (1986)

Fletcher, D. and Parker, M.R. *Double layer contribution to diffusion effects in colloids* J. Phys. D: Appl. Phys. **17**, L119 (1984)

Foner, S. *Vibrating Sample Magnetometer* Rev. Sci. Instrum. **27**, 548 (1956)

Foner, S. *Versatile and Sensitive Vibrating-Sample Magnetometer* Rev. Sci. Instrum. **30**, 548 (1959)

Gerber, J.A., Burmester, W.L. and Sellmyer, D.J. *Simple vibrating sample magnetometer* Rev. Sci. Instrum. **53**, 691 (1982)

Gerber, R., Takayasu, M. and Friedlaender, F.J. *Generalization of HGMS Theory: The Capture of Ultra-Fine Particles* IEEE Trans. Magn. **MAG-19**, 2115 (1983)

Gerber, R. *Magnetic Filtration of Ultra-Fine Particles* IEEE Trans. Magn. **MAG-20**, 1159 (1984)

Gibbs, M.R.J., Evetts, J.E. and Leake, J.A. *Activation energy spectra and relaxation in amorphous materials* J. Mater. Sci. **18**, 278 (1983)

Goodhew, P.J. *Specimen Preparation in Materials Science* in *Practical Methods in Electron Microscopy, Volume 1* Ed. A.M. Glauert, North Holland, Amsterdam, p7 (1972)

Gorter, E.W. *Some Properties of Ferrites in Connection with Their Chemistry* Proc. Inst. Radio Eng. **43**, 1945 (1955)

Granqvist, C.G. and Buhrman, R.A. *Ultrafine metal particles* J. Appl. Phys. **47**, 2200 (1976)

Guy, C.N. *Frequency doubling—a new approach to vibrating sample magnetometers* J. Phys. E: Sci. Instrum. **9**, 433 (1976*a*)

Guy, C.N. *A simple approach to coil design for vibrating sample magnetometers* J. Phys. E: Sci. Instrum. **9**, 790 (1976*b*)

Hamaker, H.C. *The London-van der Waals Attraction between spherical particles* Physica **4**, 1058 (1937)

Heisenberg, W. *Zur Theorie des Ferromagnetismus* Z. Phys **49**, 619 (1928)

Hetherington, M.G., Jakubovics, J.P., Szpunar, J.A. and Tanner, B.K. *High-voltage Lorentz electron microscopy studies of domain structures and magnetization processes in pearlitic steels* Phil. Mag. B **56**, 561 (1987)

Hoon, S.R. *An inexpensive, sensitive vibrating sample magnetometer* Eur. J. Phys. **4**, 61 (1983)

Hoon, S.R. *Ac Multipolar Sources for Vibrating and Rotating Sample Magnetometer Modelling* IEEE Trans. Magn. **MAG-24**, 1963 (1988)

Hoon, S.R. and Willcock, S.N.M. *The direct observation of magnetic images in electromagnet vibrating sample magnetometers* J. Phys. E: Sci. Instrum. **21**, 480 (1988*a*)

Hoon, S.R. and Willcock, S.N.M. *The design and operation of an automated double-crank vibrating sample magnetometer* J. Phys. E: Sci. Instrum. **21**, 772 (1988*b*)

Huisman, H.F. *Particle Interactions and H_c: An Experimental Approach* IEEE Trans. Magn. **MAG-18**, 1095 (1982)

Hull, T.E. and Creemer, A.L. *Efficiency of Predictor-Corrector Procedures* J. Assn. for Computing Machinery **10**, 291 (1963)

Hwang, J.H. and Lord, W. *Finite Element Modeling of Magnetic Field/Defect Interactions* J. Test. Eval. **3**, 21 (1975)

Ida, N. and Lord, W. *3-D Finite Element Predictions of Magnetostatic Leakage Fields* IEEE Trans. Magn. **MAG-19**, 2260 (1983)

Jacobs, I.S. and Luborsky, F.E. *Magnetic Anisotropy and Rotational Hysteresis in Elongated Fine-Particle Magnets* J. Appl. Phys. **28**, 467 (1957)

Josephs, R.M., Crompton, D.S. and Krafft, C.S. *Application of Digital Signal Processing to Vibrating Sample Magnetometry* IEEE Trans. Magn. **MAG-23**, 241 (1987)

Kaiser, R. and Miskolczy, G. *Magnetic Properties of Stable Dispersions of Subdomain Magnetite Particles* J. Appl. Phys. **41**, 1064 (1970)

Kilner, M., Hoon, S.R., Lambrick, D.B., Potton, J.A. and Tanner, B.K. *Preparation and Properties of Metallic Iron Ferrofluids* IEEE Trans. Magn. **MAG-20**, 1735 (1984)

Kittel, C. *Physical Theory of Ferromagnetic Domains* Rev. Mod. Phys. **21**, 541 (1949)

Kittel, C. *Introduction to Solid State Physics, 5th Edition* John Wiley, New York (1976)

Kloepper, R.M., Finkelstein, B. and Braunstein, D.P. *Time Decay of Magnetization in Particulate Media* IEEE Trans. Magn. **MAG-20**, 757 (1984)

Kneller, E.F. and Luborsky, F.E. *Particle Size-Dependence of Coercivity and Remanence of Single-Domain Particles* J. Appl. Phys. **34**, 656 (1963)

Knowles, J.E. *Magnetic Measurements on Single Acicular Particles of γFe_2O_3* IEEE Trans. Magn. **MAG-16**, 62 (1980)

Lamb, H. *Hydrodynamics, 6th Edition* Cambridge University Press, London (1932)

Lambrick, D.B. *Magnetic Properties of Metallic Fine Particle Systems* Ph.D. Thesis, University of Durham (1986)

Lambrick, D.B., Mason, N., Harris, N.J., Russell, G.J., Hoon, S.R. and Kilner, M. *An Iron-Cobalt 'Alloy' Magnetic Fluid* IEEE Trans. Magn. **MAG-21**, 1891 (1985)

Lambrick, D.B., Mason, N., Hoon, S.R., Kilner, M. and Chapman, J.N. *The Preparation of Co/Fe Alloy Fine Particles from* $HFeCo_3(CO)_{12}$ IEEE Trans. Magn. **MAG-24**, 1644 (1988)

Lord, W. and Hwang, J.H. *Defect Characterization from Magnetic Leakage Fields* Brit. J. Non-Destr. Testing **19**, 14 (1977)

Lord, W. *Applications of Numerical Field Modeling to Elecromagnetic Methods of Nondestructive Testing* IEEE Trans. Magn. **MAG-19**, 2437 (1983)

Lovejoy, D.J. *The Nature of Magnetic Inks and Powders* Brit. J. Non-Destr. Testing **23**, 242 (1980)

Lumb, R.F. and Winship, P. *Magnetic particle crack detection, Part 2—Flux generation and potential applications to offshore structures* Metal Construction **9**, 331 (1977)

Lyklema, J. *Fundamentals of Electrical Double Layers in Colloidal Systems* in *Colloidal Dispersions*, Ed. J.W. Goodwin, The Royal Society of Chemistry, London (1982)

Mallinson, J. *Magnetometer Coils and Reciprocity* J. Appl. Phys. **37**, 2514 (1966)

Mann, S. *Structure, Morphology, and Crystal Growth of Bacterial Magnetite* in *Magnetite Biomineralization and Magnetoreception in Organisms*, Ed. J.L. Kirschvink, D.S. Jones and B.L. Macfadden, Plenum, New York, p311 (1985)

Menear, S. and Bradbury, A. *The Effects of Weak Dipolar Interactions on the Magnetic Properties of Systems of Fine Ferromagnetic Particles* J. Magn. Magn. Mat **51**, 103 (1985)

Metcalf, M. and Fuller, M. *Domain observations of titanomagnetites from room temperature to Curie point and the nature of thermo-remanent magnetism in fine particles* Nature **321**, 847 (1986)

Morrish, A.H. and Watt, L.A.K. *Coercive Force of Iron Oxide Micropowders at Low Temperatures* J. Appl. Phys. **29**, 1029 (1958)

Morrish, A.H. *The Physical Principles of Magnetism* John Wiley, New York (1965)

Moskowitz, B.M. and Banerjee, S.K. *Grain Size Limits for Pseudosingle Domain Behavior in Magnetite: Implications for Paleomagnetism* IEEE Trans. Magn. **MAG-15**, 1241 (1979)

Nagata, N., Fujita, E., Ebisu, S. and Taniguchi, S. *Optimum Design of Detection Coil System for Vibrating Sample Magnetometer* Japan. J. Appl. Phys. **26**, 92 (1987)

Néel, L. *Propriétés Magnétiques des Ferrites; Ferrimagnétisme et Antiferromagnétisme* Ann. de Phys. **3**, 137 (1948)

Néel, L. *Théorie du Trainage Magnétique des Ferromagnétiques en Grains Fins avec Applications aux Terres Cuites* Ann. Geophys. **5**, 99 (1949)

O'Grady, K., Chantrell, R.W., Popplewell, J. and Charles, S.W. *Time Dependent Magnetization of a System of Fine Cobalt Particles* IEEE Trans. Magn. **MAG-17**, 2943 (1981)

O'Grady, K. and Bradbury, A. *Particle Size Analysis in Ferrofluids* J. Magn. Magn. Mat. **39**, 91 (1983)

O'Grady, K. and Chantrell, R.W. *The Temperature Variation of the Coefficient of Magnetic Viscosity* J. Magn. Magn. Mat. **54-57**, 755 (1986)

Oseroff, S.B., Clark, D., Schultz, S. and Shtrikman, S. *Temperature Dependence of the Time Decay of the Magnetization in Particulate Media* IEEE Trans. Magn. **MAG-21**, 1495 (1985)

Parpia, D.Y., Tanner, B.K. and Lord, D.G. *Direct optical observation of ferromagnetic domains* Nature **303**, 684 (1983)

Pauthenet, R. *Variation thermique de l'aimantation spontanée des ferrites de nickel, cobalt, fer et manganèse* Comptes Rendu Acad. Sci. (Paris) **230**, 1842 (1950)

Popplewell, J. and Charles, S.W. *Ferromagnetic Liquids—Their Magnetic Properties and Applications* IEEE Trans. Magn. **MAG-17**, 2923 (1981)

Potton, J.A., Daniell, G.J. and Melville, D. *A new method for the determination of particle size distributions from superparamagnetic measurements* J. Phys. D: Appl. Phys. **17**, 1567 (1984)

Raine, G.A. *Private communication* (1988)

Rosensweig, R.E., Nestor, J.W. and Timmins, R.S. *Ferrodynamic Fluids for Direct Conversion of Heat Energy* A.I.Ch.E.-I. Chem. E. Symp. Ser. No. 5, 104 (1965)

Rosensweig, R.E. *Ferrohydrodynamics* Cambridge University Press, Cambridge (1985)

Sato, T., IIjima, T., Seki, M. and Inagaki, N. *Magnetic Properties of Ultrafine Ferrite Particles* J. Magn. Magn. Mat. **65**, 252 (1987)

Schieber, M.M. *Experimental Magnetochemistry* North Holland, Amsterdam (1967)

Sharrock, M.P. and Bodnar, R.E. *Magnetic materials for recording: An overview with special emphasis on particles* J. Appl. Phys. **57**, 3919 (1985)

Shcherbinin, V.E. and Zatsepin, N.N. *Calculation of the Magnetostatic Field of Surface Defects. II Experimental Verification of the Principal Theoretical Relationships* Defektoskopiya **2**, 394 (1966)

Shcherbinin, V.E. and Pashagin, A.E. *Influence of the Extension of a Defect on the Magnitude of its Magnetic Field* Defektoskopiya **8**, 74 (1972)

Shelikhov, G.S. and Aleksandrov, A.G. *Coagulation of the Particles in a Magnetic Suspension and its Influence on the Sensitivity of the Magnetic-Powder Method of Testing* Defektoskopiya **13**, 26 (1977)

Shull, C.E., Wollan, E.O. and Koehler, W.C. *Neutron Scattering and Polarization by Ferromagnetic Materials* Phys. Rev. **84**, 912 (1951)

Smith, D.O. *Development of a Vibrating-Coil Magnetometer* Rev. Sci. Instrum. **27**, 261 (1956)

Stacey, F.D. and Banerjee, S.K. *The Physical Principles of Rock Magnetism* Elsevier, Amsterdam (1974)

Stadhaus, M. *Beurteilung der Magnetpulver mit Hilfe der Messung der Erkennbarkeit von Magnetpulveranzeigen* Materialprüf **21**, 157 (1979)

Stoner, E.C. and Wohlfarth, E.P. *A Mechanism of Magnetic Hysteresis in Heterogeneous Alloys* Phil. Trans. Roy. Soc. **A-240**, 599 (1948)

Street, R. and Woolley, J.C. *A Study of Magnetic Viscosity* Proc. Phys. Soc. A. **62**, 562 (1949)

Swartzendruber, L.J. *Magnetic Leakage and Force Fields for Artificial Defects in Magnetic Particle Test Rings* Proc. 12th. Symp. of Nondestructive Evaluation (San Antonio, Texas), Ed. W.W. Bradshaw, p150 (1979)

Swoboda, T.J., Arthur Jnr, P., Cox, N.L., Ingraham, J.N., Oppegard, A.L. and Saddler, M.S. *Synthesis and Properties of Ferromagnetic Chromium Oxide* J. Appl. Phys. **32**, 374S (1961)

Takayasu, M., Gerber, R. and Friedlaender, F.J. *Magnetic Separation of Submicron Particles* IEEE Trans. Magn. **MAG-19**, 2112 (1983)

Van der Biest, O. and Thomas, G. *Fundamentals of Electron Microscopy* in *Electron Microscopy in Mineralogy* Ed. H.-R. Wenk, Springer-Verlag, Heidelberg, p18 (1976)

Van Vleck, J.H. *The Theory of Electric and Magnetic Susceptibilities* Oxford University Press. Oxford (1932)

Verwey, E.J.W. and Haayman, P.W. *Electronic Conductivity and Transition Point in Magnetite* Physica **8**, 979 (1941)

Verwey, E.J.W. and Overbeek, J.T.G. *Theory of the Stability of Lyophobic Colloids* Elsevier, Amsterdam (1948)

Wagg, A.W. *Private communication* (1988)

Watt, I.M. *The analytical electron microscope* J. Phys. E: Sci. Instrum. **19**, 668 (1986)

Weiss, P. *L'hypothèse du Champ Moléculaire et la Propriété Ferromagnétique* J. de Physique **6**, 661 (1907)

Weser, T. and Stierstadt, K. *Discrete Particle Size Distribution in Ferrofluids* Z. Phys. B. **59**, 253 (1985*a*)

Weser, T. and Stierstadt, K. *Magnetoviscosity of Concentrated Ferrofluids* Z. Phys. B. **59**, 257 (1985*b*)

Willcock, S.N.M. *An Investigation of the Magnetic Properties of High Tensile Steels* Ph.D. Thesis, University of Durham (1985)

Wohlfarth, E.P. *The Physics of Magnetic Recording Media* MMIS International Newsletter **4**, 87 (1981)

Wohlfarth, E.P. *The coefficient of magnetic viscosity* J. Phys. F: Met. Phys. **14**, L155 (1984)

Wooding, A., Kilner, M. and Lambrick, D.B. *Studies of the Surfactant Double Layer Stabilisation of Water Based Magnetic Fluids* To be submitted (1988)

Zatsepin, N.N. and Shcherbinin, V.E. *Calculation of the Magnetostatic Field of Surface Defects. I Field Topography of Defect Models* Defektoskopiya **2**, 385 (1966)

Zieba, A. and Foner, S. *Detection coil, sensitivity function, and sample geometry effects for vibrating sample magnetometers* Rev. Sci. Instrum. **53**, 1344 (1982)

Zienkiewicz, O.C. *Finite Elements—The Basic Concepts and an Application to 3-D Magnetostatic Problems* in *Finite Elements in Electrical and Magnetic Field Problems* Ed. M.V.K. Chari and P.P. Silvester, John Wiley, New York, p11 (1980)

The End